9950-798

ASTRO Report

Mars Geoscience Orbiter and Lunar Geoscience Orbiter

Final Report

Prepared by
William V. Fuldner
Manager, Spacecraft Systems Engineering
Paul F. Kaskiewicz
Senior Member, Technical Staff
RCA Government Systems Division
Astro-Electronics
Princeton, New Jersey

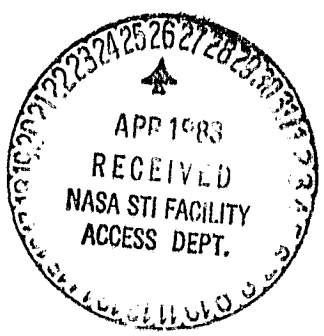

Contract No. 956291

January 28, 1983
Report No. AE R-4417

This work was performed for the Jet Propulsion Laboratory, California Institute of Technology, sponsored by the National Aeronautics and Space Administration under Contract NAS7-918.

RCA Astro-Electronics

Mars Geoscience Orbiter and Lunar Geoscience Orbiter

Final Report

Prepared by
William V. Fuldner
Manager, Spacecraft Systems Engineering
Paul F. Kaskiewicz
Senior Member, Technical Staff
RCA Government Systems Division
Astro-Electronics
Princeton, New Jersey

Contract No. 956291

January 28, 1983
Report No. AE R-4417

This work was performed for the Jet Propulsion Laboratory, California Institute of Technology, sponsored by the National Aeronautics and Space Administration under Contract NAS7-918.

ABSTRACT

This report summarizes the findings of a study done by RCA Astro-Electronics for JPL to determine the feasibility of using the AE/DE earth-orbiting spacecraft design for the LGO and/or MGO missions. During the course of the study, configurations were developed and subsystems analysis was carried out to optimize the suitability of the spacecraft to the missions.

The primary conclusion is that the basic AE/DE spacecraft can readily be applied to the LGO mission with relatively minor, low risk modifications. The MGO mission poses a somewhat more complex problem, primarily due to the overall maneuvering hydrazine budget and power requirements of the sensors and their desired duty cycle. These considerations dictate a modification (scaling up) of the strucure to support mission requirements. While this can be accomplished at low risk, the MGO mission represents about the limit for the AE/DE class spacecraft. However, for missions up to and including the MGO (and certainly for the LGO) the basic AE/DE concept provides and extremely low cost option consistent with mission needs.

TABLE OF CONTENTS

TABLE OF CONTENTS (Continued)

LIST OF ILLUSTRATIONS

LIST OF ILLUSTRATIONS (Continued)

LIST OF ILLUSTRATIONS (Continued)

LIST OF ILLUSTRATIONS (Continued)

LIST OF TABLES

LIST OF TABLES (Continued)

SECTION 1.0
INTRODUCTION AND SUMMARIZED FINDINGS

SECTION 1.0
INTRODUCTION AND SUMMARIZED FINDINGS

This report documents the findings of a study performed by RCA Astro-Electronics in response to contract No. 956291 with JPL for the study of the application of existing Earth orbiter designs to the Mars Geoscience Orbiter and Lunar Geoscience Orbiter (MGO/LGO). This study was based on the application of previously flown technologies from the Atmosphere Explorer (AE) and Dynamics Explorer (DE) programs utilizing spacecraft designed and built by RCA for NASA Goddard Space Flight Center. Both of these heritage programs accommodated science-type missions and stressed cleanliness, both in the chemical contaminant and electromagnetic domains, to minimize contamination of the measurements to be performed. Also, both programs required spacecraft designs which minimized interaction of the spacecraft with the local plasma to optimize in situ measurement instruments carried on board; with the additional constraint placed on the Atmosphere Explorer design - that it be aerodynamically stable during the low perigee (120 km altitude) passes encountered in that program's mission. These conditions led to the physical configuration of both spacecraft approximating a right circular cylinder with a 16-sided polygon.

While the identified payload for the two missions does not, to the first approximation, require the interaction with the local plasma be as minimized as the predecessor missions (other than the EMC environment for the magnetometers), the retention of these features in the spacecraft design studies allows for growth and flexibility in mission design without major impact. As will be shown in the mass budgeting and power budgeting, Sections 6 and 10 respectively of this study report, significant margins for growth have been allocated to allow for such modification within the design capacity of the common MGO/LGO system.

The payload considered for the two missions is summarized in Table 1-1.

TABLE 1-1. MISSION PAYLOADS

MGO	LGO
Magnetometer γ-Ray Spectrometer Multi-Spectral Mapper Radar Altimeter	Magnetometer γ-Ray Spectrometer Multi-Spectral Mapper Radar Altimeter X-Ray Spectrometer Electron Reflectometer
Alternatives	
Laser Altimeter	Laser Altimeter

1.1 EARTH ORBITER TO NON-EARTH ORBITER HARDWARE DESIGNS

A fundamental element in understanding implications of the results of this study is agreement to the interpretation of "applicability of existing design" of hardware from Earth orbiter missions to non-Earth orbiter missions. Additionally, agreement to the "scaling" or extension of existing designs, and

attendant risk associated with same, must receive objective assessment to make the study results useful. The position taken in performance of the analyses documented herein is that, to the first order, the orbited body is not itself a prime driver in the features of the architecture or detail design of the "bus" or "platform."

Elements of the spacecraft which do not require sensing of the body being orbited are designed to perform specific functions internal to the operation of the spacecraft and are, therefore, independent of the body orbited. An example of this is the command and data handling subsystem which is configured for optimal internal digital signal manipulation in decoding and distributing commands, synchronization signals, and the assemblage and formatting of telemetry data for transmission.

In similar fashion, the power subsystem, the thermal subsystem, and the communications subsystem are not affected by the orbited body directly, but rather are affected by its distance from the Sun. For the power and thermal subsystems, this translates into the total incident energy on the spacecraft, thus driving the size of the solar array and establishing one of the baseline parameters for the α/ε (absorbance to emittance ratio) of the thermal subsystem. Internal to the spacecraft, the designs of the power system and of the thermal subsystem are not influenced by the orbited body. In the case of the communications subsystem, the orbited body and its orbital relation to the Earth (and the Sun) establish the combined parametric requirements on transmitter size and antenna gain for required data rates: an extension, due to the distances involved, of exactly the same solutions for low altitude to geosynchronous and beyond Earth orbiters.

In the case of the attitude determination and control subsystem and the reaction control subsystem, the control function deals with manipulation of the physical orientation of the spacecraft's body either propulsively or by momentum interchange. Interaction with the orbited body is limited to the method of attitude sensing should the system design require sensing of the body orbited (e.g., infrared horizon sensors). This feature also can become insensitive to the orbited body if the sensing system employs celestial sensors and/or Sun sensors. It should be noted that this configuration is employed in the RCA-built DMSP spacecraft (Defense Meteorological Satellite Program).

Finally, the structure subsystem design is dominated by the launch vehicle to be employed and, moreover, by the initial stages wherein the maximum loads (sustained accelerations, acoustic environment) are encountered. Additional solid upper stages such as those used to enter the cruise phase of the mission or the orbit injection motor do not, in general, drive the structure design. Thus, in the case of the structure subsystem, the body to be orbited is not a major design influence.

There are second order effects of the orbited body to be considered in assessment of design adequacy. An example of this is the presence (or lack) of a magnetic field which would allow the existence of the radiation belts around the body for which appropriate electronic hardening/shielding would be required. For the missions considered in this study, neither Mars nor the moon has magnetic fields of comparable magnitude to the Earth's; therefore, earth orbiter hardware designs will more than suffice for both missions.

In this study, applicability of the design and system architecture of equipment from the Atmosphere Explorer Program and the Dynamics Explorer Program is assessed primarily from the point of view of mission adequacy to support the defined payloads and to provide the means for data retrieval. When specific instances arise where the orbited body influences the design or creates the requirement of extension to these designs, they are identified.

1.2 SPACECRAFT CONFIGURATIONS

Spacecraft configurations resulting from the study are shown in Figures 1-1 and 1-2, for the MGO and LGO, respectively, in their on-orbit configurations. Section 3 of this report summarizes the evolution of the equipment layouts which resulted in these configurations and also addresses the stowed, or launch configurations of each. With the information base used to address the sensor requirements, all viewing aspects for both the sensor detectors and their associated coolers (if applicable) have been accommodated. Similarly, the resulting configuration has allowed the achievement of mass properties of the spacecraft resulting in a "benign" design, namely that the system, which is a strong momentum biased system, is a principal axis spinner in failure modes (subsequent to burn and ejection of the orbit insertion motor). This feature significantly simplifies the nature of mission planning for anomalous events because the design is "self-surviving" without immediate or rapid intervention by the mission operations center.

1.3 STUDY EVOLUTION

The following paragraphs summarize the approach taken in the performance of the study, both from the point of view of existing design legacy and mission implications. This latter point addresses the sensitivity of the design to certain mission objectives and resulting implications for the design of hardware.

A number of parallel activities were initiated simultaneously to arrive at a spacecraft design which would accomplish the mission objectives. These included an initial field-of-view study to achieve the sensing requirements of the MGO payload. In parallel, preliminary hydrazine budgeting for the mission maneuvering was performed. This latter task resulted in "sizing" the spacecraft based on use of existing-design propellant tanks with the objective of achieving most of the mission maneuvering requirements. In the MGO case, an initial highly elliptical orbit is desired for instrument calibration. Maneuvering from this orbit to the final 350 km circular orbit, followed by the end-of-mission maneuver to a 525 km stable circular orbit (to preclude spacecraft re-entry to Mars) results in an initial elliptical orbit period of approximately 5.1 hours. While this is less than the desired 24 hour period, the relative "softness" of the time requirement was taken as the least stringent requirement of the mission maneuvering specifications. As the MGO maneuvering requirements are the more demanding of the two missions, they were used to physically size the spacecraft.

Given that sizing, the power system was then examined for ability to perform the mission. No attempt was made to optimize the available area for solar array of the body mounted array. A rather detailed analysis of the available array designs was performed, and a comparison to an AE- or DE-size spacecraft was made to develop a scaling in performance for the rather modest physical scale change in the spacecraft dimensions that resulted from the propellant sizing study addressed above. Similarly, the performance prediction technique

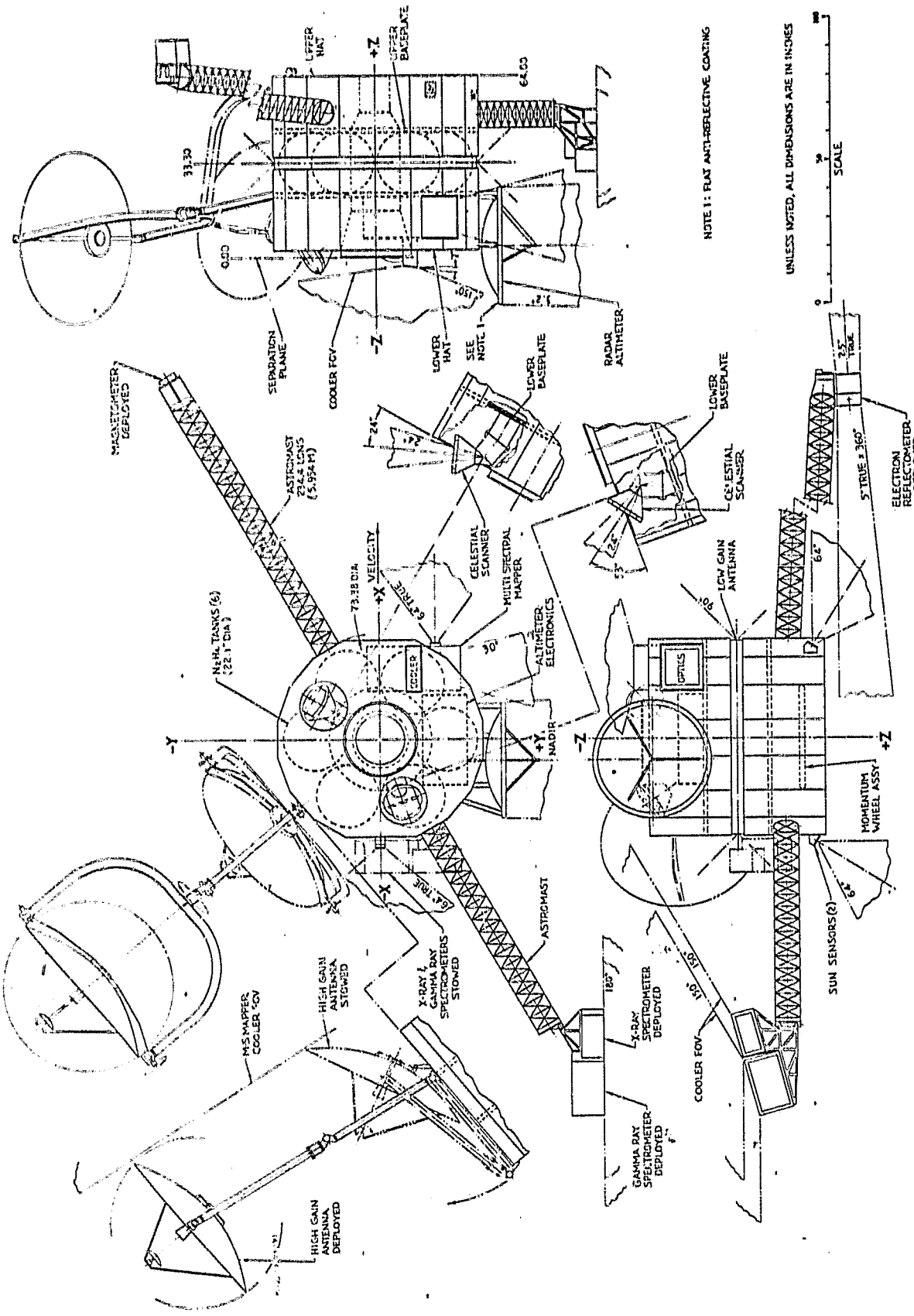

Figure 1-1. LGO Spacecraft On-Orbit Configuration

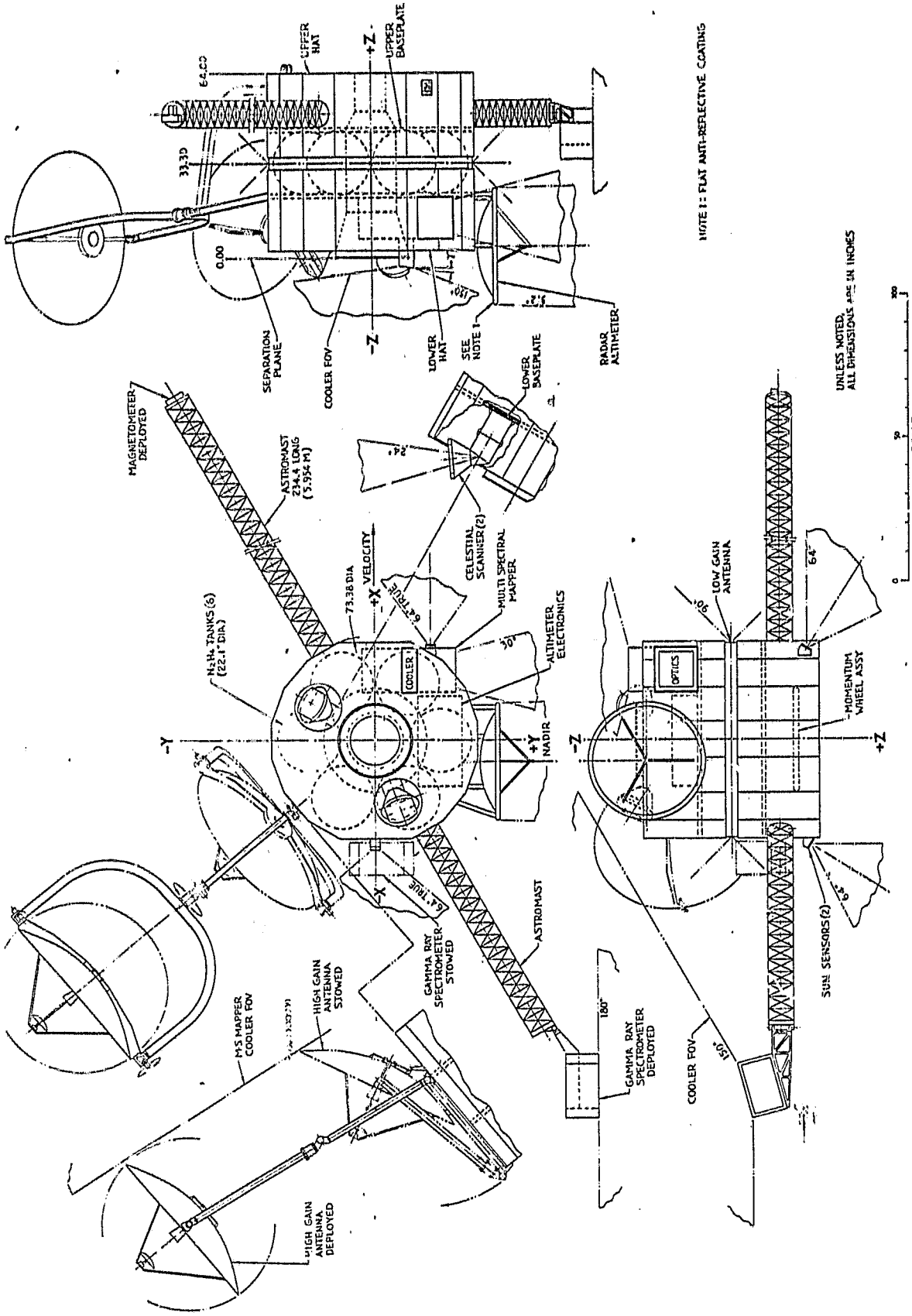

Figure 1-2. MGO Spacecraft On-Orbit Configuration

used to assess power performance (addressed in detail in Section 10 of this study) is extremely conservative in its "worst case" predictions. When compared to expected performance, use of the worst case technique results in a ratio of 1.6:1, expected case to worst case. The mission performance, which is stated in terms of full instrument operation for all orbits, is achieved in the expected case but not the worst case for the MGO mission. Adapting the same design to the LGO mission results in, as would be expected, ready accommodation of instrument operation due to the solar constant change between the two bodies to be orbited. In all of the analyses performed in this area, significant amounts of power margin were allocated, both for the instrument operation and for the data transmission period, again incorporating conservatism into the results reported. It should also be noted that, for the high inclination orbits for both the MGO and LGO missions, operation of "all the instruments all the time" results in a significant amount of "redundant data" in the polar regions. Thus, to ensure mission performance when cases of less than full orbit instrument operation are encountered, the time available for data gathering can be apportioned, by prudent planning of when, during a particular orbit sequence, the instrument payload is operated.

Having physically sized the spacecraft, a detailed mass budget was established and the maneuvering profile refined for the available amount of hydrazine. The mass budget was then used to select the orbit insertion motors and launch vehicles appropriate to the two missions. Also, as noted above, key parameters of the attitude determination and control system were sized, addressing both the cruise phase and the mission phase for the two spacecraft. In general, the MGO mission was the dominant system driver. However, in assessing the method of control for the in-orbit phase of the two missions for maintenance of the 1-rpm orientation, LGO became the driver.

Assessment of the IR spectrum of the moon, especially on the dark side, resulted in a departure from the bolometer-type horizon sensors used in both the AE and DE programs. An alternate system of sensing has been introduced and has been employed in both the MGO and LGO designs. This change is judged to be the largest departure from the design legacy of the heritage Atmosphere Explorer and Dynamics Explorer programs.

The communications requirements for both missions were addressed, on a parametric basis, in parallel with the above activities. The equipment selection was limited to known existing designs, with dependency on the use of high power amplifiers presently employed in on-going communications satellite programs at RCA. While elements of the communications subsystems are not derived from either AE or DE, their use and application to MGO and LGO requirements is not judged to be of significant impact to the system designs evolved during the study.

Application of both AE and DE thermal designs to the MGO and LGO missions was addressed during the study. Again, the MGO requirements became the driver. For the spacecraft design which evolved from the above trades, it was determined, to the first approximation, that direct application of the techniques used on both heritage programs results in a viable thermal design. Both the cruise phase and the mission phase were addressed. However, detailed analyses in this area, which were judged to be beyond the scope of the study, are required to refine the assessment of the thermal performance.

1.4 CONCLUSION

In summary, application of the designs and much of the hardware from the Atmosphere Explorer and Dynamics Explorer programs to the Mars Geoscience Orbiter and the Lunar Geoscience Orbiter missions has been examined and found to be compatible. The subsystems of the spacecraft which evolved during the course of the study have been assessed to varying levels of detail to establish credibility and/or identify limitations on the proposed missions should they be implemented using the design legacy afforded by the two heritage explorer designs. No fundamental problem which precludes mission performance using this technical approach was identified during the study.

SECTION 2.0
MGO/LGO SCIENCE ACCOMMODATIONS

SECTION 2.0
MGO/LGO SCIENCE ACCOMMODATIONS

2.1 THE INNER PLANETS - OVERVIEW

The importance of the study of the inner planets to our understanding of the Earth as a planet cannot be overemphasized. In order to provide a framework for understanding of the physical processes which shape the inner planets, it is critical to comprehend both their differences, which are striking, and their similarities, which may, in many ways, be quite subtle.

A current snapshot of the state of our knowledge reveals a relatively sophisticated understanding of the dynamics and composition of the atmosphere and surface of Venus, good enough to warrant the high resolution of the upcoming Venus Radar Mapper which will push our state of knowledge from phenomological observation to a basic understanding of the geological processes which occur on the planet. Likewise, the basic composition of the atmosphere is known, based on Pioneer Venus and Venera data, and the next step is a detailed, high accuracy measurement of relative isotopic composition which could be accomplished by a follow-on Venus probe.

The situation with respect to another member of the key inner planet trilogy, Mars, is quite different. The Viking mission provided detailed data on specific samples tested by the Lander to a level unequalled in the planetary program, save the Apollo mission. Likewise, the Viking orbiter provided an excellent cartographic understanding of the Martian surface. However, while the Viking data provides detail on certain points, it does not address major questions of surface composition and morphology (which requires a more detailed multi-spectral analysis) and provides only meager information on the atmosphere, ionosphere, magnetic field and solar wind interaction. The detailed data points of Viking, however, do provide an excellent basis for the design of the next mission, the MGO, and will provide a context for the interpretation of the MGO data that will greatly increase the scientific value of both missions.

The same premise holds with respect to the relationship of the LGO to the Apollo mission. The argument is made, why go back to the moon? Since we have lunar samples in the laboratory, what could we learn? This argument is best answered by analogy. Suppose our entire body of geological knowledge of the Earth were based on a few hundred pounds of rocks gathered near the Equator by a handful of localized missions. Certainly no one would argue that our knowledge of geology would be complete.

This analogy holds true almost verbatim when applied to the Moon. We have never explored the composition of the lunar polar areas, we do not know what the state of the volatile content near the poles is (if any), and our knowledge of lunar mineralogy is predicated only on very localized samples, which again, as the case with Viking and Mars, will provide a critical context for the interpretation of the LGO data.

It is also important to note that several of the key LGO science questions have significant bearing on the practical question of the use of lunar material as a potential source of resources for large space structures. Examples of this are the mineralogy and, more importantly, the volatiles inventory

questions. Both of these areas are key to the exploitation of raw materials and the feasibility of processing materials on the Moon for use in these structures. If materials processing on the Moon is feasible, it may prove to be the key to large space structures because delivery of material from the Moon has significant energetic advantages over delivery of material from the surface of the Earth.

2.2 BASIC MGO SCIENCE

In the context of our current state of understanding of the inner solar system, it becomes relatively straightforward to define the key areas which are prime candidates for study in the next Mars mission. High on the list of priorities are:

- Mars Geochemistry
- Mars Climatology
- Mars Aeronomy

These missions address key areas such as chemical and mineral composition of the planet, planetary weather and climate volatiles content, solar wind/planetary interaction and atmospheric evolution, all key areas to comparative planetology. The MGO (Mars Geoscience Orbiter) is the key area of study of this report; however, it is possible to combine several elements of each of these missions into a common mission while still maintaining, at minimum cost, the use of currently available spacecraft.

The major objectives of the MGO mission are fourfold. First, to understand the evolution and structure of the planet as a solid body it is necessary to understand the details of chemical and mineralogy composition and its variation over the entire planet. This will provide a basis for the study of Martian geology and structure on a global scale. Second, it is important to understand the surface features and morphology of Mars to understand the geologic evolution and crustal dynamics of the planet to try to infer its past history. Third, it is important to understand the details of the gravity field (and its gradients) of the planet to develop an understanding of the details of the structure of the planet. Finally, the intrinsic magnetic field (or lack thereof) of Mars is a key element not only for the study of the planet itself but it also provides a key for comparative planetology.

The basic MGO instrument complement addresses these questions directly. Other measurements, pertinent to the volatile content of the planet and atmosphere and seasonal variation, are provided directly by the gamma ray spectrometer. In fact, the gamma ray spectrometer and radar altimeter are also key instruments to the Mars Climatology Mission (MCO), which is basically structured to observe the atmosphere, as opposed to the MGO main objective of observing the planet as a solid body. This commonality among missions suggests the possibility of combining the MGO and the MCO to form the MCGO.

The basic payload of the MGO consists of the gamma ray spectrometer (GRS), the multi-spectral mapper (MSM), the magnetometer (MAG) and the radar altimeter (ALT). The primary function of the GRS is a chemical and mineralogical survey of the entire planet (hence the polar orbit). The GRS can also provide significant information about the planet's atmosphere. The purpose of the MSM is to get surface composition and morphology on a global basis, the ALT aids in this

objective by providing information on the gravitational aspects of the planet. The primary purpose of the MAG is for global magnetic field determination. A summary of the instruments and their basic physical accommodation requirements is presented in Tables 2-1 through 2-6.

One of the basic instruments carried by the MGO is the gamma ray spectrometer. Table 2-1 summarizes the key properties of the GRS. The major impact on the spacecraft is the fact that the GRS is boom mounted and it is desirable to perform a calibration, with boom extended, when the spacecraft is in its final on-orbit configuration (with orbit insertion motor gone). While it is, of course, impossible to provide a rigorous solution to this problem, good approximations are available by a cruise calibration (boom extended) or an initial highly elliptical orbit. Both of these alternatives are possible and have been considered.

Table 2-2 shows the basic accommodation requirements for the MSM. While there are no particular drivers to spacecraft design here, it is desirable, from a scientific point of view, to further tighten the attitude stability and knowledge criteria on the spacecraft. Depending on spacecraft choice this may or may not prove to be a significant problem.

Tables 2-3 and 2-4 show the accommodation requirements for the MAG and the ALT, respectively. No particular problems are associated with either.

2.3 BASIC LGO SCIENCE

Since the primary scientific objectives of the LGO are the same as those of MGO, minus, of course, those objectives that relate to the atmosphere, it is not surprising that the instrument complement is similar. The one difference is that in the lunar case, the complete lack of an atmosphere allows for observation of surface properties by means of x-rays and secondary electrons generated directly on the surface. In the MGO case, surface generated x-rays and secondary electrons are unable to penetrate even the tenuous atmosphere. Therefore, in the case of the LGO, all MGO instruments are retained and two additional instruments, the x-ray spectrometer (XRS) and electron reflectometer (ER) are added. The data from these complement and enhance the GRS and address the same science objectives. Tables 2-5 and 2-6 show the accommodation requirements for the XRS and ER, respectively. Again, in these instances, no particular problems are associated with either instrument.

2.4 NEW TECHNOLOGY DEVELOPMENT

As a baseline for the Pioneer class missions we have restricted the systems so as to require no new technology developments. This is absolutely essential for success given the schedule and cost constraints imposed by assumption. It is important to note that this assumption has, in no way, constrained the systems concept development or affected the mission science return since no mission-specific new technology requirements have been identified for any of the missions under consideration. Of course, normal next-generation state-of-the-art subsystem design updates will take advantage of applicable new technology developments. More importantly, several R&D areas could be of cost and/or performance benefit to the Pioneer class spacecraft and will be used if independently developed. For example, in the context of Mariner Mark II, a complete X-band system could be used which would eliminate the need for an S-band transponder.

TABLE 2-1. GRS INSTRUMENT PROPERTIES

• PRIMARY DATA	- Gamma ray pulse height spectra from the Martian/Lunar surface
• CALIBRATION	- Spectra obtained prior to mid- and post-boom deployment mid-course boom deployment required - Spectra should be obtained at various orientations with respect to the galactic background and at various levels of solar flare activity and periodically repeated as the mission progresses (special maneuvers may be desirable for this purpose)*
• CONSTRAINTS	- Passive cooler pointed at deep space - No strong EMI sources or susceptibility - No radioisotopes of any kind carried and/or used by the spacecraft or other instruments
• ATTITUDE CONTROL	- Control approximately $\pm$50 mrad ($\sim$ 2.9°) - Knowledge approximately $\pm$50 mrad ($\sim$ 2.9°) - Stability - Not specified (Note: The better and longer the nadir pointing can be held, the better the signal-to-noise ratio of a given pulse height spectra and therefore the more components which can be identified)
*NOTE: An on-board monitor such as an ionization chamber to monitor total dose of galactic/solar cosmic rays would be helpful.	

TABLE 2-2. MSM INSTRUMENT PROPERTIES

• PRIMARY DATA	- IR images (several bands) of the surface
• CALIBRATION	- Two reference targets, one reflective and one active thermal - Cruise calibration internal
• CONSTRAINTS	- Keep optics away from Sun - Cooler pointing at deep space required - No strong EMI sources or susceptibility - Thruster plume impingement excluded from optics/cooler - Covers are required
• ATTITUDE CONTROL	- Control ∿ ±30 mrad (1.73°) - Knowledge ∿ ±30 mrad (1.73°) - Stability ∿ 100 μrad/min (0.006°/min) - Nadir pointing

TABLE 2-3. MAG INSTRUMENT PROPERTIES

• PRIMARY DATA	- Magnetic field measurements near Mars or the Moon (to determine the magnetization state of the body and the nature of the body/solar wind interaction)
• CALIBRATION	- Internal, no spacecraft impact
• CONSTRAINTS	- Boom mounted - No S/C magnetic fields (AC or DC) > 0.01 gamma at sensor - EMI susceptibility concerns
• ATTITUDE CONTROL	- Control - N/A - Knowledge ∿ ±20 mrad (1.2°) - Stability - N/A

TABLE 2-4. ALT INSTRUMENT PROPERTIES

• PRIMARY DATA	- Surface roughness/height variations
• CALIBRATION	- Internal, no spacecraft impact
• CONSTRAINTS	- Possible EMI source
• ATTITUDE CONTROL	- Control ∿ ±30 mrad (1.73°) - Knowledge ∿ ±30 mrad (1.73°) - Stability ∿ ±100 μrad/min (0.006°/min) - Nadir pointing
NOTE: Replacing the radar alitmeter by a laser altimeter is an option that has yet to be fully assessed; however, to the first order, no substantial additional problems are apparent.	

TABLE 2-5. XRS INSTRUMENT PROPERTIES

• PRIMARY DATA	- X-ray pulse height spectra from the lunar surface
• CALIBRATION	- Reference target solar pointing, continuously monitored
• CONSTRAINTS	- Passive cooler pointed at deep space, reference target solar pointing - No strong EMI sources or susceptibility - Possibly boom, possibly body mounted
• ATTITUDE CONTROL	- Control ∿ ±50 mrad (2.9°) - Knowledge ∿ ±50 mrad (2.9°) - Stability ∿ ±100 μrad/min (0.006°/min) - Nadir pointing (see note on GRS)

TABLE 2-6. ER INSTRUMENT PROPERTIES

• PRIMARY DATA	-	Secondary electrons from the lunar surface, energy analysis
• CLAIBRATIONS	-	All internal, no significant spacecraft impact
• CONSTRAINTS	-	Low spacecraft magnetic field
	-	Must be flown with magnetometer (preferential geometry on boom)
	-	Spacecraft "bare area" (conducting surface/ insulating surface) constraints
	-	Nadir and zenith viewing required
• ATTITUDE CONTROL	-	Control $\sim \pm 30$ mrad (1.73°)
	-	Knowledge $\sim \pm 30$ mrad (1.73°)
	-	Stability $\sim \pm 100$ μrad (0.006°/min)

SECTION 3.0
INSTRUMENT ACCOMMODATION

SECTION 3.0
INSTRUMENT ACCOMMODATION

The instrument complement for the two missions, tabulated in Table 1-1, have the characteristics and accommodation requirements as listed in Tables 3-1 through 3-7 for:

Gamma Ray Spectrometer; Table 3-1
X-ray Spectrometer; Table 3-2
Multi-Spectral Mapper; Table 3-3
Magnetometer; Table 3-4
Radar Altimeter; Table 3-5
Electron Reflectrometer; Table 3-6
Laser Altimeter; Table 3-7 (alternate instrument)

3.1 MGO FIELDS-OF-VIEW

The initial activities in assessing the fields-of-view of the instruments commenced with a spacecraft the same physical size as an Atmosphere Explorer spacecraft or a Dynamics Explorer spacecraft. As shown in Figure 3-1, the radar altimeter and the multi-spectral mapper quickly erode the design, indicating the need for mounting the mapper externally, resulting in major surface blockages from the square antenna sensor of the radar altimeter. Additionally, it became evident that the system required use of six 22.1 inch diameter propellant tanks, resulting from a parallel activity to size the required hydrazine storage (the hydrazine storage technique is addressed in Section 5). Accordingly, the system was scaled up by a factor of 24:17.5 in each dimension. The scaling factor was derived as follows; the AE spacecraft design employed a six tank storage system with the six tanks (16.5 inch diameter sphere equivalents) in the center toroid of the spacecraft, between the two baseplates. The separation distance between the baseplates in the AE design is 17.5 inches to accommodate the 16.5 inch tanks. Increasing that dimension to 24 inches to accommodate the 22.1 inch diameter tanks and scaling all other dimensions of the structure by the same ratio to retain the basic load paths and structure design, as well as retaining the basic analytically proven loads, resulted in a physical configuration as shown in Figure 3-2. Since all dimensions were similarly scaled, including all section thicknesses, and all relative structure relationships were retained, it is claimed that the basic structure design has been retained. Further, as evidenced in the mass summaries of Section 6, where the structure masses were scaled up by a factor of $(24/17.5)^3$, it is claimed that this results in a conservative design as, for non-critical load path structure areas, many elements may require only scaling in two dimensions rather than all three. Note that in Figure 3-2, the decision to abandon the bolometer horizon sensors had not yet been made, as the momentum wheel mounted scanning mirror is still shown in the system.

At this time, it was evident that the square radar altimeter antenna was a major factor in instrument accommodation; after consultation with JPL, it was determined that a 1 meter diameter circular dish could be employed instead. It was also determined that the volume representing the radar altimeter could be packaged separately from the antenna and housed inside the spacecraft, so long as it was in close proximity to the antenna.

TABLE 3-1. GAMMA RAY SPECTROMETER CHARACTERISTICS

Heritage	Apollo 15, 16 plus developments
Mass (incl. Electronics & Cooler)(kg)	12
Power (W)	10
Size (cm)	29 x 32 x 50
Mounting	Full instrument on boom, @ >1 S/C dia. Prefer extendable rather than articulated
Axis Orientation(s)	Detector: Nadir Cooler: Space
Field-of-View	Detector: 180° (2 π st) Cooler: ∿150°
Exclusion Angle (View)	180°
Cooling	Passive Radiator 100 - 110K
S/C Environment Restrictions	No radioisotopes, (e.g., RTG's thoriated alloys, potassium paints, etc.). No strong magnetic field (>1 γ)
Environment Output	Some weak magnetic field from photomultiplier tubes
Mechanisms, etc.	Cooler shield
Calibrations	1. At apoapsis > 10 planetary radii 2. Before, mid, and after boom extension 3. During cruise also (All nadir pointing)
Modes	Single (on-off)
Duty Cycle	Continuous, day and night, full mission time
Data Rate(s) (kbps)	1.5
Data Volume (bits/day)	1.3 x 108
Pointing Accuracy (±mrad)	∿50
Pointing Knowledge (1 mrad)	∿50
Pointing Stability (μrad/min.)	--
Typical Proponent(s)	Al Metzger, JPL; Jim Arnold, U.C. San Diego

TABLE 3-2. X-RAY SPECTROMETER CHARACTERISTICS

Heritage	Apollo 15, 16
Mass (incl. Elect. & Cooler) (kg)	11
Power (W)	10
Size (cm)	20 x 20 x 40
Mounting	Bus or boom (same requirement as gamma ray spectrometer. Maybe can share same boom)
Axis Orientation(s)	Detector: Nadir Sun Monitor: Sun Cooler: Space
Field of View	Detector: ∿180° Cooler: ∿150°
Exclusion Angle (View)	Collimated, 20°
Cooling	Passive radiator ∿170°K
S/C Environment Restrictions	No outstanding sensitivities
Environment Output	None
Mechanisms, etc.	Cooler shield
Calibrations Required	Reference target sun illuminated, with separate detector, continuous operation
Modes	Single, (on-off)
Duty Cycle	Collect data on daylight side only
Data Rate(s) (kbps)	0.3
Data Volume	2.6×10^7
Pointing Accuracy (± mrad)	∿30
Pointing Knowledge (± mrad)	∿30
Pointing Stability (μrad/min.)	100
Typical Proponent(s)	Al Metzger, JPL; Jack Trombka, Goddard

TABLE 3-3. MULTISPECTRAL MAPPER CHARACTERISTICS

Heritage	Galileo (NIMS)
Mass (Incl. Elect. & Cooler) (kg)	17
Power (W)	8 average, 12 peak, 120 transient
Size (cm)	Optics: 83 x 37 x 39; Electr: 20 x 25 x 13
Mounting	Bus
Axis Orientation(s)	Optic: Nadir Cooler: Space
Field of View	Optic: 4.1 x 0.2 mrad Cooler: ∿150°
Exclusion Angle (View)	∿30°
Cooling	Passive radiator
S/C Environment Restrictions	Sensitive to gas and particulate contaminants on optics and thermal control surfaces (instrument is a 130°K cold trap)
Environment Output	None
Mechanisms, etc.	Optic drives, covers (2), purge heaters
Calibrations Required	Periodic view of two reference targets, one reflective, one active thermal
Modes	Several internal
Duty Cycle	Collect data on daylight side of planet only, until full surface mapped
Data Rate(s) (kbps)	1.5, 3, 6, 12 commandable
Data Volume (bits/day)	UP to 0.5×10^9
Pointing Accuracy (± mrad)	∿3
Pointing Knowledge (± mrad)	∿3
Pointing Stability (μrad/min.)	∿10
Typical Proponent(s)	Tom McCord, Univ. Hawaii; Bob Carlson, JPL

TABLE 3-4. MAGNETOMETER CHARACTERISTICS

Heritage	Voyager, Pioneers, ISPM
Mass (Incl. Elect. & Cooler) (kg)	Sensor(s) 1; Electronics 2
Power (W)	
Size (cm)	Sensor: 8 x 5 x 5; Electr: 22 x 11 x 15
Mounting	Sensor(s) on boom @ 3 S/C diameter Electronics on bus
Axis Orientation(s)	Orthogonal Sensors
Field of View	NA
Exclusion Angle (View)	NA
Cooling	None
S/C Environment Restrictions	No S/C Magnetic fields > 0.01 gamma at sensor location
Environment Output	Radiates weak sweep magnetic fields ($\sim$100γ) in sensor coil
Mechanisms, etc.	No moving parts
Calibrations Required	Internal, on command
Modes	Several internal
Duty Cycle	Continuous
Data Rate(s) (kbps)	0.4
Data Volume (bits/day)	3.2×10^7
Pointing Accuracy (μ mrad)	-
Pointing Knowledge ($\pm$ mrad)	$\sim$20
Pointing Stability (μrad/min.)	-
Typical Proponent(s)	Chuck Sonnett, Univ. Arizona; Chris Russell, UCLA

TABLE 3-5. RADAR ALTIMETER CHARACTERISTICS

Heritage	Pioneer Venus (ORAD)
Mass (incl. Elect. & Cooler)(kg)	Electr: 8; Antenna: 2
Power (W)	18
Size (cm)	Antenna: 120 x 120 x 5*; Electr: 120 x 60 x 10
Mounting	Bus
Axis Orientation(s)	Antenna: Nadir
Field of View	2°
Exclusion Angle (View)	30°
Cooling	Passive Thermal Control
S/C Environment Restrictions	None
Environment Output	None other than radar beam
Mechanisms, etc.	No moving parts (except possible deployment of antenna)
Calibrations Required	Internal, automatic or on command
Modes	Several antenna
Duty Cycle	Continuous until full surface mapped
Data Rate(s) (kbps)	0.6
Data Volume (bits/day)	5.2×10^7
Pointing Accuracy (± mrad)	∿30
Pointing Knowledge (± mrad)	∿30
Pointing Stability (μrad/min.)	∿100
Typical Proponent(s)	Steve Saunders, JPL; Charles Elachi, JPL

*Changed to 100 cm circular antenna during course of study

TABLE 3-6. ELECTRON REFLECTOMETER CHARACTERISTICS

Heritage	Apollo 16 subsatellite charged particle instrument
Mass (incl. Elect. & Cooler)(kg)	5
Power (W)	5
Size (cm)	20 x 20 x 20
Mounting	Boom preferred. Bus OK but away from non-conducting S/C surfaces
Axis Orientation(s)	Nadir/zenith plane
Field-of-View	5° fan x 360° revolution in nadir/zenith
Exclusion Angle (View)	Same as field-of-view
Cooling	None
S/C Environment Restrictions	1. Must be flown with magnetometer 2. S/C magnetic fields to satisfy magnetometer 3. Sensitive to S/C electrostatic charging
Environment Output	None outside instrument package
Mechanisms, etc.	No moving parts
Calibrations Required	Internal
Modes	Several Internal
Duty Cycle	Continuous
Data Rates(s) (kbps)	0.3
Data Volume (bits/day)	2.6×10^7
Pointing Accuracy (± mrad)	∿30
Pointing Knowledge (± mrad)	∿30
Pointing Stability (μrad/min.)	∿100
Typical Proponent(s)	Kinsey Anderson, U.C. Berkeley; Bob Lin, U.C. Berkeley

*Understood to be parallel (or roughly parallel to orbit plane)

TABLE 3-7. LASER ALTIMETER CHARACTERISTICS

Heritage	Apollo 15-17, plus developments
Mass (incl. Elect. & Cooler)(kg)	∿10
Power (W)	∿18
Size (cm)	40 x 20 x 20
Mounting	Bus
Axis Orientation(s)	Nadir
Field-of-View	5 mrad
Exclusion Angle (View)	30°
Cooling	Passive thermal control
S/C Environment Restrictions	None
Environment Output	None other than light beam
Mechanisms, etc.	No moving parts
Calibrations Required	Internal
Modes	Single (on-off)
Duty Cycle	Continuous until full surface mapped
Data Rate(s) (kbps)	∿10
Data Volume (bits/day)	$\sim 4 \times 10^8$
Pointing Accuracy (± mrad)	∿3
Pointing Knowledge (± mrad)	∿3
Pointing Stability (μrad/min.)	∿10
Typical Proponent	Mike Kobrick, JPL; Charles Elachi, JPL

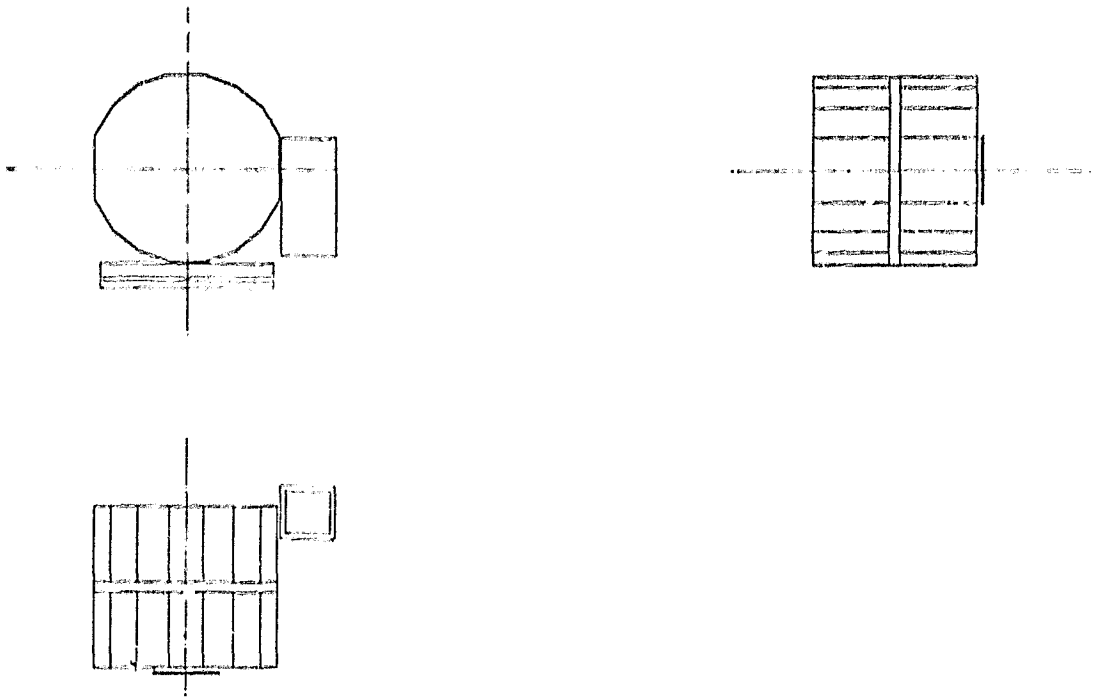

Figure 3-1. Initial MGO Configuration Using AE/DE Size Spacecraft

With these revisions, the field-of-view studies were continued on the MGO spacecraft using the scaled up structure. (Herein, this size spacecraft is referred to as "big bird" while the original AE/DE size spacecraft is referred to as "little bird.")

The resulting spacecraft configuration for the MGO is shown in Figure 3-3. The following comments address the intrument accommodation requirements.

- The booms used to extend the gamma ray spectrometer and the magnetometer are astromasts in the identical application as that of the DE program for its magnetometers and plasma wave instruments. The astromast length was selected to achieve the "greater than one spacecraft diameter separation" requirement.

- The hinge technique for the gamma ray spectrometer to achieve the desired field-of-view orientation relative to nadir and to allow for a stowed configuration; wherein a "hard point" release mechanism can be found to carry launch loads directly to the spacecraft structure via the upper baseplate identical to that used for the large plasma wave instrument antenna assembly of the DE program.

- While existing astromasts can be deployed and retracted, the cruise calibration requirement has been understood to be in the stowed mode to preclude a significant design of a mechanism to re-lock it, in the stowed mode, prior to orbit insertion motor firing.

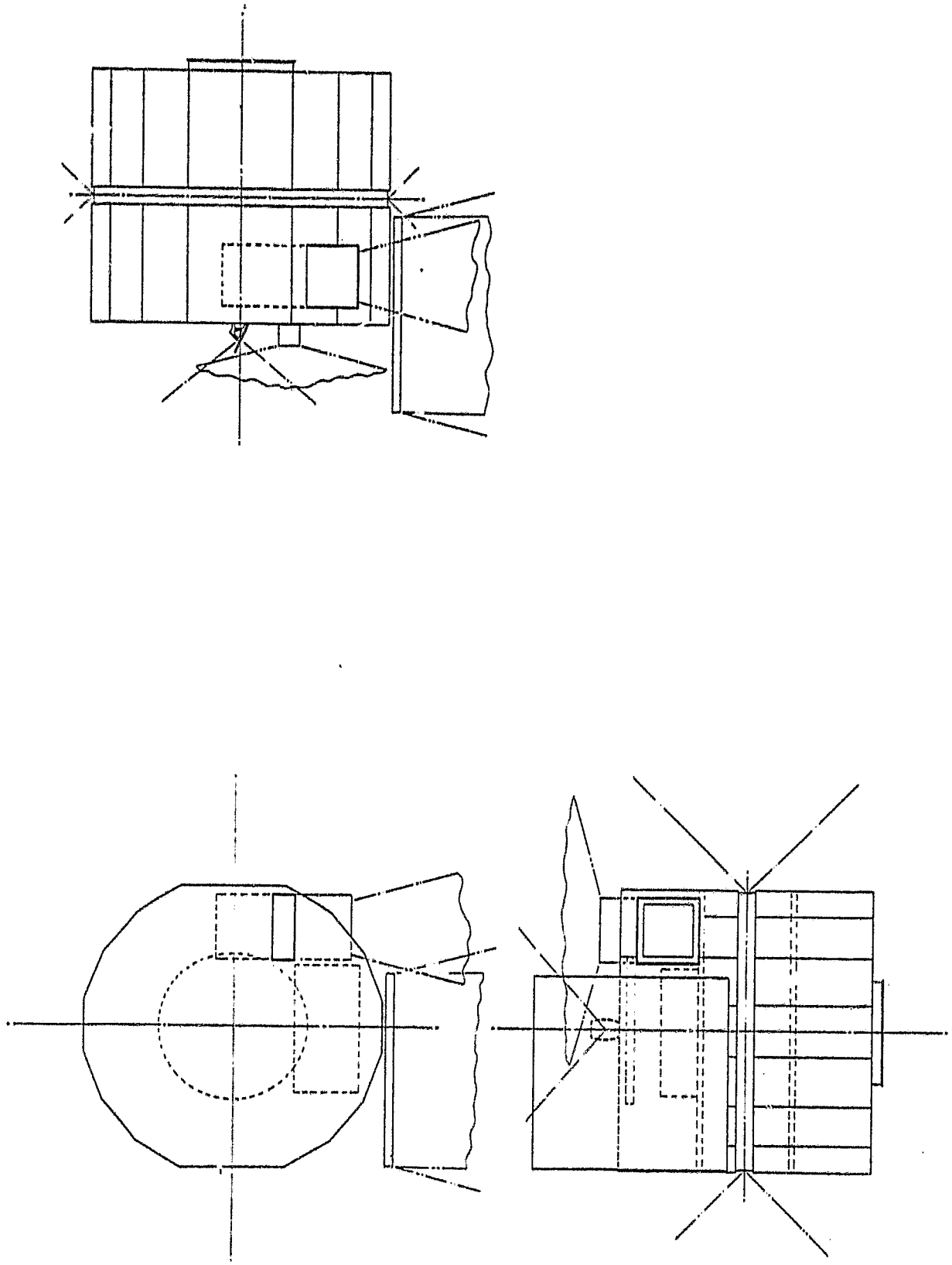

Figure 3-2. Initial MGO Configuration Using Scaled Up AE/DE Spacecraft

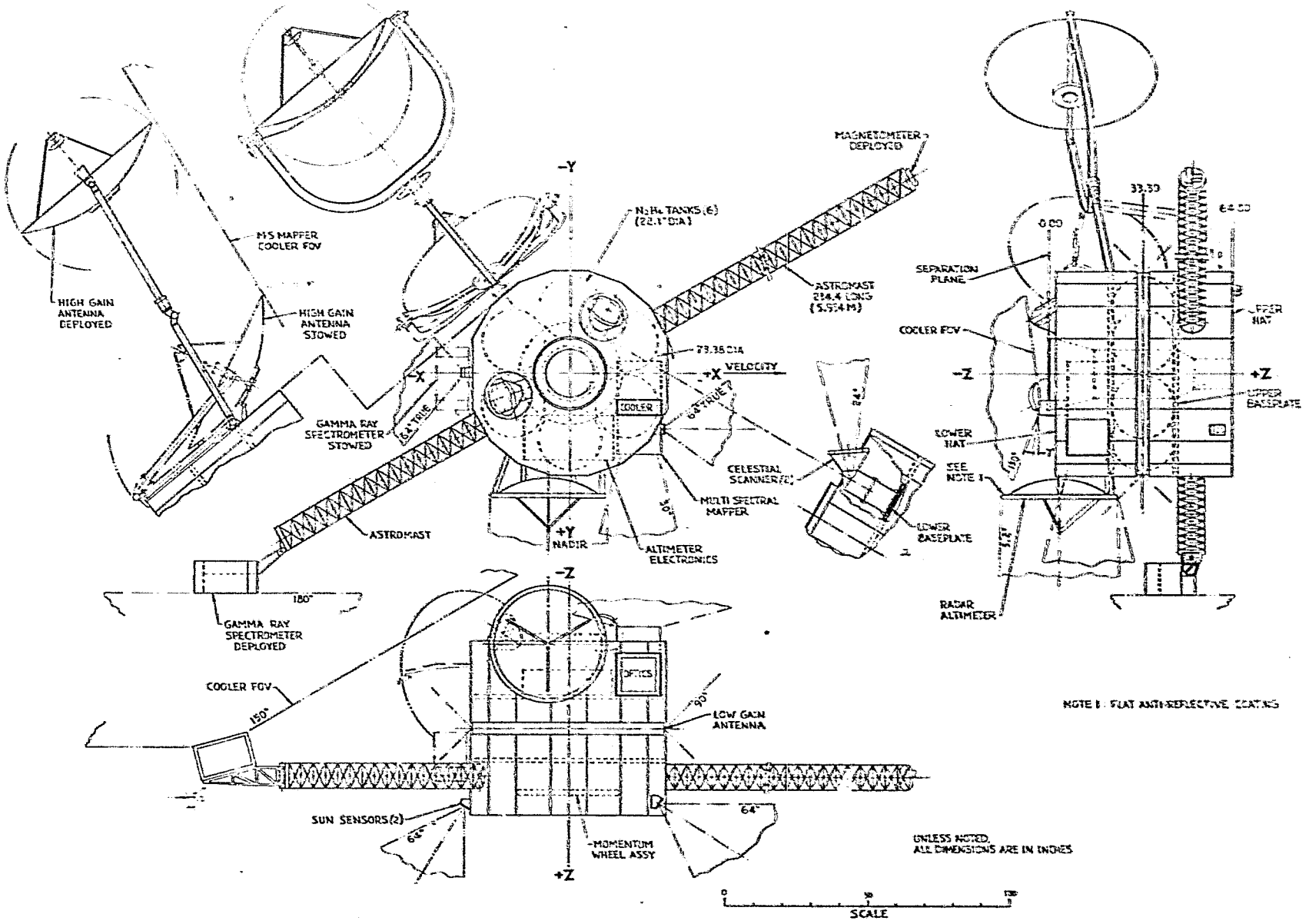

Figure 3-3. MGO Spacecraft On-Orbit Configuration

- The initial apoapsis altitude achieved for the on-orbit calibration is approximately 2 Mars radii above the surface as compared to the required 10 planetary radii, based on the hydrazine budgeting as described in Section 4.

- The calibration requirement at mid-deployment can be achieved as, in fact, the instrument can be operated throughout the deployment. However, the nature of the astromast during deployment is to "unwind" in spiral fashion about its axis. Thus, the possibility exists of stopping during the deployment with the cooler field-of-view facing Sunward. It is understood that the cooler shield will prevent damage to the instrument during this deployment sequence. Finally, it should also be noted that in the partially deployed (or partially retracted) state, the astromast does not display the same structureal rigidity as in the fully deployed state. Thus the pointing accuracy and knowledge would probably not be met given such a partially deployed state.

- The magnetometer detector has been mounted flush on the end of the astromast. If there is a requirement to orient the detectors relative to the spacecraft coordinates, a clocking plate (not shown) can be employed in like manner to those used in the DE design.

- Assuming comparable electromagnetic behavior of this spacecraft to the DE spacecraft, there is no problem foreseen in achieving the magnetometer required magnetic background of 0.01 gamma at the sensor.

- Both the radar altimeter and the multi-spectral mapper have been mounted on the lower baseplate which is closer to the end of the spacecraft that always faces the anti-Sun hemisphere.

- While not specifically characterized in the instrument data sheets, the cooler of the multispectral mapper is understood to be roughly of the dimensions and location shown. Note that the cooler field-of-view has been "shaped" with a clocking angle in the cooler aperture to offset the 150° field-of-view by 7° to clear the edge of the radar altimeter antenna. Also, the location and extension of the celestial sensors is below the cooler field-of-view.

- The high gain antenna, in both the stowed and deployed configurations, is positioned to be outside the field-of-view of the mapper-cooler field-of-view.

- The high gain antenna, in the deployed condition, is shown with its boom extended at an angle out of the x-y coordinate plane of the spacecraft. This allows for a controlled inertia cross product to permit active nutation damping in a manner identical to that performed on the DE-B spacecraft.

- The rotation yoke assembly shown for the high gain antenna was selected to support the active nutation damping concept as it results in rotation of the antenna about an axis through its center of mass, thereby maintaining the aforementioned controlled inertia cross product.

- While there is no interference between the multi-spectral mapper cooler field-of-view and the radar altimeter, design practices would include

the use of flat, anti-reflective coatings on surfaces facing the cooler fields-of-view as called out in Note 1 of Figure 3-3.

- In both the stowed and deployed configurations, both of the two axis sun sensors and the two celestial sensors have unobstructed fields-of-view.

- As shown, the low gain belt antenna is a direct design repeat of the type of antenna used on the Atmosphere Explorer spacecraft. The 90° pattern shown is typical to indicate the nature of the toroidal pattern generated by such an antenna.

3.2 LGO FIELDS-OF-VIEW

Having addressed the fields-of-view for the MGO spacecraft, the additional instrument complement for the LGO mission was addressed. The approach taken was to retain, to the greatest degree possible, the same layout for the common instruments, thereby making MGO fields-of-view essentially a subset of the LGO configuration. The resulting design is shown in Figure 3-4. As shown, the multi-spectral mapper, radar altimeter, gamma ray spectrometer, magnetometer, sun sensors, and celestial sensors have been retained from their MGO locations. The following observations apply to the inclusion of the additional LGO instruments:

- The x-ray spectrometer has been co-located on the astromast with the gamma ray spectrometer. The comments dealing with the relative orientation of the MGO gamma ray spectrometer cooler and detector during the astromast deployment sequence apply equally to this instrument.

- The magnetometer astromast mounting has been canted slightly to deploy the combined magnetometer and electron reflectometer to an angle where the electron reflectometer toroidal fan beam senses a field-of-view parallel to the top surface of the spacecraft. This results in a 360° swept fan which is not quite parallel to the orbit plane, with the plane of the boresight of the fan intercepting the orbit plane at an angle of 2.5°.

- It is unclear from the data available whether the magnetometer and electron reflectometer can be co-located on a common astromast in terms of mutual magnetic compatibility. If the instruments pose no electromagnetic contamination problems to each other and if the modest offset from the orbit plane of the instrument boresight is acceptable, then the configuration shown in Figure 3-4 accommodates their requirements.

- Two alternate configurations for accommodation of their electron reflectometer are shown in Figure 3-5. If co-location of the reflectometer and magnetometer is unacceptable, utilization of a third, short astromast, aligned with the spin axis of the spacecraft, can position the instrument away from the spacecraft body, with the fan beam boresight axis plane of revolution parallel to the plane of the orbit, shown as Alternate 1 of Figure 3-5. Conversely, if the two instruments can be co-located and the angle of the boresight plane to the orbit axis is not critcal, then the magnetometer mast can be erected co-linearly with the axis of the spectrometer mast with a 5.2°

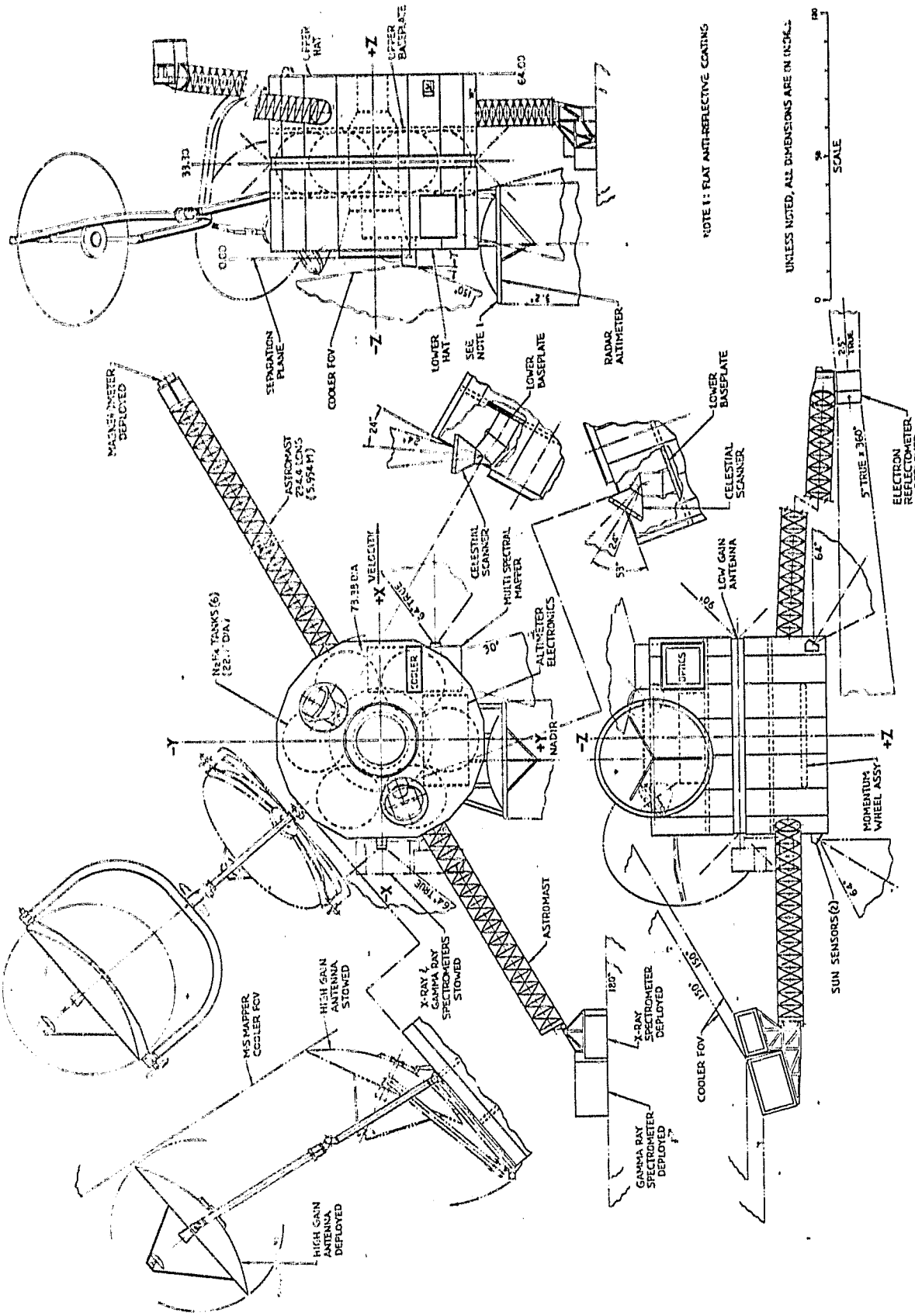

Figure 3-4. LGO Spacecraft On-Orbit Configuration

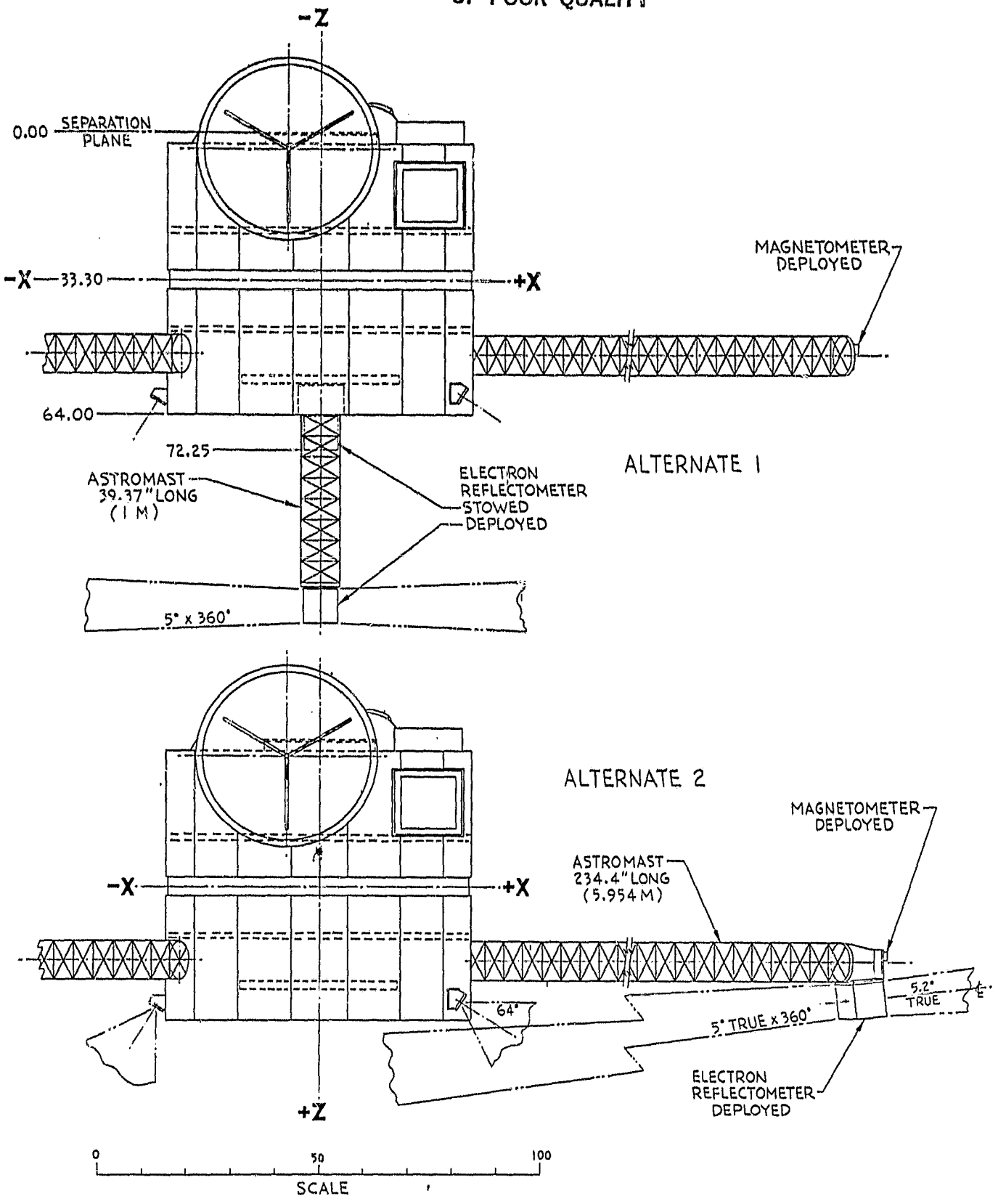

Figure 3-5. LGO Spacecraft Alternate Configuration

offset of the beam. This allows the fan beam to "miss" the spacecraft as shown in alternate 2 of the figure.

- Referring back to Figure 3-4, it can be seen that the mounting angle for the two celestial sensors has been changed for the LGO design from that of the MGO by introducing unique angles to their mounting brackets. This has been provided for a problem unique to the LGO mission. As shown in Figure 3-6, there are conditions during the mission life of the LGO spacecraft when the field-of-view of the celestial sensors, while looking into the anti-Sun hemisphere, will, during one rotation of the spacecraft, scan across the sunlit surface of the Earth. While this condition will not permanently degrade the sensor, a question remains as to whether the sensor can recover its operating response during the remainder of the revolution enough to allow for satisfactory data gathering. Accordingly, the fields-of-view of the two sensor's have been offset from each other with a "guard band" of 5° between the edges of the fields-of-view of the sensors. Thus, when one sensor's field-of-view can encounter the Earth, the other cannot. Since the Earth is approximately 2° wide as viewed from the Moon, the 5° guard band precludes all conditions for which the Earth renders both sensors inoperative at the same time. This offset also results in the edge of the field-of-view of the high angle sensor "missing" the large orbital injection motor (OIM) protrusion in the cruise configuration.

- While the power analyses of the LGO addressed in Section 10 of this report address operation of the spacecraft with and without the high gain antenna, all LGO field-of-view studies have included it to assure accommodation of the "worst case."

3.3 LAUNCH CONFIGURATIONS

Our having arrived at acceptable field-of-view accommodation, the next question addressed was the launch configuration. For this study, the three orbit insertion motor candidates identified in the mission analysis for the MGO mission were considered. In addition to delineating the MGO cruise phase configuration, specific attention was paid to the separation clamp hardware, with the objective being to achieve a configuration which utilized existing clamps rather than imply the additional programmatic costs of a new clamp development program. The configurations achieved are shown in Figures 3-7, 3-8 and 3-9 for the Star 30C, Star 37F and Star 37S OIMs, respectively. (The DMSP Block 5D clamp is an existing design taken from the on-going Defense Meteorological Satellite Program at RCA with the USAF).

3.4 ALTERNATE INSTRUMENT ACCOMMODATION

The physical characteristics of the alternate instrument candidate, namely the laser altimeter, are such that, for the data available, no major problems in accommodation (in lieu of the radar altimeter) are foreseen. Referring to Figures 3-3 and 3-4, if the large radar antenna and its associated electronics are removed, ample space is available for the mounting of the laser altimeter. The radar altimeter location is near the anti-Sun end of the spacecraft. In like manner to the technique used to accommodate the multi-spectral mapper cooler, the cooler for the laser altimeter can be accommodated. While no cooler field-of-view specifications have been identified, it is reasonable to assume a 150° requirement similar to the other detector cooler requirements in the instrument complement.

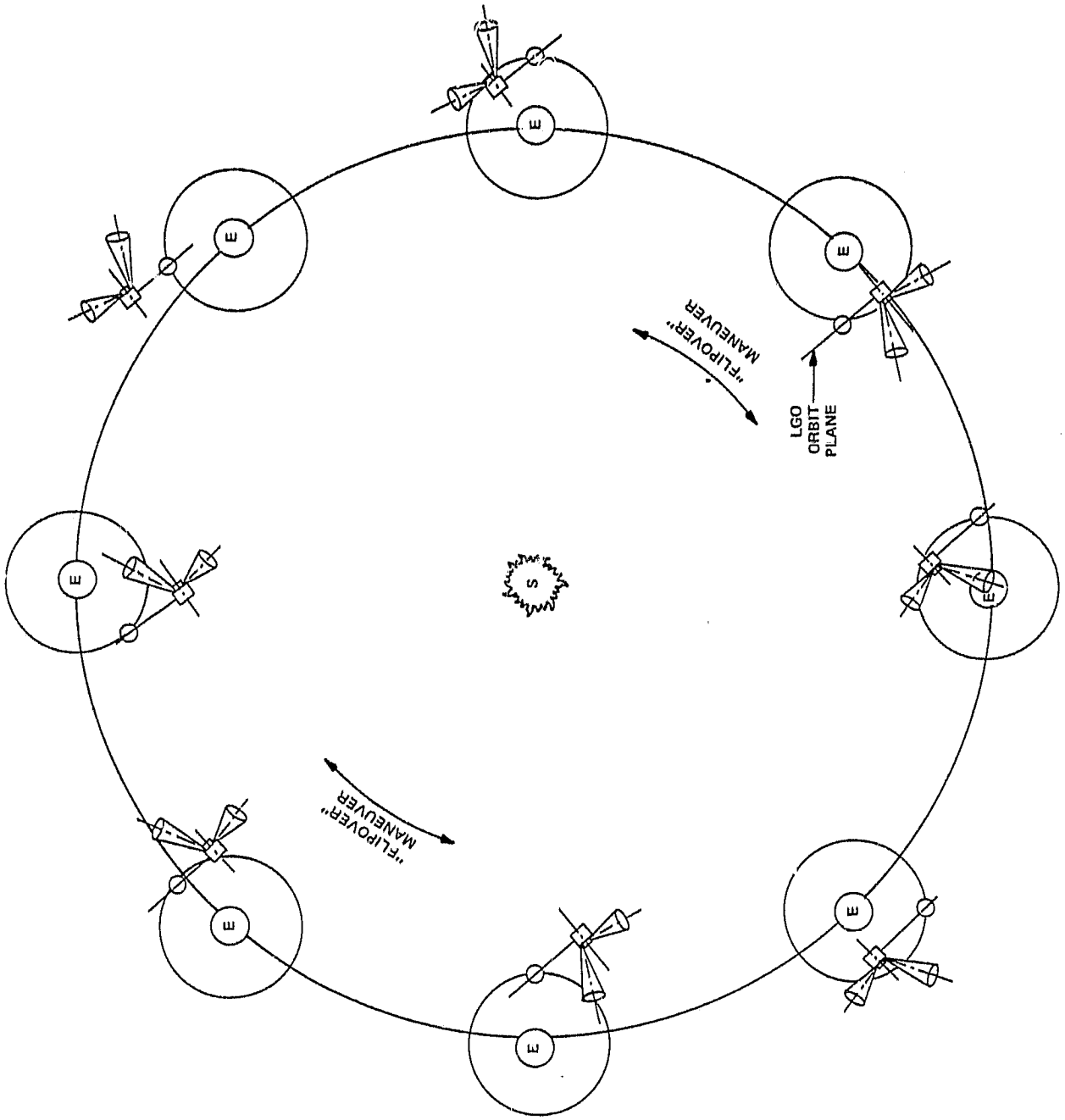

Figure 3-6. LGO Thermal Orientation and Star Sensor Configuration

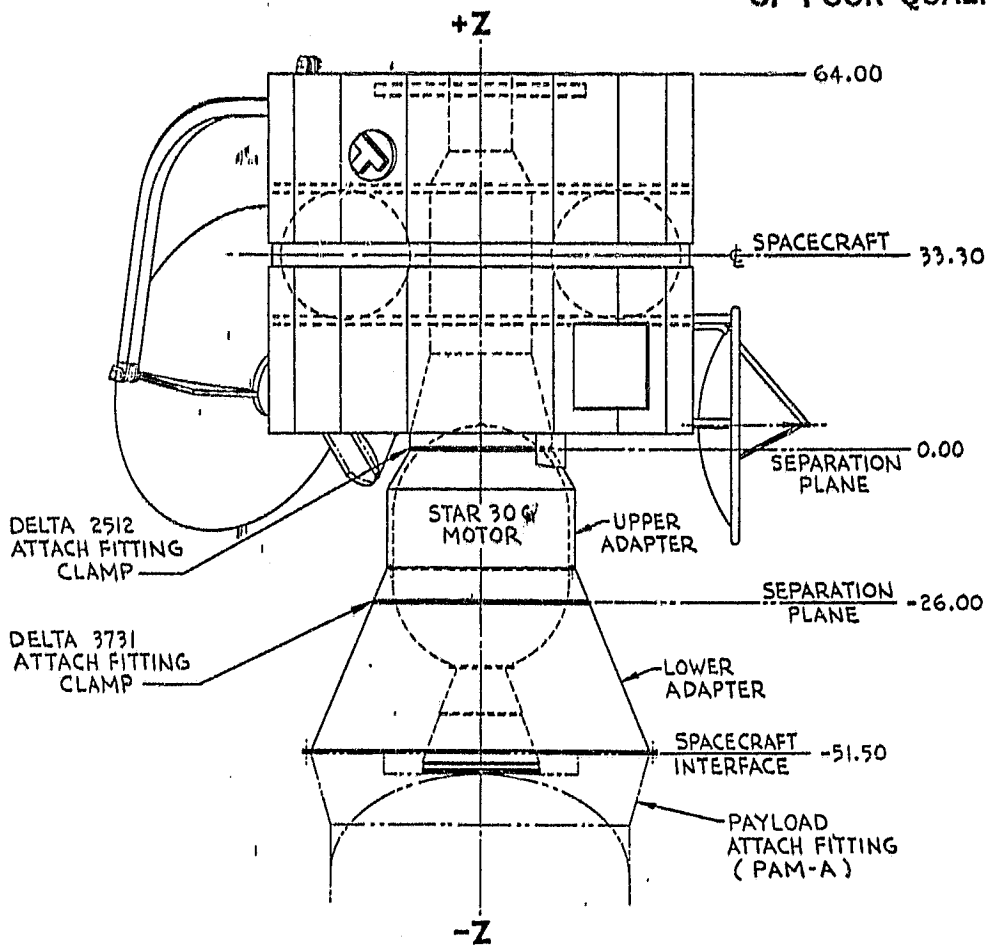

Figure 3-7. MGO-Star 30C Launch Configuration

Similarly, the field-of-view of the sensor (and its aperture) falls inside the radar altimeter aperture and beam width such that the same region may be equally applied for the laser altimeter. As can also be seen from Figures 3-3 and 3-4, the 30° exclusion angle can be readily accommodated using the radar altimeter mounting location; the closest object being the spectrometer(s) on their astromast which instruments are well outside the required exclusion angle.

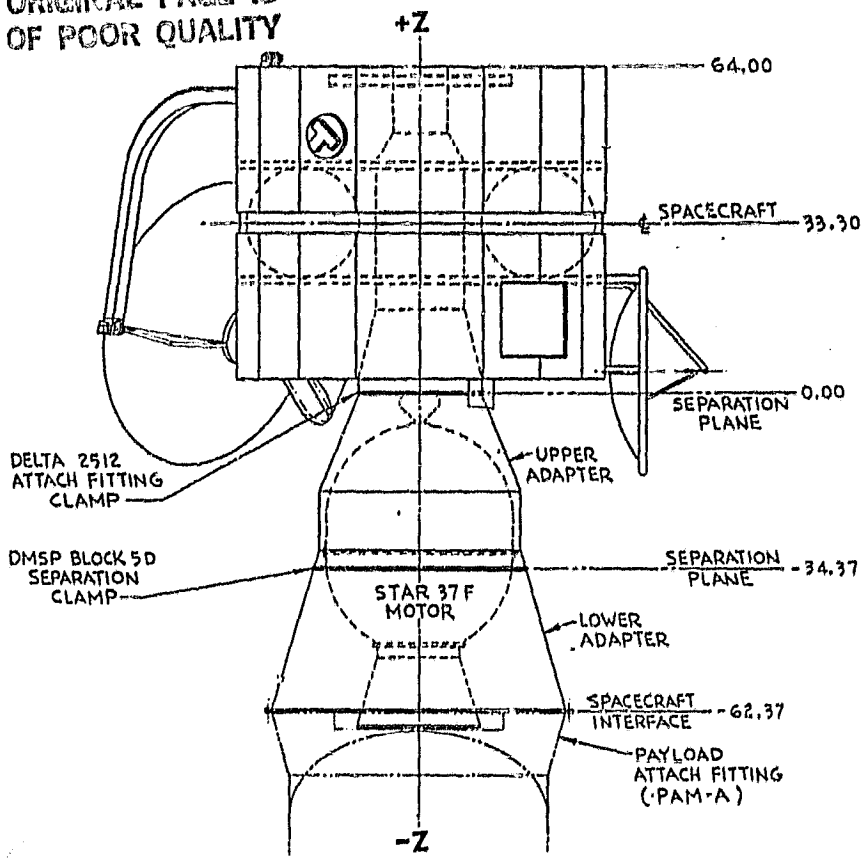

Figure 3-8. MGO-Star 37F Launch Configuration

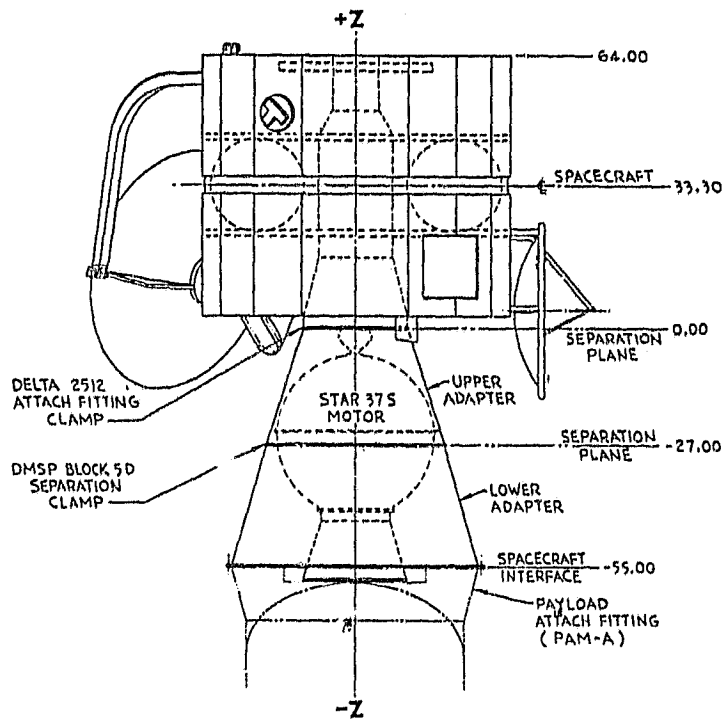

Figure 3-9. MGO-Star 37S Launch Configuration

SECTION 4.0
MISSION ANALYSIS

SECTION 4.0
MISSION ANALYSIS

4.1 BACKGROUND

The MGO and LGO missions will be second-phase explorations of Mars and the Moon, Mars having been visited first through the exploratory Viking and Mariner missions and the Moon through the Apollo program. The goal of these missions is the global mapping of geochemical and geophysical features, with an eye to the future exploitation of the resources of these bodies. This aim will be best accomplished by using polar (or near polar) orbiting spacecraft and, in later missions, also entry bodies and landers. Accordingly the subjects of this study are the development of a single basic spacecraft suited to making global remote sensing surveys of either Mars or the Moon, with only minor differences between versions for each specific mission, and the deployment and operation of this spacecraft in a nominally polar orbit for one year. Whenever possible, features of the mission design will aid in the minimization of the total cost of achieving the specified goals. The mission design described in this section reflects these criteria in its use of the Dynamics Explorer (DE) design concept as the basis of the development of a compliant spacecraft design.

While commonality is emphasized and achievable for the spacecraft, the MGO and LGO missions are treated independently herein because of the respective differences in mission profiles, time lines and ΔV requirements. This independent-treatment approach does not compromise the spacecraft commonality but, as indicated in other sections of this report, further establishes the MGO as generally the greater challenge. The LGO requirements for communications, weight control, navigation, nutation control and propulsion, for example, are subsets of the MGO requirements. On the other hand, the requirement for attitude sensing using star mappers and sun sensors in the initial insertion orbit at the Moon is a harder design driver than the similar requirement at Mars.

4.2 MGO MISSION ANALYSIS

4.2.1 Orbit Achievement - Outline

For the purpose of introducing the mission analysis for MGO it is worthwhile outlining the baseline orbit-achievement plan. This will in effect summarize the results of the various sections of the orbit-achievement analysis discussed in fuller detail in Sections 4.2.2 through 4.2.4.

In the baseline mission, launch of the MGO will be performed by the STS with a spinning IUS-1 upper stage. A type I transfer to Mars has been selected for 1988 launch and a type II transfer for each of the 1990 and 1992 launches. Ten-day launch windows have been considered. These transfer trajectories together with the STS/IUS-1 baseline launch system feature high launch payload margins.

Injection from the STS park orbit will occur without plane change. The IUS-1 will be controlled before its ignition either by the MGO attitude determination and control system (ADACS) or adapted PAM-A avionics. Mid-course maneuvers will be performed in order to effect corrections for the IUS-1 trajectory error and for targeting trims as Mars is approached. The IUS-1 will be separated early enough so as to be biased to miss Mars.

Mars orbit insertion (MOI) will be performed using a solid rocket motor over one of the polar regions of Mars, at the periapsis of the arrival hyperbola, which will be targeted to be at an altitude of approximately 500 km. The insertion orbit will be highly elliptical, with an apoapsis as high as possible so that the gamma ray spectrometer may be calibrated as far away from Mars as possible after the deployment of its boom following MOI. The apoapsis radius will be limited by the capacity of the on-board propulsion system which will be used to achieve the mission orbit at 350 km altitude. The JPL supplied Mars Reference Data Package specifies upper-stage correction-maneuver ΔV's of 200 m/s for a spinner and 60 m/s for an inertial reference unit (IRU) controlled stage. For the two types of upper stage stabilization, therefore, there will be different amounts of hydrazine available for orbit circularization and, accordingly, the maximum apoapsis altitude of the Mars insertion orbit for the two cases will be either $\sim$ 7016 km (5.1 hr period orbit) or $\sim$ 12,423 km (8.25 hr period orbit), respectively, as shown in Section 4.2.6.

The spacecraft will be left in this insertion orbit for approximately 20-130 days, depending principally upon the angle between the arrival plane and the Sun direction for the individual transfer trajectory used, until the desired 45° phase angle (3 AM or 3 PM local time of ascending node) is achieved. During this drift period the booms carrying the gamma ray spectrometer and the magnetometer will be deployed and these instruments calibrated near apoapsis.

At the end of the drift-orbit phase, the insertion orbit will be circularized at 350 km altitude using the on-board hydrazine propulsion system. The spent solid rocket motor and instrument hatches and covers will be jettisoned in the insertion orbit. It is necessary to ensure that neither this debris nor the spacecraft itself impacts the surface of Mars before the end of the expiration date of the NASA planetary quarantine policy at the end of the year 2018.

At the end of the drift-orbit phase, the insertion orbit will be circularized at 350 km altitude using the radial thrusters of the on-board hydrazine RCS. In this orbit the spacecraft will operate for nominally one year collecting and sending data on the geophysics and geochemistry of Mars back to Earth.

At the chosen end of life (EOL) of the mission, the orbit will be raised by the on-board hydrazine propulsion system into a stable circular orbit at $\geq$500 km altitude in order to satisfy the planetary quarantine requirement.

4.2.2 Earth-Mars Trajectory Selection

Paired, low-energy, two-impulse Earth-Mars transfer opportunities of types I and II (typically separated by one or two months at launch), occur approximately biannually (usually 24-28 months, the synodic period for Earth and Mars being 780 days, i.e., $\sim$ 25.6 months). Significant, even great, differences between the magnitudes of the propulsive impulses required to effect these transfers exist between the individual opportunities. Table 4.2-1 lists summary characteristics of the six Earth-Mars transfer opportunities with

TABLE 4.2-1. SUMMARY CHARACTERISTICS OF MGO TRANSFER OPPORTUNITIES (FROM REFERENCE DATA PACKAGE)

(Based on 1st day of 10-day launch period selected to maximize mass in Mars orbit)[a]

Opportunity, Year	1988		1990		1988	
Trajectory Type	I[b]	II	I	II[b]	I	II[b]
Launch						
Date	7/2/88	5/23/88	9/3/90	8/22/90	10/12/92	9/21/92
Injection Energy C_3, km^2/s^2	11.83 (11.81)	23.57	20.38	15.94 (15.87)	22.57	12.26 (12.19)
Declination, deg	20.2	-12.2	51.1	5.0	59.5	14.5
Arrival						
Date	1/25/89	2/2/89	4/24/91	8/16/91	6/27/93	8/31/93
Approach Velocity, V_∞	2.666 (2.672)	2.653	2.776	2.741 (2.783)	2.822	2.468 (2.511)
Transfer Time, days	207	255	233	359	258	344
Days Before Mars Perihelion	521	513	392	278	278	213
Earth-Mars Range, AU	1.2	1.23	1.7	2.48	1.97	2.32
Insertion ΔV, m/s[c]	905	899	960	942	983	814
Total ΔV Req'd, m/s[c, d]	2327	2321	2382	2364	2405	2236

[a]Values in parentheses are for last day of 10-day launch period

[b]Cases selected for reference trajectories

[c]Not including gravity and pointing/execution losses

[d]Values applicable to Shuttle/IUS and Titan/IUS launch vehicles utilizing inertial reference unit in upper stage.

launches occurring during the period 1988-1992 for the first days of 10-day launch windows. These transfers have been optimized to enable the delivery of the maximum mass into Mars orbit. From each of these three pairs of trajectories the 1988 I, 1990 II and 1992 II trajectories have been selected for the baseline missions discussed further in this study since they require the lowest launch energies, C_3's, and ultimately feature the highest mass in orbit for the use of a given STS upper stage. In fact, however, the results of the launch system selection process turned out to feature very large payload margins, as discussed in Section 4.2.3. It remains a possibility, therefore, that the other three transfer trajectories shown in Table 4.2-1 may be suitable. Other trajectories may be calculated according to other optimization criteria and may also be suitable, while yielding further advantages. For example Table 4.2-2 lists summary characteristics of six other opportunities with launches in the period 1988-1992, for 10-day launch windows, optimized to feature minimum ΔV requirements for the MOI maneuver. The confirmation of the suitability of these other potential trajectories remains a subject of investigation for a follow-on MGO study.

Realistic launch considerations dictate that at least 10 consecutive days be available for launching a planetary mission. For the baseline missions (superscripted "b") in Table 4.2-1, accordingly, the values of C_3 and arrival hyperbolic excess velocity, V_∞, for the last days of the 10-day launch windows are shown in parentheses in order to indicate the penalties associated with the 10-day launch windows.

Values of declination of launch assymptote, DLA, are also shown in Tables 4.2-1 and 4.2-2. The relevance of DLA is illustrated in Figure 4.2-1. If the inclination of the park orbit is denoted by I, it may be seen from the figure that any value of DLA satisfying the relationship $-I \leq DLA \leq I$ may be achieved without a plane change being effected by the upper stage. All that is required is injection at the appropriate time and position in the park orbit. Of course the correct alignment of the launch assymptote must be ensured by correct orientation of the STS park orbit, which is determined through STS launch window selection.

Further, regarding DLA, it may be shown that for MOI into near-polar orbits, no plane charge will be necessary at Mars, any necessary plane-orientation adjustment being achievable at very little propulsive cost by a mid-course maneuver. This would not be the case were the Mars insertion orbit required to be near-equatorial. The value of DLA, therefore, is not very significant in regard to MOI for the MGO mission.

4.2.3 Launch System Selection

A group of fourteen launch systems, which are either currently available, soon to be available or are proposed concepts, were considered for the MGO launch. They are:

1. STS/PAM-D
2. STS/PAM-A
3. STS/IUS Two-Stage
4. STS/Centaur F
5. STS/Injection Module (IM)
6. STS/PAM-D2
7. STS/IUS-1 (Spinner)
8. STS/IUS-1 (IRU Controlled)

TABLE 4.2-2. SUMMARY CHARACTERISTICS OF MGO TRANSFER OPPORTUNITIES (FROM REFERENCE DATA PACKAGE)

(Based on 1st day of 10-day launch period selected to minimize approach velocity V_∞)

Opportunity, Year	1988		1990		1992	
Trajectory Type	I	II	I	II	I	II
Launch						
Date	7/21/88	5/13/88	9/22/90	7/8/90	10/24/92	8/30/92
Injection Energy C_3, km^2/s^2	13.79	24.18	26.86	31.76	25.34	17.91
Declination, deg	14.48	-6.8	37.6	4.4	47.1	11.5
Arrival						
Date	2/9/89	1/13/89	5/21/91	5/10/91	7/20/93	7/31/93
Approach Velocity, V_∞	2.533	2.674	2.345	2.399	2.413	2.401
Transfer Time, days	203	245	241	306	269	335
Days Before Mars Perihelion	506	533	279	290	255	244
Earth-Mars Range	1.35	1.09	1.98	1.89	2.12	2.18
Insertion ΔV, m/s[a]	943	909	761	784	790	784
Total ΔV Req'd, m/s[a, b]	2365	2331	2183	2206	2212	2206

[a]Not including gravity and pointing losses

[b]Values applicable to Shuttle/IUS and Titan/IUS launch vehicles utilizing inertial reference unit in upper stage.

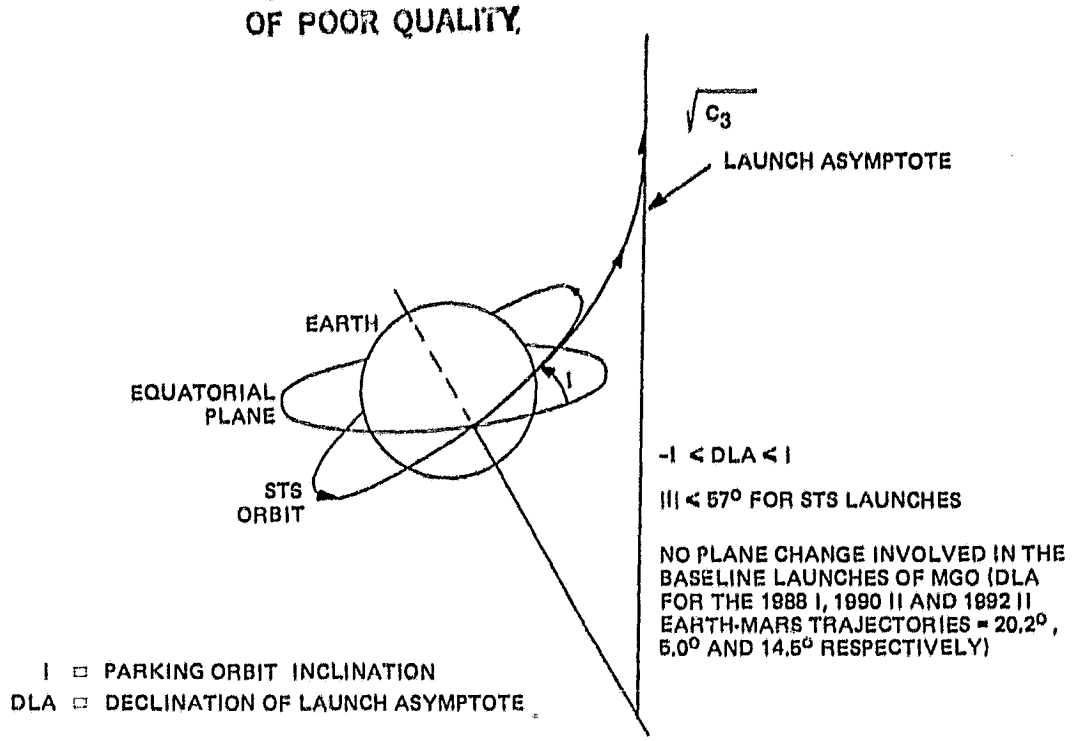

Figure 4.2-1. STS Launch Geometry

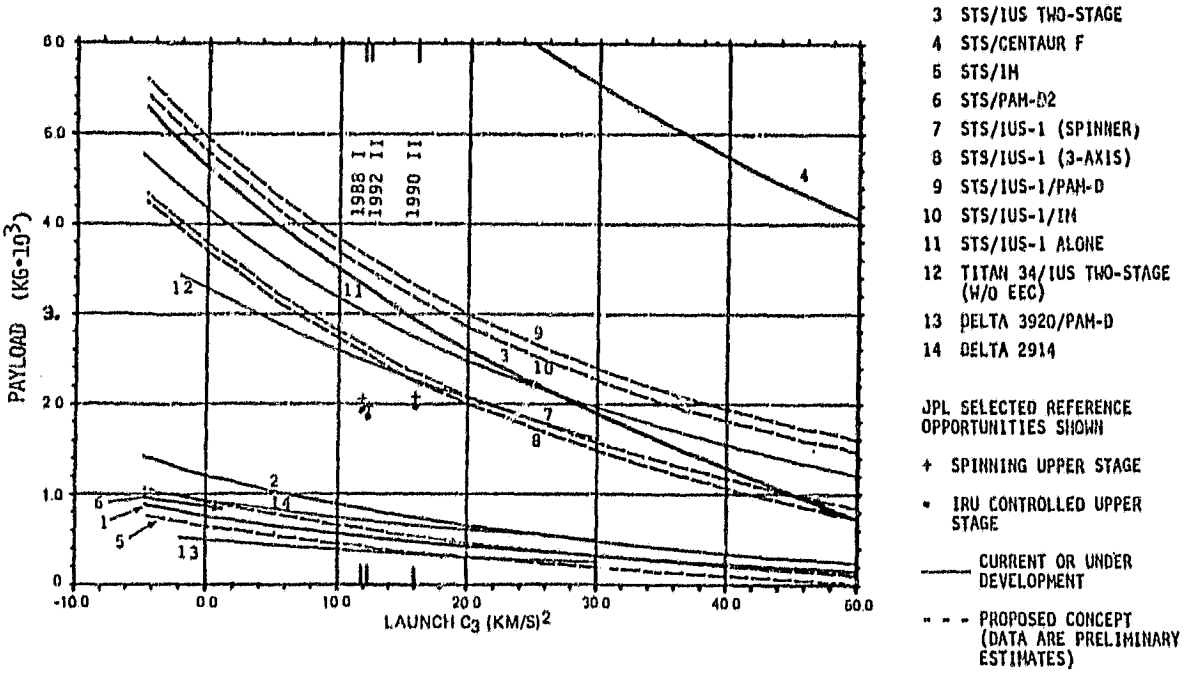

Figure 4.2-2. Match of Launch Systems with 650 kg Class DE-Based MGO Using a Hybrid Propulsion System

9. STS/IUS-1/PAM-D
10. STS/IUS-1/IM
11. STS/IUS-1
12. TITAN 34/IUS Two-Stage (W/O EEC)
13. Delta 3920/PAM-D
14. Delta 2914

The choice between these launch systems was narrowed initially by matching the calculated launch throw masses for the three baseline missions with the planetary performance curves of the launch systems as illustrated summarily in Figure 4.2-2.

The values for throw mass were developed starting from the end-of-life (EOL) mass of the spacecraft, of 651 kg, which includes 72 kg of growth margin. Intermediate results in these calculations for the three baseline missions are shown in Tables 4.2-3 to 4.2-5 for three values of the period of the Mars insertion orbit: 12, 8 and 3.5 hr, respectively.

Requirements and constraints that were figured into the calculations of these tables are:

- ΔV = 76 m/s to raise orbit altitude to 525 km at EOL
- ~25 kg allowance of hydrazine for possible extended data gathering phase
- ΔV for lowering insertion orbit to circular at 350 km altitude (magnitude of ΔV dependent on dimensions of insertion orbit)
- Component masses of suitable, available STAR solid rocket orbit insertion motors (OIMs)
- 60 kg adapter between OIM and spacecraft
- Hydrazine used for mid-course maneuvers (ΔV = 200 m/s for spinning upper stages, 60 m/s for inertially controlled upper stages)
- 100 kg launch adapter

The paired values enclosed by square brackets in Tables 4.2-3 to 4.2-5 correspond to the use of a spinning upper stage, whereas the unenclosed paired values correspond to the use of an upper stage controlled by an IRU, i.e., a "3-axis stage."

The tables show the altitudes of apoapsis, 18015, 12022 and 3841 km corresponding to Mars insertion orbits with a periapsis altitude of 500 km and periods of 12, 8 and 3.5 hr respectively. Also included are the values of the ΔVs required to lower these insertion orbits to become circular at 350 km altitude, i.e., 1044, 924, and 527 m/s, respectively.

The bottom lines of these tables show the calculated launch throw masses. These are plotted in Figure 4.2-2. The term "throw mass" is used here to represent all mass above the mating interface of the launch vehicle, i.e., does include the mass of the launch adapter.

TABLE 4.2-3. DE-BASED MGO MASS HISTORY - 12 HOUR PERIOD INSERTION ORBIT

#	Launch Year and Trajectory Type / Item	1988 I	1990 II	1992 II
			Mass (kg)	
1	EOL S/C	651	651	651
2	Hydrazine for EOL Orbit Raising (350 → 525 km Alt., ΔV = 76 m/s)	22.3	22.3	22.3
3(=1+2)	S/C Pre-EOL Orbit Raising	673.3	673.3	673.3
4	Approximate Hydrazine for 3-4 yr Data Gathering Phase	25	25	25
5(=3+4)	BOL S/C	698.3	698.3	698.3
6	Hydrazine for Apoapsis Lowering (18015 → 350 km Alt., ΔV = 1031 m/s)	404.5	404.5	404.5
7	Hydrazine for Periapsis Lowering (500 → 350 km Alt., ΔV = 13 m/s)	6.4	6.4	6.4
8(=5+6+7)	S/C Pre-Orbit Circularization	1109.0	1109.0	1109.0
9	Candidate-OIM Star Designation	30C	37S	30C
10	OIM at Burnout + 60* kg Adapter	91.3	107.5	91.3
11(8+10)	Assembly at OIM Burnout	1200.3	1216.5	1200.3
12	Mars Orbit Insertion ΔV (km/s)	1.083	1.139	1.005
13	Solid Propellant Mass	566.9	604.8	518.3
14	% OIM Off-Loading	3.1	8.1	11.4
15	OIM Mass	601.9	657.9	553.3
6(=8+15+60kg)	Planetary Approach Mass	1770.9	1826.9	1722.3
17	Hydrazine Used in Earth-Mars Transit**	47.7 [164.2]	49.2 [169.3]	46.4 [159.6]
18	Upper Stage Adapter	100	100	100
19(=16+17+18)	Launch Payload	1918.6 [2035.1]	1976.1 [2096.2]	1868.7 [1981.9]

*Current Estimate
**ΔV = 60 m/s for 3-Axis Upper Stages [Δv = 200 m/s for Spinning Upper Stages]
Mars Insertion Orbit of 500 x 18015 km Altitude, i.e., 12 hour Period.

TABLE 4.2-4. DE-BASED MGO MASS HISTORY - 8 HOUR PERIOD INSERTION ORBIT

#	Launch Year and Trajectory Type / Item	1988 I	1990 II	1992 II
			Mass (kg)	
1	EOL S/C (Including 71.5 kg Margin)	651	651	651
2	Hydrazine for EOL Orbit Raising (350 → 525 km Alt., ΔV=76m/s)	22.3	22.3	22.3
3(=1+2)	S/C Pre-EOL Orbit Raising	673.3	673.3	673.3
4	Approximately Hydrazine for 3-4 yr Data Gathering Phase	25	25	25
5(=3+4)	BOL S/C	698.3	698.3	698.3
6	Hydrazine for Apoapsis Lowering (12022 → 350 → km Alt., ΔV = 908 m/s)	346.0	346.0	346.0
7	Hydrazine for Periapsis Lowering (500 → 350 km Alt., ΔV = 16 m/s)	7.4	7.4	7.4
8(=5+6+7)	S/C Pre Orbit Circularization	1051.7	1051.7	1051.7
9	Candidate-OIM Star Designation	37S	37S	30C
10	OIM at Burnout + 60* kg Adapter	107.5	107.5	91.3
11(=8+10)	Assembly at OIM Burnout	1159.2	1159.2	1143
12	Mars Orbit Insertion ΔV (km/s)	1.207	1.263	1.129
13	Solid Propellant Mass	618.6	654.3	567.7
14	% OIM Offloading	5.9	0.5	2.9
15	OIM Mass	671.7	707.4	602.7
16(=8+15+60kg)	Planetary Approach Mass	1783.4	1819.1	1714.4
17	Hydrazine Used in Earth-Mars Transit**	48.1 [165.3]	49.0 [168.6]	46.2 [158.9]
18	Upper Stage Adapter	100	100	100
19(=16+17+18)	Launch Payload	1931.5 [2048.7]	1968.1 [2087.7]	1860.6 [1973.3]

*Current Estimate
**ΔV = 60 m/s for 3-Axis Upper Stages [ΔV = 200 m/s for Spinning Upper Stages]
Mars Insertion Orbit of 500 x 12022 km Altitude, i.e., 8 hour Period

TABLE 4.2-5. DE-BASED MGO MASS HISTORY - 3.5 HOUR PERIOD INSERTION ORBIT

#	Launch Year and Trajectory Type / Item	1988 I	1990 II	1992 II
			Mass (kg)	
1	EOL S/C (Including 71.5 kg Margin)	651	651	651
2	Hydrazine for EOL Orbit Raising (350 → 525 km Alt., ΔV = 76 m/s)	22.3	22.3	22.3
3(=1+2)	S/C Pre-EOL Orbit Raising	673.3	673.3	673.3
4	Approximate Hydrazine for 3-4 yr Data Gathering Phase	25	25	25
5(=3+4)	BOL S/C	698.3	698.3	698.3
6	Hydrazine for Apoapsis Lowering (3841 → 350 km Alt., ΔV = 501 m/s)	173.6	173.6	173.6
7	Hydrazine for Periapsis Lowering (500 → 350 km Alt., ΔV = 26 m/s)	10.1	10.1	10.1
8(=5+6+7)	S/C Pre Orbit Circularization	882.0	882.0	882.0
9	Candidate-OIM Star Designation	37F	37F	37F
10	OIM at Burnout +60* kg Adapter	121.7	121.7	121.7
11(=8+10)	Assembly at OIM Burnout	1003.7	1003.7	1003.7
12	Mars Orbit Insertion ΔV (km/s)	1.616	1.672	1.538
13	Solid Propellant Mass	780.7	816.6	731.8
14	% AKM Off-Loading	9.8	5.7	15.5
15	OIM Mass	847.8	883.7	798.9
16(=8+15+60kg)	Planetary Approach Mass	1789.8	1825.7	1740.9
17	Hydrazine Used in Earth-Mars Transit**	48.2 [165.9]	49.2 [169.2]	46.9 [161.4]
18	Upper Stage Adapter	100	100	100
19(=16+17+18)	Launch Payload	1938.0 [2055.7]	1974.9 [2094.9]	1887.8 [2002.3]

*Current Estimate
**ΔV = 60 m/s for 3-Axis Upper Stages [ΔV = 200 m/s For Spinning Upper Stages]
Mars Insertion Orbit of 500 x 3841 km Altitude, i.e., 3.5 hour Period.

It is immediately clear that the baseline MGO spacecraft lies well beyond the capability of the STS/PAM-A launch system, represented by curve 2 in Figure 4.2-2.

The next more powerful launch system beyond the STS/PAM-A is the Titan 34/IUS Two-Stage. This is not a favored launch system for several reasons. First, both the Titan 34 booster and the IUS Two-Stage upper stages will be much more expensive than the baseline choices which are an STS launch with an IUS-1 upper stage. Second, the IUS Two-Stage has a limited expected production run, especially now that the development of the STS/Centaur F has been recommended. Third, by the time of the baseline mission launches, 1988-1992, the STS will be fully operational.

The baseline launch system is the STS/IUS-1, which is the basis of the next group of more powerful launch systems. The IUS-1 motor is currently being developed under a firm program; an off-loaded IUS-1 will be used as the perigee kick motor for the Intelsat VI. The planetary performance of this system is represented by curve 11 in Figure 4.2-2. Its use would yield very large margins in launch payload (throw mass) over the requirements for the baseline missions, which are also shown in the figure.

This baseline launch system features use of the IUS-1 as a simple solid rocket motor, not as a self-controlled stage. This concept is discussed more fully in Section 4.2.4. If this concept ultimately proves to be infeasible or unattractive, the proposed launch system would become either STS/IUS-1 (spinner) or STS/IUS-1 (3-axis). The two versions of the IUS-1 referred to are conceptual stages proposed and studied at the NASA Marshall Space Flight Center. The spinning stage is controlled by modified PAM-A avionics which are capable of holding the inertial orientation of the stack steady through separation from the Shuttle and through spin-up and up to ignition. The discrepancy between the measurement of attitude by the Shuttle and the position of the IUS cradle is currently predicted to be $\leq 0.5°$, and the pointing error of the IUS-1 (spinner) stage will, therefore, be at least as high as this error. The 3-axis stage referred to is controlled by modified Galileo Insertion Module avionics, which are capable of holding the inertial orientation of the stack as it is within the Shuttle and then, if required, reorienting by a preselected bias amount before ignition. Under control of the avionics the stage is then inertially held (in three axes) during the burn, and mid-course maneuvers are also possible.

It may be seen from Figure 4.2-2 that the throw mass margins for the baseline missions are still high, in the range of approximately 200-700 kg, for these two IUS-stages. The margins are slightly greater for the IUS-1 (3-axis) stage. These launch system options are clearly less desirable than the baseline system since they require development. They may still be cheaper and more feasible than the Titan 34/IUS Two-Stage system, however.

4.2.4 Launch Phase

The launch phase of the mission will consist of boost from the Kennedy Space Center on-board the Shuttle into a circular park orbit at 296 km attitude, followed by deployment from the cargo bay and injection into the interplanetary transfer trajectory.

Since the baseline launch system is the STS/IUS-1 (see Section 4.2.3), there will be few constraints on spacecraft hardware, weight and volume for launch. Throw mass margins have been discussed in Section 4.2.3. The DE based MGO design, being evolved from designs for expendable launch vehicles, will fit easily into the Shuttle bay and on top of the IUS-1 even with any necessary environmental protection shroud. A simple conical adapter will connect the spacecraft and the IUS-1. Since the maximum thrust level of the IUS-1 will be ∿27,000 kg f (∿267000 N) and the mass of the integrated stack at launch will be ∿12,500 kg, the peak acceleration of the stack will be ∿2.2g. This level of acceleration is very mild compared with, for example, Shuttle emergency landing load factors which typically may be ∿ 4.5g in the Shuttle X and Z directions. The AE/DE design legacy of the MGO features compatibility with spinning about the axis of symmetry at rates of up to 60 rpm. The use of the spinning IUS-1 in the baseline, therefore, is perfectly matched to the spacecraft design.

While inside the Shuttle bay the MGO spacecraft will probably require thermal shielding. The spacecraft will be partially operational while inside the Shuttle bay since the momentum wheel and the ADACS will be required during the period between separation from the Shuttle and injection. In fact, in order to ensure reliability, the momentum wheel will be spinning throughout the entire launch phase. A small amount of heat will be generated, therefore, and a full thermal analysis will be necessary in further studies, but the design will be made to feature passive thermal control only. The zones of focused sunlight caused by the concave radiator panels on the inside of the bay doors will be avoided by the injection stack.

The baseline concept features control of the injection stack by the ADACS of the DE-based MGO following separation from the Shuttle and up to the time of ignition. The stack will be deployed from the Shuttle by the standard spring actuated IUS deployment system. The Shuttle orientation at separation will be held so that the orientation of the stack will be as close as possible to that required at ignition. The stack will be momentum biased during and after separation by means of the momentum wheel in the spacecraft. Following separation there will be a period, covering between a half to one orbit, during which the stack will drift to a clearance distance from the Shuttle safe for ignition. Also during this period, the orientation of the stack will be trimmed and stabilized. The ADACS of the spacecraft will employ its sun sensors, star sensors, gyro package, momentum wheel and hydrazine thrusters to trim the orientation of the stack. The level of gyroscopic stiffness of the stack already provided by the momentum wheel of the spacecraft will then be increased just prior to the IUS-1 burn by the spinning up of the stack to typically 60 rpm using the hydrazine thrusters of the spacecraft. This spinup will also serve to prevent any secular launch error due to thrust-vector misalignment effects during motor firing. Spin control of the stack in this way is performed very economically in terms of hydrazine used.

Since the attitude of the stack may be set and held, as described, following separation from the Shuttle and prior to IUS-1 ignition, the stack will not be spun up much earlier than necessary prior to ignition. In this way there will be no significant buildup of nutation prior to ignition and no nutation damping system is required on board the spacecraft or the stack.

At the appropriate moment the IUS-1 is ignited. The nominal burn time is 146 seconds. At burnout the orbital velocity (with respect to the Earth) will have been increased from 7.728 km/s to the value corresponding to the required C_3. For the 1988 I, 1990 II and 1992 II baseline trajectories are $C_3 \simeq 11.83$, 15.94 and 12.26 km^2/s^2, respectively, as shown in Table 4.2-1.

Accordingly the relationship

$$V_{injection} = \left(C_3 + \frac{2\mu_E}{r_o} \right)^{1/2}$$

where C_3 = square of the departure hyperbolic excess velocity
μ_E = gravitational constant for Earth = 398,601 km^3/s^2
r_o = initial orbit radius = 6,674 km

gives the injection velocities of 11.458, 11.636, and 11.477 km/s, respectively. The IUS-1, therefore, imparts velocity increments of 3.730, 3.908, and 3.749 km/s, respectively, to the stack for the three baseline missions. The geometry of the injection is illustrated in Figure 4.2-1 and has been discussed in Section 4.2.2.

4.2.5 Earth-Mars Transfer Phase

The heliocentric transfer phase of the mission basically consists of a "coasting" trajectory which is essentially a section of an elliptical orbit around the Sun. The trajectory for the baseline mission with the launch in 1988 is described as being a Type I trajectory since the spacecraft will travel outside the heliocentric orbit of the Earth less than 180° around the Sun. The trajectories for the baseline missions with launches in 1990 and 1992 are Type II trajectories since the heliocentric angle traveled through is greater than 180°.

The transfer times for these baseline missions are shown in Table 4.2-1 and are 207, 359, and 344 days, respectively.

Since the inclination of the Mars heliocentric orbit is only 1.85° to the ecliptic, the Earth-Mars transfer is very nearly in the ecliptic plane.

Plots of the histories of pertinent spatial and geometrical relationships for the three baseline transfers, relating to the time-changing geometry between the spacecraft, Mars, the Earth and the Sun, are shown in Figures 4.2-3 to 4.2-5. The chase diagram is very useful in aiding visualization of the relative orientation of the spacecraft to these celestial bodies and of the bodies to each other. The information shown graphically has been incorporated into the analyses of the communications, thermal and power subsystems described in Sections 8, 9 and 10.

It may be seen that for all three transfer trajectories there are no conjunctions, or close conjunctions, of the Sun and the spacecraft as seen from the Earth, nor of the Earth and the Sun as seen from the spacecraft, to cause degradation or interruption of communications.

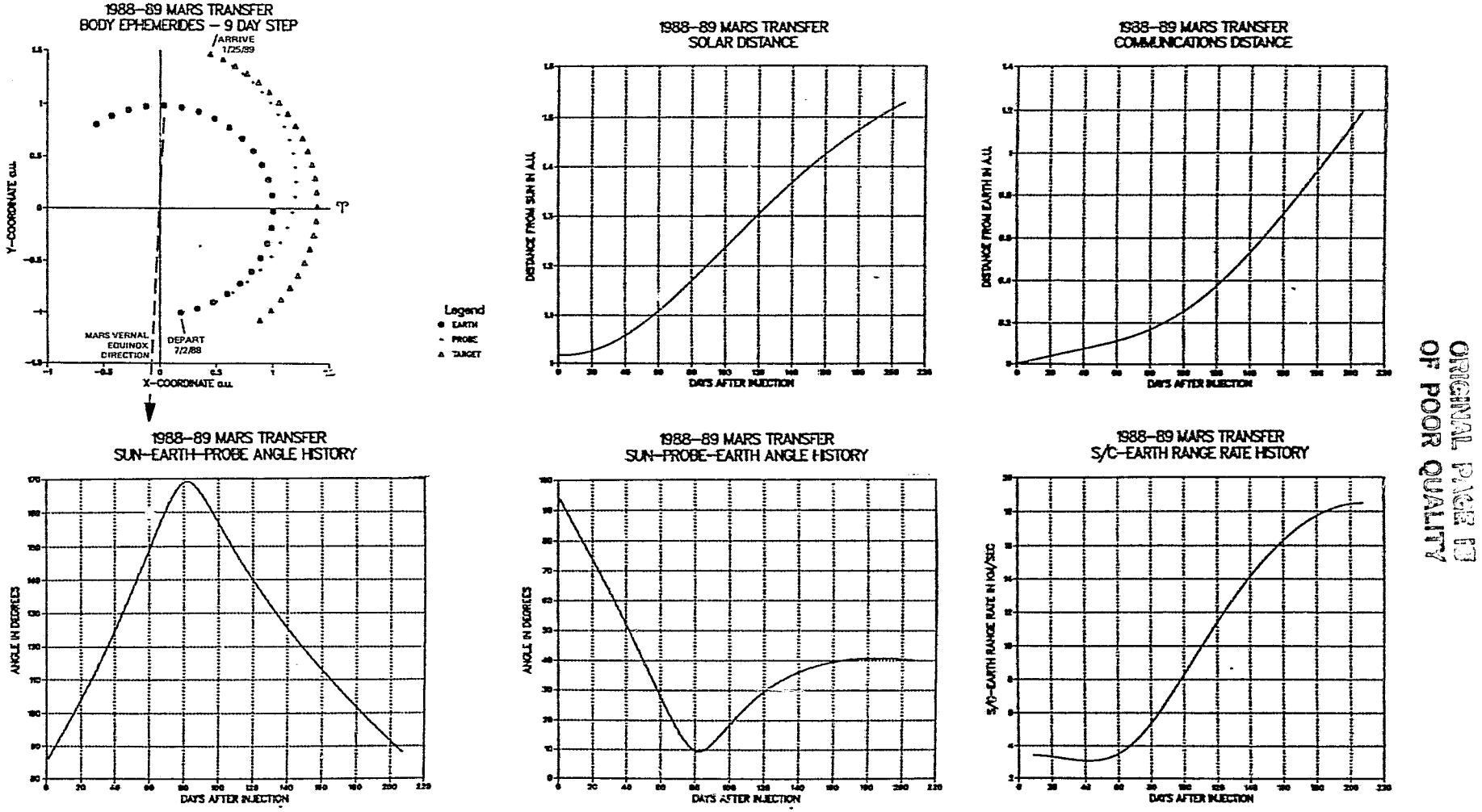

Figure 4.2-3. 1988 I Earth-Mars Transfer Geometry

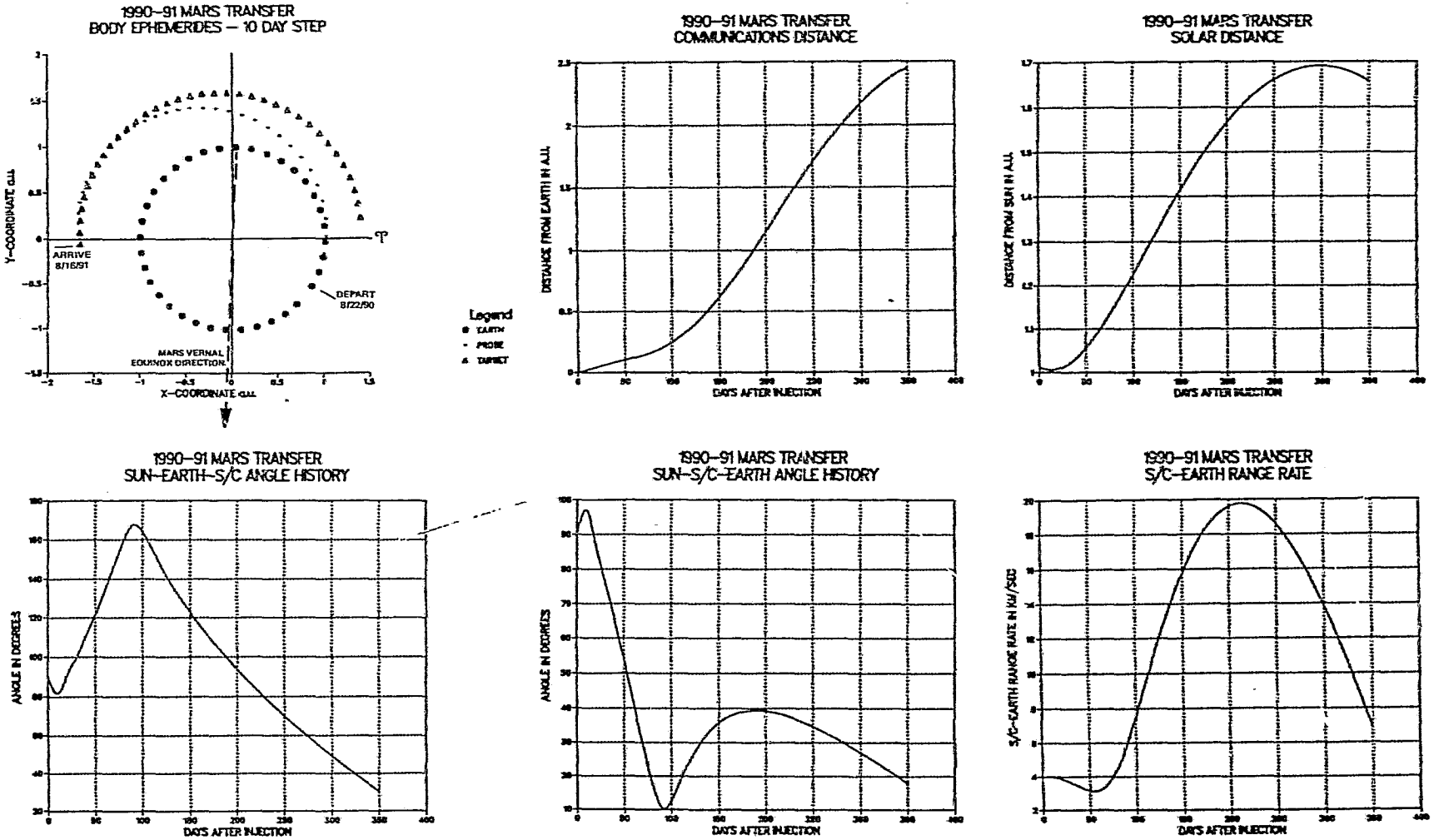

Figure 4.2-4. 1990 II Earth-Mars Transfer Geometry

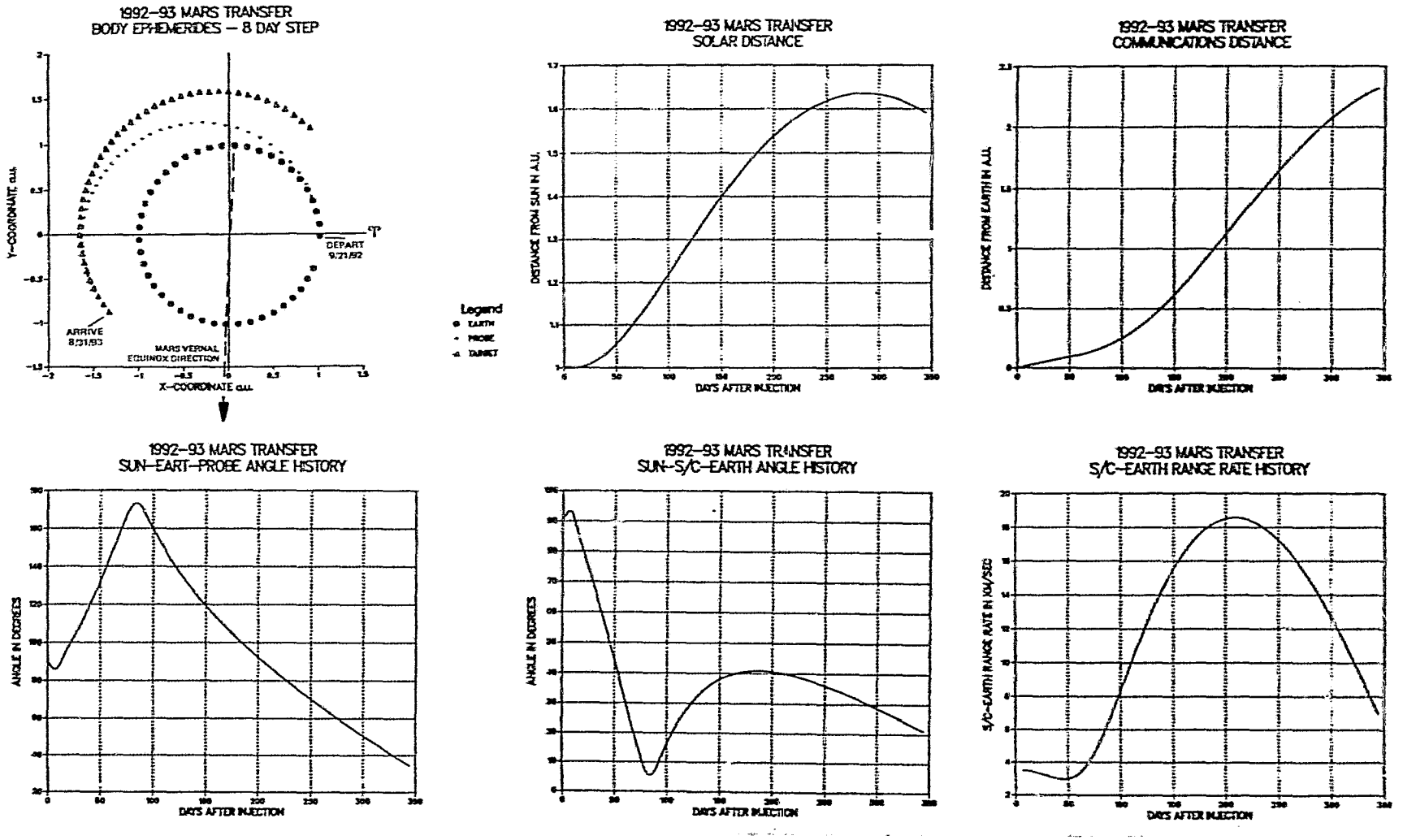

Figure 4.2-5. 1992 II Earth-Mars Transfer Geometry

Following very soon after burnout of the IUS-1, the spacecraft will be separated from the spent stage and the launch adapter. The jettisoned stage will not be targeted accurately enough at this time to intercept Mars and will not be of concern regarding planetary quarantine. The spacecraft body will then be despun quickly, using the on-board hydrazine propulsion system, before significant nutation can develop (see Section 7). The momentum wheel will be kept spinning even during the IUS-1 burn and will now provide gyroscopic stability of the axis of symmetry of the spacecraft.

During the transfer the spacecraft will spin very slowly, e.g., 0.1 rpm, about its axis of symmetry which will be oriented according to considerations arising from the thermal control of the spacecraft and orbit insertion motor and the sensing of the attitude of the stack using the star and Sun sensors. More than 90 percent of the angular momentum of the stack will reside in the momentum wheel. Generally the spin axis may be aligned anywhere between parallel and perpendicular to the ecliptic plane as long as the star and Sun sensors can view their reference bodies. In the baseline mission plan the spin axis will lie approximately parallel to the ecliptic plane with the OIM in the shadow of the spacecraft. In this orientation the solar arrays, predominantly the one on the face of the spacecraft opposite the OIM, will provide ample power for housekeeping and communications requirements. If the OIM temperature starts to fall significantly, the spin axis will be shifted temporarily in order to allow direct heating of the OIM by obliquely incident solar radiation.

While the stack is within $\sim 5 \times 10^7$ km of the Earth during the transfer phase, downlinks via the omni antenna will be strong enough for the planned science and spacecraft functions checkouts. For such higher data-rate checkouts at greater distances, however, either the fan-beam antenna or the high-gain antenna (HGA) will be used. Since the HGA will remain in its stowed configuration until after Mars orbit insertion, the stack will be temporarily reoriented from its "rotisserie" alignment, and the stack will be despun (except for the momentum wheel) for the purpose of performing the downlinks for these checkouts carried out at the greater distances from the Earth. This reorientation procedure is described more fully in Section 7.

Occasional minor and mid-course corrections will be made using the on-board hydrazine propulsion system in order to ensure the correct arrival geometry at Mars. These will involve a total ΔV of the order of 0.01 km/s, which for the typical values of the planetary approach mass for the baseline missions, shown in Tables 4.2-3 to 4.2-5, i.e., $\sim$1800 kg, corresponds to the use of $\sim$ 8 kg of hydrazine. For these mid-course maneuvers, reorientation of the stack will be performed as for the HGA downlinks, as described in the previous paragraph.

Before the closest approach to Mars and the simultaneous Mars orbit insertion, the stack will be aligned with the MOI thrust vector. This realignment will be performed open loop, and a trim maneuver will then be made under ground command. The realignment will be performed early enough that thorough verification of its accuracy may be made using the on-board attitude determination system. Also prior to MOI, the temperature of the OIM will be assured at the preselected value, possibly by the use of heater elements, as indicated by the full thermal analysis that will be a subject of a detailed follow-up MGO study. Immediately before MOI the stack will be spun up to $\sim$ 60 rpm using the on-board hydrazine propulsion system in order to stabilize the alignment of the OIM thrust vector.

4.2.6 Mars Orbit Insertion

4.2.6.1 Arrival Conditions

The Earth departure geometry, timing and injection Δ_∞ determine the Earth-Mars transfer trajectory. This in combination with mid-course corrections determines arrival conditions at Mars.

Before entering the gravitational sphere of influence of Mars, the stack of spacecraft plus OIM has an approach velocity relative to Mars, V_∞, of nominally 2.666, 2.741 and 2.468 km/s for the three baseline transfer trajectories, as shown in Table 4.2-1. It can be seen easily, therefore, that the stack will have positive energy in the Mars reference frame if one considers that, by comparison, a body with zero energy in the Mars reference frame, ejected from the planet with the escape velocity, would arrive at infinity with zero velocity relative to Mars. The stack will therefore follow a planar, hyperbolic trajectory around Mars unless it is targeted to impact the planet or is acted upon by the on-board propulsion system. The deflection angle between the approach and departure assymptotes depends upon the closeness of approach to Mars.

In the baseline missions the stack will be targeted so as to have a hyperbolic periapsis altitude of 500 km at Mars. At the periapsis point the stack, prealigned and spun up as described in Section 4.2.5, will be injected into an elliptical Mars insertion orbit by means of the solid rocket motor. The insertion orbit will be coplanar with the hyperbolic approach trajectory, which will have been arranged by mid-course targeting to produce a near-polar orbit, at 92.5° inclination for the baseline missions. The approach trajectory, accordingly, will be targeted over either Mars's North or South polar region; there will be an accompanying choice to be made between ascending nodes approximately 180° apart. The approach geometries for the three baseline missions are shown in Figures 4.2-6 to 4.2-8 which represent views from the Mars North Pole looking southwards. These figures and Table 4.2-6 show that in the Mars reference frame the stack arrives from the dawn sector with periapsis phase angles (Sun-Mars-periapsis angles) of 97(105), 77(66) and 93(68) degrees (first value of a pair corresponding to a South approach, second value, in parentheses, corresponding to a North approach) for the three optimum, low energy baseline mission trajectories. As described later in Section 4.2.7, a drift orbit will ensue, therefore, during which the desired periapsis phase angle of 45° will be achieved.

4.2.6.2 Selection of Mars Insertion Orbit

The baseline MOI geometry is shown in Figure 4.2-9.

The selection of the elements of the Mars insertion orbit involves the careful matching of many constraints and requirements such as arrival geometry (see Section 4.2.6.1), propulsion system type(s) and capability, mission science requirements, spacecraft requirements (e.g., power), planetary quarantine restrictions, etc. The interactive process is illustrated schematically in Figure 4.2-10 and is discussed in this section.

The feasible orbit insertion scenarios, while differing widely among themselves, are all very sensitive to the choice of the interplanetary transfer trajectory and the performance capabilities of the on-board hydrazine reaction control subsystem (RCS) and the available solid rocket OIMs. It

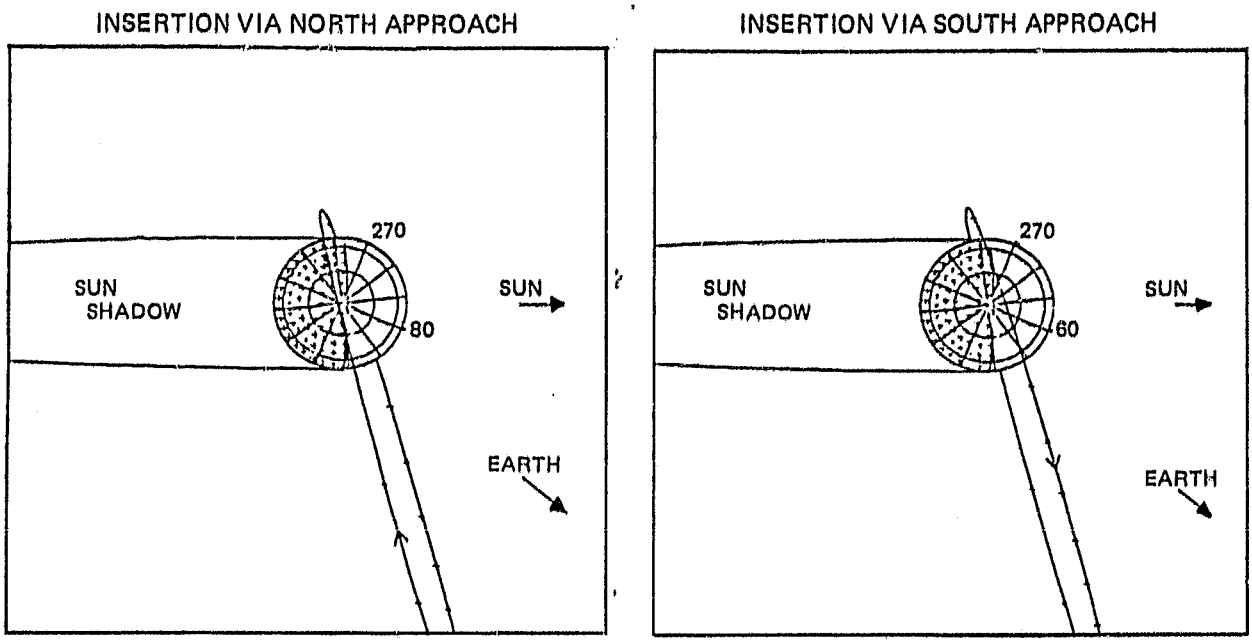

Figure 4.2-6. Initial Mars Orbit Viewed from North Pole - 1988 Type I

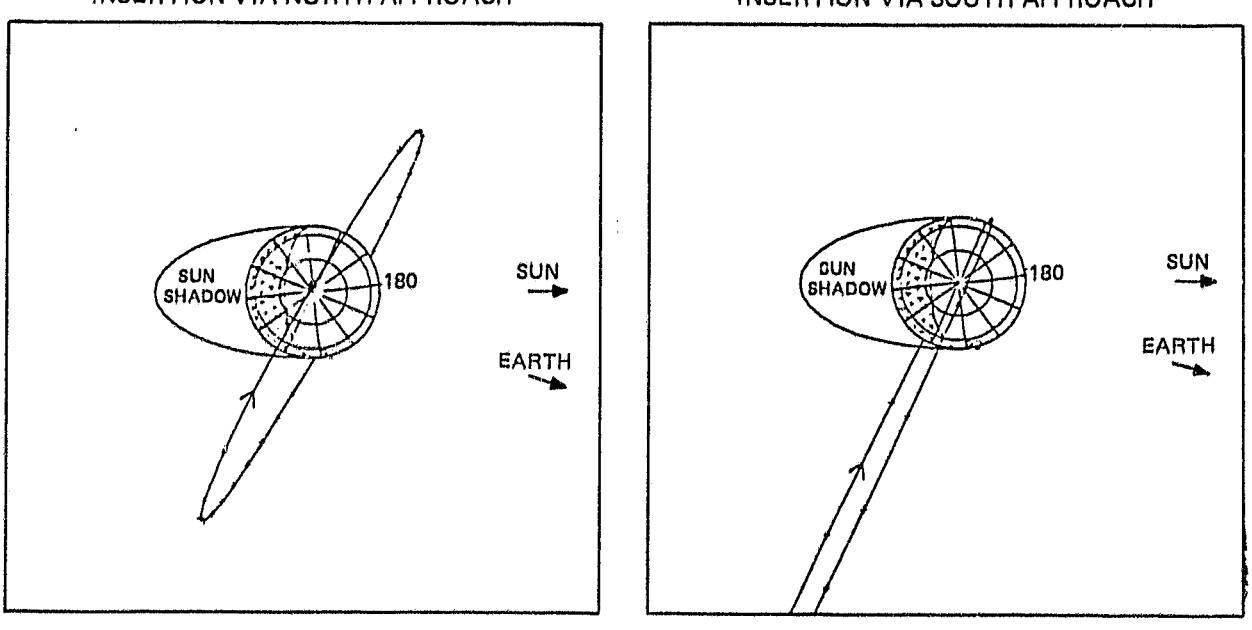

Figure 4.2-7. Initial Mars Orbit Viewed from North Pole - 1990 Type II

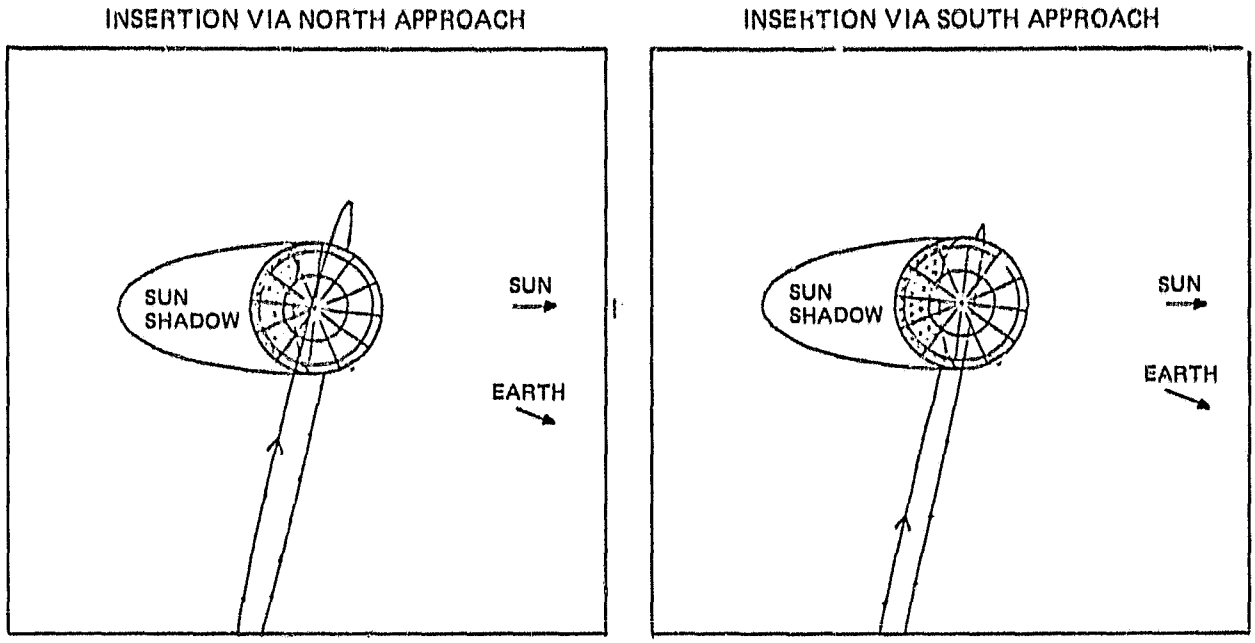

Figure 4.2-8. Initial Mars Orbit Viewed from North Pole - 1992 Type II

should be that while the three baseline Earth-Mars transfers taken for the baseline mission design are based on the optimization of delivered on-orbit mass at Mars, the baseline calculations shown in Tables 4.2-1 and 4.2-2 have been backed away from the absolute optimum values in order to allow for 10-day launch windows.

The baseline mission design incorporates a hybrid (solid plus liquid) propulsion system for the MOI and subsequent maneuvers. The incorporation of a wholly liquid propulsion system would have necessitated the design and development of a new stage, in effect, the expense and technical risk of which is inconsistent with the current scheme of modifying an existing Earth orbiter spacecraft design to give a low cost mission. Futhermore the effective efficiency of a solid OIM is at least as high as that of an integrated bipropellant stage using monomethyl hydrazine and dinitrogen tetroxide.

The on-board hydrazine propulsion system, therefore, was sized in accordance with the available volume for tanks inside the spacecraft. The size of the baseline spacecraft was principally dictated by power requirements, power being produced by solar arrays covering all available external surfaces. Accordingly the baseline design features six 22-inch (nominal) spherical hydrazine tanks as described in Section 5.

A Mars insertion orbit having a period of at least 24 hours would be preferred for purposes of calibrating the gamma ray spectrometer as far away from Mars as possible at apoapsis, following deployment of the boom carrying the instrument. This boom cannot be deployed any earlier and still survive the MOI maneuver intact. The question arises naturally, therefore, as to what is the

TABLE 4.2-6. SUMMARY CHARACTERISTICS OF MGO ORBITAL PHASE[b]

(Based on launching 1st day of 10-day period selected to maximize mass in Mars orbit)

Launch Opportunity, year	1988	1990	1992
Transfer Trajectory Type[a]	I	II	II
Elliptical Orbit (1-day period)			
Insertion Date (MOI)	1/25/89	8/16/91	8/31/93
Initial Orbit Phase Angle, deg	76(74)	52(54)	64(68)
Initial Periapsis Phase Angle, deg (Sun-Mars-Periapsis Angle)	97(105)	77(66)	93(68)
Inclination, deg	93	93	93
Duration, days	123(130)	23	61
Final Orbit Phase Angle, deg	45	45	45
Final Periapsis Phase Angle, deg	51	66	64
Circular Orbit (350 km)			
Insertion Date	5/28/89 (6/4/89)	9/8/91	10/31/93
Days Before Perihelion	398(391)	61	57
Reference Dates			
Solar Conjunction	9/30/89	11/8/91	12/27/93
Mars Perihelion	6/30/90	5/18/92	4/5/94
End of Mission	5/28/90 (6/4/90)	9/8/92	10/31/94

[a]Cases selected for Reference Trajectories

[b]Where values differ between cases for Mars Orbit Insertion from North or South approach, values for approach from North are shown in parentheses

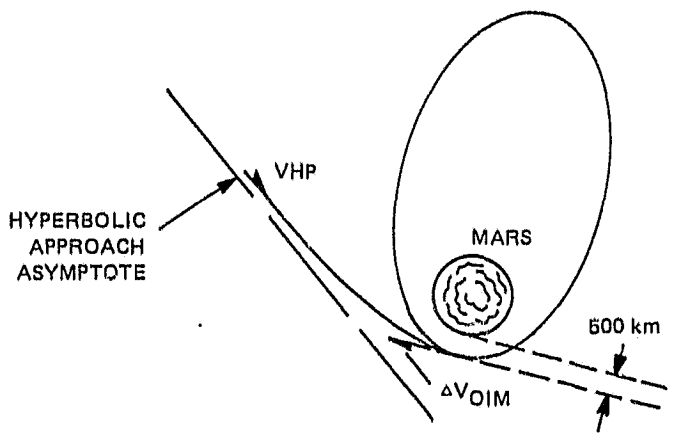

Figure 4.2-9. Mars Approach and Orbit Insertion Geometry

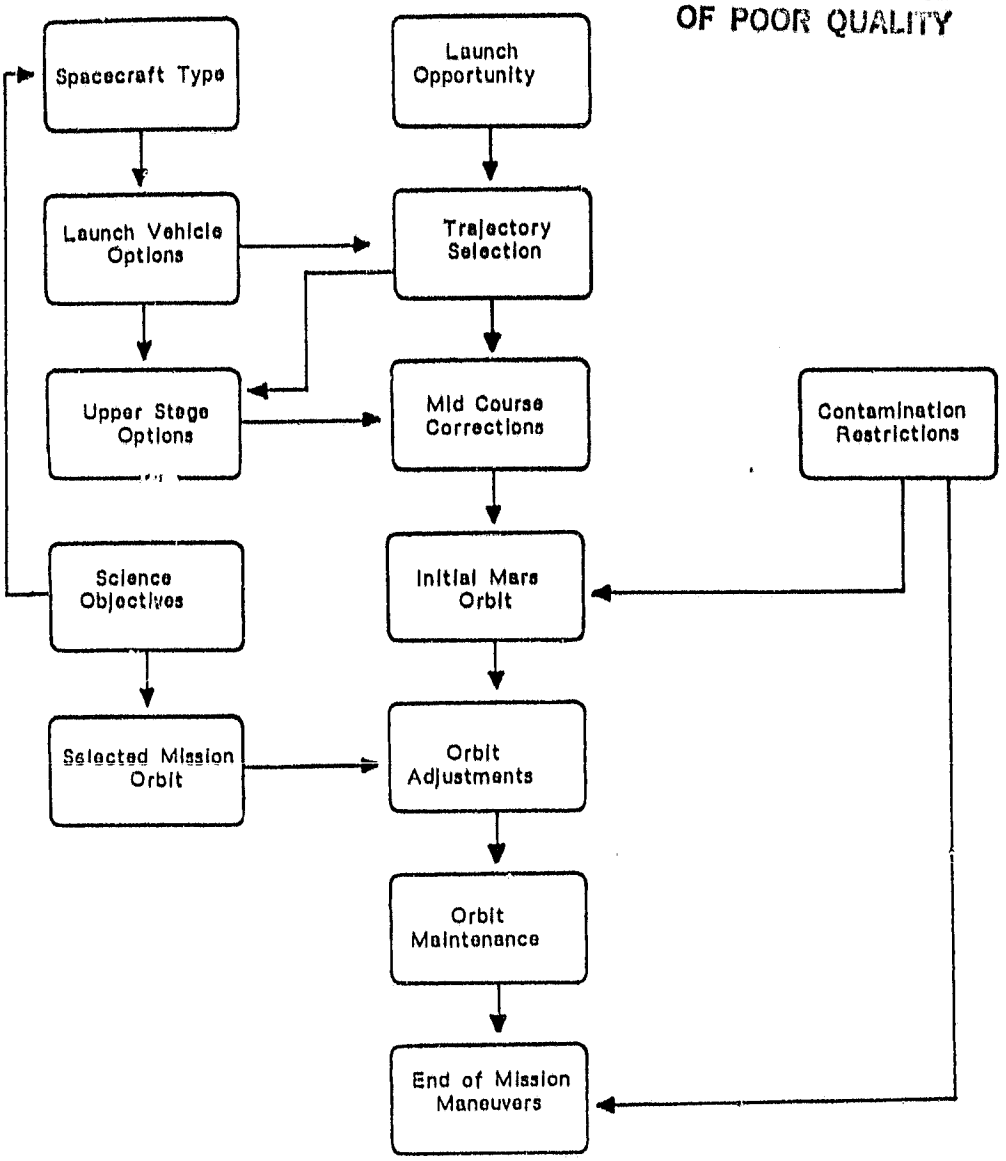

Figure 4.2-10. MGO Orbit Selection Process

largest Mars insertion orbit compatible with the bounding (maximum) capability of the on-board hydrazine propulsion system for the subsequent propulsive maneuvers.

This question was resolved graphically, as shown in Figure 4.2-11, which shows curves of the required spherical hydrazine tank diameter versus the period of the Mars insertion orbit. The upper curve corresponds to the use of a spinning STS upper stage (launch vehicle error correction ΔV of 200 m/s required) and the lower to use of an inertial reference unit (IRU) controlled upper stage (correction ΔV of 60 m/s required). The figure is consistent with baseline missions featuring the three baseline Earth-Mars transfer trajectories and possibly any of the Earth-Mars transfer trajectories described in Section 4.2.2 as well. The curves were drawn through the two triplets of data points which were derived from Tables 4.2-7 to 4.2-9. These tables correspond to Tables 4.2-3 to 4.2-5 which show the summarized MGO mass history for Mars insertion orbits with periods of 12, 8 and 3.5 hours respectively. Tables 4.2-7 to 4.2-9 show the MGO hydrazine budget for missions featuring the same

TABLE 4.2-7. DE-BASED MGO HYDRAZINE BUDGET - 12 HOUR PERIOD INSERTION ORBIT

#	Item Launch Year and Trajectory Type	1988 I	1990 II	1992 II
1	Hydrazine Used During Earth-Mars Transit*	47.7 [164.2]	49.2 [169.3]	46.4 [159.6]
2	Hydrazine for Periapsis Lowering** (kg) (500 + 350 km Altitude)	6.4	6.4	6.4
3	Hydrazine for Apoapsis Lowering** (kg) (18015 + 350 km Altitude)	404.5	404.5	404.5
4	Hydrazine for Approximately 3-4 yr Data Gathering Phase (kg)	25	25	25
5	Hydrazine to Raise S/C into 525 km Altitude Circular Orbit at EOL (kg)	22.3	22.3	22.3
6(=1+2+3+4+5)	Total Hydrazine Requirement (kg)	505.9 [622.4]	507.4 [627.5]	504.6 [617.8]
	Required Spherical Tank Diameter† (in)	22.8 [24.4]	22.8 [24.5]	22.8 [24.4]

*ΔV = 60 m/s for 3-Axis Upper Stages [ΔV = 200 m/s For Spinning Upper Stages]
**Solid OIM Used to Achieve 500 x 18015 km Altitude (12 hour Period) Mars Insertion Orbit
†Assuming Hydrazine Density = 1.04 kg/litre and 6 Tanks with 20% Initial Pressurant Volume

TABLE 4.2-8. DE-BASED MGO HYDRAZINE BUDGET - 8 HOUR PERIOD INSERTION ORBIT

#	Item Launch Year and Trajectory Type	1989 I	1990 II	1992 II
1	Hydrazine Used During Earth-Mars Transit*	48.1 [165.3]	49.0 [168.6]	46.2 [158.9]
2	Hydrazine for Periapsis Lowering** (kg) (500 → 350 km Altitude)	7.4	7.4	7.4
3	Hydrazine for Apoapsis Lowering** (kg) (12022 → 350 km Altitude)	346	346	346
4	Hydrazine for Approximately 3-4 yr Data Gathering Phase (kg)	25	25	25
5	Hydrazine to Raise S/C into 525 km Altitude Circular Orbit at EOL (kg)	22.3	22.3	22.3
6(=1+2+3+4+5)	Total Hydrazine Requirement (kg)	448.8 [566.0]	449.7 [569.3]	446.9 [559.6]
	Required Spherical Tank Diameter† (in)	21.9 [23.7]	21.9 [23.7]	21.9 [23.7]

*ΔV = 60 m/s for 3-Axis Upper Stages [ΔV = 200 m/s For Spinning Upper Stages]
**Solid OIM Used to Achieve 500 x 12022 km Altitude (8 hour Period) Mars Insertion Orbit
†Assuming Hydrazine Density = 1.04 kg/litre and 6 Tanks with 20% Initial Pressurant Volume

TABLE 4.2-9. DE-BASED MGO HYDRAZINE BUDGET - 3.5 HR. PERIOD INSERTION ORBIT

#	Item Launch Year and Trajectory Type	1988 I	1990 II	1992 II
1	Hydrazine Used During Earth-Mars Transit*	48.2 [165.9]	49.2 [169.2]	46.9 [161.4]
2	Hydrazine for Periapsis Lowering** (kg) (500 + 350 km Altitude)	10.1	10.1	10.1
3	Hydrazine for Apoapsis Lowering** (kg) (3841 + 350 km Altitude)	173.6	173.6	173.6
4	Hydrazine for Approximately 3-4 yr Data Gathering Phase (kg)	25	25	25
5	Hydrazine to Raise S/C into 52[illegible] Altitude Circular Orbit at EOL (kg)	22.3	22.3	22.3
6(=1+2+3+4+5)	Total Hydrazine Requirement (kg)	279.2 [396.9]	280.2 [400.2]	277.9 [392.4]
	Required Spherical Tank Diameter† (in)	18.7 [21.0]	18.7 [21.1]	18.7 [20.9]

*ΔV = 60 m/s for 3-Axis Upper Stages [ΔV = 200 m/s For Spinning Upper Stages]
**Solid OTM Used to Achieve 500 x 3841 km Altitude (3.5 hr. Period) Mars Insertion Orbit
†Assuming Hydrazine Density = 1.04 kg/l and 6 Tanks with 20% Initial Pressurant Volume

three Mars insertion orbits with subsequent maneuvers as described in later subsections of Section 4.2. In calculating the tables it was assumed that there would be six identical hydrazine tanks with an initial pressurant volume fraction of 20% (i.e., 5:1 blowdown ratio) and that the density of hydrazine is 1.04 kg/litre (which corresponds to 25°C).

It may be seen from Figure 4.2-11 that use of 22 inch diameter tanks will allow Mars insertion orbits of ∿ 8.25 hour period (15,816 km apoapsis radius) and ∿ 5.1 hour period (10,409 km apoapsis radius) for the missions featuring an IRU controlled and a spinning STS upper stage, respectively. Since the baseline STS upper stage is a spinner (Section 4.2.3) it will be considered herein that the largest Mars insertion orbit consistent within the baseline design has a period of ∿ 5.1 hours. In fact, though, further analysis in a later study could well show that the baseline ADACS scheme described in Section 4.2.4 will reduce the launch vehicle error correction ΔV allotment of 200 m/s and correspondingly enlarge the limiting Mars insertion orbit.

Table 4.2-4 shows that for a Mars insertion orbit with a period of 8 hours the MOI ΔVs are 1.207, 1.263 and 1.129 km/s for the three baseline missions and that these would be best performed by STAR 37S, 37S, and 30C OIMs, respectively. The corresponding ΔVs for an insertion orbit with a 3.5 hour period are 1.616, 1.672 and 1.538 km/s and the most suitable OIM is the STAR 37F in all three cases.

4.2.7 Drift Orbit Phase

Following MOI the stack of the spacecraft and spent OIM will be quickly despun to about 4 rpm using the on-board hydrazine propulsion system before significant nutation develops. The spin axis of the stack will then be precessed until it is normal to the orbit plane, so that the spacecraft orbits Mars in a cartwheel mode.

The requirement for an initial orbit phase angle of 45° slightly complicates the orbit achievement strategy if efficiency regarding propulsive energy is to be maintained. The baseline mission design incorporates a drift orbit phase following MOI so that in the Mars-Sun reference frame the insertion orbit will precess from its arrival value (see 4.2.6.1) to the specified 45° prior to achievement of the Sun-synchronous mission orbit, as described in Section 4.2.6.1. The drift periods are shown in Table 4.2-6.

Alternative schemes of achievement of the specified phase angle are more costly regarding propulsion requirements and, therefore, have been rejected. For example, a similar Earth-Mars transfer trajectory which results in an arrival periapsis phase angle of 45° features an injection from Earth orbit on 12 July 1988 and MOI on 22 December 1988. The value of V_∞ for this trajectory, however, is 3.376 km/s. This is much higher than the values of V_∞ of 2.666, 2.741 and 2.468 km/s for the baseline trajectories, shown in Table 4.2-1, and a correspondingly much greater retrovelocity maneuver of ∿ 2.6 km/s, instead of ∿ 1.1 to 1.3 km/s, would be required on arrival at Mars. Bearing in mind the large throw mass margins for the baseline trajectories described in Section 4.2.3 and illustrated in Figure 4.2-2, however, this option might be considered in a future study for MGO. Summary results of a ΔV budget analysis for the MGO mission using this less efficient, direct transfer trajectory are shown in Table 4.2-10.

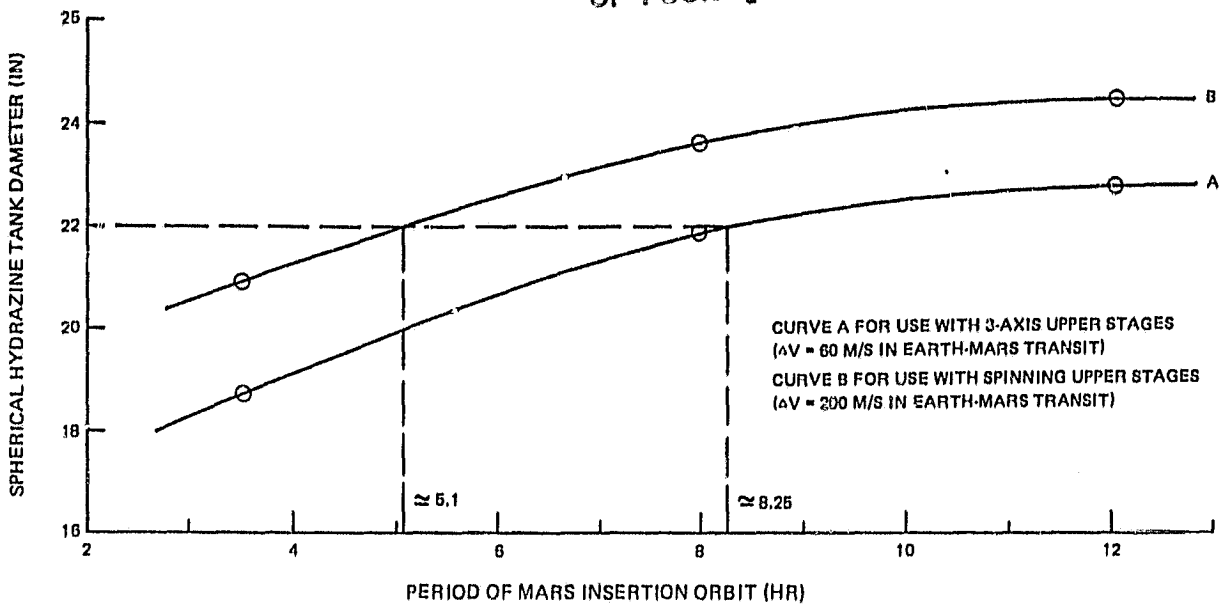

NOTES

- SOLID ROCKET MOTOR USED TO ACHIEVE ELLIPTICAL MARS INSERTION ORBIT WITH PERIAPSIS AT 500 KM ALTITUDE
- 6 SPHERICAL HYDRAZINE TANKS WITH 20% INITIAL PRESSURANT VOLUME
- END OF LIFE SPACECRAFT MASS = 651 KG (INCLUDING 71.5 KG MARGIN)

Figure 4.2-11. MGO Spherical Hydrazine Tank Diameter vs Period of Mars Insertion Orbit for the 1988 I, 1990 II, and 1992 II Launch Opportunities

Another inefficient route to arrive at the desired 45° periapsis phase angle involves first the utilization of the energy-efficient, baseline Earth-Mars transfer trajectories followed by the propulsive changing of the orbit phase angle. Fuller analysis would determine the optimum timing and magnitude of the required plane change maneuver(s). If the plane changing were performed following circularization of the insertion orbit to 500 km altitude, however, it is readily calculated that the required ΔV would be $\sim$ 5.8 m/s/degree.

For the baseline drift orbits (periapsis altitude of 500 km and periods in the range 3.5 - 8.25 hr approximately) the phase angle precession due to the motion of Mars around the Sun will be dominant, averaging $\sim$ 0.457 degree/day over Mars's significantly elliptical heliocentric orbit. The precession due to the oblateness of Mars (J_2 = 0.00197) for an orbit with inclination = 92.5°, periapsis altitude = 500 km and period = 24 hr is only $\sim$ 0.011 degree/day, and in the opposite direction as the heliocentric-orbit induced precession. The exact drift orbit periods necessary for the three baseline missions (assuming a periapsis altitude of 350 km and an orbit period of 24 hours) are shown in Table 4.2-6. It may be seen that, after arrival along the 1988 I baseline trajectory, the drift period following MOI on a North approach is seven days longer, at 130 days, than the 123 days required following MOI on a South approach. This is due to the difference in initial periapsis phase angle between arrival on the North and South approaches for an on-orbit inclination of 92.5°.

Figure 4.2-12 illustrates two high Mars orbits after 50 and 100 days from arrival along the 1992 II baseline trajectory with MOI on a North approach.

TABLE 4.2-10. MGO ΔV BUDGET FOR MISSION WITH 7/12/88 - 12/22/88 EARTH-MARS TRANSFER, FEATURING DIRECT MARS ORBIT INSERTION

Orbit	V_p(km/s)	V(km/s)	ΔV_{OIM}(km/s)	$\frac{M_{RSP}}{M_{PA}}$ (I_{sp}=300s)	ΔV_{AKF}(km/s)	ΔV_{PKF}(km/s)	ΔV_{circ}(km/s)	$\frac{M_{CSP}}{M_{NOM}}$ (I_{sp}=230s)
4 hrs/ell. @ 300 km p./(a=6081.8051 km)	4.0186835	5.8814351	1.8627516	0.4689734	0	0.6134025	0.6134025	0.2380407
12 hrs/ell. @ 300 km p./(a=12650.664 km)	4.4504391	5.8814351	1.430996	0.3850641	0	1.0451581	1.0451581	0.3707444
24 hrs/ell. @ 300 km p./(a=20081.678 km)	4.5890266	5.8814351	1.2924085	0.3554137	0	1.1837456	1.1837456	0.4082317
4 hrs/ell. @ 600 km p./(a=6081.8051 km)	3.795728	5.7314059	1.9356779	0.4819703	0.0485294 † (0.5853949)	0.5911851 (0.0658145)	0.6397145 (0.6512094)	0.2468747
12 hrs/ell. @ 600 km p./(a=12650.664 km)	4.2501932	5.7314059	1.4812127	0.3954678	0.0259216 (1.0398601)	1.0405917 (0.0658145)	1.0665133 (1.1056746)	0.3766720
24 hrs/ell. @ 600 km p./(a=20081.678 km)	4.3950995	5.7314059	1.3363064	0.3649571	0.01683 (1.1847664)	1.1815965 (0.0658145)	1.1988265 (1.2505809)	0.4121739
4 hrs/ell. @ 1000 km p./(a=6081.8051 km)	3.5291156	5.5584278	2.0293122	0.4981925	0.1108255	0.5595404	0.6703669	0.2570369
12 hrs/ell. @ 1000 km p./(a=12650.664 km)	4.0138819	5.5584278	1.5445459	0.4083383	0.0591813	1.0343224	1.0935037	0.3840837
24 hrs/ell. @ 1000 km p./(a=20081.678 km)	4.167014	5.5584278	1.3914138	0.3767375	0.0383976	1.179622	1.2180196	0.4171530
circ. @ 300 km	3.405281	5.8814351	2.4761541	0.5688808	0	0	0	0
circ. @ 600 km	3.2748749	5.7314059	2.456531	0.5659966	0.0645418	0.0658145	0.1303563	0.0561371
circ. @ 1000 km	3.1222362	5.5584278	2.4361916	0.5629868	0.1381898	0.1443236	0.2825134	0.1176892

NOTES:

V = Planetocentric-conic arrival velocity at phasetocentric radius R_p
R_p = Perigee radius of insertion orbit
V_p = Velocity @ periapsis of insertion orbit
a = semi-major axis of insertion orbit

p. = periapsis
ell. = elliptical (orbit)
circ. = circular (orbit)
V_∞ arrival = 3.3763 km/s

M_{RSP} = Retrostage (OIM) propellant mass
M_{PA} = Planetary approach mass
ΔV_{AKF} = ΔV for lowering periapsis of Mars insertion orbit to 300 km alt.
ΔV_{PKF} = ΔV for lowering the apoapsis of the intermediate orbit (=apoapsis of Mars insertion orbit) to 300 km alt.
ΔV_{circ} = ΔV to circularize insertion orbit to 300 km alt. ($\Delta V_{circ} = \Delta V_{AKF} + \Delta V_{PKF}$) Hydrazine burns have been considered impulsive, as an approximation
† = Figures in brackets show the ΔV's for the cases in which apoapses were lowered before the periapses

M_{CSP} = Circularization stage (hydrazine) propellant mass
M_{NOM} = Net S/C mass before firing hydrazine system

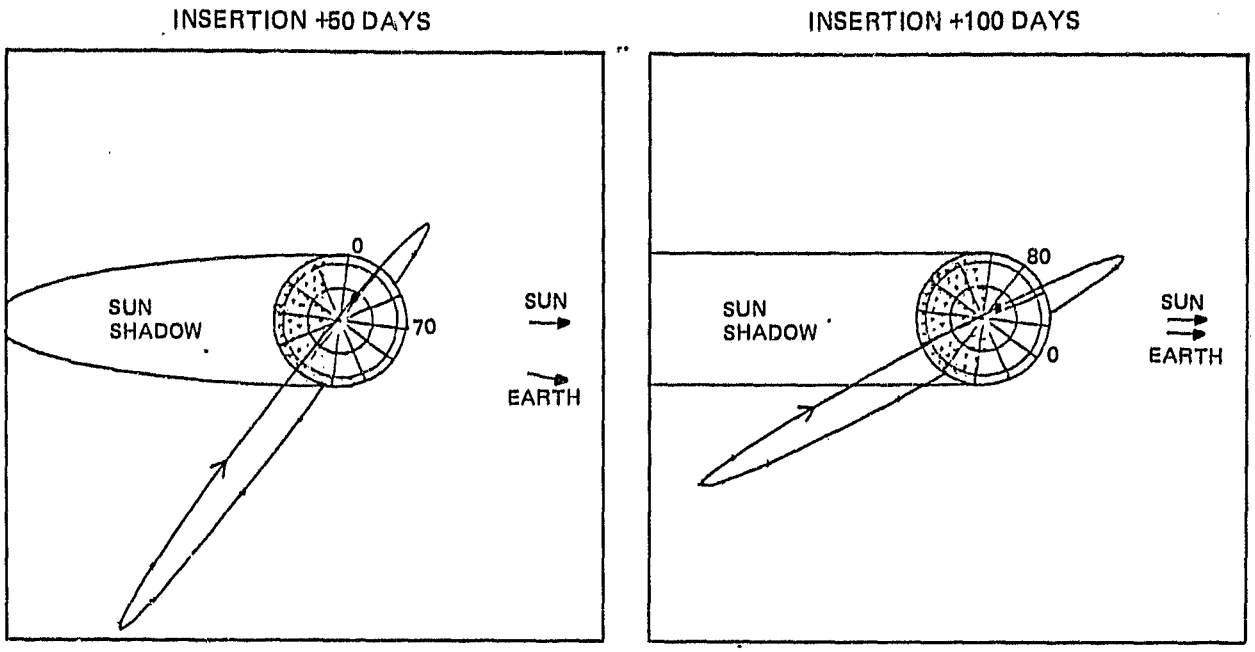

Figure 4.2-12. Mars Orbits after 50, 100 Days Viewed from North Pole - 1992 Type II (Insertion Via North Approach)

4.2.8 Planetary Quarantine

The task of baseline science accommodation in the spacecraft design is greatly simplified if the spent OIM is jettisoned. The NASA policy on planetary quarantine as applied to the MGO mission, however, requires that all passive space hardware around the planet must be left in orbits that will survive the expiration date of the policy as applied to the MGO mission, which is the end of the year 2018. The Mars insertion orbit is a candidate for storing the jettisoned spent OIM and instrument hatches and covers. Furthermore, the related MOI at 500 km altitude, described in Section 4.2.6, will more safely accommodate potential dispersions of the arrival trajectory arising from such causes as ephemeris errors than will MOI directly at the mission orbit altitude of 350 km.

A circular orbit at 525 km altitude is proposed in the baseline for the final storage of the spacecraft at the end of its mission life. A ΔV budget allowance of 90 m/s was specified for the purpose of this end-of-life orbit raising. Such high altitude circular orbits are the longest lived.

The determination of the stability of an orbit around Mars is a complicated process which must take into account several influencing factors. For example, third-body effects from the Sun and the planetary asphericity are significant contributing factors. For low orbits, atmospheric drag is important. The study of the orbital motion of a satellite of Mars grows rapidly in complexity as one tries to generalize the situation since the oblateness coefficient, J_2, is twice as large as the similar coefficient for the Earth.

Researchers in the field have shown that resonant situations between oblateness and long-period third-body effects can occur at several inclinations. The effect of this is to cause large variations in the periapsis altitude over short periods of time. A semi-analytic method of predicting the variation of a Mars orbit over long periods of time has been reported in the literature. It has been used to simulate the specific MGO baseline insertion orbit with periapsis at 525 km altitude, inclination of 92.6° and a period of 12 hours, and also to simulate the EOL orbit, circular at 525 km altitude at the same inclination. Fortunately, these orbits, selected for jettisoning the expended OIM and for EOL parking of the spacecraft, do not exhibit these resonances.

The results of simulations for a 525 km circular orbit are displayed in Figure 4.2-13. Variation of semi-major axis, eccentricity, and inclination remain well-bounded until at the earliest the year 2014, and should remain so well beyond 2018. Specifically, the eccentricity ranges between 0.003 and 0.014. There are slight high-frequency oscillations but nothing of significance which might cause orbit decay. Based on these simulations, it is concluded that the selected parking orbit is sufficiently stable to satisfy the NASA planetary quarantine policy requirements. On the other hand, elliptical orbits and circular orbits at around 300 km to 400 km altitude may decay too fast.

Results of the simulations for the elliptical orbit are illustrated in Figures 4.2-14 and 4.2-15. The difference between the two sets of simulation is that Figure 4.2-14 corresponds to a drag-free simulation while Figure 4.2-15 corresponds to the model for the atmosphere of Mars contained in "Models of Mars Atmosphere (1967)," NASA Space Vehicle Design Criteria (Environment), NASA SP-8011, December 1968, which may be considered to represent the extreme, worst case. Figure 4.2-15 indicates that the baseline Mars insertion orbit may not be stable until 2019, or may be only marginally stable. A more appropriate simulation in a follow-on MGO study should be able to clear this matter up. In any case the choice of jettisoning hardware in the insertion orbit rather than the EOL orbit would be virtually insignificant regarding the baseline mission design.

4.2.9 Mission Orbit Achievement

At the end of the drift orbit phase the insertion orbit will be circularized at 350 km altitude using the on-board hydrazine propulsion system. For this and subsequent adjustments to orbit altitude in the baseline design, the pitch control of the spacecraft will be employed to hold the radial hydrazine thrusters parallel or antiparallel to the orbit velocity. The orbit will be circularized by multiple apoapsis-pass and periapsis-pass retrofirings on-ground command. The associated total ΔV and hydrazine usage depend upon the size of the insertion orbit and may be read from the data presented in Tables 4.2-3 to 4.2-5.

Once the spacecraft is in the mission orbit, pitch lock will be obtained. The HGA will then be deployed and will acquire Earth pointing through initial, approximate pointing, commanded from Earth, followed by a raster search in pitch of the gimbal mount, at slowly changing gimbal pitch offset angle, until Earth lock is achieved. A backup acquisition mode will also be programmed into the spacecraft in case the acquisition command from Earth is not received. In this mode, the despin control system or the HGA gimbal pitch-control will be used to slowly rotate the HGA relative to inertial space. After the entire

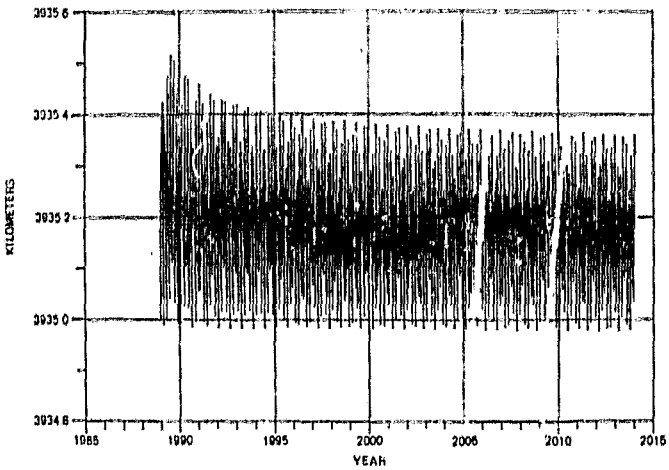

A. SEMI-MAJOR AXIS

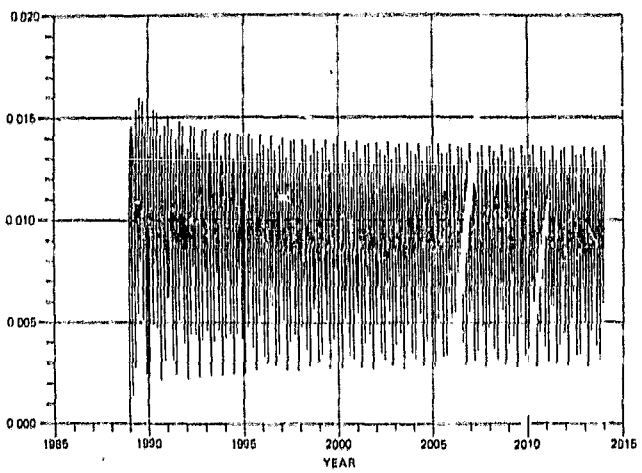

B. ECCENTRICITY

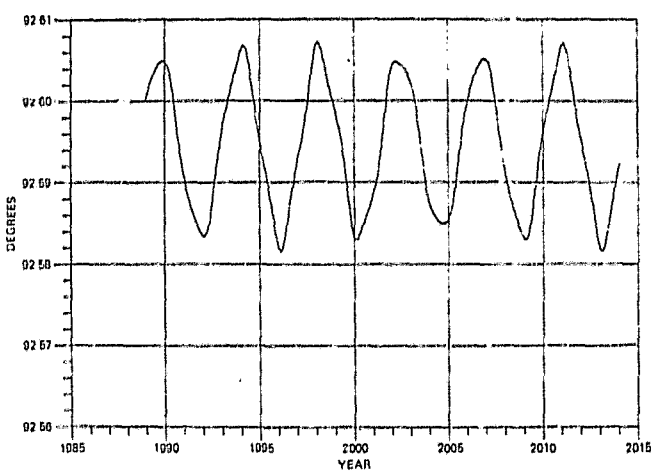

C. INCLINATION

Figure 4.2-13. Stability of Circular Orbit at 525 km Above Mars

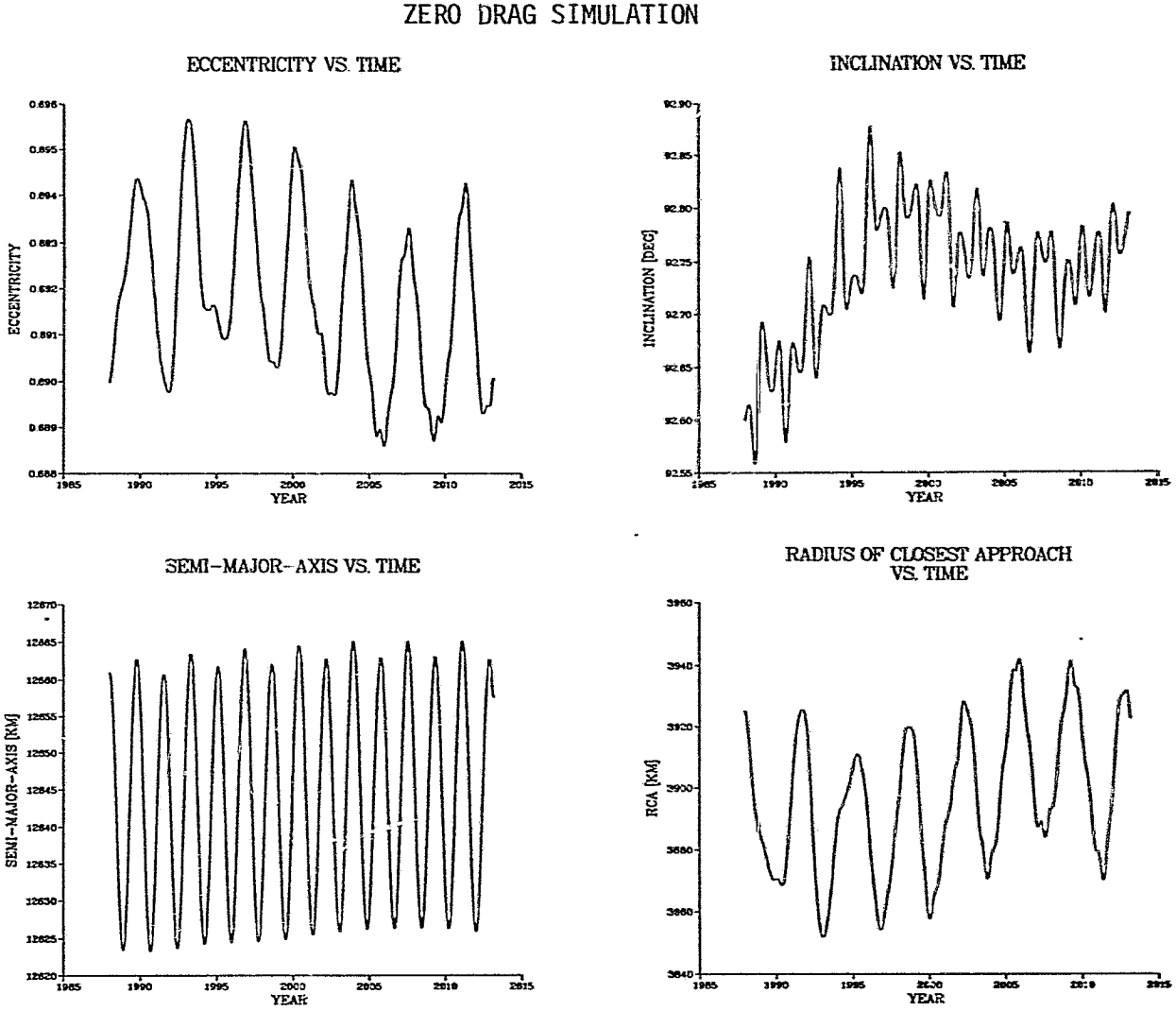

Figure 4.2-14. Evolution of 12 Hour Period Mars Insertion Orbit with 525 km Altitude Periapsis

MAXIMUM DRAG SIMULATION

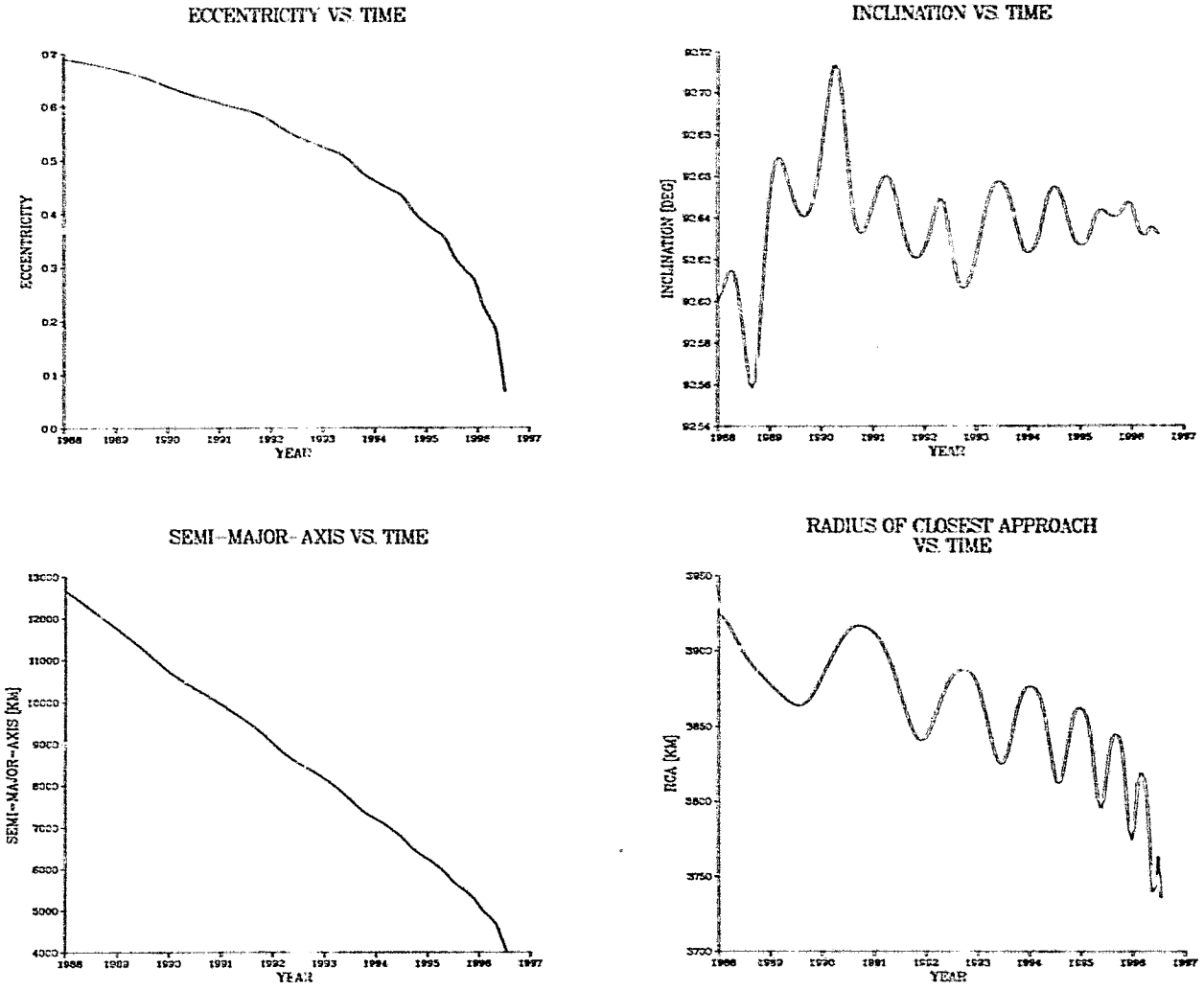

Figure 4.2-15. Evolution of 12 Hour Period Mars Insertion Orbit with 525 km Altitude Periapsis

cone has been searched for Earth signal, either attitude thrusters or the gimbal mount will increment the spin axis or the pitch offset angle, respectively, by approximately one antenna beam-width, and the new cone of rotation will be examined. The process will be continued until the HGA receives Earth signal. The pitch control system will then acquire lock with the spacecraft orbiting in the 1-rpo cartwheel mode. Using an antenna spin rate of 2 rpm and a beam width of 1.8° (X-band) or 6.6° (S-band), for a 1.5m diameter antenna, this search should ideally take at the most 100 or 28 minutes, respectively.

4.2.10 Mission Orbit Phase

The baseline mission orbit will be circular at 350 km altitude and approximately 93° inclination. It will, therefore, be approximately Sun synchronous.

Orbit and attitude maintenance during the one-year mission life will involve counteracting the small perturbations due to solar pressure, solar and lunar gravity, aerodynamic drag, RCS thrusting and the effects of the asphericity of Mars associated with terms of higher order than that of J_2 in the spherical harmonic expansion of the Mars gravitational potential. The spin or pitch axis will be precessed at the average rate of one revolution per 687 days (one Mars year) by precession thrusting in order to maintain its alignment with the normal to the Sun synchronous orbit. In fact, these effects will only be corrected insofar as they affect the attitude control of the spacecraft, or overly reduce the coverage of the surface of Mars by the scientific instrument; otherwise they will be allowed to accumulate.

Since the orbit inclination will be $\sim$ 93°, for any sensor there would eventually be total latitudinal coverage of Mars for latitudes L, where L <87°; i.e., the 3° polar caps will not be passed over directly. In the nominal one year of mission, however, there will be 4541 orbits at 350 km altitude. If orbit control were possible, so that no two sensor swaths overlapped at the Equator, then full coverage at the sunlit Equator could be achieved with a swath width of 4.70 km, i.e., 0.079° or 1.38 milliradians subtended at the center of Mars. This is narrower than the narrowest swaths of the baseline sensors, i.e., 4.0 x 0.2 milliradians for the MSM and 5 milliradians for the laser altimeter. Such perfect swath control is extremely unlikely, even if possible, and the most practical solution to maximizing surface coverage might well be to trim the orbit inclination, perhaps several times during the mission, according to the results of simulations, and to extend the mission life as much as possible. Inclination and node trims can be achieved propulsively for ΔV = 59 m/s per degree, which corresponds to an expenditure of hydrazine of 18 kg/degree for a 700 kg spacecraft (i.e., beginning of life, as in Tables 4.2-3 to 4.2-5) and 15 kg/degree for a 600 kg spacecraft. A detailed orbit-control simulation might be a subject for a follow-on MGO study.

Since in the baseline design the full capacity of the spacecraft for hydrazine storage has already been utilized (see Tables 4.2-7 to 4.2-9 for example), the use of hydrazine for inclination or node control would further decrease the size of the largest possible Mars insertion orbit (see Section 4.2.6.2) and a corresponding, slightly larger mass of propellant would be required for the OIM. In view of the large throw mass margins for the baseline mission using the STS/IUS-1 launch system (see Section 4.2.3), however, this scheme is certainly feasible.

Plots of the histories of several pertinent spatial and geometrical relationships in the mission phases for the three baseline missions, relating the

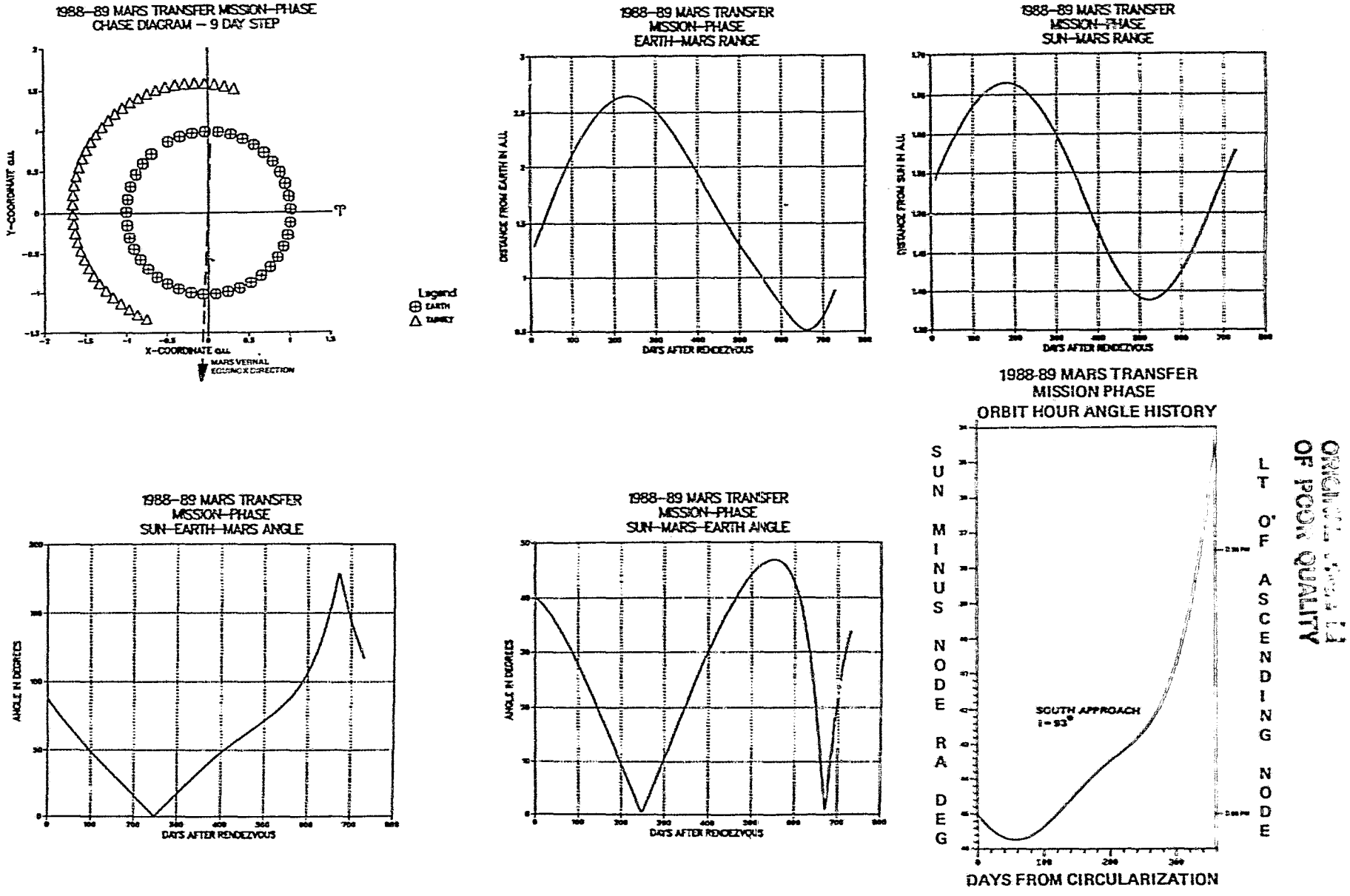

Figure 4.2-16. 1988 I Earth-Mars Transfer-Mission Phase Geometry

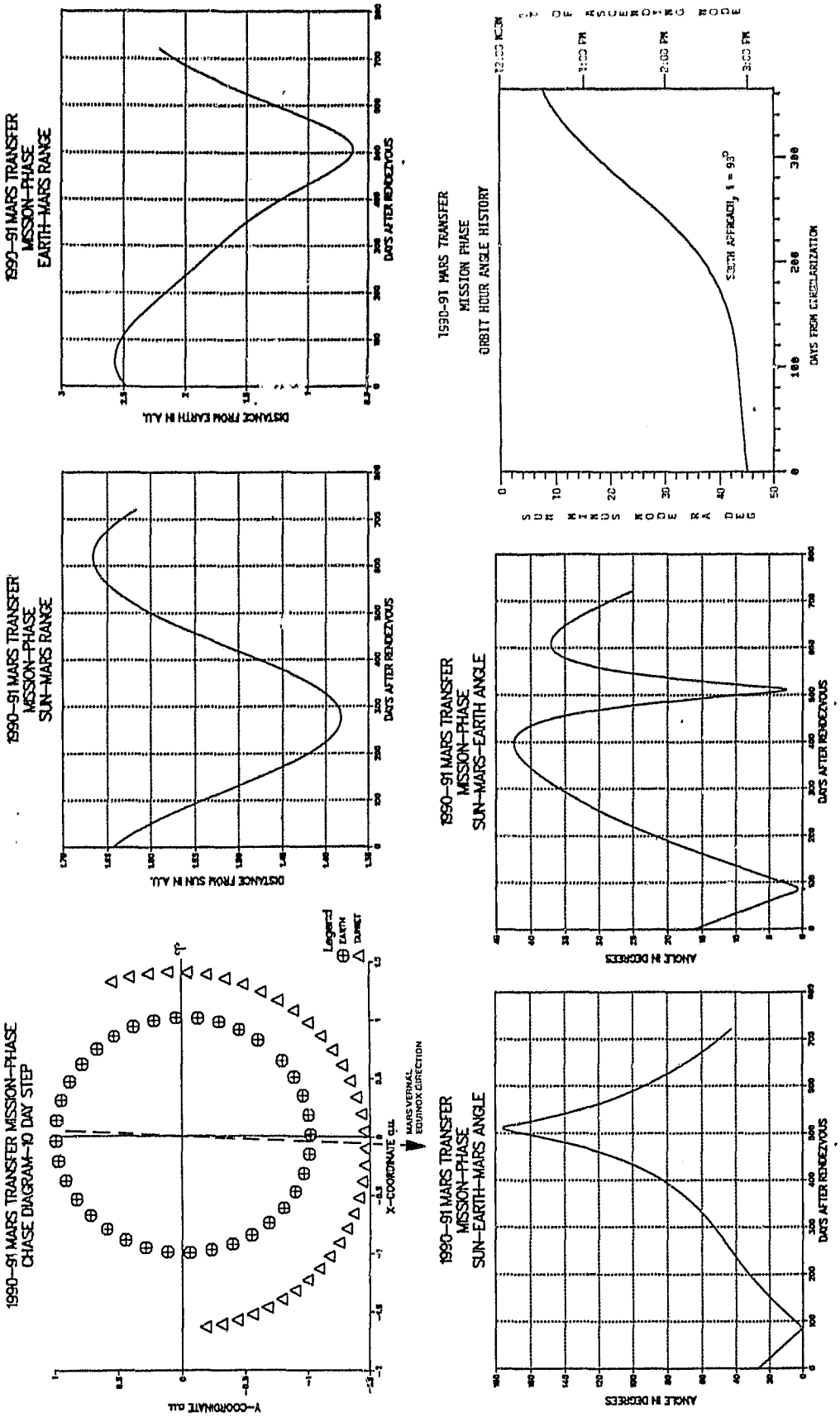

Figure 4.2-17. 1990 II Earth-Mars Transfer--Mission Phase Geometry

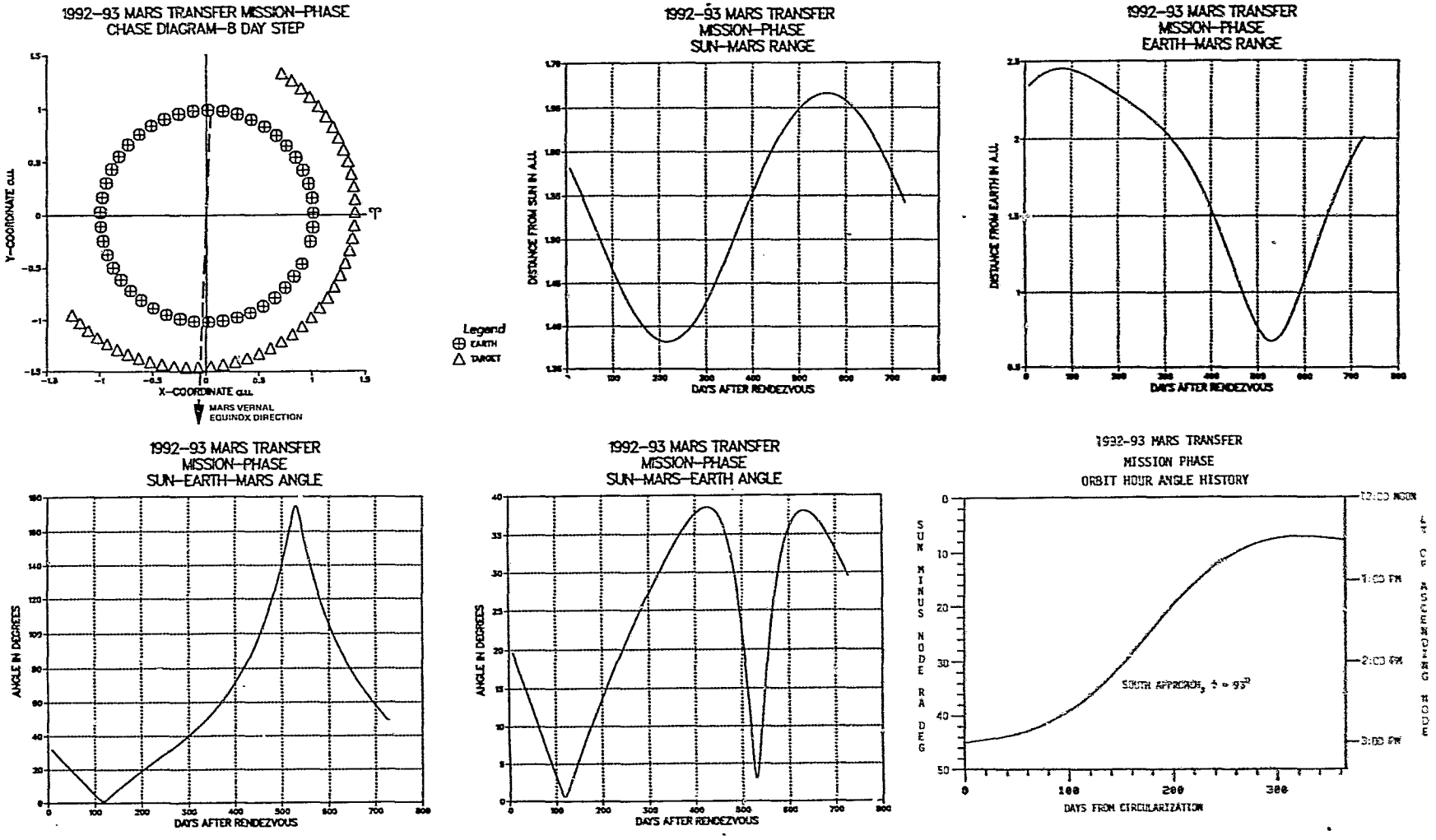

Figure 4.2-18. 1992 II Earth-Mars Transfer-Mission Phase Geometry

time-changing geometry between the spacecraft, Mars, the Earth and the Sun, are shown in Figures 4.2-16 to 4.2-18. The heliocentric plots in these figures are very useful in aiding visualization of the relative orientation of the spacecraft to these celestial bodies and of the bodies to each other. The information shown graphically has been incorporated into the analyses of the communications, thermal and power subsystems described in Sections 8, 9 and 10.

It may be seen from the figures that opposition occurs approximately 250, 80 and 120 days after MOI for the 1988 I, 1990 II and 1992 II baseline missions, respectively. It may be seen from Table 4.2-6 that the mission phases begin after drift-orbit periods of ∿ 130, 23 and 61 days, respectively. The oppositions, therefore, occur approximately 120, 57 and 59 days after the beginning of mission life in the 350 km altitude orbit. Consequently, a short shutdown-period, typically of the order of 30 days, as in the Viking missions, will be unavoidable. Temporal relationships between the different orbit phases, the seasons, seasonal effects such as dust storms, and other heliocentric-orbit features such as perihelion are shown in the baseline orbital-phase timelines in Figures 4.2-19 to 4.2-21.

The evolution of the orbit phase angle through the mission is also shown in Figures 4.2-16 to 4.2-18. The initial value at circularization of the insertion orbit is 45°, by definition, and corresponds to local times of the ascending node of 1500 hours for South approaches and 0300 hours for North approaches. It may be seen that for all three baseline missions the orbit plane precesses towards the noon-midnight sectors following circularization, as preferred in the mission specifications. The precession rate might well be speeded up for the 1988 I mission by selecting a lower value of inclination than the baseline value of 93°. On the other hand, at the end of the nominal one-year mission, the ascending and descending nodes for the 1990 II and 1992 II missions will be within 30 minutes of local noon or midnight, for the baseline value of inclination of 93°.

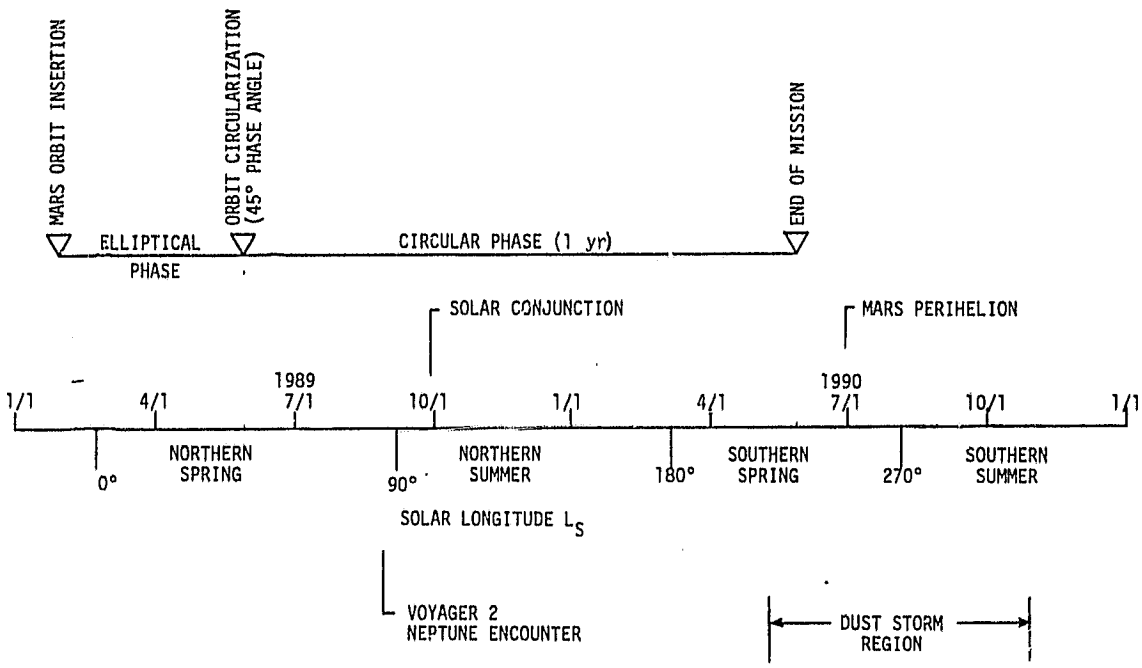

Figure 4.2-19. Orbital Phase Timeline - 1988 Type I

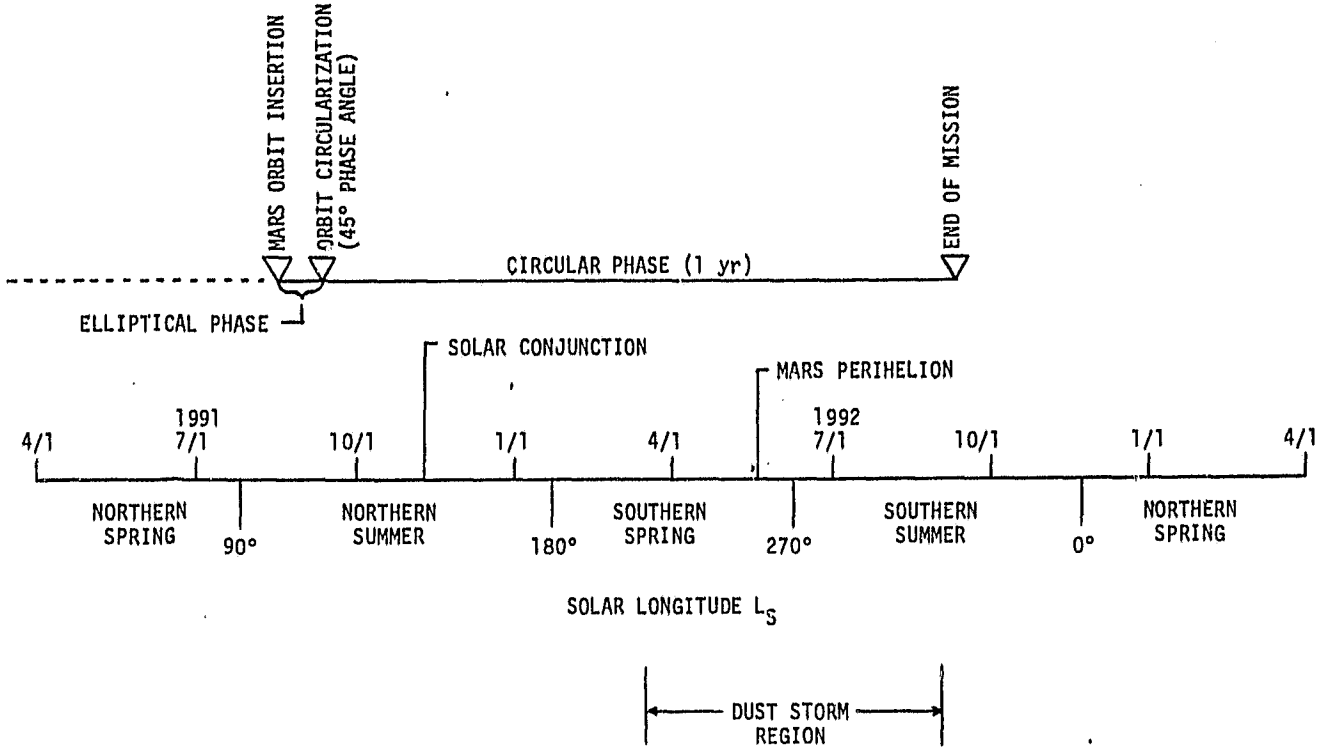

Figure 4.2-20. Orbital Phase Timeline - 1990 Type II

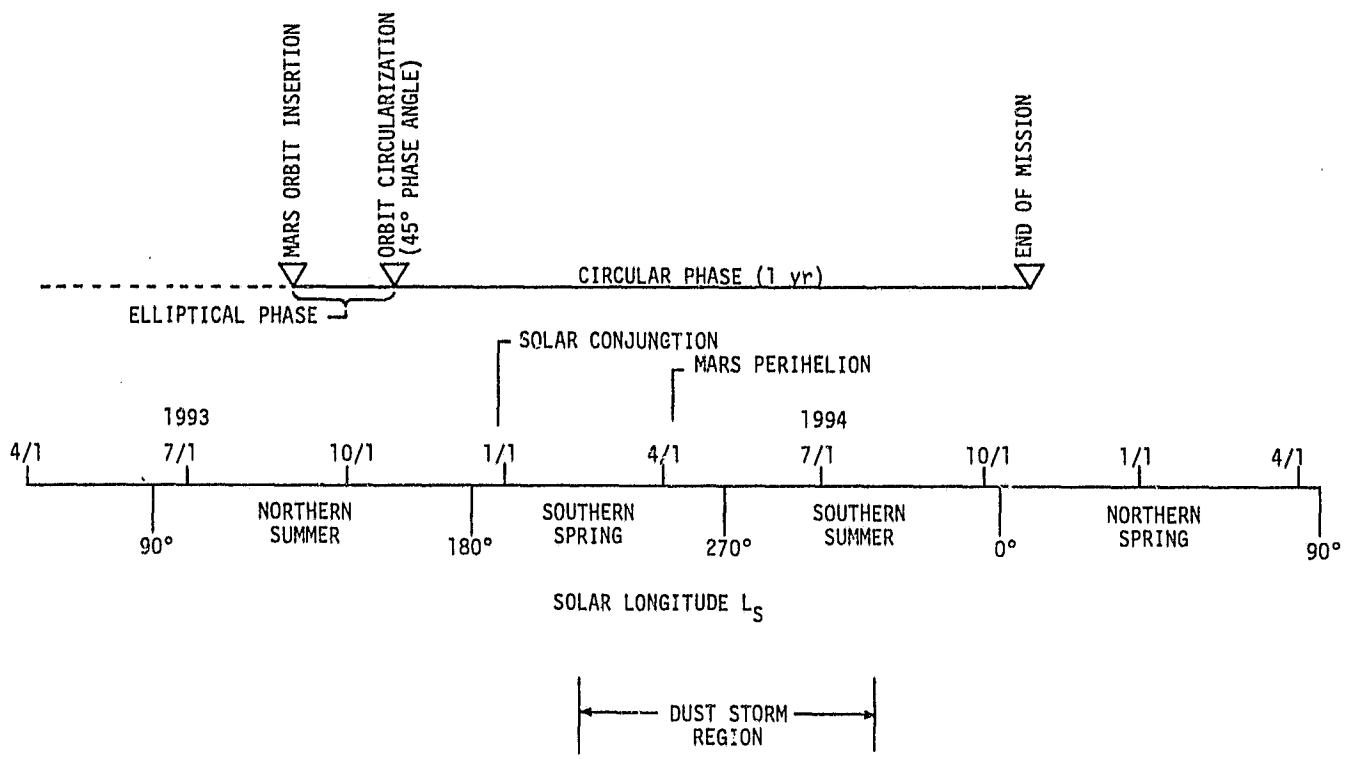

Figure 4.2-21. Orbital Phase Timeline - 1992 Type II

It may be seen from the orbit geometry that the HGA tracking will consist of rotation of the dish about the pitch axis at 1 rpo, with a roll-yaw offset which varies slowly from day to day. The roll-yaw offset, measured with respect to the orbit normal, may be referred to as the antenna offset angle. The evolution of the antenna offset angle for the three baseline missions for both North and South approaches is shown in Figure 4.2-22. The ranges shown are all within the capability of the gimbal-mount design when used together with temporary spacecraft reorientation by pitch offset control as necessary.

The solid angle swept by the HGA axis through the mission during Earth-communications operations for one year is approximately 8 steradians for the baseline missions. A similar example, corresponding to a slightly different baseline mission orbit commencing 1/17/89 and lasting for two years with ascending node at 1945 hours local time, is shown in Figure 4.2-23. The dots in the figures show sample traces of the locus of the end of the unit pointing-vector with respect to the spacecraft axes. The zenith lies in the direction of the positive radial axis. Unit circles in the radial and orbit-normal (yaw-pitch) plane and the velocity and orbit-normal (roll-pitch) planes are also shown, to facilitate interpretation. The similar figure corresponding to a 0745 local time ascending node is the mirror image of Figure 4.2-23 in the orbit plane. The baseline design for the mounting of the HGA accommodates pointing of the dish for all appropriate orbit hour angles and Earth-Mars orientations, as well as its stowage for launch. In order to ensure clearance of the spacecraft body by the HGA beam, the spacecraft may have to be temporarily flipped through 180° in pitch prior to communication, for some Earth-Mars orientations.

If the mechanism for effecting rotation of the HGA about the pitch axis (thus maintaining Earth-pointing against the pitch rotation at 1 rpo) were to fail, Earth-pointing could still be easily achieved by maintaining the appropriate programmable body pitch offset using the attitude control subsystem.

Occultation of the Earth by Mars will occur for those HGA pointing directions at angles greater than $\sim$ 115° away from the local zenith. As the relative orientations of the Sun, the Earth and Mars change through the mission, the length of time per orbit during which the Earth is eclipsed by Mars as seen from the spacecraft will also change. The histories of this eclipse duration for the three baseline missions are shown in Figure 4.2-24 for both South and North approaches. It may be seen that the longest time per orbit that the spacecraft is out of view of the Earth is $\sim$ 43 minutes, i.e., $\sim$ 37 percent of the 116 minute orbit period. This presents no problems regarding opportunities to transmit data gathered between down links.

4.2.11 End of Mission-Life

In the baseline mission design, the mission phase will be ended by raising the 350 km altitude orbit to approximately 525 km altitude using the on-board hydrazine RCS. This will be achieved over several orbits each involving a slight raising. The necessary total ΔV will be $\sim$ 76 m/s which corresponds to the usage of $\sim$ 22.3 kg of hydrazine for the baseline spacecraft design (EOL mass = 651 kg) as shown in Tables 4.2-3 to 4.2-5. It has already been shown in Section 4.2.8 that this orbit will be stable until, at the earliest, the end of the current NASA policy on planetary quarantine for the MGO mission, the end of the year 2018.

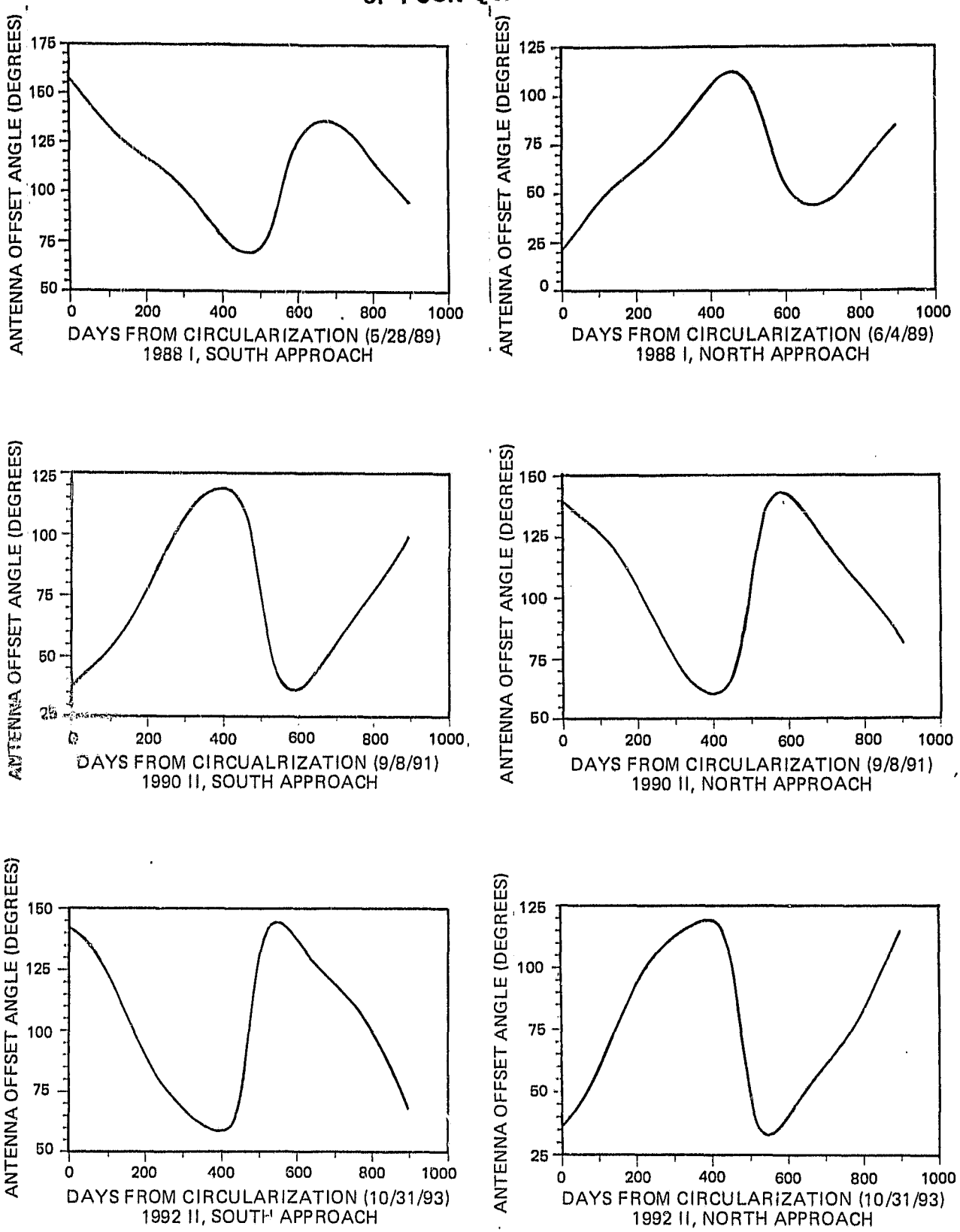

Figure 4.2-22. Evolution of Antenna Offset Angle

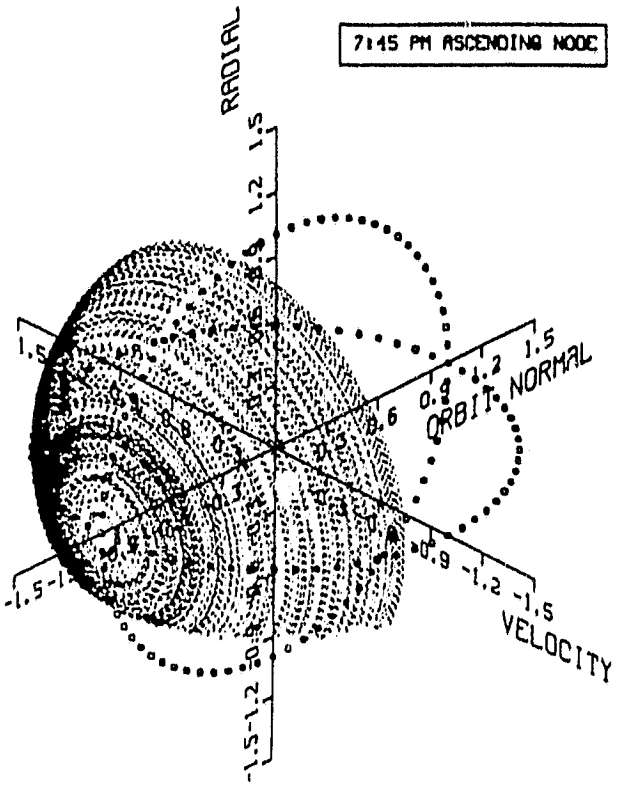

Figure 4.2-23. Example of Solid Angle Swept by HGA Axis during Earth Communication Opportunities for Two Years From 1/17/89

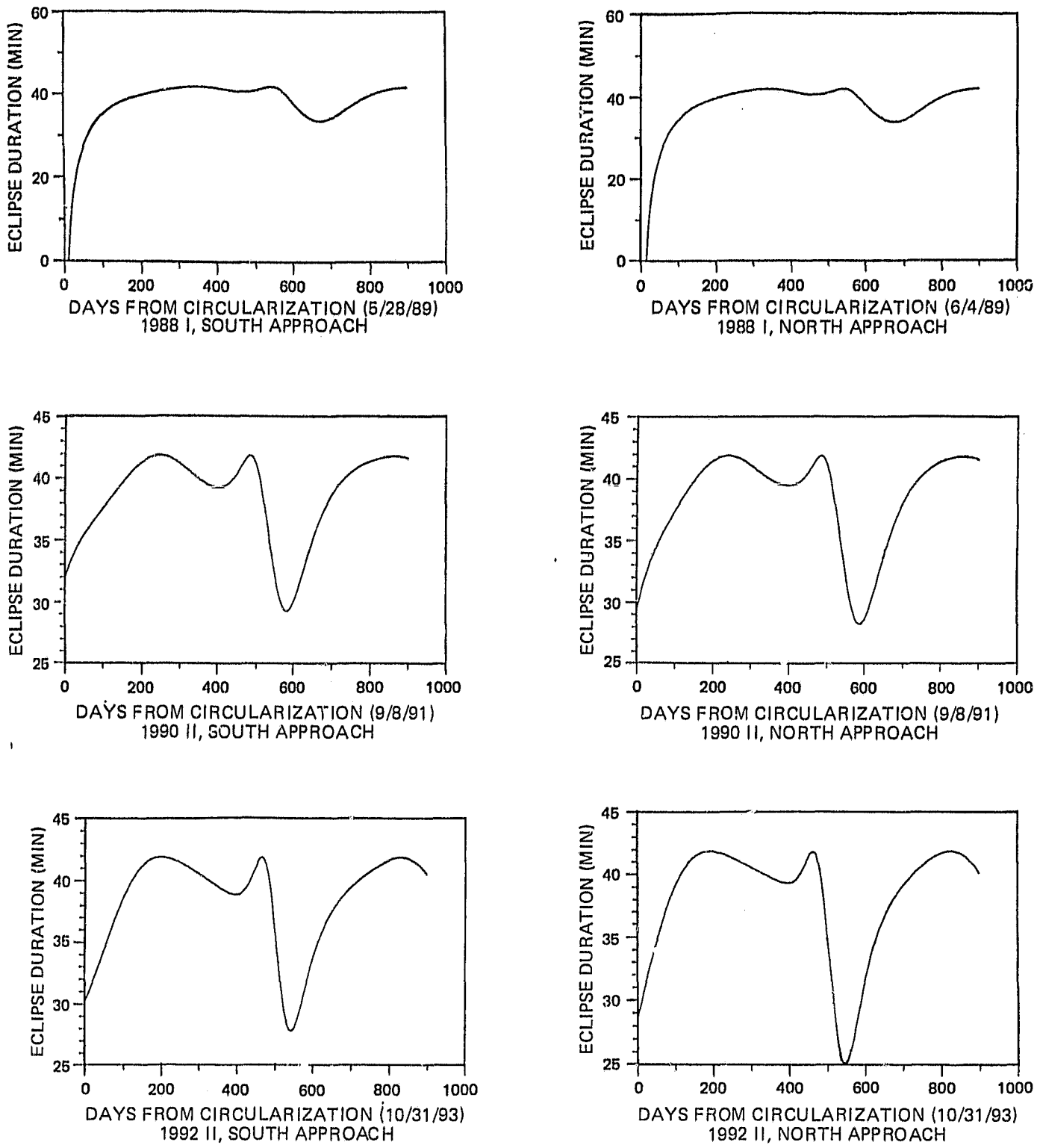

Figure 4.2-24. History of Earth Occultation Duration

4.3 LGO MISSION ANALYSIS

4.3.1 Orbit Achievement Outline

The highlights of the orbit achievement outline for the baseline LGO mission are shown in the mission timeline presented in Figure 4.3-1. This timeline presents a baseline sequence of mission events from lift-off through the end of the mission, which will be one year after lunar orbit insertion. Although the level of the detail is limited at this stage of mission planning, such a timeline is a good starting point from which to develop a comprehensive mission plan. It presents all anticipated mission maneuvers in a logical sequence and incorporates the assumptions made in Section 4.3, where appropriate.

The launch phase of the mission will consist of boost from the Kennedy Space Center by a Delta 3920 or the Shuttle, followed by injection into the translunar trajectory by a PAM-D or PAM-D2 upper stage, respectively. The launch energy, C_3, necessary for an Earth-Moon transfer is negative due to the ellipticity of the orbit of the Moon around the Earth, varying between approximately -2.1 and -1.9 km^2/s^2.

The momentum wheel will be spinning throughout the mission, with the body rate reduced to a very low rate following translunar injection, so that gyroscopic stiffness is high and nutation will not become significant during the transfer phase. Following launch, attitude determination and control will be performed by the spacecraft using the star sensors, sun sensors, gyro-package, momentum wheel and the onboard RCS thrusters.

The JPL specified allowance of 100 m/s has been made for launch vehicle error corrections and mid-course maneuvers for lunar targeting.

In the baseline mission design there is a choice available between an all-hydrazine on-board RCS and a hybrid solid plus hydrazine system. The all-hydrazine option was incorporated into the baseline design late during the current LGO study but is the preferred option. The feasible hybrid option has been left in as part of this study report.

Use of an all-hydrazine RCS will allow deployment and calibration of the gamma ray spectrometer along the Earth-Moon transfer trajectory.

If a solid lunar orbit insertion motor is used, the injection stack will be spun-up to $\sim$ 60 rpm using the hydrazine RCS just prior to the lunar orbit insertion (LOI) maneuver.

The LGO will be injected into a lunar insertion orbit using either a solid OIM or the hydrazine RCS. If the hybrid RCS is used, the baseline insertion orbit will be 100 x 4000 km altitude. If the all-hydrazine RCS is used, the baseline insertion orbit will be nominally identical with the mission orbit, i.e., circular at 100 km altitude, although an elliptical insertion orbit for calibration of the gamma ray spectrometer could be included in the baseline mission design if desired.

The approach assymptote will take the insertion stack either under the South Lunar Pole or over the North Lunar Pole so that a near-polar orbit, probably at an inclination of 85° or 95°, can be established without any plane change being performed on arrival at the Moon. For the mission orbit, which is

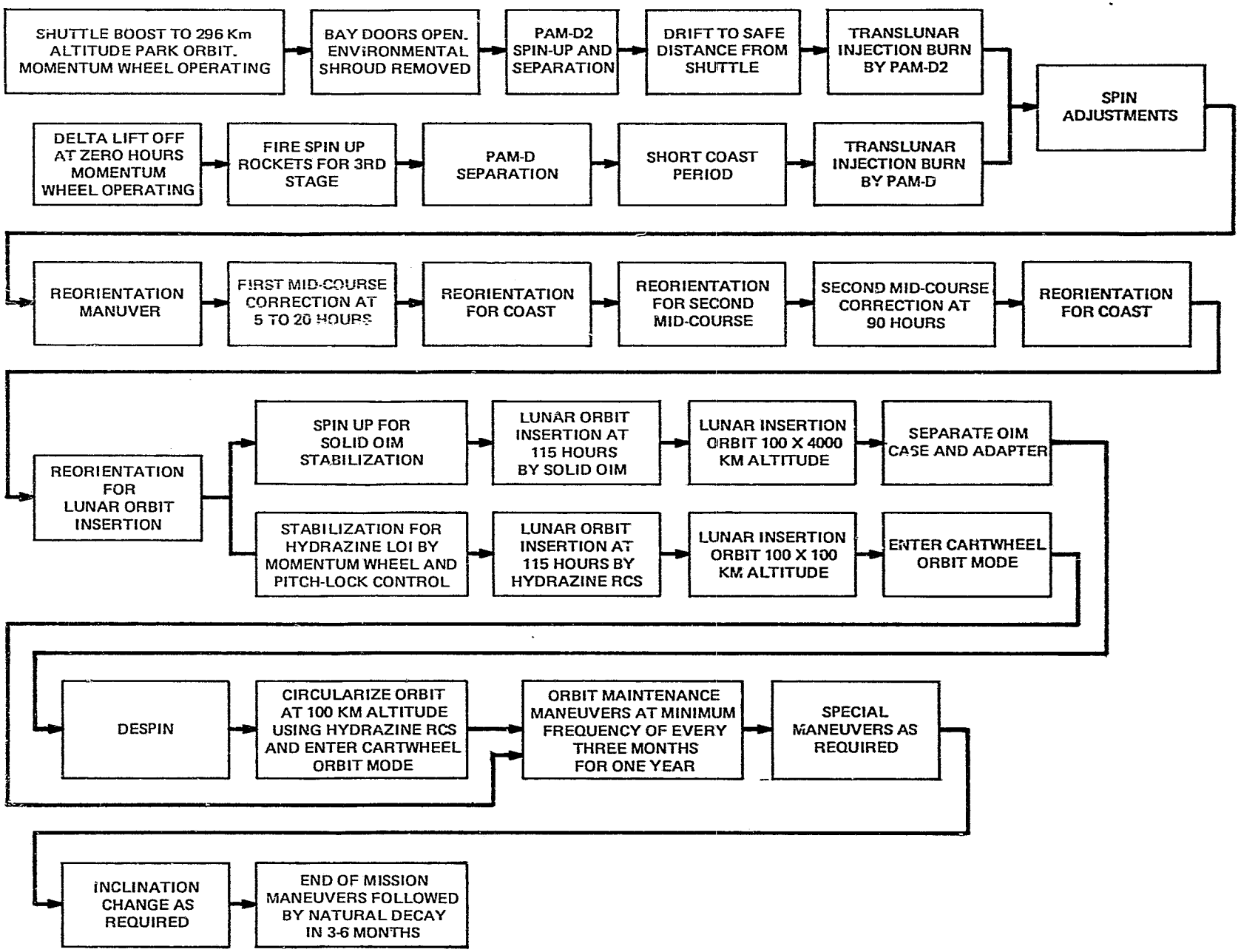

Figure 4.3-1. LGO Baseline Mission Events and Timeline

circular at 100 km altitude, an inclination within several degress of 90° is undesirable since instabilities become amplified and orbit eccentricity builds up rapidly in such an orbit.

No relay satellite is included in the baseline mission design as there was in earlier lunar orbiter proposals. Communications and tracking using Earth ground stations, therefore, will be limited to line of sight situations during the entire mission.

If a hybrid RCS is used, an additional sequence of operations will be necessary. Following LOI, the spacecraft will be quickly despun and the spent OIM separated and allowed to impact the lunar surface as a result of natural orbit decay. The spacecraft will then be precessed using the on-board hydrazine RCS so that it orbits in the cartwheel mode. Following LOI, the gamma ray spectrometer and magnetometer booms will be deployed and the spectrometer calibrated at the high altitude of the apolune. The hydrazine RCS will then be used on successive perilune passes to circularize the orbit at 100 km altitude.

Perilune passage will probably occur over the far side of the Moon. It may not be possible, therefore, to monitor the injection and circularization maneuvers as they are performed.

In the baseline plan, the mission-phase orbit will be maintained nominally at 100 km altitude for one year. The ΔV incorporated into the baseline mission design for this purpose is the JPL-specified 100 m/s.

In the mission orbit, the spacecraft will orbit in the cartwheel mode, spinning at 1 rpo so that the imaging sensors will be held pointing continuously towards the nadir. Since the orbit inclination will probably be about 5° away from exactly polar, the spacecraft will not pass directly over the polar caps.

The extensive lunar orbiter mission studies that have been performed in the past have been reviewed. Table 4.3-1 is presented as a summary comparison of the current baseline mission design with the previous mission designs, which were proposed by GSFC (1975), JPL (1977) and ESA (1979). References for these earlier studies are provided at the bottom of the table.

4.3.2 Launch Window and Earth-Moon Trajectory Selections

Typical flight profiles for the LGO spacecraft are depicted in Figures 4.3-2 and 4.3-3. The transfer time for the most efficient Earth-Moon transfers is approximately 115 hours, i.e., 4 days, 19 hours. In such a transfer the LGO will move in a single plane. Thus, the initial Earth orbit and trans-lunar planes must be coincident and, at least approximately, contain the Moon at arrival. For a given launch azimuth, an inertial orientation of the Earth orbit is a function only of launch timing. Thus, on any given day there are two instances in which the parking orbit plane contains the Moon. The launch window can be lengthened by widening the range of launch azimuths, but the cost is an increase in required ascent energy.

The inclination of the transfer plane to the plane of the orbit of the Moon about the Earth is a function of the Moon's declination and the launch azimuth. The maximum and minimum inclinations occur when the Moon is on its descending and ascending nodes on the Earth's Equator, and the inclinations are approximately equal when the Moon is near its maximum or minimum declination with respect to the Earth's Equator. During 1988, the inclination of the Moon's

TABLE 4.3-1. COMPARISON OF LUNAR POLAR ORBITER MISSION PLANS BY GSFC (1975), JPL (1977), ESA (1979) and RCA (1982)

Feature	GSFC	JPL	ESA	RCA
Orbit Achievement Strategy	Independent targeting of LPO and Relay (each using own solid retro for insertion)	Insert stack into Relay orbit using retro. Separate and lower LPO using N_2H_4 RCS.	(1) Insert stack into elliptical polar Relay orbit using restartable bipropellant RCS on Polo to separate and lower Polo; or (2) Independent targeting of Polo and Relay (each with own bipropellant RCS); or (3) As in (1) but Relay maneuvers to circular orbit of 7000 km alt and 70° inclination using N_2H_4 RCS.	Single spacecraft mission (i.e., no Relay)
Launch Energy considered in Reference, C_3 (km^2/s^2)	-2.15 to -1.93	-2.1 to -1.9	?	-2.1 to -1.9
LPO/Polo Orbit	• 150 km mean alt. nominally circular (period 123 min.) • 85° - 95° inclination • Passes within ±1° of all points on surface twice per month	• 100 km alt. nominally circular (period 118 min.) • 95° inclination • Nodal Rate 1.1°/rev westwards • 14-day repeat	• 100 km alt. nominally circular with decay to 50 km x 150 km alt. allowed before correction • 85° - 95° inclination	• 100 km alt. circular maintained by frequent RCS thrusting, or 100 km alt. nominally circular with decay to 50 x 150 km allowed before correction • 85° - 95° inclination
Relay Orbit	• 5000 km alt., circular • 10° - 15° inclination	• 100 km x 3424 km alt. • 95° inclination • 5.3 hr. period	• Elliptical with apolune at 7000 km alt. and polar inclination for strategy (1) above • Circular at 7000 km alt. and with 70° inclination for strategies (2) and (3) above	Not applicable

TABLE 4.3-1. COMPARISON OF LUNAR POLAR ORBITER MISSION PLANS BY GSFC (1975), JPL (1977), ESA (1979) and RCA (1982) (Continued)

Feature	GSFC	JPL	ESA	RCA
Separated Mass (kg) with Breakdown	495 using Delta 2914 Launch Vehicle • 285.4 – LPO (incl. 6.2 kg stationkeeping N_2H_4) • 72.4 – Relay • 95.5 – LPO solid retro propellant • 17.6 – Relay solid retro propellant • 24.1 – Orbit Achievement N_2H_4	482 using Delta 2914 Launch Vehicle • 297 – LPO, dry • 28 – Relay • 69.5 – Solid propellant • 87.5 – N_2H_4 + pressurant	1087* using Ariane I + 4th stage (leaving 63 kg reserve capability) • 493 – Polo • 102 – Relay • 430 – Bipropellant • 42 – N_2H_4 • 20 – Polo-Relay adapter	See Table 4.3.3-1 for optional mass budgets with the Delta 3920/ PAM-D or STS/PAM-D2 launch systems
Launch Vehicle Error Correction (m/s)	84 (99% probability)	83	Not Specified	100 (including targeting maneuvers)
LPO-Retargeting Correction following Separation from Relay (m/s)	25.4	N.A.	Not Specified	N.A.
Final LPO Trajectory Correction (m/s)	7	Not Specified	Not Specified	Included in 100 m/s allowance for launch vehicle error correction (probably ~7 m/s)
Retrovelocities (m/s)	820 – LPO (mostly or all by a solid, but perhaps 50 m/s by LPO N_2H_4 RCS) 620 – Relay (solid)	458 (solid inserts stack into Relay orbit) 357 (N_2H_4 RCS lowers LPO)	Not Specified	See Table 4.3.3-1 for options
LPO Stationkeeping ΔV (m/s)	50	50	For 1 year (not specified)	100
Reference	GSFC Interim Technical Report X-703-75-141 (1975)	JPL Report 77-51, Vol. IV, (1977)	ESA Assessment Study SCI (79)7, (1979)	This Report

*Figures given here are for strategy (3), though strategies (1) and (2) would be designed to give a 63 kg reserve in throw mass too.

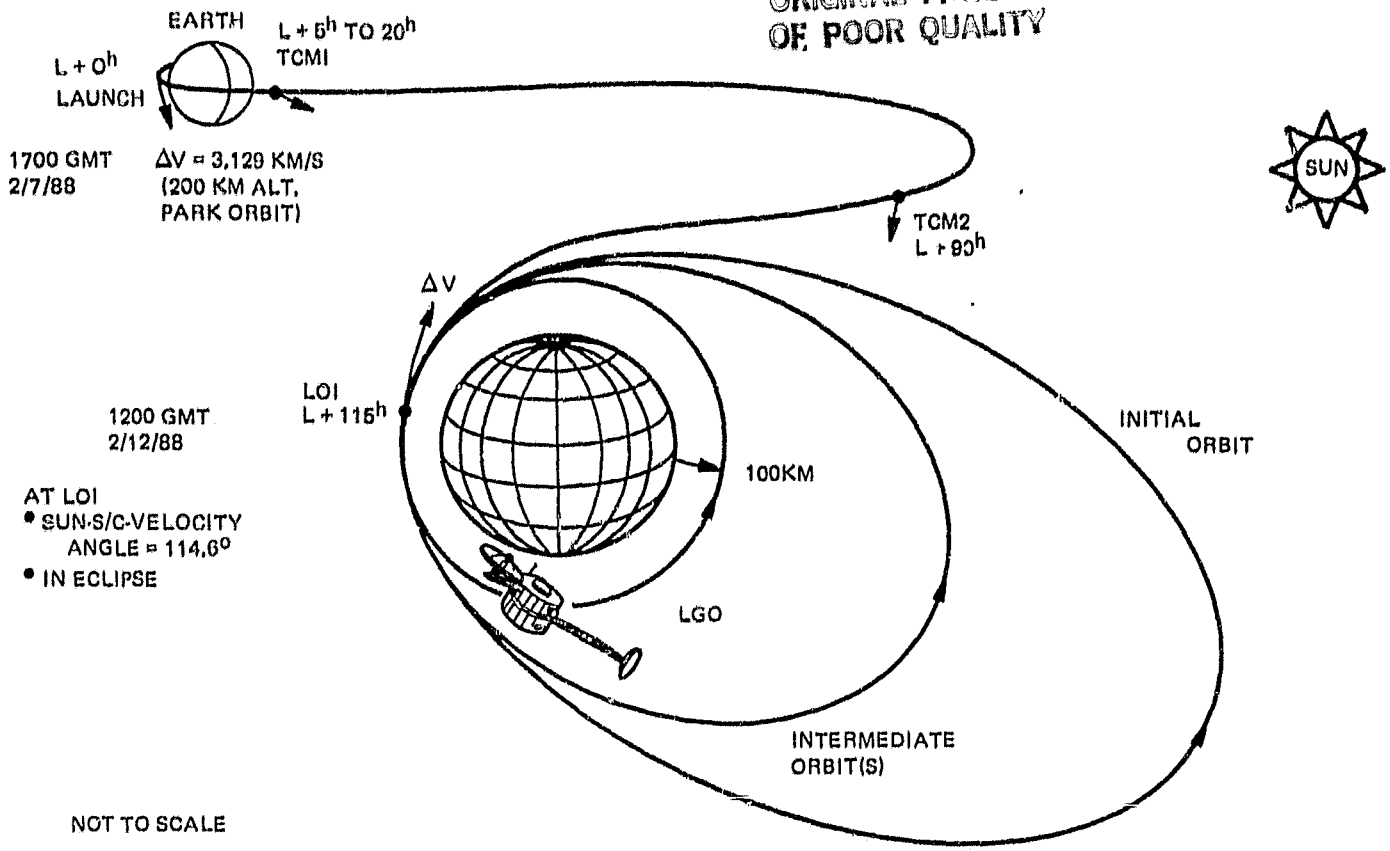

Figure 4.3-2. LGO Orbit Achievement Sample Case - Arrival 1200 GMT 21/12/88

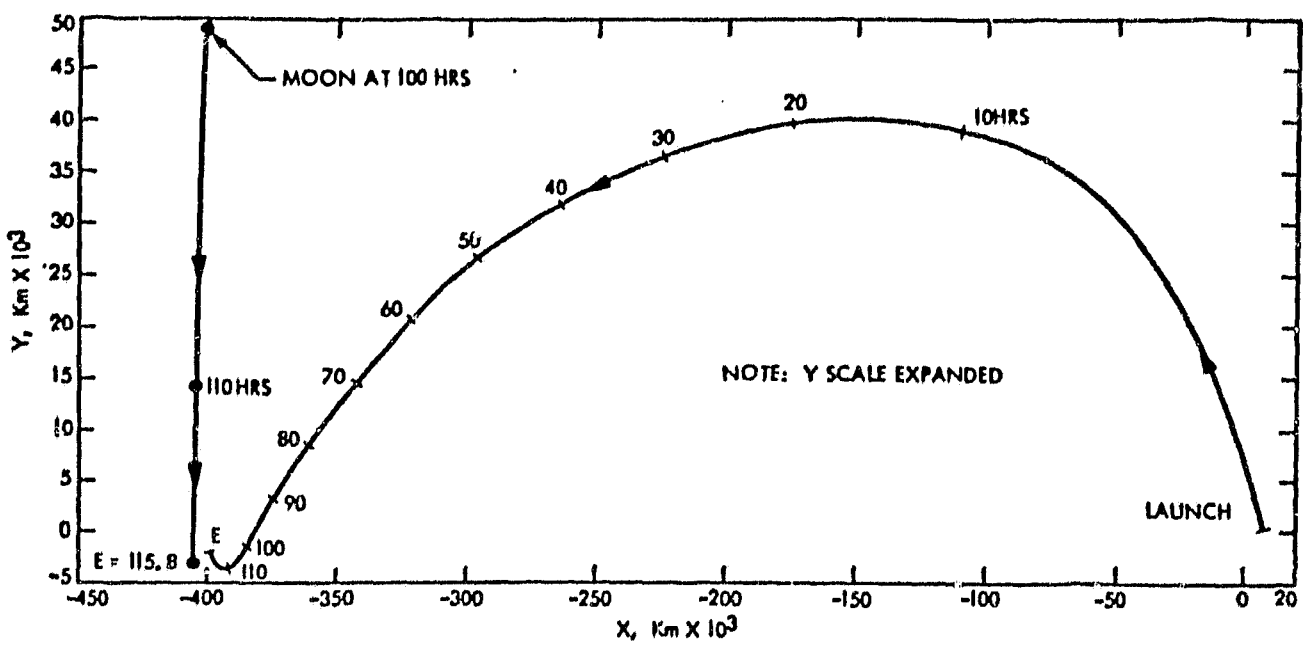

Figure 4.3-3. Typical LGO Earth-Moon Trajectory (Ecliptic Plan View)

orbit is approximately 29° to the Earth's equator; for a 90° launch azimuth, the parking orbit is inclined approximately 28°. Therefore, the maximum and minimum inclinations of the transfers would be approximately 57 and 1 degree, respectively. The two solutions on a given day are referred to as "high" and "low" with reference to their inclinations. Figure 4.3-4 illustrates these solutions, and shows that the difference in inclinations is approximately 10 degrees.

The transfer trajectory geometry within the Earth-Moon system is approximately the same for all launch dates. As the Moon revolves around the Earth, however, the transfer changes with respect to the Sun. If the right ascensions of the line of nodes and the Sun are plotted with respect to the Earth-Moon line as a function of launch date, as in Figure 4.3-5 for July 1979, it becomes apparent that twice during the lunar month the line of nodes aligns approximately with the Moon-Sun line. Once the orbit around the Moon is established, however, an alignment occurs only twice per year, and, since the Moon-Sun line moves approximately 1°/day, an alignment may take a very long time. If such an alignment early into the mission is scientifically desirable, the acceptable launch opportunities may be limited to two periods per month as shown.

Scientific and engineering constraints may have the effect of restricting otherwise acceptable launch opportunities. For example, thermal and power subsystem requirements may impose conditions at launch, during park orbit coast, or in translunar trajectory, which conditions affect launch time or park orbit coast time and thus limit the number of acceptable launch dates per month. Further classification of launch window constraints follows.

There are two basic categories of launch window constraints, i.e., monthly and daily. Table 4.3-2 summarizes the elements of each and gives some insight into the significance of each. Monthly launch window constraints come about because the Moon is circling the Sun with the Earth once per year. To further complicate this, the lunar orbit precesses once every 18.3 years about the ecliptic pole.

Daily launch window constraints are dictated primarily by the combination of the choice of launch azimuth and the lunar geometry for that launch day. This relationship is shown in Figure 4.3-6. To provide an optimum trans-lunar insertion (TLI) maneuver from an Earth parking orbit, the Earth parking orbit plane must contain the lunar position vector at the desired time of arrival at the Moon. The transfer occurs in the vicinity of the negative of the lunar right ascension and declination of the desired time of arrival at the Moon. The vicinity is referred to as the lunar antipode. To achieve the required TLI geometry in the presence of a rotating Earth, the launch azimuth at Cape Kennedy must be continually varied in order to produce an Earth parking orbit plane containing the lunar positive vector. Therefore, the limits on the launch azimuth dictate the duration of the daily launch window. Launch azimuth restrictions are due to range safety considerations.

Examples of other constraints may be cited. Two more potential launch window guidelines affecting the design of the daily launch window are the requirements for both a Pacific TLI and a daylight launch. These two requirements are interrelated. For a given launch day and a fairly narrow range of allowable launch azimuths for the Cape, two basic categories of TLI possibilities exist, a Pacific Ocean TLI or an Atlantic Ocean TLI. These two categories refer to whether the TLI maneuver is made on the portion of the Earth parking orbit over the Pacific Ocean as it ascends from southwest to northeast or over the general

C-2

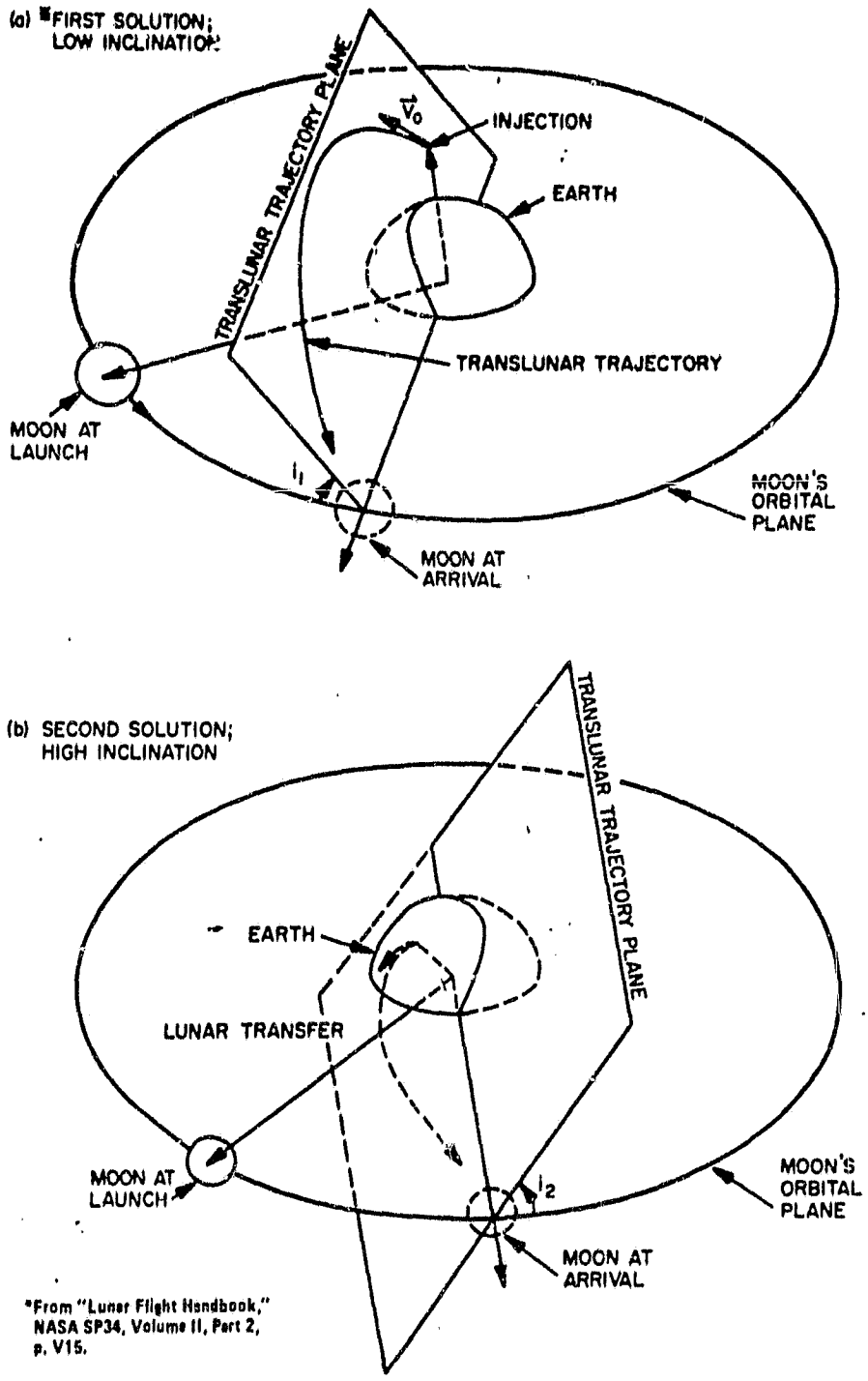

Figure 4.3-4. Lunar Transfer Geometry

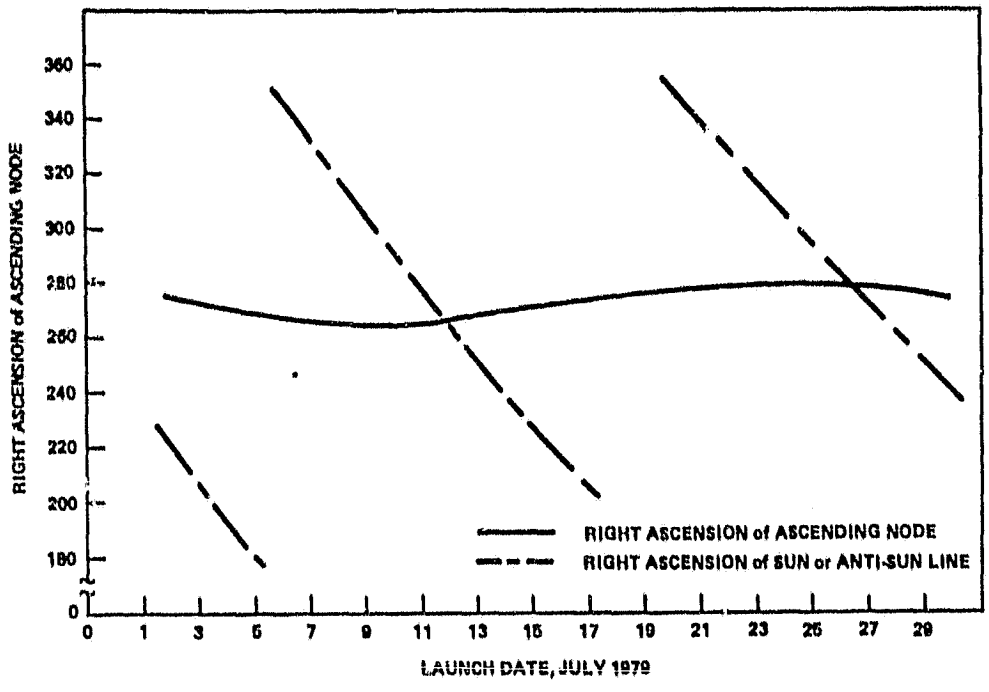

Figure 4.3-5. Right Ascension of Polar Orbiter Ascending Node with Respect to Moon-Earth Line vs Launch Date

TABLE 4.3-2. SUMMARY OF LGO LAUNCH WINDOW CONSTRAINTS

Window Category	Why Important
Monthly Window	
Choice of month	Lunar orbit precession
Mission profile	Affects arrival geometry
Lighting at lunar arrival	Sensor and power aspects
Ground station coverage	Command and telemetry
Daily Window	
Choice of day	Lunar orbit phasing
Mission profile	Affects arrival geometry
Ground station coverage	Command and telemetry
Launch azimuth restrictions	Limits lunar transfer
Launch vehicle ascent constraints	Affects trans-lunar insertion (TLI) options

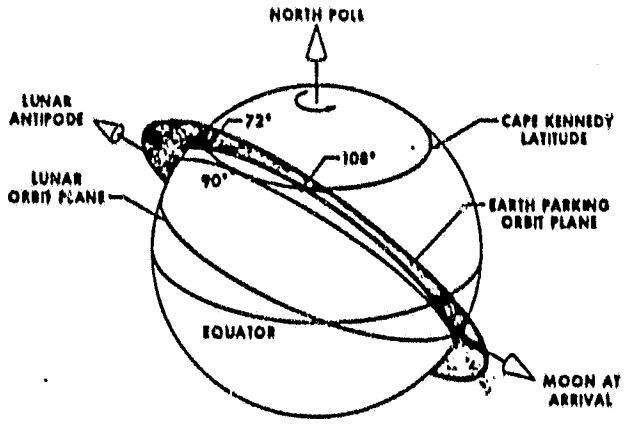

Figure 4.3-6. Daily Launch Window Geometry

vicinity of the Atlantic Ocean as the parking orbit trajectory descends from northwest to southeast, as shown in Figure 4.3-7. For a given launch azimuth, either of the two injection opportunities is available, but they correspond to two significantly different launch times. These differences in launch time range from nearly 24 hours to several minutes; however, the general case is usually a 6- to 18-hour difference with the average being approximately 12 hours. If the two respective launch times differ by several hours, the probability is great that one will be a night launch and one a day launch. The combination of these two factors could be an important consideration in launch planning.

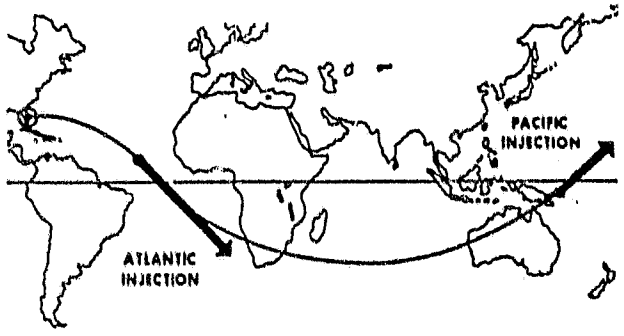

Figure 4.3-7. Pacific and Atlantic Trans-lunar Injection

As part of the current study effort a software package that simulates the Earth-Moon transfer trajectory has been developed. This Lunar Transfer and Insertion Simulation Package was installed at RCA towards the end of the current study and is now available for detailed investigation of launch window constraints for specific launch dates. To begin its description, it was assumed that there are four orbit adjustment maneuvers:

- ΔV_1 to inject into the trans-lunar ellipse
- ΔV_2 to effect a plane change
- ΔV_3 for lunar orbit insertion
- ΔV_4 to circularize the insertion orbit

It was assumed that the translunar injection occurs at the perigee of the geocentric transfer ellipse from low Earth orbit. A mid-course plane change at the point of minimum velocity allows insertion into a polar approach hyperbola. On arrival at the Moon the spacecraft is inserted into an elliptical insertion orbit. The lunar insertion maneuver is performed at the perilune of the approach hyperbola at the altitude of the mission orbit, 100 km.

The selected approach is one which has as its basis the patched-conic method. The accuracy is greatly enhanced, however, by imposing corrections to account for gravity perturbations on each basic conic trajectory segment. The computational procedure can be quickly summarized. To begin the sequence a geocentric ellipse segment is generated between two points. This is called the "Lambert calculation." An Encke refinement follows, and a corrected or Encke trajectory segment is produced. This correction allows an offset aimpoint in the Lambert calculation which accounts for perturbations. Near the Moon, a similar procedure is used in selenocentric space. The geocentric and selenocentric segments are fitted together at a "patch point" at the lunar sphere of influence. This is accomplished by elimination of the velocity mismatch.

The geometrical relationships investigated using the program are depicted in Figure 4.3-8. The output information consists of the histories of angles, ranges, range rates, eclipses and occultations, as well as the calculated ΔV vectors and their times. A sequence of runs of the program for various total flight times yields the minimum total ΔV. Some preliminary results are presented throughout this section (i.e., Section 4.3).

4.3.3 Launch System Selection

The launch system performance requirement may be evaluated by reference to either the launch energy, C_3, for the trans-lunar trajectory or the ΔV required to inject from the park or boost orbit.

The value of C_3 is indicative of the type of trajectory being used. Most commonly, C_3 is used in connection with interplanetary flight and has positive values. When $C_3 = 0$ this corresponds to an escape (or parabolic) trajectory. If C_3 is negative in value, then it refers to an elliptical orbit. For lunar flights, Earth escape is not necessary, and C_3 has negative values. The associated range of values for minimum energy transfers is -2.1 to -1.9 km^2/s^2. This range is a result of the eccentricity of the lunar orbit around the Earth. The value -1.9 km^2/s^2 corresponds to the higher energy and higher ΔV than does -2.1 km^2/s^2. In general, one can define C_3 for LGO as

$$C_3 = v^2 - v_{esc}^2 = v^2 - \frac{2\mu_E}{r}$$

where velocity, v, occurs at radial distance, r. For example, if $C_3 = -1.9$ km^2/s^2, then the required value of v at 200 km altitude above Earth is 10.92 km/s. The ΔV to achieve this from a circular orbit is 3.14 km/s, which is imparted by the upper stage. The values of injection ΔV for LGO launches over 13 days through early September 1990 were computed and are shown in Figure 4.3-9 together with the corresponding values of the lunar orbit insertion ΔVs.

The launch systems considered for the LGO mission were the same 14 considered for the MGO mission and described in Section 4.2.3. The objective here is to compare launch capabilities to required spacecraft mass as injected into the

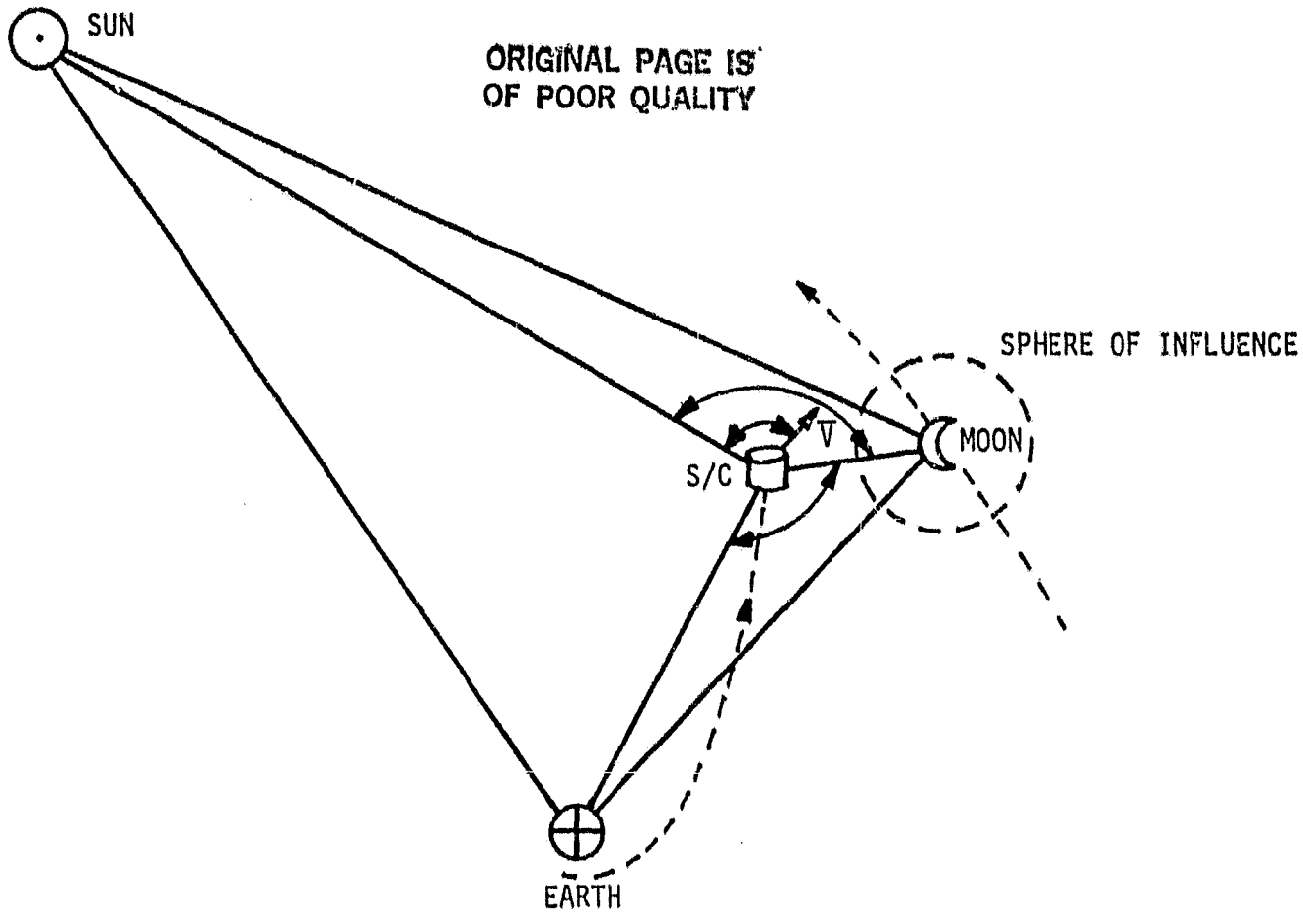

Figure 4.3-8. Geometry of Earth-Moon Transfer Investigated using RCA Lunar Transfer and Insertion Simulation Package

trans-lunar trajectory. This includes the mission spacecraft mass plus the lunar orbit insertion motor and adapters. Given the baseline spacecraft configurations, the comparison leads to realistic launch options.

For the greater part of the current, limited LGO study the baseline spacecraft body had conceptually grown from the size of DE (53 inches diameter) to that of the current baseline MGO/LGO (72 inches diameter) in order to give more solar power for MGO; but the decision to optionally replace the originally baselined 16.5 inch diameter hydrazine tanks, which would fit inside the 53 inch body, with 22 inch diameter tanks had not been made. Accordingly, the selection of the lunar insertion orbit (see Sections 4.3.6 and 4.2.6.2) and the details of the mass history through the LGO mission, presented in Table 4.3-3, still include the viable option of using six 16.5 inch diameter hydrazine tanks. For this option, the corresponding EOL mass of the LGO used in the launch vehicle selection calculations was 556 kg, which is actually 23 kg less than the current baseline prediction for the EOL LGO mass. In fact this could be taken account of by removing the HGA from the MGO/LGO baseline design and using the fan beam antenna together with a higher power amplifier, and by the fact that the 16.5 inch diameter tanks would weigh less than the baseline 22 inch tanks.

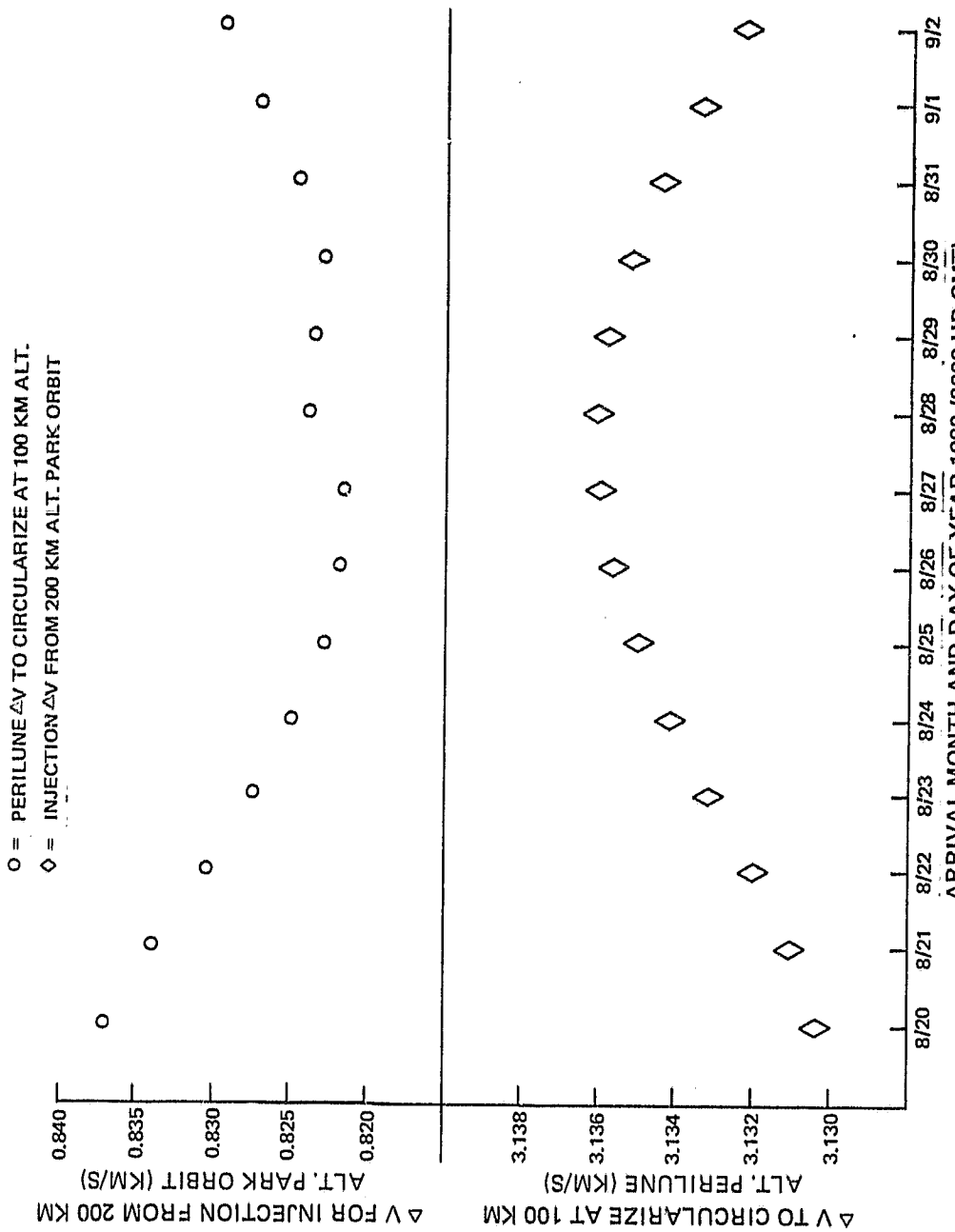

Figure 4.3-9. LGO Injection and Insertion ΔV Requirements for Launches Between 8/20/90 and 9/2/90

TABLE 4.3-3. MASS HISTORIES OF LGO OPTIONS (kg)

Item \ Option	A Zero Growth Margin, 3-Axis Upper Stage, Monoprop RCS, 22" Hydrazine Tanks	B Zero Growth Margin, Spinning Upper Stage, Monoprop RCS, 22" Hydrazine Tanks	C 72 kg Growth Margin, 3-Axis Upper Stage, Monoprop RCS, 22" Hydrazine Tanks	D 72 kg Growth Margin, Spinning Upper Stage, Monoprop RCS, 22" Hydrazine Tanks	E Zero Growth Margin, Spinning Upper Stage, Hybrid RCS, 16.5" Hydrazine Tanks
EOL S/C	579	579	651*	651*	556
Mission N_2H_4 (ΔV = 100 m/s)	26.2	26.2	29.5	29.5	25
EOL S/C	605.2†	605.2†	680.5†	680.5†	581
Circularization N_2H_4	–	–	–	–	106** (ΔV = 376.3 m/s)
S/C Pre-Circularization	–	–	–	–	687
S/C – OIM Adapter	–	–	–	–	25
OIM AT Burnout	–	–	–	–	12
Burnout Assembly	–	–	–	–	724
OIM Propellant	–	–	–	–	115(3% Augmented) (ΔV = 415 m/s)
OIM STAR Designation	–	–	–	–	17A
OIM Mass	–	–	–	–	129
Lunar Arrival Assembly	864.7	864.7	972.3	972.3	839
Earth-Moon Transit N_2H_4 (ΔV = 100 m/s with Spinners) = 30 m/s with 3-Axis)	11.6	39.2	13	44.1	38
Total N_2H_4 Requirement (kg)	297.3 (ΔV = 935 m/s)	324.9 (ΔV = 1005 m/s)	334.3 (ΔV = 935 m/s)	365.3 (ΔV = 1005 m/s)	169
Trans-Lunar Injection Assembly	876.3	903.9	985.3	1016.3	877
Launch Vehicle Adapter	70	70	70	70	70
Launch Payload	946.3	973.9	1055.3	1086.3	947

*Includes 72 kg growth margin.

**For lunar insertion orbit at 100 x 4000 km altitude, set by hydrazine capacity of DE-based LGO (6 x 16.5 in tanks)

†Direct insertion into circular orbit at 100 km altitude assumed.

Note: N_2H_4 for Attitude Control to be included throughout when available.

The optional LGO configurations presented in Table 4.3-3 feature launch throw masses in the range 946-1086 kg. The launch vehicle adapter was sized conservatively at 70 kg. For options A through D, the total hydrazine requirement, corresponding to the specified total post-injection ΔV requirement of 935/1005 m/s, is in the range 297-365 kg. For option E, the specified ΔV allowance of 100 m/s for launch vehicle error corrections and lunar targeting translates into a hydrazine usage of 38 kg for the 877 kg trans-lunar injection assembly; a lunar injection orbit of 100 x 4000 km altitude suitably matches the assumption of 16.5 inch diameter hydrazine tanks; the corresponding OIM is a Star 17A with 3% propellant augmentation, a launch mass of 129 kg and an OIM adapter mass of 25 kg; circularization of the insertion orbit accounts for 106 kg of hydrazine; and the specified total ΔV of 100 m/s for mission-orbit maintenance and orbit adjustments accounts for another 25 kg of hydrazine; it may be seen that the total hydrazine load of 169 kg closely approaches the maximum capacity of the six 16.5 inch diameter hydrazine tanks, ~180 kg assuming a 5:1 blow-down ratio. It was considered that hydrazine necessary for attitude control through the mission is included in the two JPL-specified ΔV allowances of 100 m/s each.

The match of the calculated optional throw masses for LGO with the planetary performance curves of the closest matched of the 14 candidate launch systems is shown in Figure 4.3-10. The optional baseline LGO payloads described in this section may be launched very efficiently by the Delta 3920/ PAM-D combination or its expected, more powerful development versions. It may be seen from the figure that the currently promised performance of the STS/PAM-D2 combination is inadequate; but it should be borne in mind that 15-20% growth in this payload capability is envisaged.

In comparison, it may be seen that the relatively low values of C_3 for the LGO mission allow smaller launch vehicles and stages than those necessary for the MGO mission.

4.3.4 Launch Phase

The LGO spacecraft and its optional solid rocket OIM will be boosted from the Kennedy Space Center by the Delta 3920 or the Shuttle into a circular parking orbit, followed by injection into the translunar trajectory by the PAM-D/D2.

Since there are no tightly constrained bi-annual launch windows as in the MGO case, the lunar mission has significantly more flexibility from a programmatic and STS operations point of view. Launch parameters do vary slightly throughout the month for the minimum energy Earth-Moon transfers which are those at low inclinations to the lunar orbit. Values of C_3, ΔV and, consequently, the net orbited mass vary accordingly. For example, C_3 varies within the approximate range of -2.15 to -1.95 km^2/s^2. For the launch of an expendable launch vehicle (ELV) such as the Delta 3920, the timing of the ascent and insertion into the parking orbit and the velocity of injection into the translunar trajectory may be varied independently to match the launch parameters. Some of the flexibility might be lost with a shared STS launch; however, the details of the mission timeline must be assessed before the effects of any possible constraints can be evaluated.

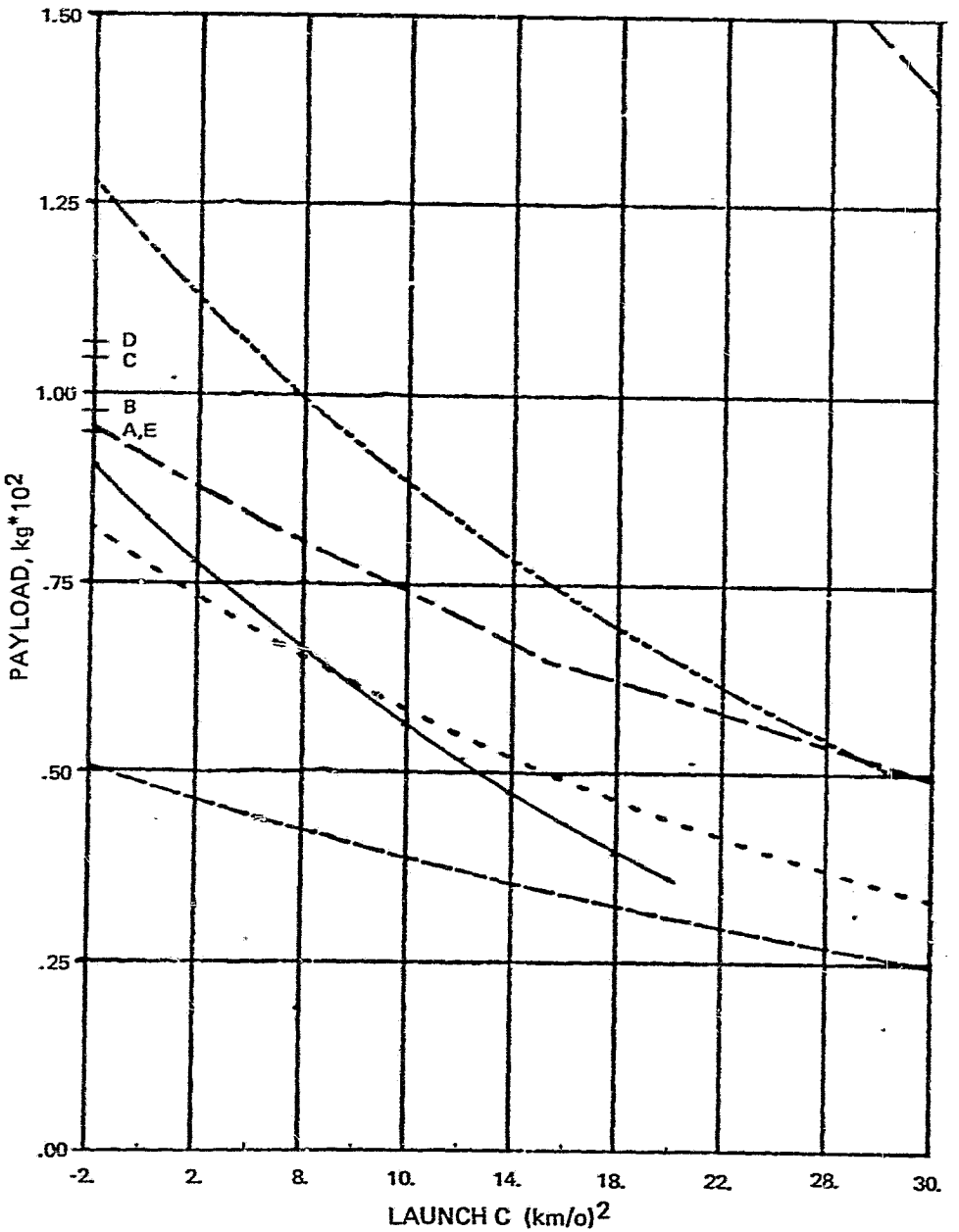

STS/PAM-A
DELTA 3920/PAM-D
STS/PAM-D2
STS/PAM-D (MAX PROPELLANT LOAD)
DELTA 2914

OPTION*	LGO MASS (KG)	THROW-MASS (KG)	RCS TYPE	UPPER-STAGE TYPE
A	579	946	N_2H_4	3 AXIS
B	579	974	N_2H_4	SPINNER
C	651	1055	N_2H_4	3 AXIS
D	651	1086	N_2H_4	SPINNER
E	556	947	N_2H_4 + SOLID	SPINNER

*CF. TABLE 4.3-3

Figure 4.3-10. Match of Launch System Performance Curves With Throwmasses for LGO Options

The use of the Delta 3920/PAM-D or STS/PAM-D2 launch systems imposes more constraints on the LGO design than the STS/IUS-1 does on the MGO design. In view of the smallness of the margins in throwmass shown in Figure 4.3-10, weight control will have to be very strict. On all other counts, the LGO will be entirely suited to a PAM-D/D2 injection because of its origins in DE and AE. The diameter of the main body of the LGO is 72 inches, and this, plus the extra width of appendages such as the HGA, is comfortably accommodated inside the Delta fairing, the diameter of which is 84 inches. Compatibility with the Delta and PAM-D/D2 acceleration levels and spin rates exists through design heritage. The PAM-D/D2 will probably spin at ∿60 rpm.

Attitude control through burnout will be achieved by the Delta 3920 and by spin stabilization of the PAM-D/D2. The momentum wheel will be spinning for the entire mission from before lift-off, however, for reliability.

The Sun-spacecraft-Earth angles at injection, i.e., on departure from Earth orbit on the trans-lunar trajectory, over a period of 13 days through early September 1990, were computed and are shown in Figure 4.3-11. This figure immediately shows whether the injection is sunlit or dark.

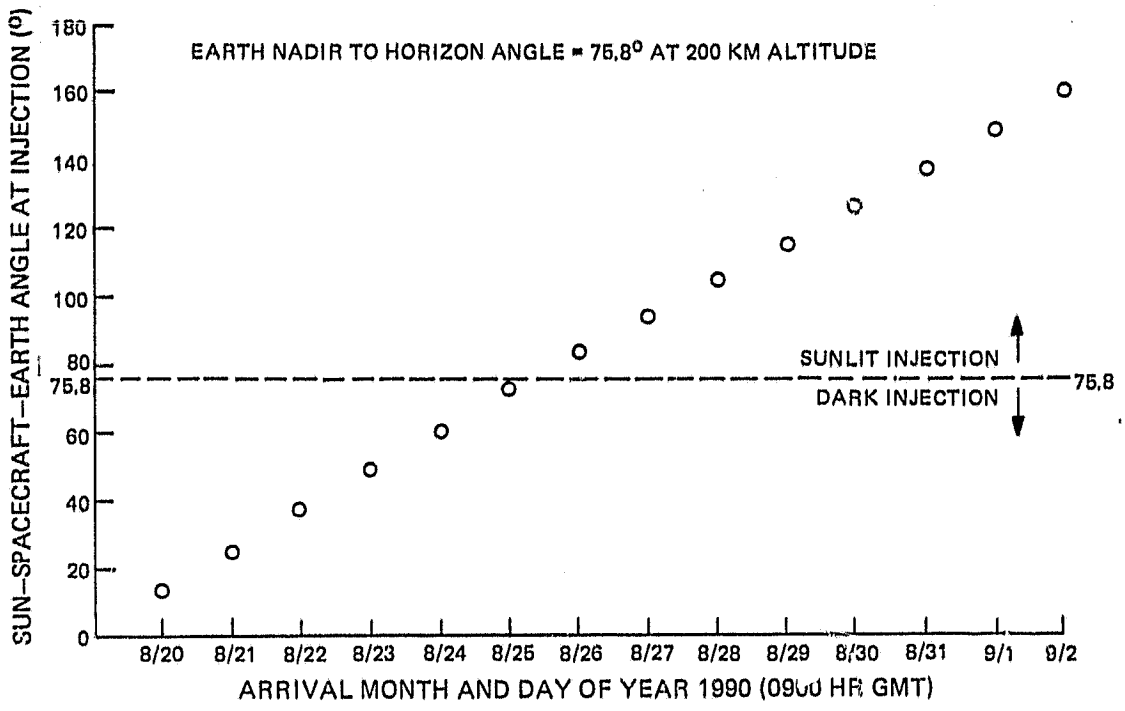

Figure 4.3-11. Sun-LGO-Earth Angle at Injection for Launches Between 8/20/90 and 9/2/90

4.3.5 Earth-Moon Transfer Phase

The Earth to Moon transfer phase of the mission consists basically of a "coasting" trajectory entirely within the gravitational spheres of influence of the Earth and the Moon. The trajectory has been discussed in Section 4.3.2. It may be shown by simulations, using for example the RCA Lunar Transfer and Injection Software Package, that for the minimum energy transfers, the transfer time is approximately 115 hours, i.e., 4 days, 19 hours.

The values of the inclination of the transfer trajectory with respect to the orbit of the Moon around the Earth, for launches over 13 days through early September 1990, were calculated and are shown in Figure 4.3-12. The low inclination solutions only are shown.

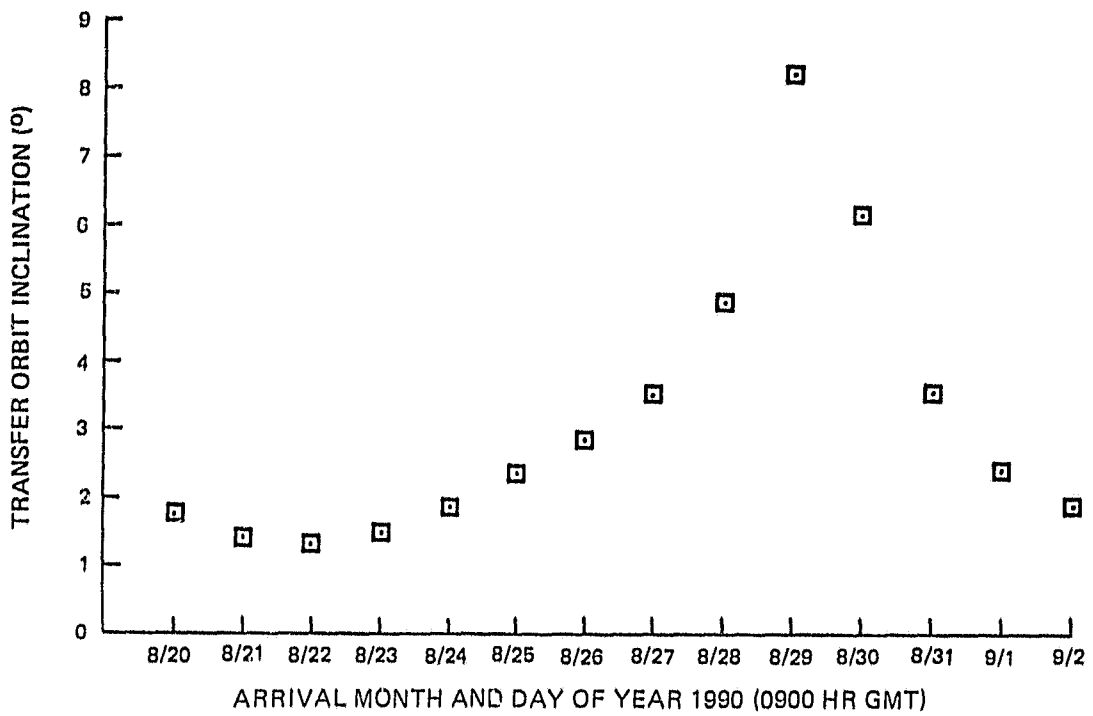

Figure 4.3-12. Inclination of LGO Transfer Orbit Relative to Orbit Plane of Moon Around Earth for Launches Between 8/20/90 and 9/2/90

Following closely after burnout of the PAM-D/D2 the trans-lunar spacecraft will be separated from the spent PAM-D/D2 and the launch adapter. The spacecraft will then be despun to a very low body-rate, using the on-board hydrazine RCS, before significant nutation develops. The momentum wheel will be left spinning and will contain $\geq$90% of the angular momentum of the trans-lunar assembly.

Attitude determination and control for the rest of the mission, except during the LOI maneuver, will be achieved by the spacecraft using its sun sensors, star sensors, gyro package, momentum wheel and hydrazine RCS thrusters. The momentum bias mode will be employed to provide gyroscopic stability during the transfer phase without concern for the build-up of nutation.

The JPL-specified ΔV allowance of 100 m/s for maneuvers during the Earth-Moon transfer has been incorporated into the baseline mission design. As shown in Table 4.3-1, the GSFC LPO study estimated the launch vehicle error correction maneuver ΔV in its baseline mission to be <84 m/s with 99% probability for a Delta 2914 launch vehicle. The 100 m/s allowance will probably also comfortably cover spin-up and -down and attitude control maneuvers. The baseline mission design features one or two mid-course targeting maneuvers with a total ΔV <7 m/s. Refinement of these current estimates may be made shortly when the RCA Lunar Transfer and Insertion Simulation Package (see Section 4.3.2) is fully operational. The mass of hydrazine corresponding to a ΔV of 100 m/s for the trans-lunar injection assembly is between approximately 11 and 44 kg for the five LGO options tabulated in Table 4.3-3.

4.3.6 Lunar Orbit Insertion

Several hours before lunar orbit insertion, the LGO will be reoriented using the precession thrusters of the on-board hydrazine RCS so that either the OIM or the large (22.3 N) thrusters of the all-hydrazine RCS are aligned with the necessary LOI thrust vector. The realignment maneuver will be performed open loop and a trim maneuver then made under ground command. The realignment will be performed early enough that thorough verification of its accuracy may be made using the on-board attitude determination system.

Also prior to LOI, i.e., if a solid rocket OIM is used, its temperature will be assured at the preselected value, possibly through the use of heater elements, as indicated by the full thermal analysis that will be a subject of a detailed follow-on LGO study. Also in this case, immediately before LOI the LGO will be spun to $\sim$60 rpm, using the on-board hydrazine RCS, in order to stabilize the alignment of the OIM thrust vector. In the case of an all-hydrazine RCS, the body rate will be held at zero, the spinning momentum wheel providing gyroscopic stiffness.

The Earth departure geometry, timing and injection ΔV determine the Earth-Moon transfer trajectory. This in combination with the mid-course corrections determines the arrival conditions at the Moon.

Before entering the gravitational sphere of influence of the Moon, the spacecraft has an approach velocity relative to the Moon. As explained in Section 4.2.6.1 for MGO, therefore, the LGO will have positive energy in the lunar reference frame and will follow a planar, hyperbolic trajectory around the Moon unless it is targeted to impact the Moon or is acted upon by the RCS. The deflection angle between the approach and departure assymptotes depends upon the closeness of approach to the Moon.

In the baseline mission options, the LGO will be targeted so as to have a hyperbolic periapsis altitude of 100 km at the Moon. At the periapsis point, the LGO, prealigned or prealigned and spun as described previously, will be injected into a lunar insertion orbit by means of either the on-board hydrazine RCS or a solid rocket motor. The insertion orbit will be coplanar with the hyperbolic approach trajectory which will have been arranged by mid-course targeting to produce a near-polar orbit, probably at approximately 85° or 95° inclination for the baseline missions. The approach trajectory, accordingly, will be targeted over either the North or South polar region of the Moon; and there will be an accompanying choice to be made between ascending nodes approximately 180° apart.

A schematic illustration of the LOI geometry is shown in Figure 4.3-2.

The selection of the elements of the lunar orbit insertion involves the careful matching of many constraints and requirements such as arrival geometry (see Section 4.2.6.1), propulsion system type(s) and capability, mission science requirements, spacecraft requirements (e.g., orientation of the attitude determination sensors), etc. The similar interactive process for the MGO is illustrated in Figure 4.2-10.

The feasible orbit insertion scenarios, while differing widely between themselves, are all very sensitive to the choice of the interplanetary transfer trajectory and the performance capabilities of the on-board hydrazine RCS and the available solid rocket orbit insertion motors (OIMs).

In the baseline mission there is a choice available between (a) a wholly hydrazine on-board RCS identical with that baselined for MGO, i.e., with six 22 inch diameter hydrazine tanks, and (b) a hybrid RCS incorporating a solid rocket OIM, such as the Star 17A for LOI, and an on-board hydrazine RCS with 16.5 inch diameter tanks for orbit circularization and maintenance and for mission maneuvers.

Unlike the result found in the current MGO study, the use of a wholly hydrazine on-board RCS does not necessitate the design or development of a new stage.

These two baseline RCS options were chosen over other candidate RCSs, solid plus bipropellant and wholly bipropellant, on grounds of hardware mass, system simplicity, handling ease and development cost. Between the baseline options the all-hydrazine system would be preferable. It allows the gamma ray spectrometer to be calibrated either along the Earth-Moon transfer trajectory (see later in this section) or following LOI if desired, is the same RCS as the on-board RCS for MGO, and is the least complex and, therefore, most reliable and least expensive design.

The LGO design option incorporating an all-hydrazine on-board RCS features a very great advantage, which is that the gamma ray spectrometer and magnetometer booms may be deployed either prior to LOI or in a lunar insertion orbit with an almost arbitrarily high apolune. Consequently, the gamma ray spectrometer may be deployed and calibrated along the Earth-Moon transfer trajectory, and the altitude of the apolune of the lunar insertion orbit need not necessarily be maximized as it must be if a solid rocket OIM is used. Detailed simulations of the LOI maneuver, a possible subject for a follow-on LGO study, would determine the optimum insertion strategy. In the current baseline mission design for an all hydrazine RCS, direct insertion into a

circular orbit at 100 km altitude is assumed. The baseline all-hydrazine on-board RCS features two 22.3N (5 lb_f) main thrusters for LOI. Since the lunar approach mass will be >840 kg, the LOI deceleration will be <0.053 m/s^2, i.e., $<5.4 \times 10^{-3}g$, which is compatible with the deployed booms.

The burn duration, t, for this hydrazine LOI may be established from the equations

$$t = \frac{M_p}{\dot{m}}$$

$$\dot{m} = \frac{T}{I_{sp}g}$$

where M_p = mass of propellant used in maneuver

$\dot{m}$ = rate of use of propellant

T = thrust

I_{sp} = specific impulse of propellant-engine combination

g = acceleration due to gravity at sea level

and pointing and gravity losses are neglected.

Since $M_p \lesssim 290$ kg for insertion into a 100 x 100 km insertion orbit, $t \lesssim 245$ minutes. This burn time is clearly very long compared to the 22 seconds for a Star 17A solid OIM, but it is perfectly compatible with the baseline mission design. The LOI maneuver will be planned accordingly, rather than for an impulsive LOI. In fact, by breaking the LOI into a group of smaller hydrazine burns the velocity may be almost continuously checked and trimmed, allowing great accuracy to be achieved in the lunar orbit insertion maneuver.

On the other hand, for the LGO option incorporating a solid rocket OIM the booms could not survive the LOI maneuver in their deployed state. Consequently, the booms will have to be deployed following the LOI maneuver and the gamma ray spectrometer calibrated at the apolune of the elliptical insertion orbit. Accordingly the highest possible apolune is desired. The height of apolune is limited by the capability of the on-board hydrazine RCS which must subsequently perform the circularization and mission maneuvers. Six 16.5 inch diameter tanks used in a system with a 5:1 blowdown ratio have a capacity of 180 kg of hydrazine. The longest possible lunar insertion orbit suited to this hybrid propulsion option is approximately 100 x 4000 km altitude, as may be seen in column E of Table 4.3-3 in which the total hydrazine requirement is 169 kg.

Typical orbit insertion ΔV requirements are plotted versus apolune altitude in Figure 4.3-13. The paired values of LOI and subsequent circularization ΔVs corresponding to several apolune altitudes in the range 100 - 5000 km are shown in Table 4.3-4.

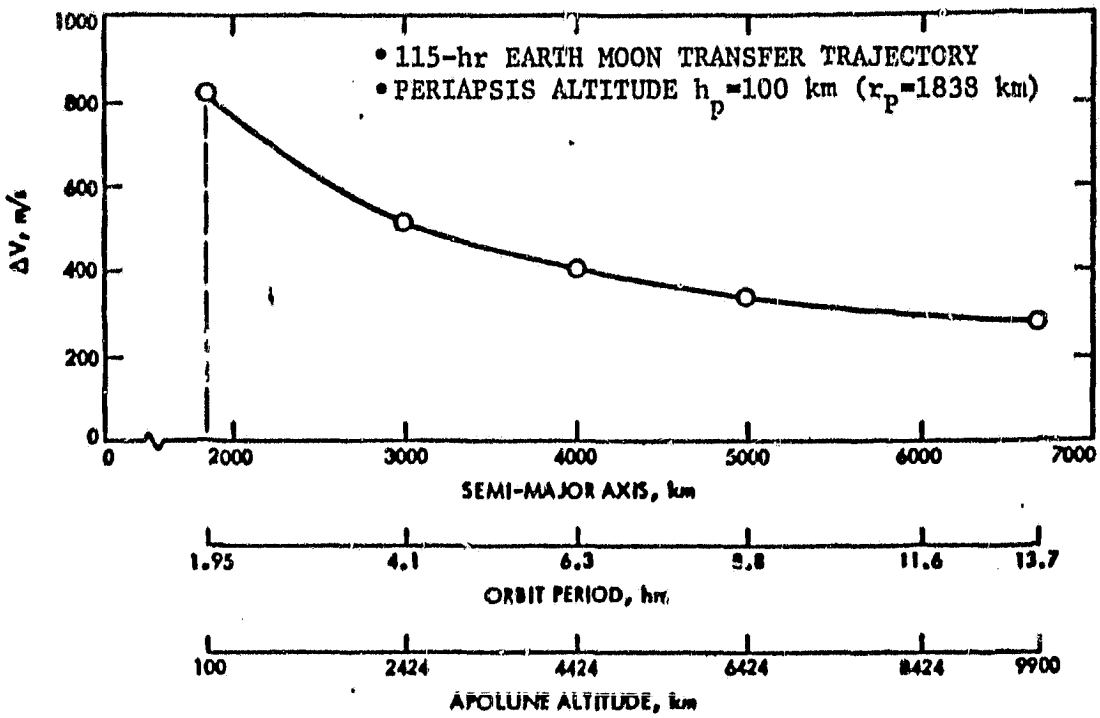

Figure 4.3-13. Typical Orbit Insertions ΔV Requirements vs. Apolune Altitude

TABLE 4.3-4. LUNAR ORBIT INSERTION AND CIRCULARIZATION ΔVs

Apolune Altitude (km)	Lunar Orbit Insertion ΔV (m/s)	Circularization ΔV (m/s)
100	805	0
500	740	78.1
1000	650	153.2
2000	530	257.5
3000	460	326.8
4000	415	376.3
5000	380	413.4
Arrival Hyperbolic Perilune Altitude = 100 km		

Table 4.3-3 shows that a good choice for the solid rocket OIM, for the LGO option with a hybrid RCS launched by the Delta 3920/PAM-D or STS/PAM-D2, is the Star 17A with ∿3% propellant augmentation, or otherwise an offloaded Star 20. After a 115 hr trans-lunar transfer, the ΔV requirement for insertion into a 100 x 4000 km orbit will be ∿415 m/s which corresponds to 115 kg of solid propellant with an I_{sp} of ∿293s.

Finally, the values of three pertinent angles at arrival hyperbolic perilune:

- Earth-spacecraft-Moon
- Sun-spacecraft-Moon
- Sun-spacecraft-hyperbolic velocity

for launches over 15 days through early September 1990, were computed and are presented in Figure 4.3-14. It may be seen from the lower curve of this figure that within the period shown, the launch window for the LGO option incorporating a hybrid RCS starts on the last day, i.e., 9/4/90. For a launch on that date, the corresponding orientation of the LOI vector, which will be parallel with the spin axis of the insertion stack, begins to be such that the Sun will be in the hemisphere scanned by the LGO Sun sensors and that the hemisphere scanned by the star scanners will be dark. On the other hand, for the LGO options with an all hydrazine RCS, the necessary orientation of the LOI thrusters is such that the Sun and star scanners will be well oriented for all values of Sun-spacecraft-hyperbolic velocity more than a few degrees away from 0° and 180°, i.e., for all of the launch dates shown in Figure 4.3-14.

4.3.7 Orbit Circularization

Following LOI the LGO option incorporating a solid OIM will be quickly despun to <4 rpm, using the on-board hydrazine RCS, before significant nutation builds up. The spent OIM will then be jettisoned. The spin axis will then be precessed until it is normal to the orbit plane so that the spacecraft orbits the Moon in the cartwheel mode for good attitude sensing. In this mode the gamma ray spectrometer and magnetometer booms will be deployed and the spectrometer calibrated at apolune.

For the LGO option featuring a solid OIM, and also for the all-hydrazine option if a direct insertion into a 100 km altitude circular orbit is not made on LOI, the next maneuver is orbit circularization at 100 km altitude. This is performed by the on-board hydrazine RCS on successive perilune passes, under ground command.

The orientation of the spacecraft for these apolune-lowering maneuvers will be held under pitch-lock control so that the total thrust vector from the two large (22.3 N) hydrazine REAs is antiparallel to the elliptical-orbit velocity around perilune. The momentum wheel will be spinning, with $\gtrsim$90% of the angular momentum of the spacecraft, to provide gyroscopic stiffness throughout.

The ΔV necessary to circularize an elliptical orbit around the Moon, with a perilune altitude of 100 km altitude, at 100 km altitude is related to the apolune altitude, h_a, by the expression

$$\Delta V = \left\{ \sqrt{2\mu_{\mathbb{C}} \left(\frac{1}{1838} - \frac{1}{3576 + h_a} \right)} - 1.631 \right\} 1000$$

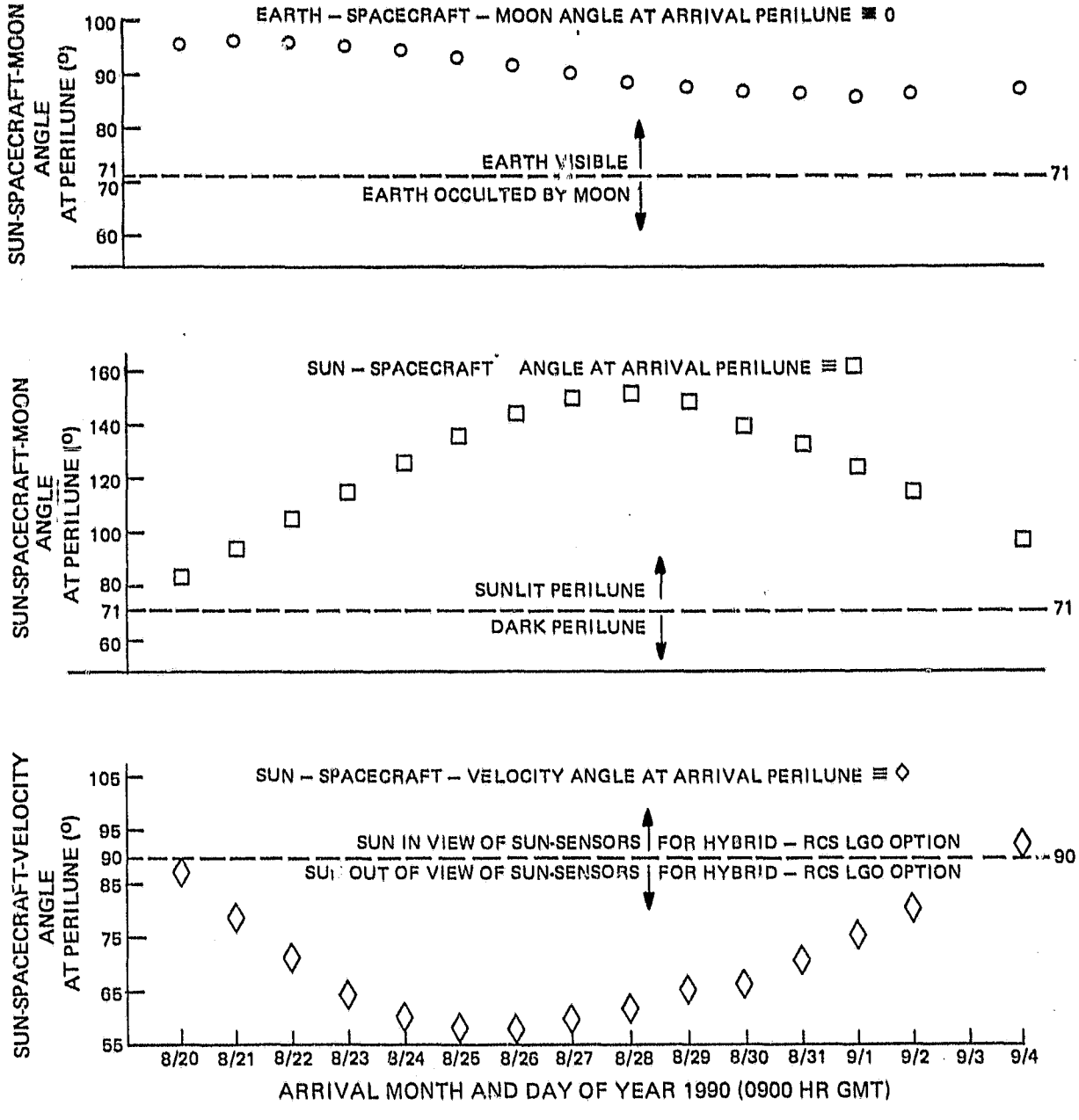

Figure 4.3-14. LGO Arrival Hyperbolic-Perilune Geometry

where

ΔV is in m/s
$\mu_{\mathbb{C}}$ = 4887 km^3/s^2
h_a = apolune altitude in km

Determination of the baseline circularization ΔV is a function of the spacecraft propellant capacity, other ΔV budget items, and the solid orbit insertion motor, as described in Section 4.3.6. Example values of the circularization ΔV, for apolune altitudes in the range 100-5000 km, are shown in Table 4.3-4. The values shown range between 0 and 414 m/s. As a specific example, it may be seen from Table 4.3-3 that, for the baseline LGO option with a hybrid RCS, the circularization ΔV is 376.3 m/s, corresponding to the starting apolune altitude of 4000 km, and corresponds to the usage of 106 kg of hydrazine.

The intermediate orbit achieved after each perilune burn will be monitored on Earth by ground tracking. The mission orbit, therefore, will be achieved very efficiently and as accurately as desired.

4.3.8 Mission-Orbit Phase

4.3.8.1 General Description

Once the LGO is in its mission orbit, pitch lock will be obtained so that the spacecraft orbits in the cartwheel mode at 1 rpo with the imaging sensors continuously nadir pointing. The high gain antenna will then be deployed. The HGA will then acquire Earth pointing through the use of the same baseline and backup techniques described for MGO in Section 4.2.9.

Attitude maintenance during the one-year mission life will involve only minor impulses for counteracting the small perturbations due to solar pressure and RCS thrusting.

The LGO orbit is virtually inertially fixed, with no significant nodal precession occurring, as shown in the example orientation of Figure 4.3-15. Accordingly, there is no practical possibility of a Sun-synchronous orbit. As another consequence, the spinning spacecraft will be precessed, using the onboard RCS, so that the spin axis is flipped through 180° in yaw once or twice during the one year long baseline mission so that the Sun and star sensors will always have a view of their reference bodies.

4.3.8.2 Lunar Orbit Stability and Maintenance

A key question in the final selection of a lunar orbit for LGO is that of stability. This is particularly true of low altitude orbits. All low altitude orbits are unstable due to the extreme anomalies in the lunar gravitational field. The resulting effect is that eccentricity increases rapidly while the orbital period remains constant. This corresponds to a lowering of perilune and raising of apolune. If not corrected periodically, the perilune altitude would go to zero and lunar impact would occur. Present models of the lunar gravity field differ drastically, causing great difficulty in predicting the frequency and magnitude of corrections. Thus, the preliminary design study should pursue a bounding of the problem in terms of correction frequency and impulse requirements.

Figure 4.3-15. Earth-Moon-Sun-Orbit Geometry

A great deal of numerical work has been done on the simulation of lunar polar orbiter lifetimes by NASA Goddard (Lunar Polar Orbiter Interim Technical Report, X-703-75-141, May 1975). The gravitational model used is the JPL (15, 8) model, which represents one of the best descriptions of the Moon's gravitational field available. However, since some of the higher order terms have standard deviations of uncertainty as large in magnitude as the terms themselves, and since a number of these higher order odd harmonics are nearly as large as some of the low-order terms, the predictions of orbit lifetime determined through the use of this model should be regarded with caution, particularly for low altitude satellites like LGO. For example, the magnitudes of the odd harmonics of the gravitational potential field significantly affect the calculated lifetimes of lunar satellites.

The orbit propagation technique uses an orbit averaging method in the MAESTRO program. Input orbit-elements are numerically integrated over one revolution, and averaged orbit-elements are then calculated from this initial orbit. The process is then restarted with the averaged elements, but now the averaged elements are used to predict the orbit elements, again averaged over a revolution of the satellite, at some time in the future. This process is much more rapid computationally than a direct propagation of the orbit through point-by-point numerical integration.

In the Goddard study a number of orbit elements were varied, i.e., semimajor axis, eccentricity, inclination and longitude of the ascending node of the initial orbits. The semimajor axes chosen were 1788, 1813, 1838, 1938 and 2038 km. These values correspond to mean altitudes of the satellite above the lunar surface of 50, 75, 100, 200 and 300 km, respectively. Up to three initial eccentricities were chosen for each value of the semimajor axis; these were chosen to produce initial perilune heights of approximately 50, 75 and 100 km, where possible. The range of inclinations of the plane of the orbit extended from 80° to 100° in 5° increments for the smaller three values of the semimajor axis. All orbits were calculated as starting on June 6, 1979. Since the southern and northern approaches to the Moon limit the longitudes of the ascending node to a range near 90° and another near 270°, only these two values were used. The initial true anomaly and argument of perilune were chosen to be zero in all cases. Thus, for each value of the semimajor axis, as many as 30 different combinations of the initial orbit-elements were investigated.

All of the initial orbits examined for the three lower values of the semimajor axis evolved such that the satellite impacted the lunar surface within one year after being launched. Many of the initial orbits examined for the two highest values of the semimajor axis were still in orbit at the end of one year, the limit of the propagation. In all cases, the semimajor axis of the initial orbit remained relatively constant during the satellite lifetime, but the eccentricity of the orbits increased until the radius of perilune was less than the radius of the Moon. The eccentricity varied in an irregular manner from orbit to orbit but exhibited an overall secular increase which became more rapid as the value of the eccentricity increased. As might be expected from this observation, larger initial eccentricities resulted in shorter satellite lifetimes, assuming all other parameters remained unchanged. On the other hand, larger initial semimajor axes resulted in longer satellite lifetimes.

The lifetimes of the satellites also tended to increase as the inclination of the initial orbits increased or decreased from a value of 90°. However, these increases in lifetime with changing inclination were not universal, and wide variations in lifetime with smoothly changing inclinations were found. The inclinations themselves were quite stable over the orbit lifetimes, however.

For the LGO case the factors of interest are inclination, initial circular altitude, and time until impact and until 30 km altitude. Results for these cases appear in Table 4.3-5. An initial altitude of 100 km is assumed in all cases. The value of longitude of ascending node in combination with inclination appears to be very important. It would seem that an inclination of 85° or 95° is preferable. With proper selection of these parameters, it is reasonable to expect three-month intervals between orbit maintenance maneuvers.

TABLE 4.3-5. LGO LIFETIME PREDICTIONS

Inclination (degrees)	Longitude of Ascending Node (degrees)	Days Until	
		Impact	30 km Perilune
80	90	61	51
85	90	83	56
90	90	41	29
95	90	237	128
100	90	37	12
80	270	37	22
85	270	98	71
90	270	40	29
95	270	168	87
100	270	52	45

The baseline LGO mission orbit is nominally circular at 100 km altitude and at an inclination of either 85° or 95°. A preliminary analysis by JPL indicates an orbit evolution to a 50 x 150 km altitude orbit in approximately three months. Thus, at least three circularizations are needed to ensure a one-year mission life. The orbit will decay progressively after the final recirculariization and impact the surface of the Moon between three and six months later. Each recircularization at 100 km altitude, starting in a 50 x 150 km altitude orbit, entails a two-burn process requiring a combined ΔV of 22.6 m/s.

It should be noted that much more frequent orbit recirculariizations, to correct for slighter orbit decay, would be equally simple to effect.

The ΔV allowance for orbit maintenance suggested by JPL in the LGO Reference Data Package is conservative at 100 m/s for the one year duration of the baseline mission. This corresponds to a hydrazine expenditure of 25-30 kg for the baseline spacecraft, as shown in Table 4.3-3.

4.3.8.3 Lunar Surface Coverage

Science coverage of the lunar surface will depend upon the orbit-maintenance strategy employed. If the orbit is allowed to decay to relatively elliptical orbits (e.g., 50 x 150 km altitude) between propulsive recircularizations at 100 km altitude performed at intervals of several months, then a significant fraction of the surface could be covered from below 100 km. This strategy may be attractive from a scientific viewpoint. Alternatively, frequent circularizations could easily be made in order to preserve a nominally circular orbit since the RCA LGO will orbit in a nadir-pointing cartwheel mode, and variable pitch-offset control to allow retrofiring and boost ΔVs is easy with the AE/DE based spacecraft design.

Surface coverage will be almost complete for orbit inclinations only a few degrees away from 90°, though if the orbit inclination were 85° or 95°, for example, the 5° poles would never be passed over directly. A mission phase at a precisely polar inclination could be included in the mission design to provide polar coverage, though a mass penalty would be incurred due to the necessary hydrazine used to effect the plane change. Pending the results of a future detailed LGO mission-orbit simulation, it may be said that it is feasible that inclination changes may be desirable for orbit maintenance or science return objectives. The ΔV required for changes of $\lesssim$5° is about 28.5 m/s for each degree of change. This is approximately equal to the excess of the JPL-specified baseline allowance of 100 m/s for the mission orbit phase over the 67.8 m/s required for three recircularizations to 100 km altitude from 50 x 150 km altitude orbits (see Section 4.3.8.2). Any additional ΔV allowance for the mission orbit phase will result in higher launch throw masses than those shown in Table 4.3-3 and will potentially lower the capability of the on-board hydrazine RCS for cirularizing an elliptical insertion orbit produced by a (larger than baseline) solid rocket OIM.

The baseline LGO orbit will be almost inertially fixed and have a period of close to 2 hours (1 hr 58 min). The Moon revolves on its axes at ∿0.5° per hour. The nodal precession rate of the LGO, therefore, will be ∿1° per orbit period. The full extent of the baseline coverage of the lunar surface, therefore, will be achieved with longitudinal spacings of ∿1° within approximately 14 days, half the period of revolution of the Moon on its axis.

4.3.8.4 Earth Communications

Low data-rate communications, e.g., for commands, will be possible through the omni antenna and also through the fan-beam antenna, provided that the spacecraft is oriented so that the fan-beam intersects the Earth.

For the baseline spacecraft, however, high data rate communications, e.g., for the regular data dumps, must be performed using the HGA. An alternative, weight-saving design would dispense with the HGA and use only the fan-beam antenna with a higher power amplifier than in the baseline design. This alternative would generally necessitate reorientation of the spacecraft for communications through the fan-beam antenna so that the fan-beam would intersect the Earth.

For the baseline spacecraft it may be seen from the orbit geometry that the HGA tracking will consist of rotation of the dish about the pitch axis at 1 rpo with a roll-yaw offset which varies slowly from hour to hour.

As described in Section 4.2.10, the programmable body pitch offset capability of the baseline MGO/LGO spacecraft serves as a backup for effecting rotation of the HGA about the pitch axis.

Due to the motions of the Moon on its axis and around the Earth, the ground track of the LGO in the baseline lunar orbit at 100 km altitude will advance westwards at the rate of approximately 1.1 deg/rev.

The Moon, however, perpetually presents almost the same hemisphere to the Earth. Only small lunar librations, or apparent rockings, of ∿7° from the mean orientation occur. The librations result from two main causes.

The geometrical libration in latitude arises from the tilt of 6.5° of the Equator of the Moon from the plane of its orbit around the Earth. The poles of the Moon, therefore, are tipped alternately towards and away from the Earth in a monthly cycle.

The geometrical libration in longitude is due to the eccentricity of the orbit of the Moon around the Earth. The rotation of the Moon on its axis is uniform, but its angular velocity around its orbit is not since the Moon moves faster near perigee than near apogee. Consequently, from Earth approximately 7.75° more of the surface of the Moon can be seen beyond the limb of the mean visible hemisphere.

Further, there is a rocking, or "physical libration," caused by the attraction of the Earth on the long diameter of the triaxial ellipsoid figure of the Moon.

These small librations apart, therefore, the LGO orbit will be seen from the Earth to precess westwards across the visible face of the Moon in about 14 days.

One baseline option regarding orbit maintenance is to keep the mission orbit circular at 100 km altitude. Another option is to allow the the ellipticity of the orbit to increase to the point where the apolune and perilune altitudes are about 150 km and 50 km respectively before recircularization. Correspondingly, as seen from the LGO, occultation of the Earth by the lunar limb will occur for LGO-Earth vectors further than 113°-103.6° from the zenith.

Consideration of these angular limits shows that for some orbits, whose planes lie approximately perpendicular to the Moon-Earth line, there will be no occultation of the Earth by the Moon. For such orbits, the greatest departure of the LGO-Earth vector from the local LGO zenith will occur when the LGO is on the far side of the most distant of the two lunar poles from the Earth, and will be about (90 + 7 + 5)° = 102°. For most orbits, however, communications will be restricted by occultation of the Earth by the Moon; and this restriction will occur throughout the entire 360° range of azimuths with respect to the LGO.

The LGO will be held nadir pointing by virtue of continuous control of its pitch offset at the orbital rate. The solid angle swept through by the LGO-Earth vector for all communications opportunities, therefore, is that bounded by a cone of half angle 113°-103.6° (depending on LGO altitude) as measured from the zenith direction. This is represented in Figure 4.3-16. A precise investigation of HGA pointing would be a subject of a follow-on LGO study.

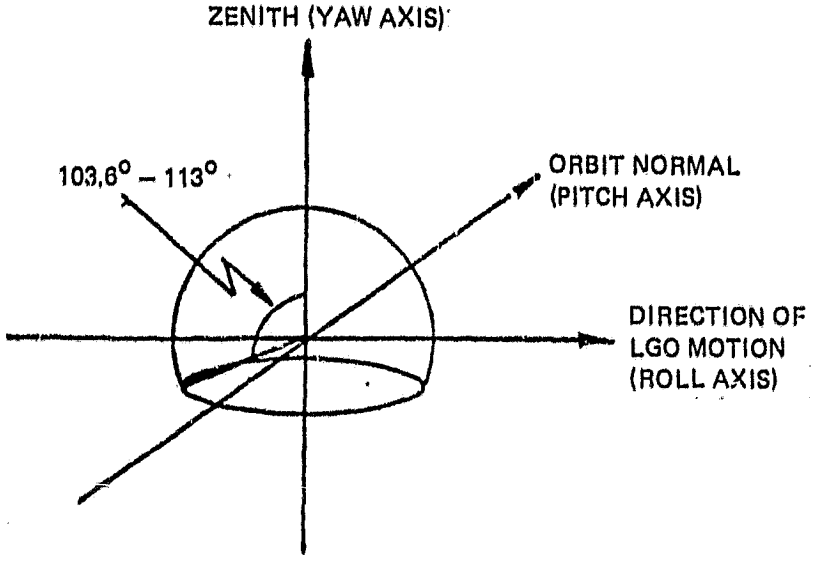

Figure 4.3-16. Solid Angle Swept by LGO-Earth Line

A 180° pitch offset maneuver will be made for HGA communications wherever necessary for the HGA beam to clear the body of the spacecraft.

4.3.8.5 Occultations and Eclipses

The history of the visibility of the LGO from Earth was simulated in the GSFC LPO study. For circular polar orbits at 100 km altitude, it was found that periods of occultations for all locations on Earth constituted ∿25% of the mission, with the longest occultation lasting ∿0.8 hour. Results for partial occultations (i.e., occulted for only part of the Earth's surface) and results for slightly decayed elliptical orbits were very close. The visibility depends upon the inclination of the orbit and the right ascension of the nodes with respect to the Earth-Moon line.

Finally, the phenomenon of solar occultation for the LGO is similar to that of Earth occultation. For the baseline circular polar orbit, the LGO will be in umbra for an average of ∿37% of the time, with the longest period being for ∿0.8 hour. Extension of these results to include time in the penumbra results in virtually insignificant differences. The duration in shadow will vary smoothly through the year since the angle between the orbit normal and the Sun varies smoothly at a rate just a little slower than 1° per day. For orbits at 100 km altitude, shadow-free periods of ∿35 days will occur twice per year at half yearly intervals, interleaved with periods that include the longest time in eclipse when the line of nodes is parallel to the Sun-Moon line. In addition, the LGO will be in darkness during eclipses of the Moon by the Earth. The dates and durations of partial and total eclipses of the Moon from August 1988 through December 1993 are shown in Table 4.3-6. The longest

TABLE 4.3-6. DATES AND DURATIONS OF LUNAR ECLIPSES

Date	Partial Eclipse Duration (minutes)	Total Eclipse Duration (minutes)
8/27/88	122	-
2/20/89	212	76
8/17/89	220	98
2/9/90	204	46
8/6/90	174	-
12/21/91	70	-
6/16/92	174	-
12/9/92	212	74
6/4/93	220	98
11/29/93	206	50

total eclipses last for 98 minutes and the longest partial eclipses for 220 minutes. If necessary, data transmission to Earth will be curtailed so that the LGO will survive these eclipse periods on battery power. Since operation in the shadow of the Moon for approximately half of each orbit for most of the year is part of the baseline mission design, there are no design-driving power and thermal impacts of lunar eclipses.

SECTION 5.0
PROPULSION SUBSYSTEM

SECTION 5.0
PROPULSION SUBSYSTEM

The MGO propulsion subsystem is a single-stage hydrazine blowdown configuration consisting entirely of flight-proven hardware. The system is designed to deliver 450 kg of hydrazine in a 5-to-1 blowdown ratio for the following attitude- and orbit-control functions: spin-rate control (spin-up and despin), orbit injection error correction, mission maneuvers, momentum management, precession maneuvers, attitude control, and end-of-life orbit adjust.

The proposed propulsion subsystem is shown schematically in Figure 5-1. All components are fully redundant and the design provides for selective isolation of any element by ground command, thus yielding a subsystem with no single-point failures.

5.1 SUBSYSTEM CONFIGURATION

To provide the required thrust levels, the baseline subsystem provides 10 rocket engine assemblies (REAs). Two of the REAs are rated at 22.3 N (5 lb_f). These engines are canted relative to each other, but the thrust vector of each REA goes directly through the spacecraft center of mass. These two REAs may be used as a pair or individually. Their primary use is for large

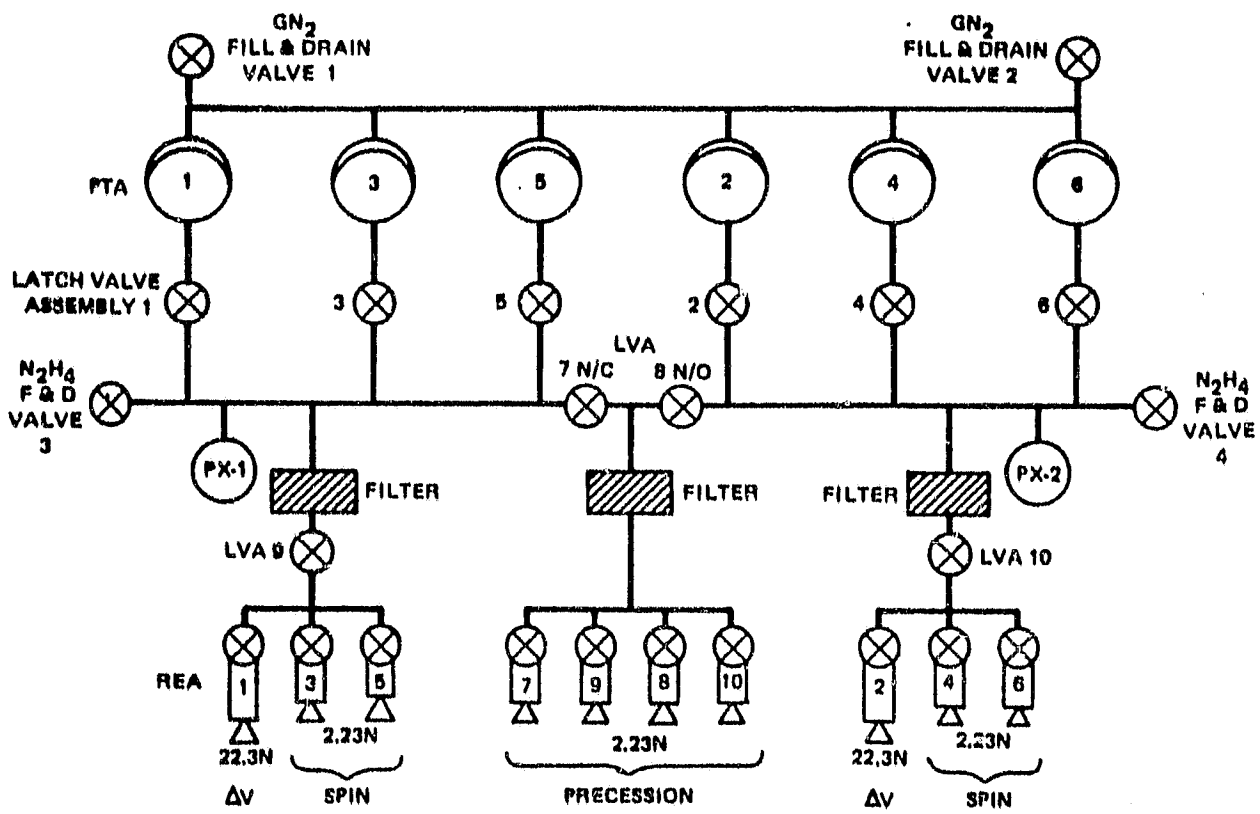

Figure 5-1. Propulsion Subsystem, Schematic Diagram

ΔV maneuvers such as for orbit lowering from the initial Mars insertion orbit to the circular, Sun-synchronous mission orbit at 350 km altitude, and for raising the orbit at EOL.

Eight 2.23 N (0.5 lb_f) REAs are provided for spin and precession maneuvers. They are capable of performing all orbit-adjust and attitude control functions that will be required throughout the mission. The locations and functions of the thrusters are shown in Figure 5-2. Note that the field-of-view studies of Section 3 do not include the thrusters. All engines are provided with a redundant, backup REA that can be used for the required maneuvers.

In like manner to AE, the hydrazine is stored in six propellant tanks, which are divided into two independent half systems. Each half system maintains a uniform pressure and can be used independently of the other half system. Each 22.1-inch diameter tank is a sphere with an elastomeric diaphragm to prevent gas ingestion in the hydrazine manifolds.

5.2 CENTER OF MASS MANAGEMENT

The tanks of each half system are alternated symmetrically around the spacecraft spin axis, as shown in Figure 5-3. As can also be seen from the field-of-view studies of Section 3, the plane containing the X, Y, Z coordinate reference (0, 0, 0), also contains the geometric center of all six tanks. The design allows for center-of-mass control by withdrawing propellant from the tanks individually. This control is accomplished by opening or closing any of the tank outlet latch valves as required. When a half system is used as a unit, the propellant mass decreases uniformly around the spin axis and does not shift the spacecraft center of mass away from the spin axis.

Two pressure transducers (PX-1 and PX-2) are provided to gauge the amount of propellant left in each half system. These gauges are normally isolated from each other, but by opening the cross-over latch valves (LVAs 7 and 8 of Figure 5-1) the transducers can be calibrated against one another.

Ten latch valves are provided for fuel isolation and to minimize propellant loss due to potential rocket engine or propellant tank leaks. In addition to filters in the latch valves, three high-capacity filters are located in the propellant pathway in front of the REAs.

Heaters, located as required to keep the N_2H_4 above the minimum temperature limit, are monitored by strategically located temperature sensors. Propulsion system parameters will be monitored via telemetry.

5.3 CONTAMINATION CONSIDERATIONS

With the type of scientific instruments on both the MGO and LGO missions, the final thruster layout is critical because of plume impingement considerations. The rocket engine assemblies shown in Figure 3-6 will be mounted on the spacecraft in the same way as was done for AE. Extensive further analysis is required to minimize this potential problem. However, AE flight data from the sensitive instruments has confirmed that no contamination problems occurred from the hydrazine plumes.

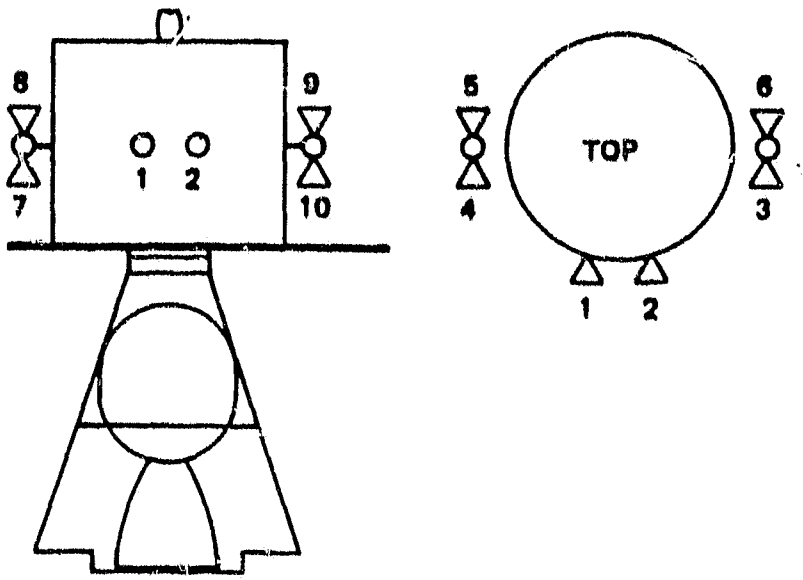

MANEUVER	REA NO.
ORBIT CIRCULARIZATION	1 + 2
SPIN AND DE-SPIN	3 + 5 OR 4 + 6
PRECESSION	8 + 10 OR 7 + 9

Figure 5-2. Rocket Engine Assembly Locations

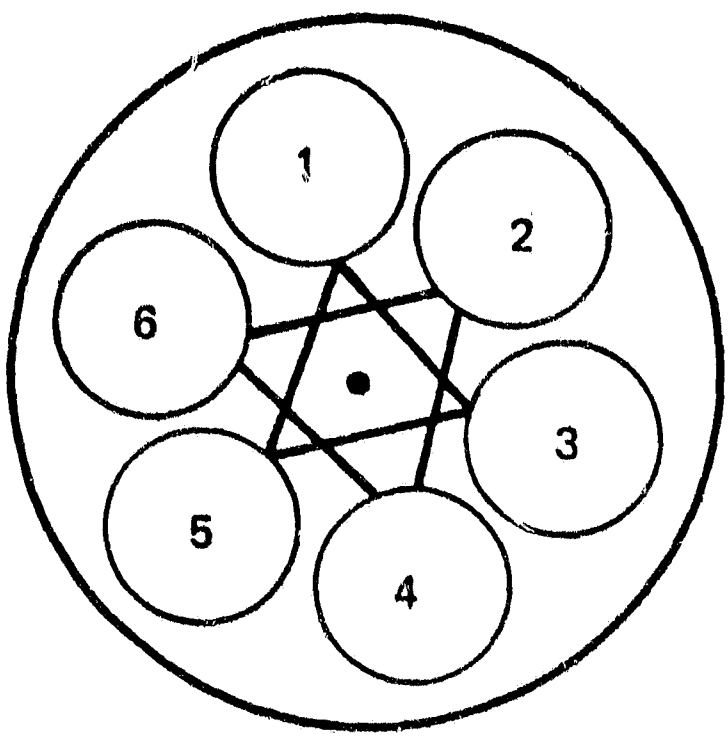

Figure 5-3. Propellant Tank Configuration

SECTION 6.0
MASS PROPERTIES

SECTION 6.0
MASS PROPERTIES

6.1 SPACECRAFT STRUCTURE ESTIMATES

As has been presented in Section 3, the physical size of the spacecraft was arrived at by scaling up the existing dimensions of the structure to accommodate 22.1 inch diameter spherical propellant tanks, as compared to the 16.5 inch tanks of the heritage Atmosphere Explorer structure design. In all of the estimates contained herein, the resulting scale factor (24/17.5) was applied to the measured values of the corresponding structure elements from the Dynamics Explorer program as a cubed factor to assure conservatism in the estimates. In the case of the solar array substrates, which are of a honeycomb construction, the factor was applied as a squared factor since no justification for the increase in honeycomb thickness has been identified. Similarly, for box mounting bracketry, since the dimensions of the electronics boxes have not changed, the "as measured support bracketry" was not scaled. In all cases of the estimated masses, various percentage margin allocations were made, with the percent allocated being a function of the degree of legacy in the equipment design. Table 6-1 contains the mass estimates for both the "big bird" configuration and the "little bird" configuration for comparison purposes.

6.2 ELECTRONIC COMPONENTS ESTIMATES

Entries in Table 6-1 for the electronics components are, for the most part, based on actual weights of the heritage design components from the DE program. It should be noted that when these weights are compared to those of the equivalent components of the AE program, significant weight reductions were achieved. While the system architecture was basically identical between AE and DE, the availability of more densely packaged, qualified piece parts allowed for reduction in the numbers of electronics cards and circuit elements to perform the same functions. It can equally be expected that similar improvements could be encountered in applying the DE designs to the MGO/LGO flight equipment, thereby rendering the estimates of Table 6-1 very conservative. No such reductions have been accounted for in the estimates herein. For those components which were non-redundant in the DE equipment complement, the measured masses were doubled. This again is conservative in that in-house RCA design practice routinely houses both redundant components in a single common "wrapper" or package.

6.3 TOTAL DRY MASSES

The dry masses of both the little bird and big bird designs for the MGO spacecraft are tabulated at the bottom of Table 6-1. The big bird mass, including the total margin, along with the total mass of hydrazine as identified in the mission analyses of Section 4, were used to assess maneuvering performance (hydrazine budget) orbit insertion motor selection and launch vehicle selection.

TABLE 6-1. MGO MASS BUDGET (kg)

ELEMENT	16.5" TANK CONFIG. LITTLE BIRD	22.1" TANK CONFIG. BIG BIRD	COMMENT
INSTRUMENT			
Gamma Ray Spectrometer	12	12	
Multi-Spectral Mapper	17	17	
Magnetometer	5	5	
Radar Altimeter	10	10	
	44	44	
20% Margin	8.8	8.8	
	52.8	52.8	
STRUCTURE			
Upper Base Plate	9.33	24.06	
Lower Base Plate	9.28	23.94	Scaled by $\left(\frac{24}{17.5}\right)^3$
Center Column/Shear Process	12.87	33.20	
Separation Adapter	6.51	16.79	
MWA Support	1.52	3.92	
	39.51	101.91	
10% Margin	3.95	10.19	
	43.46	112.10	
Solar Array Substrates (Less Cells) = 2 x 20.5 lbs	18.19	34.21	Scaled by $\left(\frac{24}{17.5}\right)^2$
10% Margin	1.82	3.42	
	26.00	37.63	
Box Support Bracketry	19.12	19.12	
10% Margin	1.91	1.91	
	21.02	21.02	
COMMUNICATIONS			
Transponder 2 x 33.2 lbs	30.12	30.12	Based on AE Antenna
Low Gain Antenna	4.54	4.54	Not Based on DE
High Gain Antenna Assembly	6.8	6.8	
Antenna 2 Axis Index	5.0	5.0	
	46.46	46.46	
10% Margin	4.65	4.65	
	51.11	51.11	

TABLE 6-1. MGO MASS BUDGET (kg) (Continued)

ELEMENT	16.5" TANK CONFIG. LITTLE BIRD	22.1" TANK CONFIG. BIG BIRD	COMMENT
C&DH			
CTP 2 x 11.9 lbs	10.79	10.79	
CDU 1.5 x 12.1 lbs	8.23	8.23	
RTM 2 x 9.9 lbs	8.98	8.98	
TR's 37.3 lbs	16.92	16.92	
	44.92	44.92	
10% Margin	4.49	4.49	
	49.41	49.41	
HARNESS S/C	23.18	31.79	Scaled by $\left(\frac{25}{17.5}\right)^2$
Intra-Inst. Harn.	1.86	1.86	No Scaling
	25.04	33.65	
10% Margin	2.50	3.37	
	27.54	37.02	
ASTROMAST 2 @ 24.1 lbs (6 meter)	21.86	21.86	Margin for Clocking Plates, Related Mechanics, etc.
10% Margin	2.19	2.19	
	24.05	24.05	
THERMAL			
2 x DE-B = 2 X 11.42 lbs	10.36	10.36	5 kg for Modified RCS & OIM Heaters
Tank & Engine Htrs	5.	5	
	15.36	15.36	
10% Margin	1.54	1.54	
	16.89	16.89	
ADACS			
2 x PCE 2 x 10.9 lbs	9.89	9.89	Scale by $\left(\frac{24}{17.5}\right)^2$
MWA 39.64 lbs	17.98	17.98	
2 x Sun Sens 2 x3.11 lbs	2.82	2.82	
Nut. DPR (Passive) 12.15	5.5	10.34	
2 CS201 STAR Sensors @ 2.95 kg	5.9	5.9	Not Based on DE
2 Gyro Packages @ 4.55 kg	9.1	9.1	Not Based on DE
	51.19	56.03	
15% Margin		8.40	
	58.87	64.43	

TABLE 6-1. MGO MASS BUDGET (kg) (Continued)

ELEMENT	16.5" TANK CONFIG. LITTLE BIRD	22.1" TANK CONFIG. BIG BIRD	COMMENT
POWER			
PSE	9.01	9.01	
Batteries (2) $\left(\frac{24}{17.5}\right)^2$	16.83	16.83	Scale Cell Mass by $\left(\frac{24}{17.5}\right)^2$
+28V REG	1.78	1.78	
Solar Cells 2 x DE-B Lower = 2 x 25.7 lbs	23.35	43.92	
	50.97	71.54	
10% Margin	5.10	7.15	
	56.07	78.69	
BALANCE DE-B = 25 lbs	11.34	29.95	Scale by $\left(\frac{24}{17.5}\right)^3$
	11.34	29.25	
RCS (DRY)			
Tanks	45.59	46.95	Per PSI Data Sheet
Plumbing	3	4	Not Based on DE
Valves	3	3	
Engines	16	16	
	67.59	69.95	
10% Margin	6.76	7	
	64.35	76.95	
S/C Dry Weight:	512.91 (Incl 51.39 kg Margin) Margin)	651.35 (Incl 71.91 kg	

6.4 INERTIA CHARACTERISTICS

The masses comprising the MGO spacecraft having been identified, a brief mass properties analysis was performed to support the attitude control analyses of Section 7. The major elements of the structure, hats, propellant tanks, and hydrazine loads, along with the masses of the payload instruments were individually modeled in an available automated analytic model. The remaining electronics components, along with the undistributed margins, are modeled as two toriodal masses, one resident on the outward facing surface of each of the two baseplates. A sample of the analytic model tabulation is contained in Appendix A of this report.

Several conditions were analyzed for the MGO design. These included:

- Fully stowed, full hydrazine load, OIM jettisoned (Case 1)
- Fully stowed, full hydrazine load, full Star 30C attached (Case 2)
- Fully stowed, full hydrazine load, full Star 37F attached (Case 3)
- Partially deployed, (astromasts only), full hydrazine load, OIM jettisoned (Case 4)
- Fully deployed, empty hydrazine load, OIM jettisoned (Case 5)

The resulting inertia characteristics are shown in Table 6-2 and are the basis for the attitude control techniques discussed in Section 7. Note that in all of the cases considered, when the OIM has been jettisoned, the ratio of the spin moment of inertia to the maximum transverse moment of inertia is greater than one. Since this includes the partially deployed case, the indication is that during the deployment scenario, if for some reason the momentum wheel should stop, the system would remain spinning about the proper axis.

TABLE 6-2. MGO INERTIA PROPERTIES

CASE 1	Stowed, No Engine, Full N_2H_4 Load I_{xx} = .325 (10^4) in-lb-sec^2 I_{yy} = .338 (10^4) in-lb-sec^2 I_{zz} = .430 (10^4) in-lb-sec^2 $I_{SPIN}/I_{TRANS(MAX)}$ = 1.272
Case 2	Stowed, Full 30C Attached, Full N_2H_4 Load I_{xx} = .119 (10^5) in-lb-sec^2 I_{yy} = .120 (10^5) in-lb-sec^2 I_{zz} = .474 (10^4) in-lb-sec^2 $I_{SPIN}/I_{TRANS(MAX)}$ = .394
Case 3	Stowed, "Full" 37F Attached Full N_2H_4 Load I_{xx} = .157 (10^5) in-lb-sec^2 I_{yy} = .159 (10^5) in-lb-sec^2 I_{zz} = .491 (10^4) in-lb-sec^2 $I_{SPIN}/I_{TRANS(MAX)}$ = 0.310
Case 4	Partial Deploy, No Engine, Full Load N_2H_4 I_{xx} = .321 (10^4) in-lb-sec^2 I_{yy} = .488 (10^4) in-lb-sec^2 I_{zz} = .588 (10^4) in-lb-sec^2 $I_{SPIN}/I_{TRANS(MAX)}$ = 1.033
Case 5	On-Orbit Full Deploy, No Engine, No N_2H_4 I_{xx} = .370 (10^4) in-lb-sec^2 I_{yy} = .522 (10^4) in-lb-sec^2 I_{zz} = .670 (10^4) in-lb-sec^2 $I_{SPIN}/I_{TRANS(MAX)}$ = 1.284
NOTE:	Inertia properties exclude Momentum Wheel

SECTION 7.0
ATTITUDE DETERMINATION AND CONTROL

SECTION 7.0
ATTITUDE DETERMINATION AND CONTROL

7.1 SPACECRAFT DESIGN

The spacecraft is designed to minimize fuel usage in the cruise orbit, to provide adequate maneuvering propulsion while in the Lunar or the Mars orbit, to account for uncertainties in the gravitation of those bodies, to provide an accurate orientation of the spacecraft in all mission modes, and to provide for momentum management. Further, the "flip over" maneuver, required for the LGO mission (See Section 9), is performed by this subsystem and the propulsion subsystem.

The requirement for a substantial quantity of propellant storage, electrical power requirements and instrument accommodation necessitate adopting the "big bird" option (See Section 3). In this configuration, the six tank geometry used in AE is retained because it eases the problem of maintaining the center of mass on the spin axis.

The spacecraft will have a large momentum bias, which provides a stable configuration with minimum nutation, so minimal fuel will be required in the cruise phase. It will be a dual spinner capable of rotating once per revolution in orbit about the Moon or Mars, and by using momentum management techniques, the spacecraft can be oriented to point towards any vector in the spacecraft X-Y plane along nadir.

A momentum biased system was selected for the MGO/LGO system designs for several reasons:

- The proven techniques from both the AE and DE programs for orientation of the instrument platform in the range of pointing accuracy required, lend themselves to this form of control and mission.
- The gyroscopically stiff spacecraft oriented in the mission mode is inherently extremely insensitive to disturbances. Furthermore, in the event of anamolous behavior, e.g., momentum wheel slowdown or stoppage, the system, being a principal axis spinner in the on-orbit configuration, is benign and does not require immediate corrective actions.
- During the cruise phase, a gyroscopically stiff system with the OIM attached will retain its desired orientation with minimum attitude correction. Further, with the system which evolved during the study, the need for propellant expenditure for active nutation damping is obviated. During the course of the study, a parallel analysis was performed for a cruise configuration MGO with inertia properties similar to the final derivation, as reported in Section 6.

This parallel study assumed inertia properties of the spacecraft OIM combination of:

$$I = 5640 \text{ in-lb-sec}^2$$

$$I_{xx} = I_{tt} = 9590 \text{ in-lb-sec}^2 \left(I_{tt} \equiv I_{\text{max transverse}}\right)$$

Assuming spin rates during the cruise phase of 1, 5, and 30 rpm, the analysis yielded the propellant utilization for nutation control of nutation angles of 1° and 3°, as shown in Table 7-1.

TABLE 7-1. PROPELLANT UTILIZATION PER DAY FOR NUTATION CONTROL (lbs/day)

Nutation Angle	Spin Rate		
	1 rpm	5 rpm	30 rpm
1°	0.7973	14.195	352.1
3°	2.393	42.515	1056.6

The detailed analysis supporting these findings is contained in Appendix B of this report.

While not exact, in that the inertia values used are somewhat different than those reported for the MGO configuration in Section 6, these valves are sufficiently close to indicate the unacceptability of active damping by propulsive means for the cruise phase.

During the cruise phase, celestial sensors will be used to determine spacecraft orientation prior to making midcourse corrections. For other attitude determination activities, the Sun sensors will be used. The sensors will be used in mission mode as one element of an attitude determination and control technique.

7.2 MOMENTUM SIZING

Fundamental to the application of the existing designs and technologies from the AE and DE programs, the basic momentum wheel design has been retained. This assembly consists of a brushless dc motor assembly, a lightly preloaded dual bearing pair and a "flywheel" inertia rim. In the AE design, the system was equipped with redundant motors; in the DE design, the second motor was omitted but the housing envelope retained the configuration to allow for a second motor. A major key to the application of the same design to a different mission is retaining the operating speed regime of the wheel to allow retention to the bearing design and especially the design of the bearing lubrication system. In sizing the momentum system for the MGO/LGO, this characteristic has been taken as the prime consideration. Thus, when the momentum magnitudes for various phases of the mission are identified, the only change to the momentum wheel design is the sizing of the inertia rim of the flywheel. In both the AE and DE applications, the momentum wheel was required to operate over several speed ranges. Given a nominal system momentum for a 1 rpo momentum biased spacecraft, by varying the wheel speed relative to the body, conservation of momentum results in imparting rotation rates to the body. This technique was used extensively in the AE program where the system operated in a 1 rpo mode and also allowed for body rotation rates, selectable from 1 to 10 rpm.

Given the system inertias as reported in Section 6, and considering the cruise case where the star 30C OIM is in place, the following sizing of momentum values was conducted. For the cruise phase, a slow rotation rate of the body is desired for thermal considerations (also see the discussion of cruise phase attitude maneuvers for thermal and communication considerations in Section 9). Likewise, during cruise, the assembled "stack" (stowed spacecraft and OIM) is stable about the pitch (Z) axis, which is also the rotation axis, of the momentum wheel if the momentum stored in the wheel is much larger than that stored in the body at its slow rotation rate. For conditions where 0.1 rpm on the body provides an adequate thermal rotation rate, and assuming roughly

a 100:1 ratio of momentum in the wheel to momentum in the body, and further assuming that acceptable wheel speeds are in the range of 200 rpm to 1500 rpm, the following conditions were derived, recognizing that the system would also require a momentum ratio which results in a 1 rpo rotation rate in the deployed, "on-or- bit" condition.

In the on-orbit condition, the deployed inertia of the spacecraft results in 6.1 in-lb-sec of momentum in the body. Thus, for a 100:1 ratio in this condition, the wheel momentum is 610 in-lb-sec yielding a wheel inertial of 29.13 in-lb-sec^2. Considering next the cruise phase, the wheel will operate in the low speed regime in the on-orbit case and the high speed regime during cruise where the momentum of the stack is 49.64 in-lb-sec. This results in a momentum ratio of 92.16, which is acceptable for the stability criteria. Alternately, given these speed limitations and inertia properties, and again starting from an "on-orbit" condition, if it were desired to force the ratio during cruise to be 100:1, this would result in reducing the stack rotation rate during the cruise phase from 0.1 rpm to 0.0922 rpm, also a totally acceptable solution.

Given these conditions, the physical size of the momentum wheel was addressed. The existing DE momentum wheel was 25 inches in diameter with an inertia of 6.366 in-lb-sec^2. For the MGO wheel inertia of 29.13 in-lb-sec^2, and assuming that the mass of the wheel is kept constant (conservative estimate) but redistributed, and since

$$I = MR^2 ,$$

then the new radius of the MGO wheel is found to be 26.74 inches. The resulting 53.5 inch diameter wheel fits nicely within the envelope of the spacecraft. Further, as the actual design of the momentum rim will, in actuality, probably result in some mass increase, the resulting wheel diameter would be somewhat smaller. By comparison, the momentum wheel assembly inertia rim employed in the AE design was 48 inches in diameter.

To achieve the desired rotation rates of the stack in the cruise phase for the candidate CS201 celestial sensors, the momentum wheel, by command, is "slowed down" thus increasing the body rate of the stack to the desired value. Having completed the precision attitude sensing activity, the wheel is returned to its normal operating speed in the cruise phase and the "stack" returns to its slow rotation rate. Futhermore, should it be required to stop the body (inertially) during cruise to orient the stowed high gain antenna toward the earth, an algorithm utilizing the Sun sensor output is employed to slightly increase the wheel speed until the body stops in the desired orientation.

A similar technique is used in the on-orbit configuration when it is desired to obtain a precision attitude data sample. This maneuver is not projected to be performed frequently during the mission, possibly once every one or two weeks. To perform the same in the on-orbit configuration, the same concept is employed, but in this condition the wheel speed is raised rather than lowered. Since momentum must be conserved, the body reduces from 1 rpo to zero and then spins up in the opposite rotational sense from the 1 rpo direction to the desired rate. Upon completion of the data gathering, the wheel speed is returned to the normal orbital rate and pitch capture is re-achieved.

7.3 MGO PITCH PERFORMANCE

Application of the pitch control system of the AE and DE programs to the MGO and LGO missions required the assessment of the existing horizon sensors for these applications. The boltmeter sensors, which were optically filtered to respond in the 14-16 micron band CO_2 horizon regime and which were used in both heritage programs, were considered for the MGO mission. In the pitch control system design, the sensors scan the body being orbited by means of a mirror mounted to the momentum wheel. The scan path so generated is offset from the orbit plane to optimize geometric sensitivity. The resulting horizon sensor output, called the body crossing envelope (BCE), is "split", and the resulting signal is compared to a reference pulse, generated once per wheel revolution. The displacement between the reference and the split pulse is a direct measure of the instantaneous pitch error. In response to this error, the wheel speed is slightly increased (or decreased) until the two pulses are aligned.

An existing in-house analytic model of the sensor and associated processing electronics was employed to determine the effects of the Mars CO_2 horizon on pitch performance. This model takes into account that the output of the sensor, due to the time constraints of the bolometer and associated processing electronics, is delayed in time from the ideal condition, thus a relatively constant delay in the location of the split pulse is encountered. (In practice, this delay is measured and the reference pulse generator is intentionally aligned to compensate for the shift). A series of 11 computer runs was made under the assumption that the bolometer assembly and optics could be modified to produce an output signal equivalent to that of the system in Earth orbit. The input conditions and the resulting shift in split point for the conditions analyzed are tabulated in Table 7-2 for the 11 cases considered. To assess the effects on pitch performance, the average value of the shift in split pulse was subtracted from the result of each case to determine the pitch error and roll error average values resulting from these 11 cases. These errors are tabulated in Table 7-3. Due to the offset in scan angle for the bolometers from the orbit plane, an instantaneous pitch error also translates into an apparent roll error which can be approximated by:

$$\frac{\text{Mars Crossing Envelope}}{2} \pm \text{Roll Error} = \frac{\text{Average Pitch Error}}{2}$$

Taking the pitch error analysis from the Dynamics Explorer program and adding in the pitch and roll errors (from Table 7-3), the resulting performance in pitch control and indicated roll error can be seen to be only about 0.02 worse than the performance in Earth orbit. This error budget is presented in Table 7-4. By comparison with the instrument pointing requirements as presented in Section 3, the system performance easily satisfied the payload.

7.4 MARS HORIZON SENSING

The key to the preceding analysis is the assumption that the horizon sensor performance in orbit around Mars can be adjusted to equal that of its Earth orbiting performance. Given comparative horizon radiance data from the Viking program, the incident energy on the bolometers in Mars orbit is approximately one-fourth that encountered in Earth orbit in the 14-16 micron band. Thus, to achieve the same signal output of the bolometer assembly, the bolometer flake length would have to be doubled as would the bolometer telescope lens diameter. Since the bolometer assemblies are housed in the momentum wheel assembly, such changes would also require modifications to this equipment.

TABLE 7-2. MGO SIMULATIONS

Orbit Alt. (km)	Run No.	Sky/Mars Latitude	Mars/Sky Latitude	Scan Rate rpm	Threshold Factor	Gain Factor	Mars Crossing Envelope (degrees)	Sensed Degrees from Sky/Mars Horizon	Hard Surface Mars/Sky Horizon (degrees)	Resulting Center Split Pulse Shift (degrees)
300	1	Jul 22°N	Jul 22°N	4500	0.4	1.0	125.114	-57.610	67.453	4.8957
300	2	Sep 48°N	Sep 48°N	4500	0.4	1.0	125.039	-57.786	67.253	4.7337
300	3	Mar 24°S	Mar 24°S	4500	0.4	1.0	124.698	-57.552	67.145	4.7965
300	4	Jul 22°N	Sep 48°N	4500	0.4	1.0	125.918	-57.682	67.236	4.7767
300	5	Sep 48°N	Jul 22°N	4500	0.4	1.0	125.221	-57.755	67.466	4.8556
300	6	Sep 48°N	Sep 48°N	4950	0.4	1.0	125.286	-57.438	67.848	5.2046
300	7	Sep 48°N	Sep 48°N	4050	0.4	1.0	124.445	-57.911	66.534	4.3119
300	8	Sep 48°N	Sep 48°N	4500	0.4	0.9	125.039	-57.786	67.253	4.7337
300	9	Sep 48°N	Sep 48°N	4500	0.4	1.1	125.039	-57.786	67.253	4.7337
300	10	Sep 48°N	Sep 48°N	4500	0.39	1.0	125.151	-57.837	67.314	4.7388
300	11	Sep 48°N	Sep 48°N	4500	0.41	1.0	124.928	-57.736	67.192	4.7284
Average							124.989			4.17736

TABLE 7-3. MPO PITCH/ROLL ERRORS

Run	Pitch Error	Roll Error
1	+0.12	+0.08
2	-0.04	+0.03
3	+0.01	-0.18
4	+0.003	-0.04
5	+0.08	+0.14
6	+0.43	+0.18
7	-0.46	-0.33
8	-0.04	+0.03
9	-0.04	+0.03
10	-0.02	+0.10
11	-0.05	-0.07
Average	0.12	0.18

$$\frac{MCE}{2} + RE = \frac{AV}{2}$$

TABLE 7-4. MPO PITCH LOOP ERROR

Error Source	(Deg. Pitch)	Roll (Deg)	Comment
Noise	0.021	0.047	From DE-B Earth Error Analysis (From Table 7-2)
Threshold Variation	0.0	0.056	
Gain Variation	0.01	0.011	
Wheel Speed Change	0.31	0.085	
IR Scanner Alignment	0.10	0.032	
Horizon Radiance Variation Errors	0.12	0.18	(From Table 7-3)
RSS of Above	0.348	0.215	(1)
RSS of Above with Wheel Speed Effects Calibrated Out	0.158	0.197	(4)
RSS (DE-B)	0.342	0.190	(2)
RSS (DE-B) with wheel Speed Effects Calibrated Out	0.143	0.170	(5)
Net Increase or MPO Sensor Over DE-B Sensor	0.006	0.025	(3) = (1) - (2)
	0.015	0.027	(6) = (4) - (5)
Rounded Off Difference	0.02	0.03	

7.5 SELECTED APPROACH

While this approach is an acceptable solution for the MGO case, and is, in fact, the solution which would probably be employed if only a Mars mission were to be considered, the lack of virtually any horizon signature in this energy band in the case of LGO indicates a different solution would be required. Accordingly, to achieve a common design, an alternate method of obtaining instantaneous pitch orientation information has been adopted which is viable for both the MGO and LGO designs.

Instead of using horizon sensors, the instantaneous attitude of the gyroscopically stiff spacecraft will be determined by an algorithm which operates on star sensor and Sun sensor data to yield a control signal for the pitch loop. This algorithm will also provide blanking orientation information to electronically blank the celestial sensors so they are not saturated by the orbited body's albedo during the spacecraft rotation. Locations of the attitude sensors, and their view angles, are shown in the on-orbit configuration figures of Section 3.

SECTION 8.0
MGO/LGO COMMUNICATIONS

SECTION 8.0
MGO/LGO COMMUNICATIONS

8.1 MGO COMMUNICATIONS

8.1.1 Science Data

Figure 8-1 shows the science channel data rates achievable as a function of Earth-to-Mars distance for both S-Band and X-Band downlinks, working into 34 meter and 64 meter ground antennas. The following assumptions apply:

- 1.5 meter dish and 20 watt transmitter on the spacecraft
- S-Band frequency is 2295 MHz; X-Band frequency is 8415 MHz
- Science data PSK-modulated on a square-wave subcarrier
- Carrier modulation index is 0.8 radian nominal
- Engineering telemetry is transmitted simultaneously on another subcarrier
- 32, 6 biorthogonal error coding is used
- Required word error rate is 1×10^{-2}

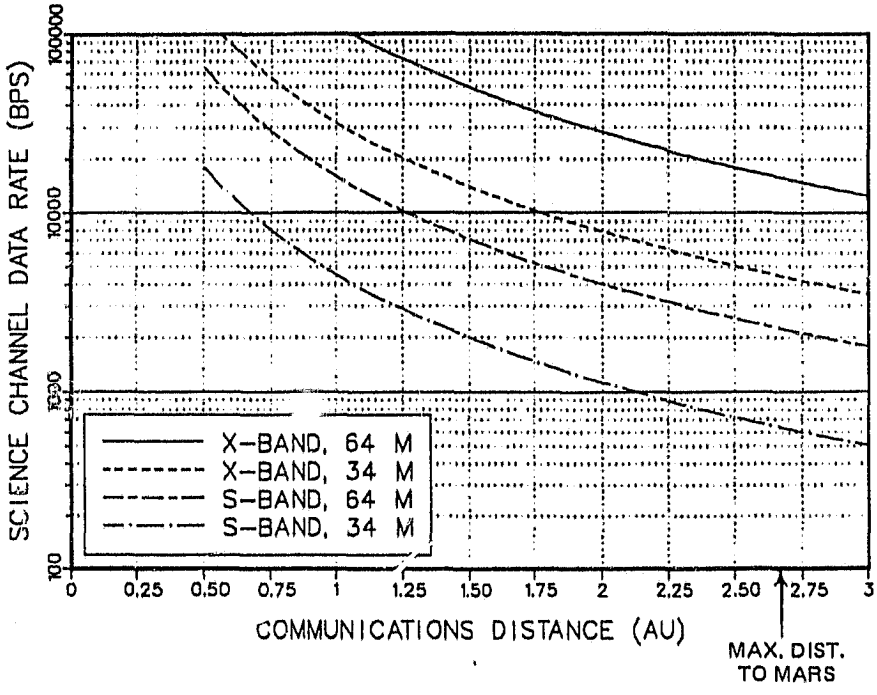

Figure 8-1. MGO Science Channel with Spacecraft High Gain Antenna (HGA)

These assumptions were influenced by the following considerations:

(a) Fitting an antenna larger than the 1.5 meters within the launch vehicle constraints would pose a significant design challenge.

(b) Space-qualified 20 watt power amplifiers are available at both S-Band and X-Band. Output powers greater than 20 watts would entail excessive dc power drain on the spacecraft. (To prelude this being a major factor in limiting the system, the power analyses of Section 10 allocated ample margin to the playback function.)

(c) The error code assumed is the same as used for Viking Lander communications. Additional study would be needed to determine the feasibility of using convolutional coding to obtain further improvement in link performance.

The data rates required for the mission depend upon the sensor raw data rates and the time available for playback. Sensor data rates are expected to be between 3.9 kbps and 14.4 kbps. The time available for playback is a function of the orientation of the spacecraft orbit plane relative to the Earth. At worst the spacecraft would be visible only slightly more than half an orbit. At best it would be continuously visible from Earth.

Table 8-1 shows the data rates needed for several assumed playback schedules with the minimum and maximum sensor data rates rounded off to 4 kbps and 16 kbps respectively. From the table it can be seen that a transmitting data rate of 16 kbps would allow continuous real-time transmission at the maximum sensor rate, or playback every other orbit with sensor data rate at minimum.

TABLE 8-1. PLAYBACK OPTIONS

Playback Schedule	At Minimum Sensor Data Rate (kbps)	At Maximum Sensor Data Rate (kbps)	Remarks
Real Time Continuous	4	16	50% to 100% coverage, dependent upon orbit orientation.
Playback of Stored Data From One Orbit	8	32	Full coverage if playback is performed every orbit.
Playback of Stored Data From Two Orbits	16	64	Full coverage if playback is performed every other orbit. Allows make-up for missed contacts.

Figures 8-2 through 8-5 show spacecraft antenna size vs. transmitter power for various data rates at maximum Earth-Mars distance (2.68 AU). Figure 8-2 shows that with a 64 meter ground antenna at X-Band, a 16 kbps data rate can be supported with a 1.5 meter antenna and a 20-watt transmitter on the spacecraft. However, use of S-Band and/or a 34 meter ground antenna (Figures 8-3 through 8-5) would reduce the available data rate significantly.

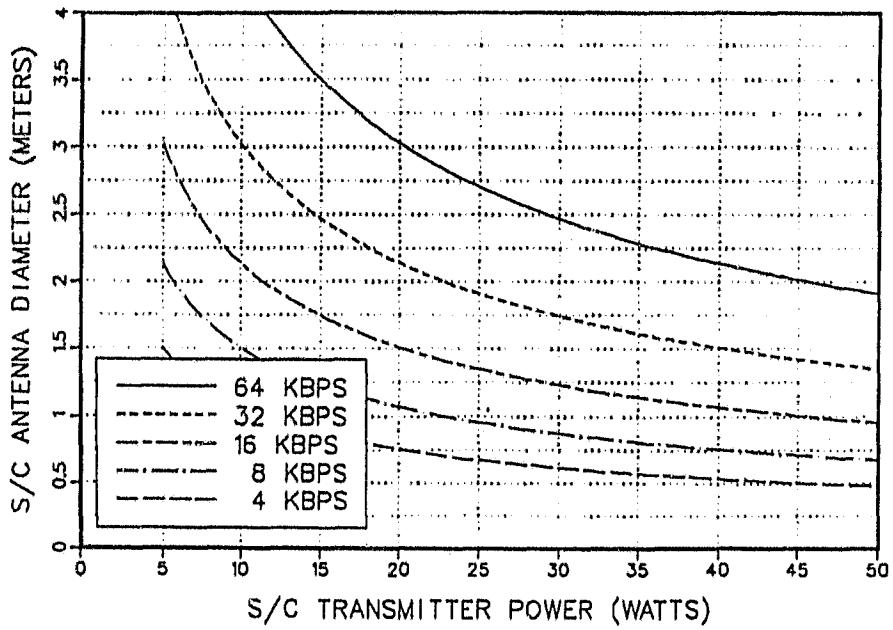

Figure 8-2. MGO Science Channel at Maximum Distance with Spacecraft High Gain Antenna to 64 Meter Antenna at X-Band

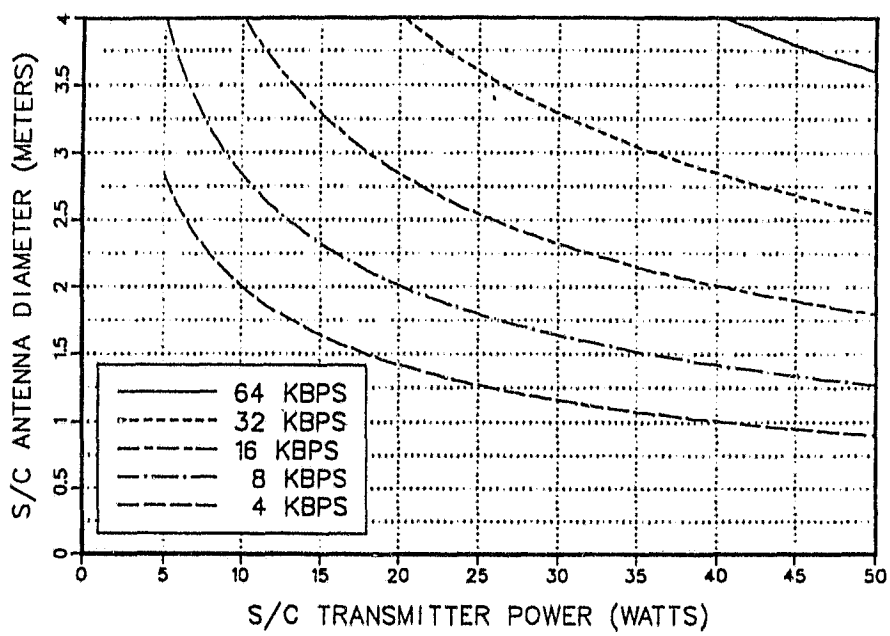

Figure 8-3. MGO Science Channel at Maximum Distance with Spacecraft High Gain Antenna to 34 Meter Antenna at X-Band

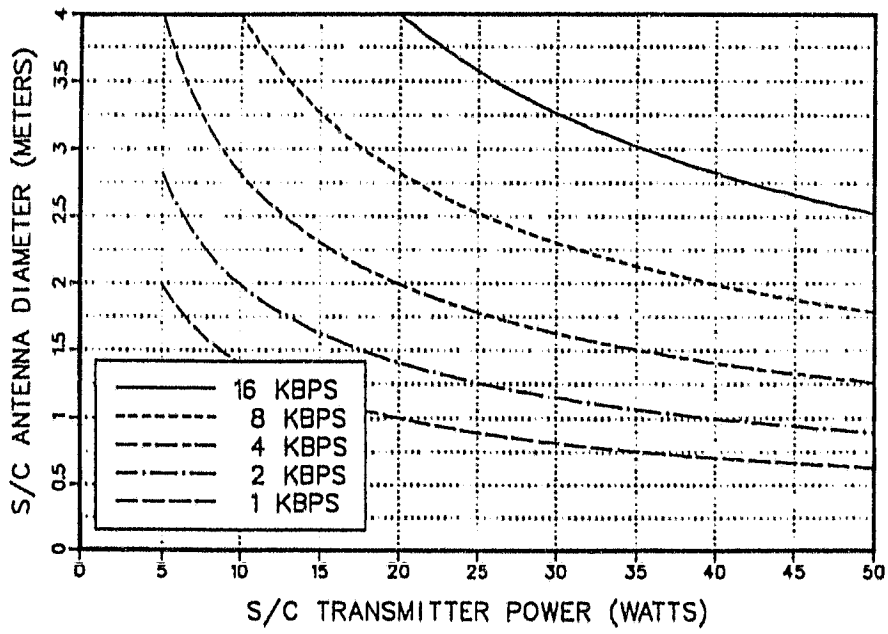

Figure 8-4. MGO Science Channel at Maximum Distance with Spacecraft High Gain Antenna to 64 Meter Antenna at S-Band

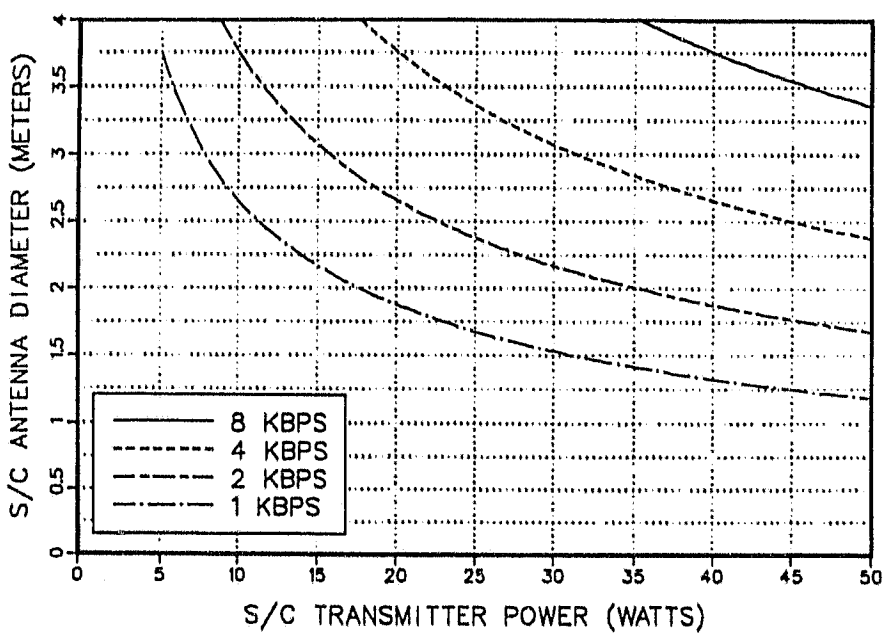

Figure 8-5. MGO Science Channel at Maximum Distance with Spacecraft High Gain Antenna to 34 Meter Antenna at S-Band

Referring to Figure 8-1, it can be seen that much better performance can be obtained near minimum Earth-Mars distance, allowing either the use of a 34 meter ground antenna or a reduced number of ground contacts per day, or combinations of both.

8.1.2 Engineering Telemetry

During mission operations, engineering telemetry will be transmitted simultaneously with science data using a separate subcarrier. Figure 8-6 shows the data rates attainable under the same conditions as in Figure 8-1 with the following additional assumptions:

- Carrier modulation due to the engineering subcarrier is 0.45 radian nominal
- Data is uncoded with a required bit error rate of 5×10^{-3}

It is expected that engineering telemetry rates in the 1 to 10 bps range will be adequate for the mission. Figure 8-6 indicates that more than adequate link capacity is available when the 1.5 meter high gain antenna is used.

During the cruise phase of the mission, there will be times when the spacecraft's orientation may prevent use of the high gain antenna, in which case, a low gain antenna with a toroidal-shaped coverage pattern can be used. Figures 8-7 through 8-10 show the engineering telemetry data rate attainable using a bifilar antenna or a belt antenna to provide the toroidal coverage.

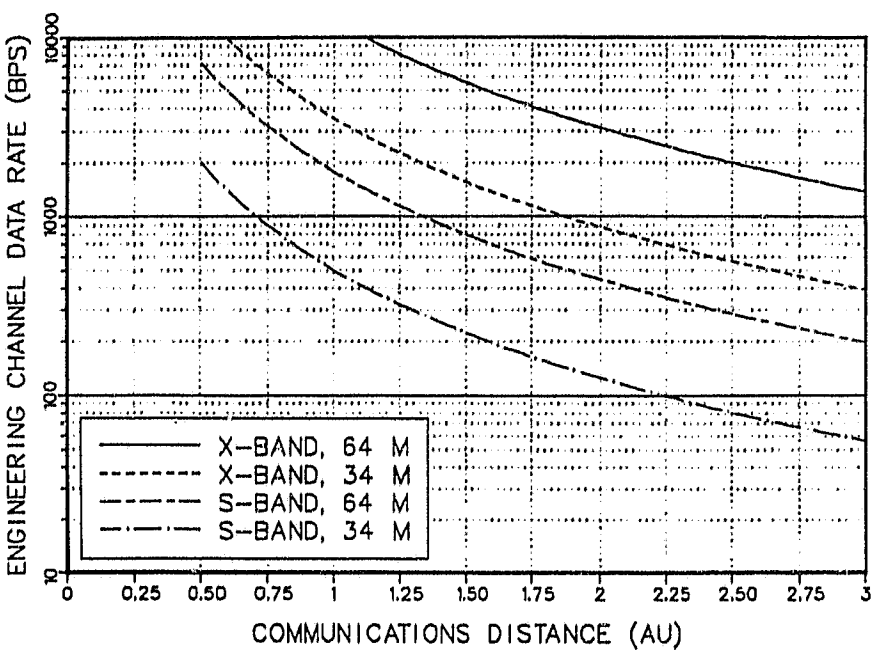

Figure 8-6. MGO Engineering Telemetry Channel with Spacecraft High Gain Antenna

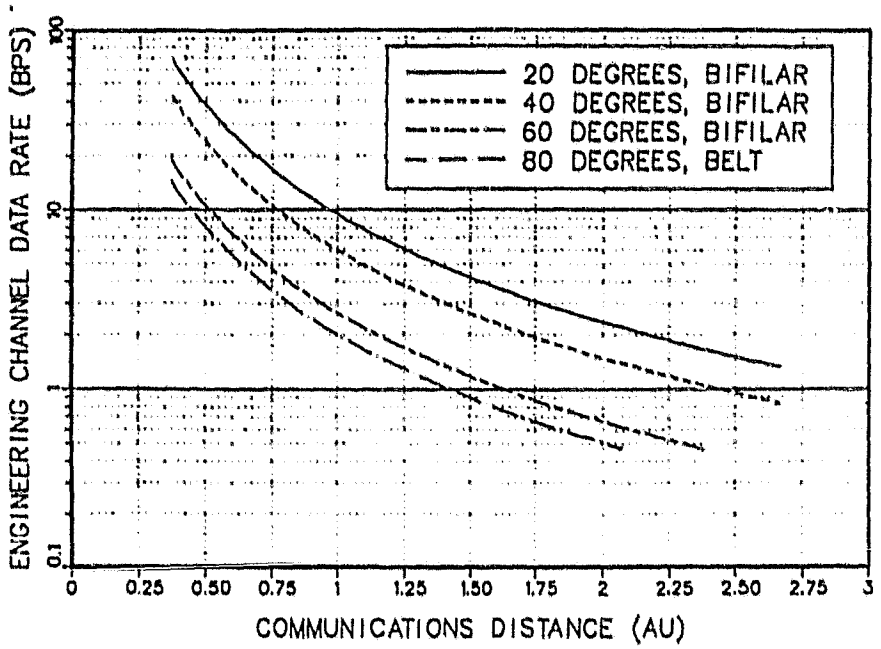

Figure 8-7. MGO Engineering Telemetry Channel with Spacecraft Low Gain Antenna (LGA) to 64 Meter Antenna at S-Band

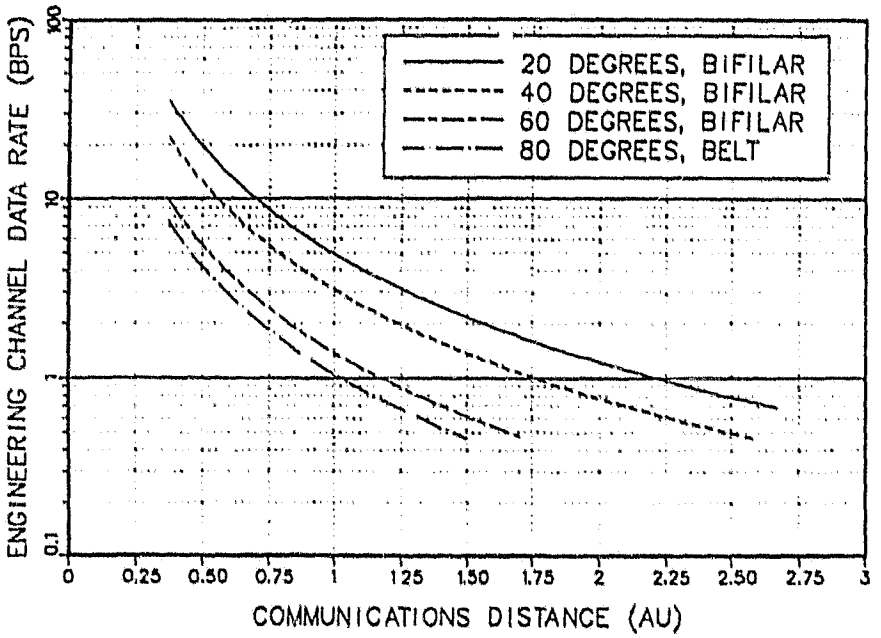

Figure 8-8. MGO Engineering Telemetry Channel with Spacecraft Low Gain Antenna to 64 Meter Antenna at X-Band

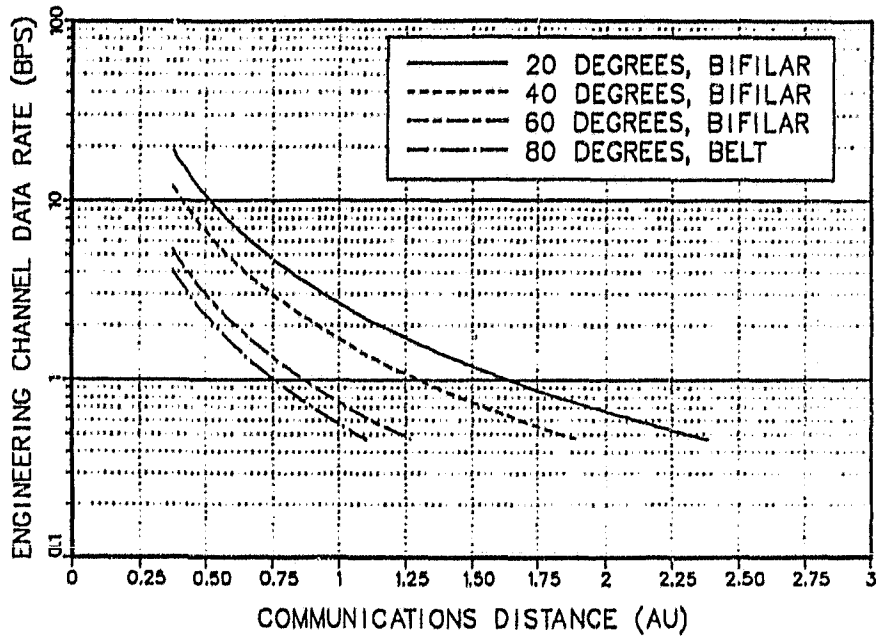

Figure 8-9. MGO Engineering Telemetry Channel with Spacecraft Low Gain Antenna to 34 Meter Antenna at S-Band

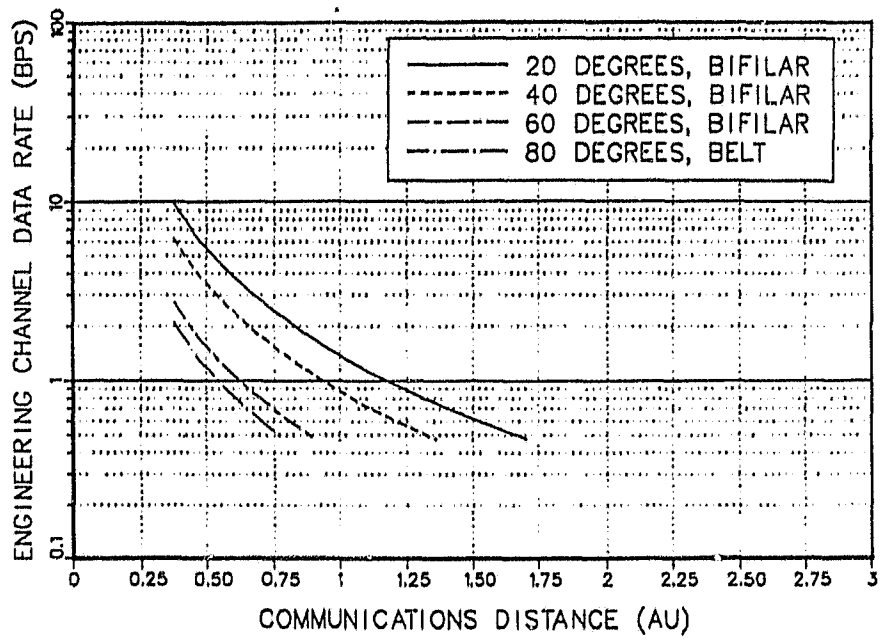

Figure 8-10. MGO Engineering Telemetry Channel with Spacecraft Low Gain Antenna to 34 Meter Antenna at X-Band

The angle quoted in the legend is the angle of each side of the plane normal to the axis of the toroidal antenna. The performance of the belt antenna is based on measured data for the antenna alone. It is anticipated that when mounted on the spacecraft its performance will be degraded in regions significantly off-axis of the toroid. Therefore, the performance shown for the belt antenna is probably somewhat optimistic. Note that many of the curves terminate before reaching maximum Earth-Mars distance. This occurs because in some cases there is inadequate link margin to support reliable carrier loop acquisition and tracking at the ground station. The figures indicate that a 64 meter ground antenna at S-Band is needed to transmit engineering data at 1 bps at maximum distance. Also, the coverage angle would be limited to approximately ±30 degrees off the plane normal to the axis of the toroid. The low gain antenna can also provide a backup capacity to recover engineering data in the event the high gain antenna is not pointed correctly.

8.1.3 Commands

S-Band was assumed for uplink communications because of the availability of deep space receivers in that band.

During mission operations at maximum Earth-Mars distance, command data rates in excess of 125 bps are possible using the spacecraft high gain antenna and a 34 meter antenna and 2 kilowatt transmitter on the ground. At this rate, the spacecraft command memory could be fully loaded in a fairly short period of time.

During the cruise phase, the low gain antenna could be used for commanding. Figures 8-11 and 8-12 show the data rates available assuming a 20 kilowatt ground transmitter. Note that most of these curves terminate before maximum Earth-Mars distance because of inadequate signal-to-noise ratio in the command receiver carrier loop. A 64 meter round antenna is needed to command through the low gain antenna at maximum distance. The low gain antenna will also provide a backup for commanding in case the high gain antenna is not pointed correctly. Although the command data rate through the low gain antenna will be limited to as low as 8 bps, this will be adequate for the mission.

8.2 LGO COMMUNICATIONS

8.2.1 Science Data

Due to the much shorter distances of the lunar mission, high data rate downlinks can be supported for playback of science data. The limiting factor in this case is the maximum playback/record ratio of the tape recorder. Assuming a maximum sensor data rate of 16 kbps and a maximum playback/record ratio of 160:1, the required transmit data rate would not exceed 2.56 Mbps. Achievable data rates as a function of the spacecraft transmitter power, when the spacecraft 1.5 meter high gain antenna is used, are shown in Figure 8-13. Even with a 1 watt transmitter, a bit rate of 2.56 Mbps can be easily supported. The high playback/record ratio will permit storing many orbits of data before playback.

If a fixed low gain antenna were used instead of the stored high gain antenna, the downlink performance would be as shown in Figure 8-14. Note that with a 20 watt transmitter at S-Band working into a 34 meter ground antenna, a data rate of 270 kbps could be supported. This would allow a 16:1 playback/record ratio, and data could be dumped as infrequently as once every eight orbits.

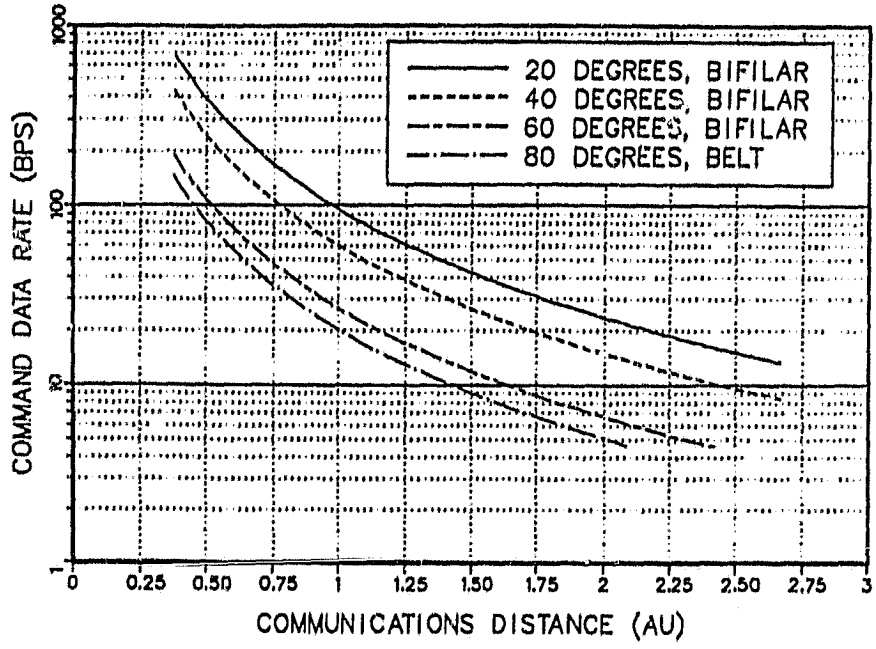

Figure 8-11. MGO Command Channel with Spacecraft Low Gain Antenna from 64 Meter Antenna at 20 kW S-Band

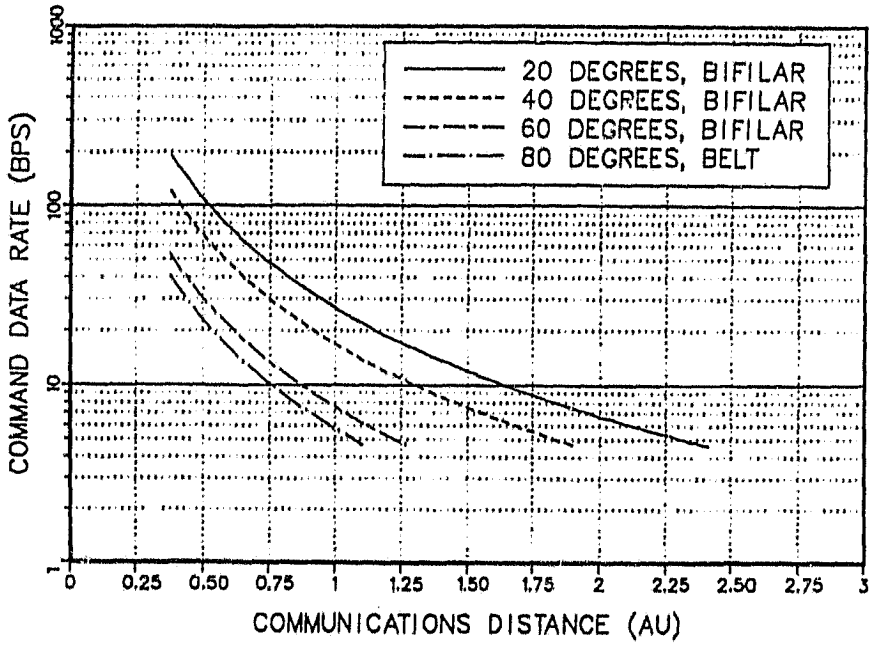

Figure 8-12. MGO Command Channel with Spacecraft Low Gain Antenna from 34 Meter Antenna at 20 kW S-Band

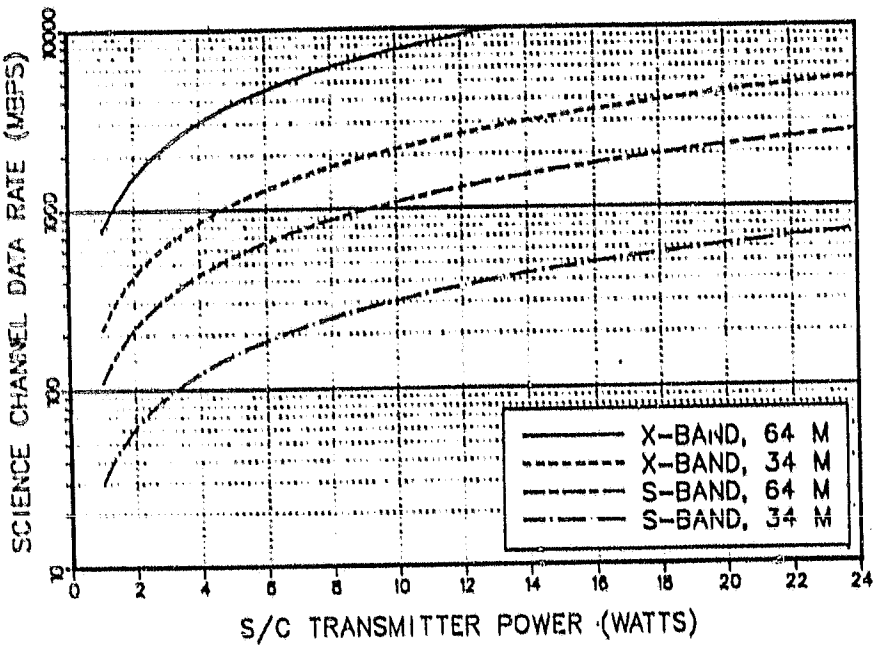

Figure 8-13. LGO Science Channel with Spacecraft High Gain Antenna

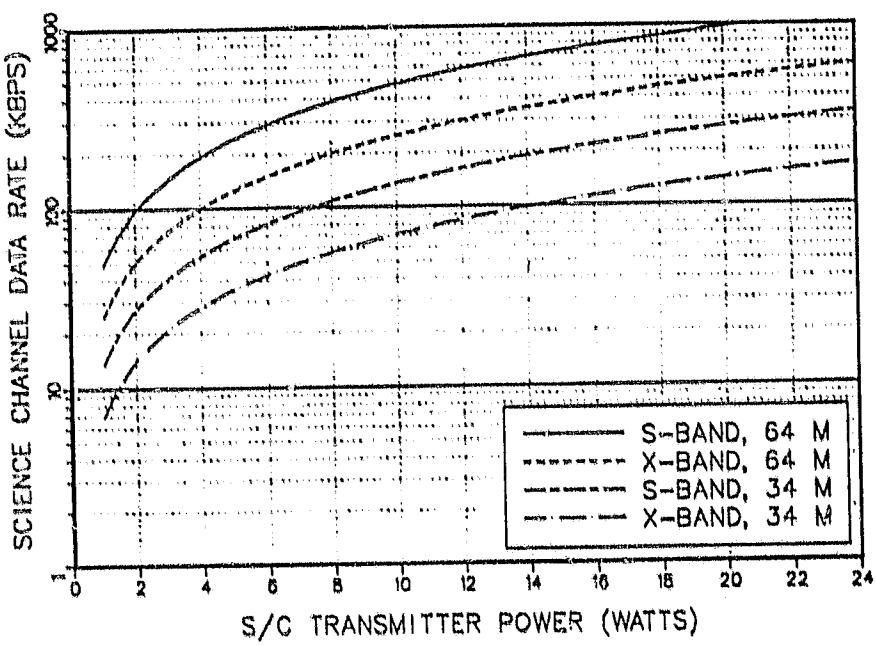

Figure 8-14. LGO Science Channel with Spacecraft Low Gain Antenna

8.2.2 Engineering Telemetry and Commands

With either a high gain antenna or low gain antenna, engineering telemetry data rates and command data rates in excess of 125 bps can easily be hand'ed simultaneously with the science data. This is more than adequate for the mission.

SECTION 9.0
THERMAL DESIGN

SECTION 9.0
THERMAL DESIGN

9.1 LGO THERMAL DESIGN

As the lunar orbiter thermal environment rather closely approximates the thermal environment of an Earth orbiter, with the largest difference being the lack of Earth albedo and IR both of which are second order effects as compared to the internal dissipations and solar influence, the Dynamics Explorer B thermal design can be adapted directly to LGO. This design consists of a set of "pinwheel" shaped louvers mounted in the anti-Sun end of the spacecraft which, in closed loop response to sensed internal temperatures, rotate to open or close apertures coupling to the deep space thermal sink. By so varying the sink coupling, the spacecraft internal temperatures are maintained at the desired levels. The remainder of the thermal system consists of blanketing the internal cavity of the spacecraft to prevent heat leakage other than through the desired apertures, as is depicted in Figure 9-1.

Since the LGO orbit is essentially inertial, this thermal design requires the maneuvering and reorientation of the spacecraft to maintain the lower end in the anti-Sun hemisphere. Such a maneuvering history is shown in Figure 9-2 where typical orientation profiles are shown for the spacecraft in lunar orbit during a one Earth-year mission. The flipover maneuver is not new to the LGO mission, having been accomplished routinely on the DE-B spacecraft and on the AE-C, -D and -E spacecraft throughout their mission lives. It is performed by

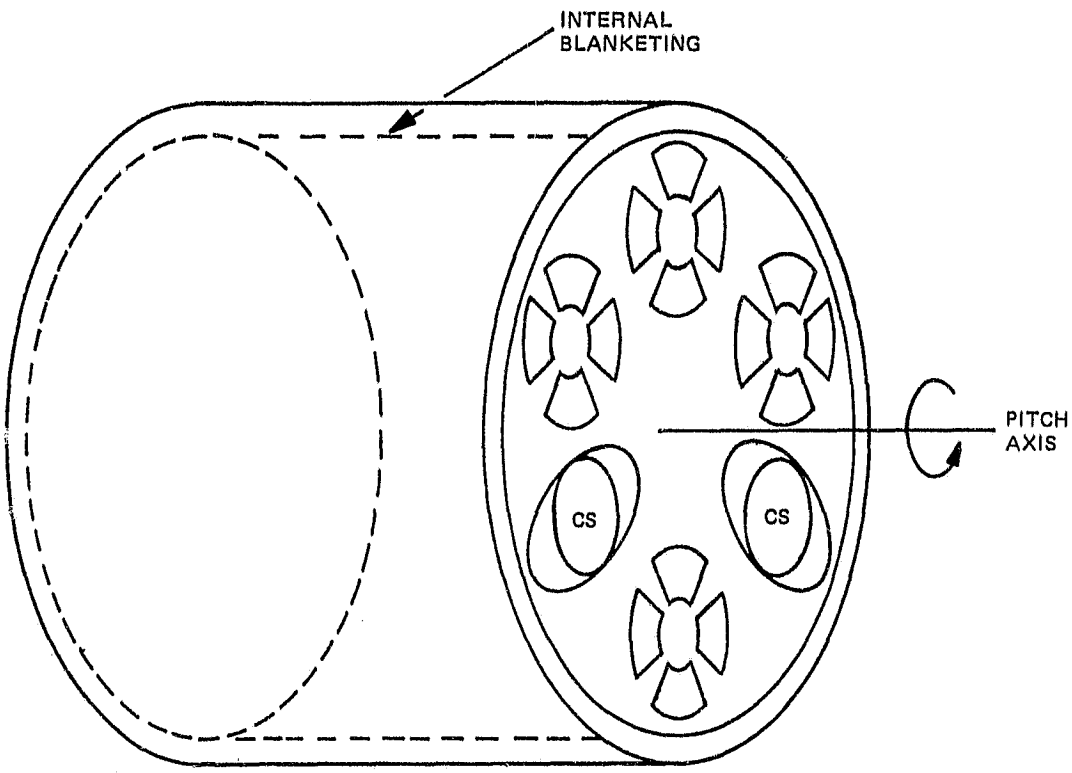

Figure 9-1. LGO Thermal Configuration

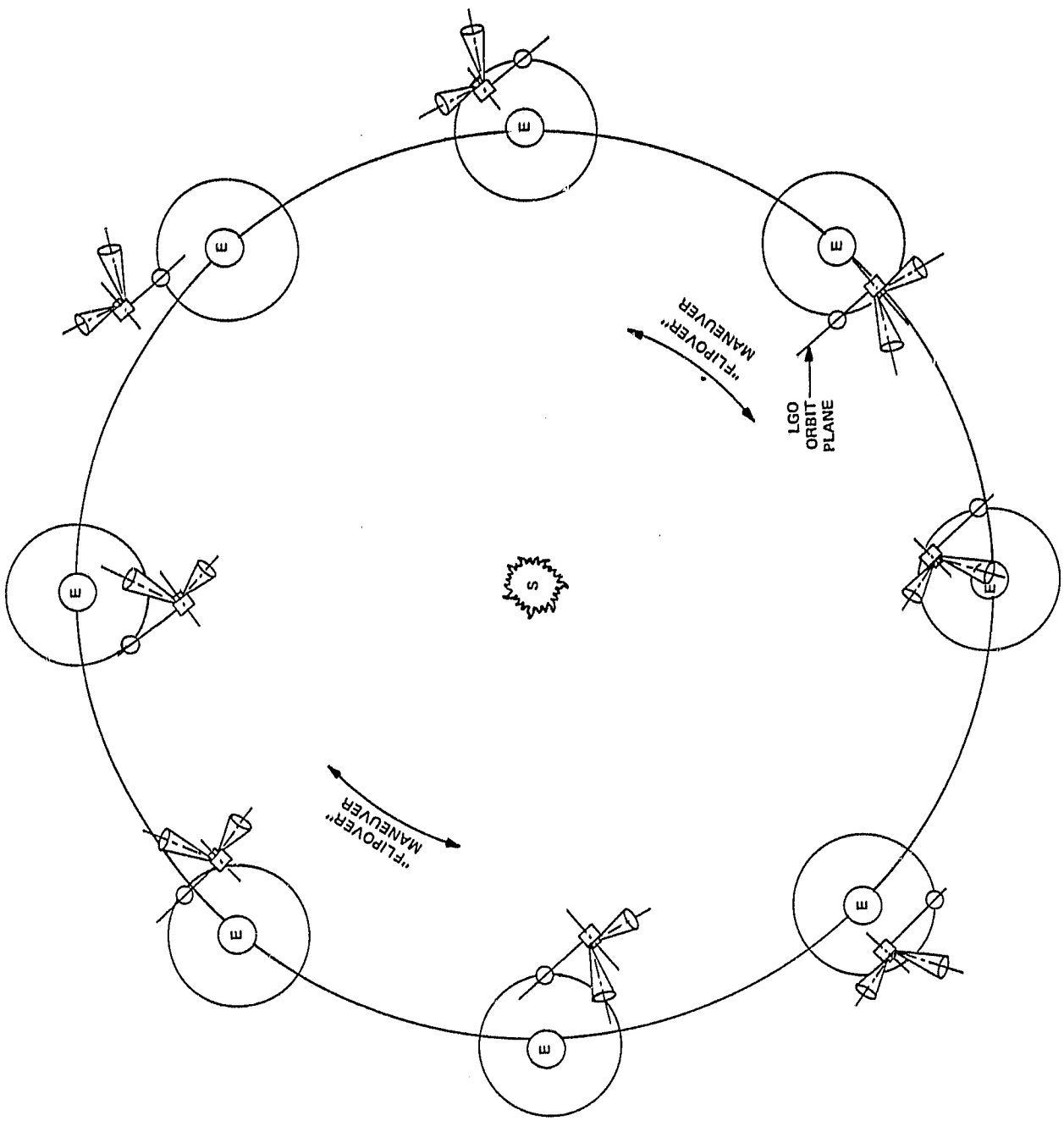

Figure 9-2. LGO Thermal Orientation and Star Sensor Configuration

first executing a 180° yaw maneuver, followed by a re-orientation in pitch of 190°, thereby re-establishing the same spacecraft azimuth vector along the velocity vector.

9.2 MGO THERMAL DESIGN

As in the case of the power system, the thermal design of the MGO spacecraft is the driving consideration for the combined LGO/MGO configuration. In the LGO configuration described above, the effective emmittance of the louvered end of the spacecraft is approximately 0.07 while the internally blanketed sides have an effective emittance of approximately 0.05. This results in a requirement of significant thermal dissipation internal to the spacecraft to maintain the internally mounted equipment at desired temperatures. As an alternative, if the LGO louvers were "left out" of the design and the entire internal spacecraft assembly were blanketed, the required internal dissipation would be reduced, as shown in Figure 9-3.

Projections of the solar array temperature in the worst case for the cruise phase of the mission are shown in Figures 9-4 and 9-5, for the side solar array and end solar array, respectively, as a function of the angle between the Sun vector and the spacecraft spin axis. For these calculations, the solar constant was taken as 0.39 watt per square inch (Sun-Mars distance) but no input from Mars, either IR or albedo, is assumed. Similar calculations for the array side and end temperatures for the spacecraft in a 300 km circular Mars orbit were made. These, as they have a more direct impact on the electrical design of the solar array, are shown in the power section (Section 10) of this report. For brevity, they will not be presented here.

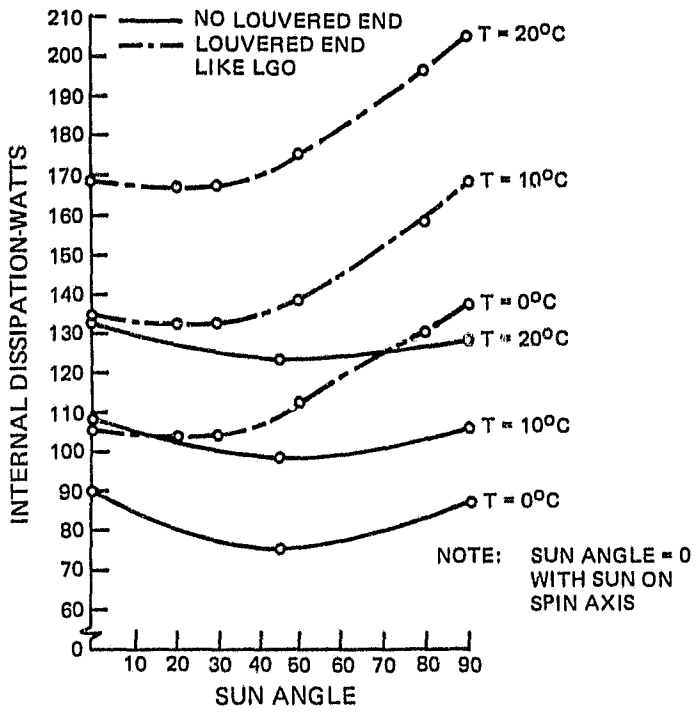

Figure 9-3. Required MGO Internal Dissipation to Maintain Internal Equipment Temperatures in 300 km Mars Orbit

The curves of Figures 9-4 and 9-5 show the thermal sensitivity of the array to Sun angle. A varying Sun angle during the cruise phase is highly desirable to control impingement of the total solar flux on the OIM, allowing the engine to be maintained in a reasonable thermal environment. Therefore, the attitude profile during the cruise phase will be varied to achieve desirable array temperatures and motor temperatures while also retaining the orientations that keep the Earth well within the beam of the belt antenna. This is depicted schematically in Figure 9-6. During the earlier phases of the cruise, the spin axis is maintained in the plane of the ecliptic at an orientation in which the spacecraft body blocks much of the solar influence from the OIM. During this phase, since the solar thermal constant is much greater than the worst case 0.39, the arrays will operate at significantly warmer temperatures. As the cruise continues, the spin axis is reoriented, still in the plane of the ecliptic, to present more and more of the OIM to the Sun. As the spin axis approaches the normal to the Sun vector during the latter stages of the cruise, the angle from the spin axis (still in the plane of the ecliptic) to the Earth is reduced, moving the Earth farther from the axis of the fan belt antenna. As this condition becomes more severe, the spin axis is then reoriented to move out of the plane of the ecliptic, thus moving the Earth closer to the center of the beam while retaining a desirable Sun angle for the motor, with the final orientation (as shown in Figure 9-6, insert 2) approaching that of the orientation preparatory to OIM ignition. Note that throughout this cruise phase (see also Section 7) the spacecraft has been slowly rotating and has utilized the capability to spin up to approximately 4 rpm to allow for operation of the celestial sensors with no condition wherein the Sun is in the field-of-view of the sensors. For the conditions shown in Figure 9-6, insert 1, note that an orientation of the spin axis relative to the ecliptic plane can be found where, during a portion of the revolution of the spacecraft, the celestial sensor field-of-view contains the ecliptic and the Sun is not in the sensor field-of-view.

9.3 THERMAL DESIGN SUMMARY

The preceding paragraphs have addressed the direct application of the thermal control techniques of both the Atmosphere Explorer and the Dynamics Explorer programs to the MGO and LGO missions. From the level of effort expended during the study, no fundamental problems have been identified which would preclude their application. The major feature that will require further, more detailed analysis, is the behavior of the system in the cruise phase. This is the area of design that maximizes the extension of the Earth orbiter system to the MGO/LGO case.

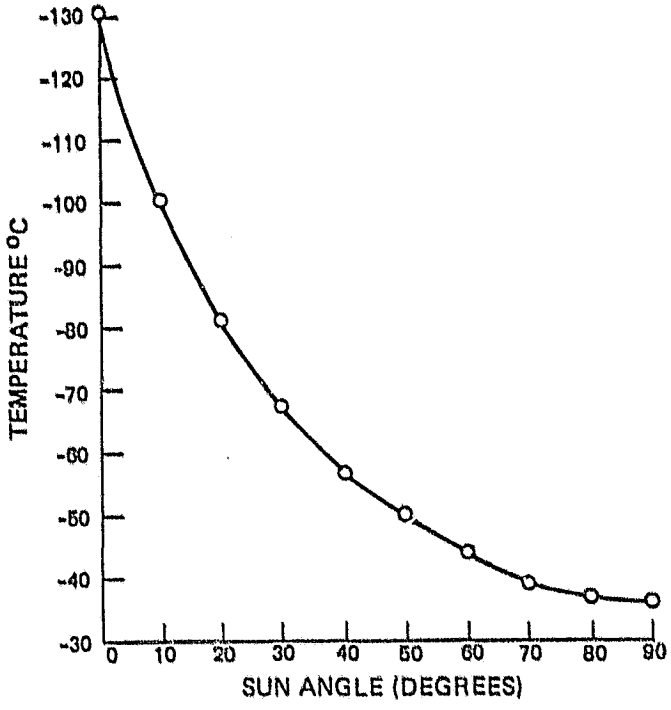

Figure 9-4. Worst Case Side Array Temperature During Cruise Phase as Function of Sun Angle (Sun Angle = 0° When Sun on Spin Axis)

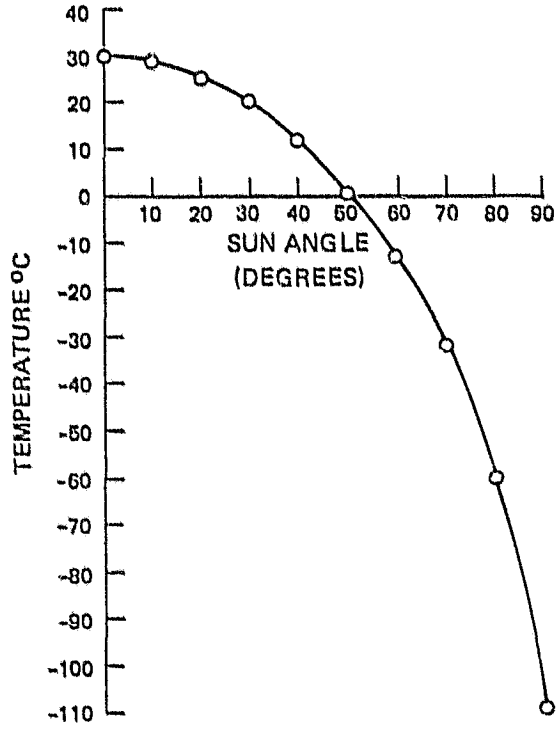

Figure 9-5. Worst Case End Array Temperature During Cruise Phase as Function of Sun Angle (Sun Angle = 0° When Sun on Spin Axis)

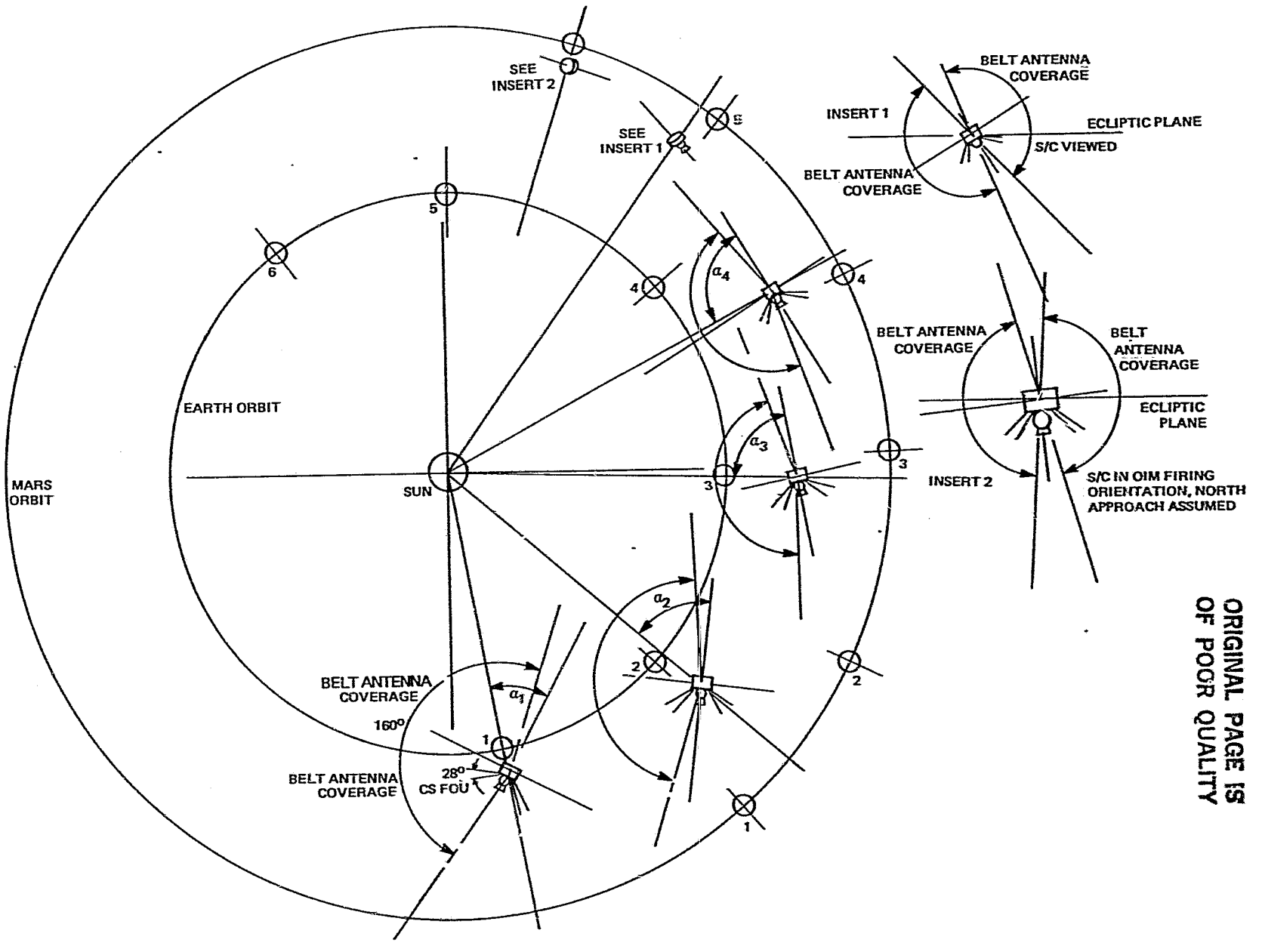

Figure 9-6. Attitude Orientation Profile During Cruise Phase

SECTION 10.0
POWER PERFORMANCE EVALUATION

SECTION 10.0
POWER PERFORMANCE EVALUATION

The assessment of the power performance for the MGO and LGO spacecraft presented herein is based on an analytic computer program originally developed for the Dynamics Explorer program. Subsequent modification has included the options to select either the Earth, Mars or the Moon as the body to be orbited. In the case of the Moon, a simplification was used whereby the Earth was replaced by the Moon rather than introducing the orbital complexities associated with modeling the Moon's motion about the Earth. This approximation is not of major significance, especially when the MGO design consideration is the driving case addressed in this study, due to the reduction in solar constant from 1.0 to approximately 0.4.

10.1 MGO/LGO POWER PROFILE

10.1.1 Configuration

A standard power-profile configuration, shown in Figure 10-1, has been adopted for use in MGO/LGO power computations. This profile is used in the Power Analysis Computer Program which uses the energy balance analysis approach to measure the power system performance for both the MGO and LGO missions.

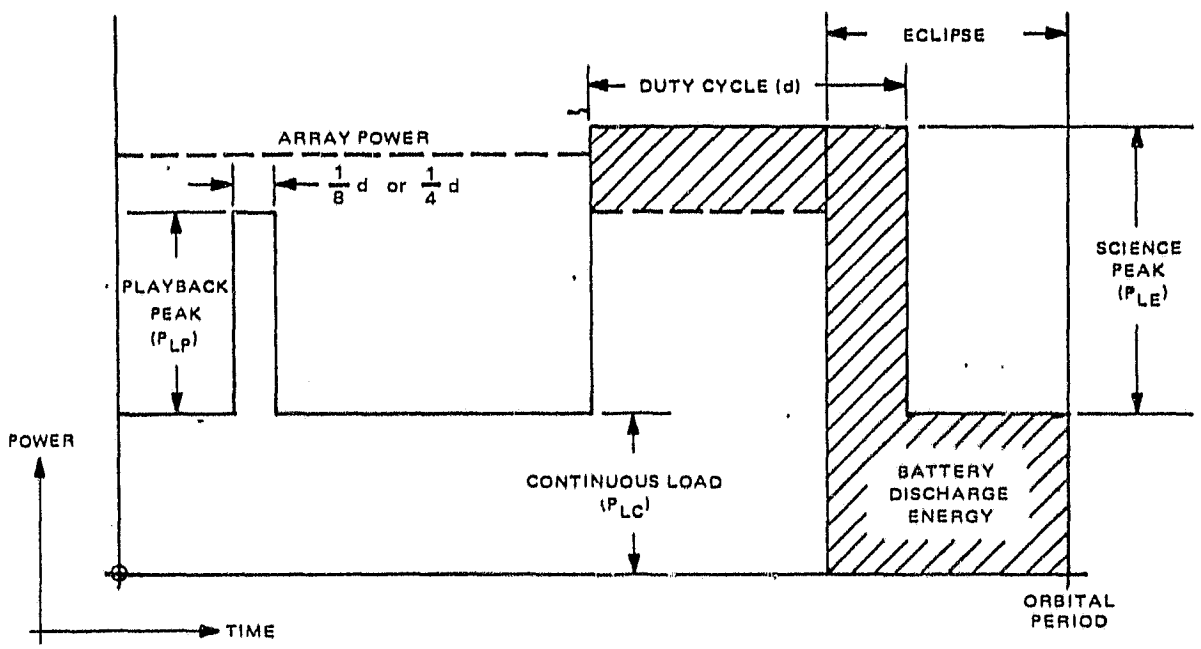

Figure 10-1. Standard Power Profile Model for MGO and LGO

Certain simplifications assumed in the standard power profile have been made necessary due to the presumption that the science loads' actual occurrence and duration are not accurately predictable and that the load, cycling in orbit, does not occur on a consistent, repetitive basis. Alternatively, energy balance, basic to all power systems analyses, does require a repetitive load cycle as a starting point; hence the need for a simplified "standard" profile, as well as a set of agreed-upon simplifications judged to be representative of the long-term, if not the exact, operating conditions in orbit.

Key features of the assumed power profile model are as follows:

(1) There are three possible fixed-load levels in the MGO or LGO power profiles, as shown in Figure 10-1, with the shaded area representing the battery discharge energy. The fixed-load levels are the continuous load, the science peak load and the playback peak load. Note the drop in the solar array power level when the total load exceeds array capability; this occurs because of the reduction of the array voltage which takes place when the batteries are discharging.

(2) The load profile, as the name implies, includes all loads, regulated and unregulated, at the output terminals of the power subsystem. Internal power supply losses, such as regulator inefficiencies, are load-dependent and are not included in the load profile. Their effect on the power supply performance is properly treated in energy balance expressions used in the Power Analysis Computer Program. An exception is the power supply electronics shunt-current (leakage) loss which is assumed to be constant and, as such, is included in the load profile as a component of the total continuous load.

(3) Continuous load is the minimum average power required to sustain the spacecraft in orbit. To maximize battery recharge, all commandable loads not essential to spacecraft operation are assumed to be OFF. These include: science instrumentation, the data transmitter, tape recorder (TR) and TR electronics, and the -24.5 volt regulator. The continuous load is not constant as implied by the adopted simplification, but varies somewhat; for instance, power needed for thermal control will vary, but an assumed orbit-average value is included as a component of the total continuous load.

(4) The science peak load magnitude is the sum total of the individual power consumptions of all the on-board instruments in the normal ON state, plus all the supporting equipment, which consists of the tape recorder in "record," the TR electronics and the -24.5V regulator.

All of the instruments and the tape recorder in "record" mode of science peak loads are assumed to be delivered at the regulated -24.5 volt bus whereas the attitude determination sensors are supplied with +28 V regulated bus.

The assumed condition of all the instruments being ON at the same time is judged to be pessimistic. The implied degree of pessimism, therefore, justifies the following additional simplifying assumptions:

- Instrument warmup time is negligible

- Data transmitter is never ON when the instruments are ON. (Note that this assumption is made only to configure a more straightforward power profile; the power system is capable of supplying the appropriate peak power magnitude if, in fact, all the instruments should be ON, together with the data transmitter, on either MGO or LGO.)

A further assumption is made that any on-board instrument can be ON anywhere along the orbital path. If so, the total science peak can also occur anywhere, e.g., either in sunlight or in eclipse, wholly or partially. To best reflect long-term operating trends, the analysis assumes that the science peak duration is proportionally divided between Sunlight and eclipse, more or less, as shown in Figure 10-1. The analytical model has the capability to shift the peak to occur entirely in eclipse as a special case for assessing "worst-case" battery operation.

(5) Playback load magnitude over and above the continuous load equals mainly the sum of the data transmitter and the tape recorder (playback) loads. While the transmitter loads are taken from the unregulated bus, the tape recorder (playback) load is supplied by the -24.5 V bus. Playback time duration is a fixed fraction of the time the science loads are ON. The value of that fraction is assumed to be one-eighth or one-fourth, consistent with the 8:1 and 4:1 playback-to-record ratios.

In actual orbital operation, the playback load can occur anywhere along the orbital path. To simplify the already complex energy-balance expressions, it has been assumed that playback occurs only when the spacecraft is in sunlight. This assumption introduces very little error in such computed quantities as the science ON time duty cycle, battery depth of discharge, or the power supply dissipation.

10.2 POWER SUPPLY PERFORMANCE SUMMARY

10.2.1 Analysis

The primary performance parameters are the science ON time duty cycle (expressed in terms of minimum, maximum and average duty cycle as well as total hours of science data-gathering through the mission life), the solar-array output power, the depth of battery discharge and the charge current magnitude. The Power Analysis Computer Program is used to compute the magnitude of these parameters as they vary with life, subject to major influencing factors such as the Sun incidence angle and eclipse duration.

10.2.2 Performance

The MGO and LGO power supply performance will be discussed in terms of the computer-aided solutions obtained as a consequence of the inputs listed in Table 10-1. Note that the star sensors are not included as their aperiodic use during the mission and not considered part of the routine mission profile (see Section 7.0).

The output power for the MGO spacecraft is based on temperature data for the side and array as discussed below.

TABLE 10-1. RUN 025 PERFORMANCE ANALYSIS INPUT

DE-BASED MGO 19881

----> SPECIFIED ORBIT: MARS

HEIGHT AT APOAPSIS =	350.000	HEIGHT AT PERIAPSIS =	350.000	ORBIT INCLINATION =	92.50
RIGHT ASCENSION OF ASCENDING NODE =	89.015	ARG OF PERIAPSE =	0.0		
EPOCH =	5/ 28/ 1989	TIME =	0: 0: 0		
PS WATTS FACTOR =	1.000/ 1.000				
LIFE OF MISSION =	8760.0 HOURS	ORBIT PERIOD =	1.9316 HOURS	SOLAR ARRAY TABLE # 1	

DRI = 3 (USE GIVEN PSFAC AS DEGRADATION FACTOR)

PWR SYSTEM

ITYPE =	3	INPUTD =	0		
VF =	24.50	VBD =	1.22	DELVD =	1.00
N =	24	VBC =	1.45	DELVCH =	1.20
EB =	0.85	EC =	0.89	R =	0.125
PLC =	45.00	C =	12.00	PSLD =	3.500
PLE =	73.00	F1 =	0.037	PSLN =	1.500
PLP =	136.60	F2 =	0.014	B =	1.50
ECC =	0.89	ECD =	0.89	K =	0.81
DUTY CYCLE MAX =	0.889	PT =	81.60	PRF =	20.00

Table 10-2 is the computer printout for Run 25 (MGO, Effective Sun Angle = 50°).

As can be seen in the table, values are computed in five-day increments for the entire mission lifetime. The "Gamma" column in the computer printouts is the sun angle listing which is plotted in Figure 10-2, together with the solar array output power (as measured at the solar bus in the PSE) given in the "PSA watts" column. Figure 10-3 shows plots of the eclipse duration as well as the average and the maximum battery depth of discharge; the latter two are listed in the computer printouts as DODAVE and DODMAX. The average depth-of-discharge values are based on the assumption that the science ON time is proportionally divided between the in-sunlight part of the orbit and the eclipse. The maximum depth-of-discharge value, however, is arrived at by departing from the "standard" profile and allowing the science ON time to be centered on eclipse instead, resulting in a "worst case" situation. Note that Run 25 is based on solar array power not degrading from beginning-of-life to end-of-life as no significant radiation environment leading to such degradation exists at Mars. In examining the graphic output of this program, the solid line curve always refers to the left ordinate, the dashed line to the first right ordinate and the dotted line to the second right ordinate.

The ON time duty cycle is plotted in Figure 10-4.

The "ICHMAX (amps)" column of the computer printouts is the result of a computation of the maximum total charge current available to both batteries.

The "Case #" column of the computer printouts refers to load profile magnitudes relative to the instantaneous magnitude of the solar array power output; for example, "3" denotes that there will be a battery discharge during the playback peak (Figure 10-1) but not during the science peak. The "QMAX subcase #" refers to the duration of the science ON time relative to the eclipse duration, necessary when computing the DODMAX value. Neither of the two "case" columns are of any great consequence to this discussion, and both are amply discussed in the referenced RCA DE File Documentation (DE 2.4.1-005, 10/14/77).

Table 10-3 contains a printout of a summary of the electrical performance. In Table 10-3, for example, it can be seen that the worst case science duty cycle over the spacecraft lifetime will range between 52 and 57 percent, with an overall life average value of 56.1 percent, corresponding to gathering science data over a total of 4918.2 hours throughout the mission.

The remainder of the data provided in the computer printouts (not provided in this report but available if required) deals with thermal dissipation. The "averaged array dissipation" column includes the combined orbit-average values of power dissipated in the shunt limiter, array wiring, and blocking diodes. Low values indicate that there is no shunt limiter dissipation and that the entire array power capability is utilized to support spacecraft and instrument loads as well as to supply the necessary battery charge. Slightly higher values mean that some shunt limiter dissipation is taking place. The "PSE dissipation" column includes all of the orbit-average power dissipated in the power supply electronics unit, including the regulator dissipation. The last column labeled simply "watts" is the orbit-average dissipation in the data transmitter.

TABLE 10-2. RUN 025 PRINTOUT

CALENDAR DATE	GAMMA	DURATION OF ECLIPSE (MINS)	FRACTIONAL SUN TIME	FSA WATTS	ON TIME DUTY CYCLE	CASE#	DODAVE	DODMAX	QMAX SUB-CASE#	ICHMAX (AMPS)
5-28-1989	48.75	37.95	0.690	173.362	0.57	3	0.179	0.241	1	3.566
6 -2-1989	48.86	36.00	0.689	173.373	0.57	3	0.179	0.241	1	3.566
6 -7-1989	48.99	36.04	0.689	173.385	0.57	3	0.179	0.242	1	3.566
6-12-1989	49.12	36.09	0.689	173.397	0.57	3	0.179	0.242	1	3.567
6-17-1989	49.25	36.14	0.688	173.410	0.57	3	0.179	0.242	1	3.567
6-22-1989	49.39	36.19	0.688	173.422	0.57	3	0.179	0.242	1	3.567
6-27-1989	49.53	36.25	0.687	173.436	0.57	3	0.179	0.243	1	3.566
7 -2-1989	49.67	36.30	0.687	173.449	0.57	3	0.180	0.243	1	3.568
7 -7-1989	49.81	36.35	0.686	173.462	0.57	3	0.180	0.243	1	3.568
7-12-1989	49.96	36.40	0.686	173.475	0.56	3	0.180	0.244	1	3.569
7-17-1989	50.09	36.45	0.686	173.465	0.56	3	0.180	0.244	1	3.568
7-22-1989	50.22	36.50	0.685	173.442	0.56	3	0.180	0.244	1	3.568
7-27-1989	50.36	36.54	0.685	173.420	0.56	3	0.180	0.244	1	3.567
8 -1-1989	50.48	36.59	0.684	173.398	0.56	3	0.180	0.245	1	3.567
8 -6-1989	50.60	36.63	0.684	173.377	0.56	3	0.180	0.245	1	3.566
8-11-1989	50.72	36.67	0.684	173.358	0.56	3	0.180	0.245	1	3.566
8-16-1989	50.82	36.70	0.683	173.340	0.56	3	0.180	0.245	1	3.565
8-21-1989	50.92	36.74	0.683	173.323	0.56	3	0.180	0.246	1	3.565
8-26-1989	51.01	36.77	0.683	173.308	0.56	3	0.180	0.246	1	3.564
8-31-1989	51.09	36.79	0.683	173.295	0.56	3	0.180	0.246	1	3.564
9 -5-1989	51.15	36.82	0.682	173.284	0.56	3	0.180	0.246	1	3.563
9-10-1989	51.21	36.83	0.682	173.275	0.56	3	0.180	0.246	1	3.563
9-15-1989	51.25	36.85	0.682	173.268	0.56	3	0.180	0.246	1	3.563
9-20-1989	51.28	36.86	0.682	173.263	0.56	3	0.180	0.246	1	3.563
9-25-1989	51.29	36.86	0.682	173.260	0.56	3	0.180	0.246	1	3.563
9-30-1989	51.30	36.86	0.682	173.260	0.56	3	0.180	0.246	1	3.563
10 -5-1989	51.29	36.86	0.682	173.262	0.56	3	0.180	0.246	1	3.563
10-10-1989	51.25	36.85	0.682	173.267	0.56	3	0.180	0.246	1	3.563
10-15-1989	51.21	36.84	0.682	173.274	0.56	3	0.180	0.246	1	3.563
10-20-1989	51.16	36.82	0.682	173.283	0.56	3	0.180	0.246	1	3.563
10-25-1989	51.09	36.79	0.683	173.295	0.56	3	0.180	0.246	1	3.564
10-30-1989	51.00	36.76	0.683	173.310	0.56	3	0.180	0.246	1	3.564
11 -4-1989	50.91	36.73	0.683	173.327	0.56	3	0.180	0.246	1	3.565
11 -9-1989	50.79	36.69	0.683	173.345	0.56	3	0.180	0.245	1	3.565
11-14-1989	50.67	36.65	0.684	173.366	0.56	3	0.180	0.245	1	3.566
11-19-1989	50.53	36.60	0.684	173.389	0.56	3	0.180	0.245	1	3.566
11-24-1989	50.39	36.55	0.685	173.414	0.56	3	0.180	0.245	1	3.567
11-29-1989	50.23	36.50	0.685	173.440	0.56	3	0.180	0.244	1	3.568
12 -4-1989	50.07	36.44	0.686	173.468	0.56	3	0.180	0.244	1	3.569
12 -9-1989	49.90	36.38	0.686	173.471	0.56	3	0.180	0.244	1	3.569
12-14-1989	49.73	36.32	0.687	173.454	0.57	3	0.180	0.243	1	3.568
12-19-1989	49.55	36.25	0.687	173.438	0.57	3	0.180	0.243	1	3.568
12-24-1989	49.38	36.19	0.688	173.421	0.57	3	0.179	0.242	1	3.567
12-29-1989	49.20	36.12	0.688	173.405	0.57	3	0.179	0.242	1	3.567
1 -3-1990	49.03	36.06	0.689	173.389	0.57	3	0.179	0.242	1	3.566
1 -8-1990	48.87	36.00	0.689	173.373	0.57	3	0.179	0.241	1	3.566
1-13-1990	48.71	35.94	0.690	173.359	0.57	3	0.179	0.241	1	3.566
1-18-1990	48.57	35.89	0.690	173.345	0.57	3	0.179	0.241	1	3.565
1-23-1990	48.44	35.83	0.691	173.333	0.57	3	0.179	0.240	1	3.565
1-28-1990	48.33	35.79	0.691	173.323	0.57	3	0.179	0.240	1	3.565
2 -2-1990	48.24	35.75	0.691	173.314	0.57	3	0.179	0.240	1	3.564
2 -7-1990	48.17	35.73	0.692	173.308	0.57	3	0.179	0.240	1	3.564
2-12-1990	48.13	35.71	0.692	173.305	0.57	3	0.178	0.240	1	3.564
2-17-1990	48.13	35.71	0.692	173.304	0.57	3	0.178	0.240	1	3.564
2-22-1990	48.15	35.72	0.692	173.306	0.57	3	0.178	0.240	1	3.564
2-27-1990	48.22	35.75	0.692	173.312	0.57	3	0.179	0.240	1	3.564
3 -4-1990	48.32	35.79	0.691	173.322	0.57	3	0.179	0.240	1	3.564
3 -9-1990	48.46	35.84	0.691	173.335	0.57	3	0.179	0.240	1	3.565
3-14-1990	48.62	35.92	0.690	173.353	0.57	3	0.179	0.241	1	3.565
3-19-1990	48.89	36.01	0.689	173.375	0.57	3	0.179	0.241	1	3.566
3-24-1990	49.17	36.11	0.688	173.402	0.57	3	0.179	0.242	1	3.567
3-29-1990	49.50	36.24	0.687	173.433	0.57	3	0.179	0.243	1	3.568
4 -3-1990	49.69	36.38	0.686	173.468	0.56	3	0.180	0.243	1	3.569
4 -8-1990	50.32	36.53	0.685	173.425	0.56	3	0.180	0.244	1	3.567
4-13-1990	50.81	36.70	0.683	173.342	0.56	3	0.180	0.245	1	3.565
4-18-1990	51.35	36.88	0.682	173.250	0.56	3	0.180	0.246	1	3.563
4-23-1990	51.94	37.07	0.680	173.150	0.55	3	0.181	0.248	1	3.560
4-28-1990	52.58	37.27	0.678	173.041	0.55	3	0.181	0.249	1	3.557
5 -3-1990	53.27	37.48	0.677	172.924	0.54	3	0.181	0.250	1	3.553
5 -8-1990	54.01	37.70	0.675	172.799	0.54	3	0.181	0.251	1	3.550
5-13-1990	54.79	37.92	0.673	172.667	0.54	3	0.182	0.253	1	3.546
5-18-1990	55.61	38.14	0.671	172.528	0.53	3	0.182	0.254	1	3.542
5-23-1990	56.47	38.36	0.669	171.997	0.52	3	0.182	0.255	1	3.528
5-28-1990	57.36	38.59	0.667	171.610	0.52	3	0.182	0.256	1	3.517

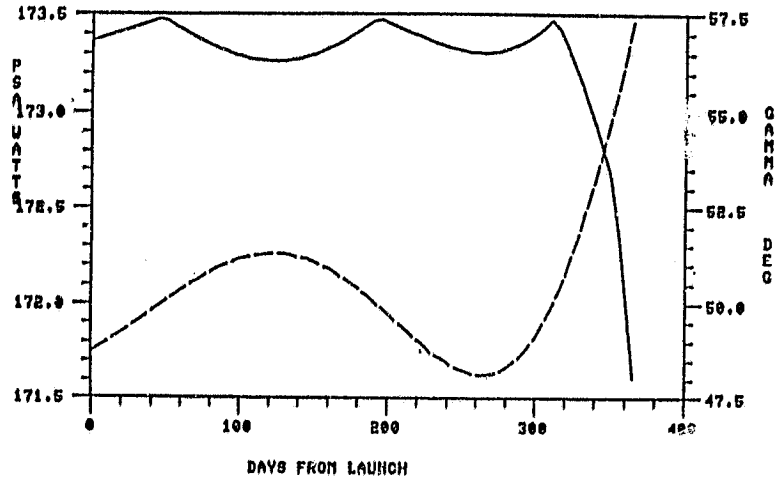

Figure 10-2. Run 025, Array Power and Sun Angle

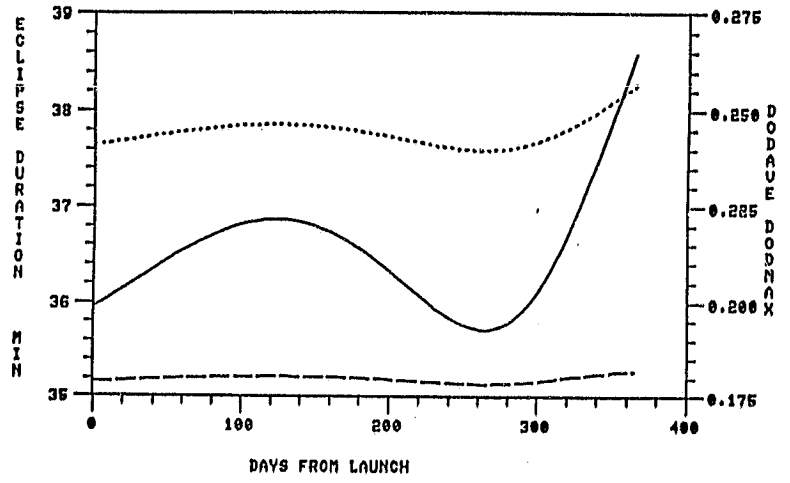

Figure 10-3. Run 025, Eclipse History and DOD Performance

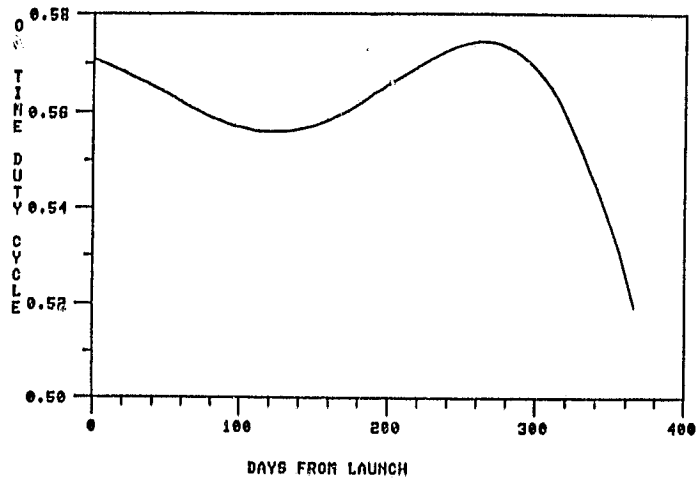

Figure 10-4. Run 025 Duty Cycle Performance

TABLE 10-3. RUN 025 PERFORMANCE SUMMARY

DOD Max Ranges from 0.240 to 0.256
Duty Cycle Ranges from 0.52 to 0.57
Average Duty Cycle = 0.561
Total Duty Cycle for Life of Mission = 4918.168 Hours

10.3 POWER SUBSYSTEM DESIGN

10.3.1 Power Supply Electronics (PSE)

A block diagram of the PSE is also shown in Figure 10-5. The design considered for MGO and LGO is identical to that of [illegible] with the exception of the number of 2 x 2 cm solar cells, a slight difference in their series/parallel connections and an increased number of "legs" in the shunt limiter.

The PSE will perform the following functions:

- Load Voltage Distribution
- Battery Charge Control
- Solar Array Shunt Regulator Control
- Regulated Bus Failure Detection
- Unregulated Bus Undervoltage Detection
- Charge-Controller Disconnect
- Ground Command Response
- Telemetry Generation

10.3.2 Load Voltage Distribution

The PSE accepts solar array and battery power at voltage levels varying between -27.0 and -38.75 volts and provides the following steady-state bus voltages:

- Unregulated bus to support instruments and non mission-critical spacecraft subsystem, -25.7 ±0.1 to -38.25 ±0.25 volts

- Unregulated bus to support spacecraft mission-essential loads, -25.5 to -38.5 volts

- Pulse load bus for use by stepper motors, electro-explosive devices, heaters and other spacecraft components with large transient power requirements, -25.5 to -36.5 volts

- Primary regulated power for use by non-mission critical loads, -24.5 volts ±2%. The -24.5 volt regulated bus is derived from the unregulated bus by a constant-frequency pulse-width-modulated (PWM) regulator which will hold the regulated bus within the specified tolerance for static loads within the range of 0.4 to 6 amperes. Two identical PWM regulators are provided but, at most, only one regulator will be "on line" at any time. Current limiting is employed in each voltage regulator to protect the circuit from overloads.

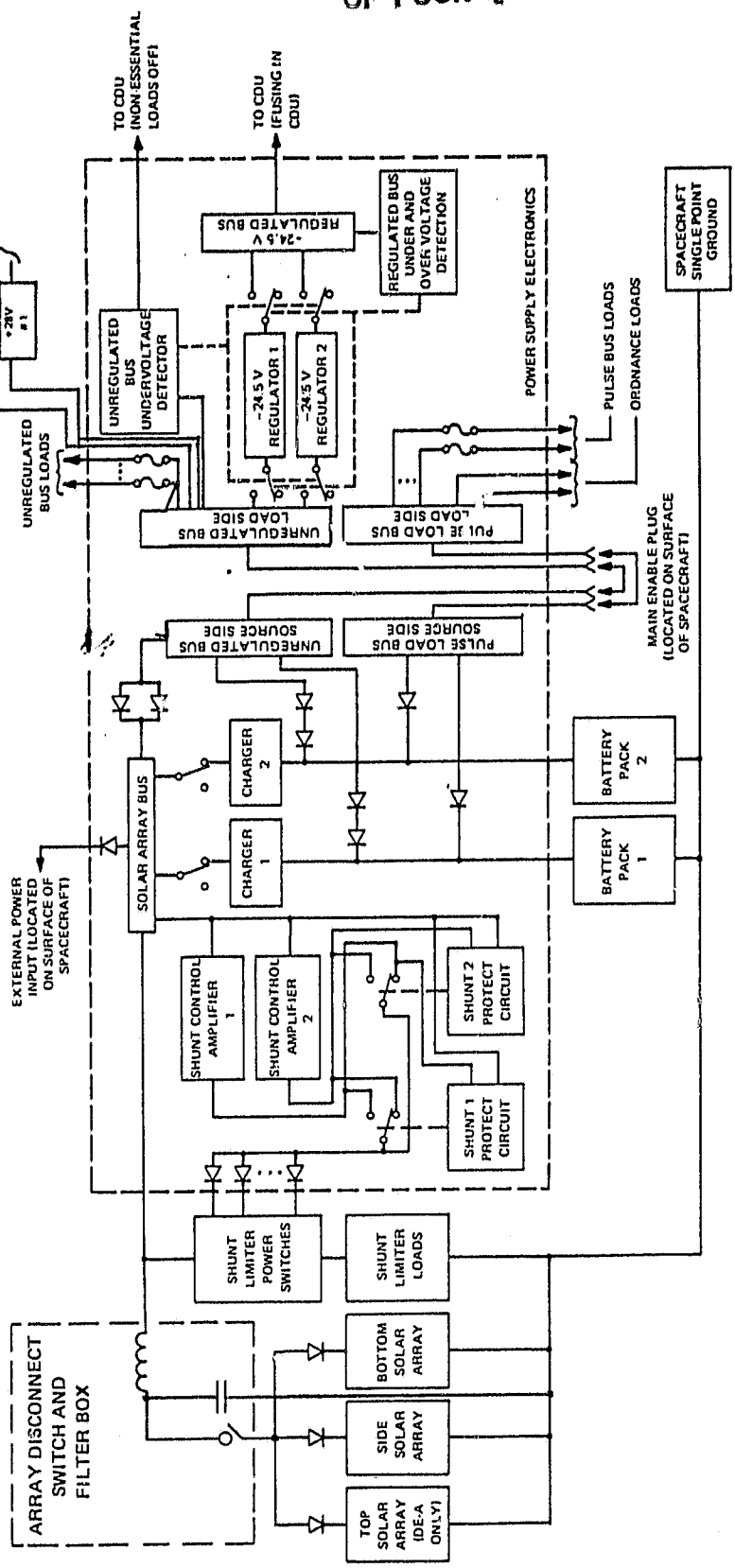

Figure 10-5. Power Subsystem Block Diagram

10.3.3 Battery Charge Control

When excess solar array power is available, circuits within the PSE control the recharging of the two batteries. The maximum charge rate of each battery is limited to approximately C/4. Separate control circuits are provided for each battery.

10.3.4 Solar Array Shunt Regulator Control

Two redundant shunt regulator control amplifiers sense the solar array bus voltage and provide a drive signal to the power-dissipating sections. The power-dissipating sections, located on the solar array panels, act as shunt loads on the solar array so as to limit the solar array bus voltage to a nominal maximum voltage of -38.5 volts.

Automatic failure detection circuitry is provided to disconnect a control amplifier which has failed in the ON state. Provision is also made to switch a "failed ON" amplifier off line, by ground command.

10.3.5 Regulated Bus Detector

Circuitry is provided to monitor the regulated bus and automatically disconnect the "on line" PWM voltage regulator if the regulated bus voltage deviates from pre-set limits. Ground command capability is also provided to disconnect the "on-line" regulator. Ground command capability also exists to control the enable/disable status of the regulated bus detector.

10.3.6 Unregulated Bus Undervoltage Detector

Circuitry is provided to monitor the unregulated bus voltage and to automatically disconnect the "on-line" PWM regulator and other non-essential loads if the unregulated bus voltage level drops below a pre-set limit. The non-essential loads can also be disconnected individually (reconnected) by ground command. Additionally, ground command capability is provided to disable or enable the unregulated bus detector.

10.3.7 Charge Controller Disconnect

In the event of a charge controller failure in a shorted or saturated mode, a charge controller automatic-disconnect circuit is provided. The disconnect circuit will also detect battery voltage as a function of temperature and disconnect the affected charge controller from the solar array bus if battery voltage/temperature condition exceeds a pre-determined level, or if the temperature at any voltage exceeds 35.0 ±2.5°C.

10.3.8 Array Disconnect and Filter Box

A means is provided to filter internally generated noise in the spacecraft, preventing it from reaching the solar array surface. Additionally, if this proves inadequate for electromagnetic interference (EMI) contamination operations, provision is also made to disconnect the array; automatic reconnect is provided. These features were incorporated to assure maximum electromagnetic compatibility (EMC) cleanliness for Electric Field and Plasma Wave measurements on DE and may be deleted for the present payloads for MGO and LGO. Should revised payload requirements dictate more stringent EMC, they are available and have been previously flown.

10.4 SOLAR ARRAY PERFORMANCE PREDICTIONS

Inherent to the operation of the power performance analysis is a table of information characterizing the solar array output power (referred to herein as a STINT Table - for Standard Interpolation Table), in watts, as a function of Sun angle. To provide this input information, an analysis was performed; it is summarized below.

In assessing the solar array design, again concentrating on the MGO case since that mission contains the driving set of constraints, the following approach was taken. The physical size of the spacecraft, both for the "as is" dimensions of the parent DE spacecraft (referred to as "little bird" herein) and for the scaled up spacecraft (referred to as "big bird" herein) to accommodate the 22.1 inch hydrazine tanks, was taken as a dual baseline. (The DE size spacecraft was considered to establish a comparison in performance for the scaled up configuration.) After establishing the basic field-of-view requirements, the side array and the end array remaining areas were allocated to solar cells using the following constraints for three different effective mission Sun angles, namely 30°, 50° and 70°. Since these Sun angles effectively project different areas of the right circular cylinder spacecraft to the Sun, the incident-flux results in different orbit average temperatures of the solar array. The projected temperatures for the sides and end are shown in Figures 10-6 and 10-7, while the geometry of the definition of Sun angle is shown in Figure 10-8. For purposes of the sizing of the solar array, the "on-orbit" condition in a 300 km circular orbit was assumed. Using the same 2 cm x 2 cm cell as was used on the DE spacecraft, a maximum of 258 cells can be placed on one hat's side panel of the little bird configuration. Before continuing, the power output of a single cell and its maximum power point for the Mars orbit were determined. The I-V curve for the cell is shown in Figure 10-9, with both Earth and Mars performance characteristics. In the Mars application, the maximum power point is indicated at 480 mV and 56.5 mA for the 25°C cell.

Using the equation

$$V = n\,(.480) + (.00223)\,(25-T)$$

where

V is the desired operating voltage of the solar array output

n is the number of series connected solar cells in one string

(.480) is the maximum power point operating voltage

(.00223) is the change in voltage, per cell, per degree Centigrade

T is the expected operating temperature in Centigrade degrees

the number of series cells per string is calculated to achieve the same output voltage from the solar array as was used in the DE design, namely 37.8 volts. (By so doing, the performance and operating characteristics of all of the remaining elements of the DE power system are retained.)

For the 30° effective Sun angle condition in the 300 km Mars orbit, it is seen from Figure 10-6 that the side array is projected to operate at +6°C. Solving the above equation for this condition yields n = 72.36 cells required in the

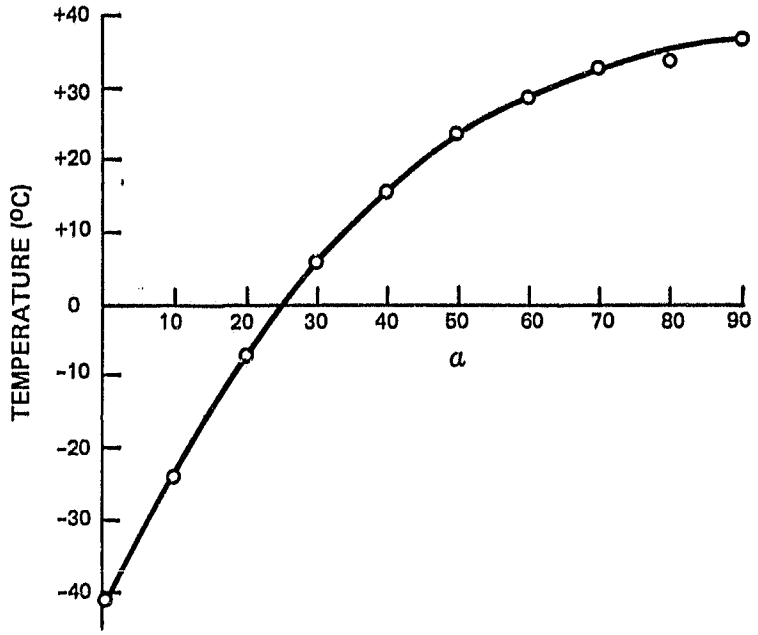

Figure 10-6. 300 km Circular Mars Orbit (Average Side Panel Temperature)

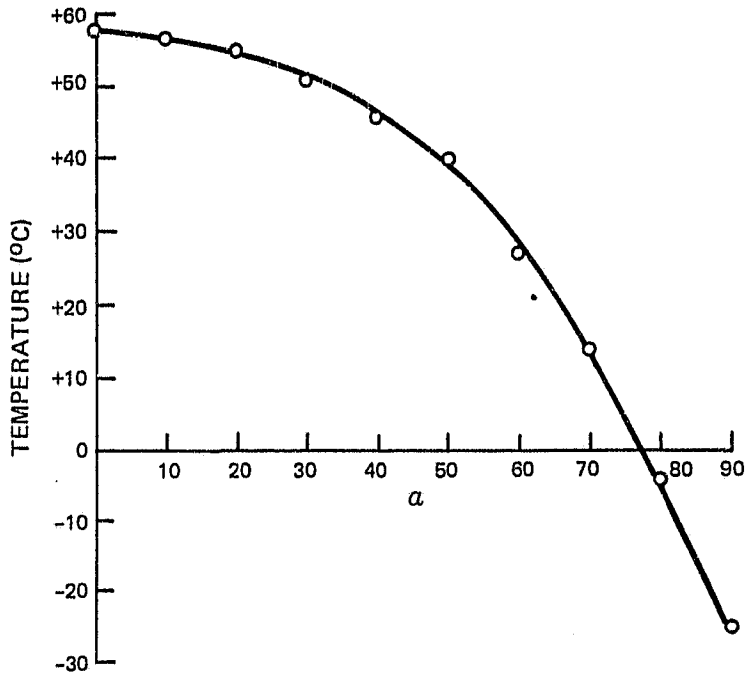

Figure 10-7. 300 km Circular Mars Orbit (Average Array End Temperature)

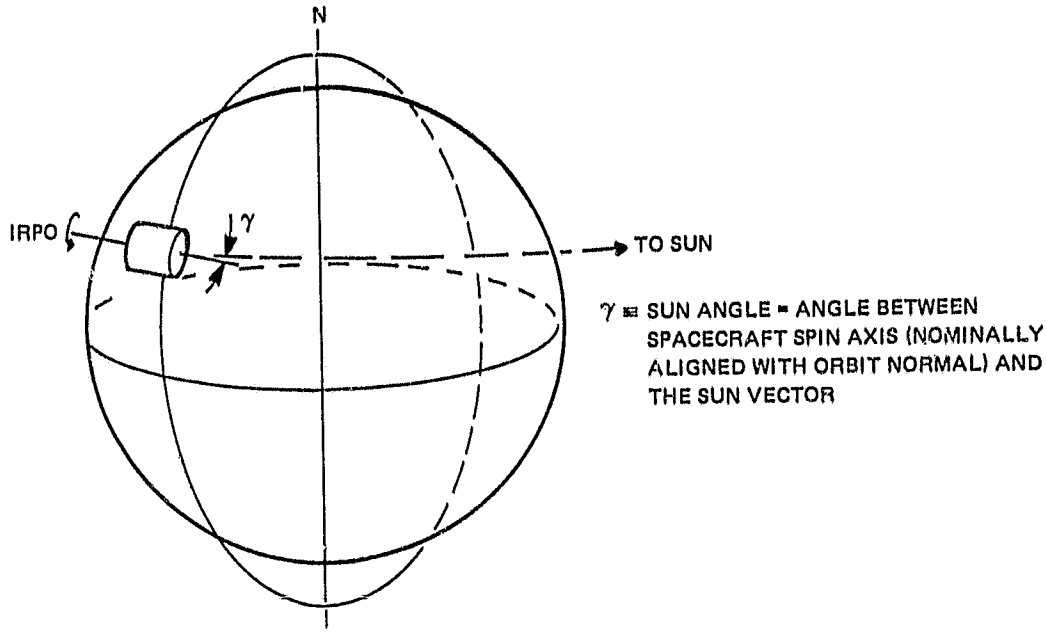

Figure 10-8. Sun Angle Geometry

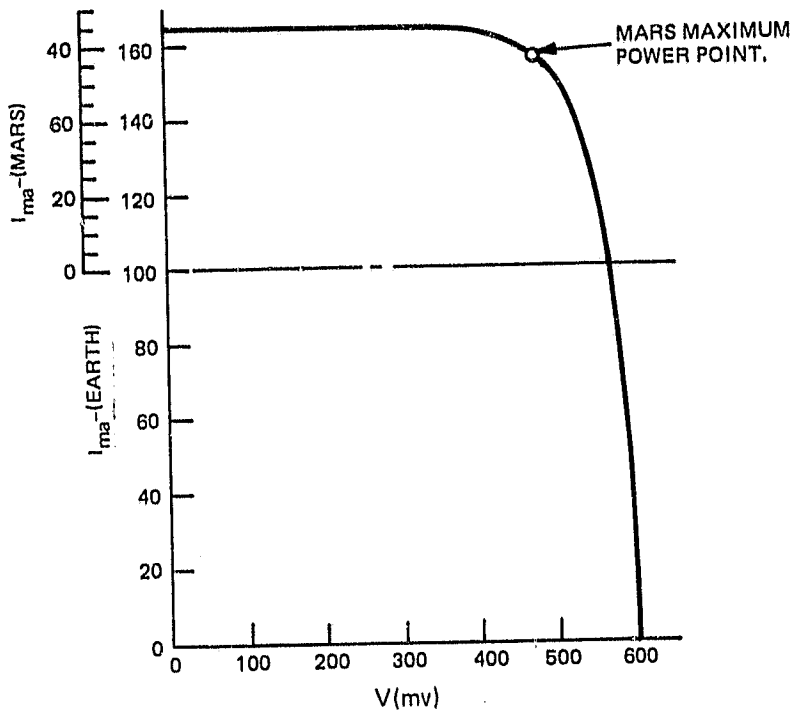

Figure 10-9. Solar Cell I-V Characteristics

series. For a full panel of 258 cells available this would allow three half-series strings to be mounted on one panel. Note that when half strings are used, the second half of the string must be placed on the adjacent facet of the spacecraft to allow both halves to be illuminated simultaneously; if the adjacent panel cannot accommodate a full complement of cells (or, more specifically can accommodate only a whole number of strings, i.e., 1, 2 or 3) the half string cannot be utilized.

In similar fashion, the end array, operating at 50°C for the 30° effective Sun angle, can mount a maximum of 2410 cells. Again applying the above equation, the number of series cells is 89 to achieve the -37.8 volt array output, and, this translates into 26 parallel strings, which for normally incident illumination would yield

$$26 \times 37.8 \text{ volts} \times 0.0565 \text{ amps} = 55.53 \text{ watts}$$

Figure 10-10 displays the developed array and the number of strings of solar cells allocated to the side panels; the shaded areas represent areas not available for mounting cells, due either to other equipment mounting or to being in the shadow of projecting equipment as was shown in the preliminary little bird field-of-view study in Figure 3-1.

To determine the available power, the generated power for each of the 16 orientations of the 16 sided spacecraft was calculated assuming that the solar input was normal to each face sequentially, as indicated in Figure 10-11. This calculation is shown in Table 10-4. To determine the average power available from the array, these calculated data were plotted and the representative points (Figure 10-12) were averaged. Because the STINT table requires, by program structure, entries of solar array output power for a full 180° range of sun angle, these were calculated by

$$P_{(end)} (\cos\gamma) + P_{(side\text{-}avg)} (\sin\gamma) = PS/A$$

For the 30° effective Sun angle array, the resulting array output is shown in Figure 10-13.

Considering next the 50° and 70° effective Sun angles, the resulting side and end temperatures, number of series cells and number of strings were similarly determined and are tabulated in Table 10-5. As can be seen from the table, both configurations can use only three strings per full side panel as compared to the 30° Sun angle array design. The STINT table data for these configurations were generated in like manner to the 30° configuration by first developing the average array power (see Figure 10-14) and then generating the actual array versus Sun angle curves (see Figures 10-15 and 10-16).

In like manner to the above, the solar array performance for the big bird spacecraft configuration was generated. The developed solar array is shown in Figure 10-17 for the 30° effective Sun angle with the resulting numbers of strings of solar cells as allocated for the available area. Table 10-6 summarizes the numbers of cells and strings for the three Sun angle conditions considered. In like manner to the calculations performed for the little bird case, the array performance was determined for these array designs. (The tabulated calculations have not been included, for brevity.) The power performance for the three cases through one orbit is shown in Figures 10-18, 10-19 and 10-20, with the resulting STINT curves shown in Figures 10-21, 10-22, and 10-23.

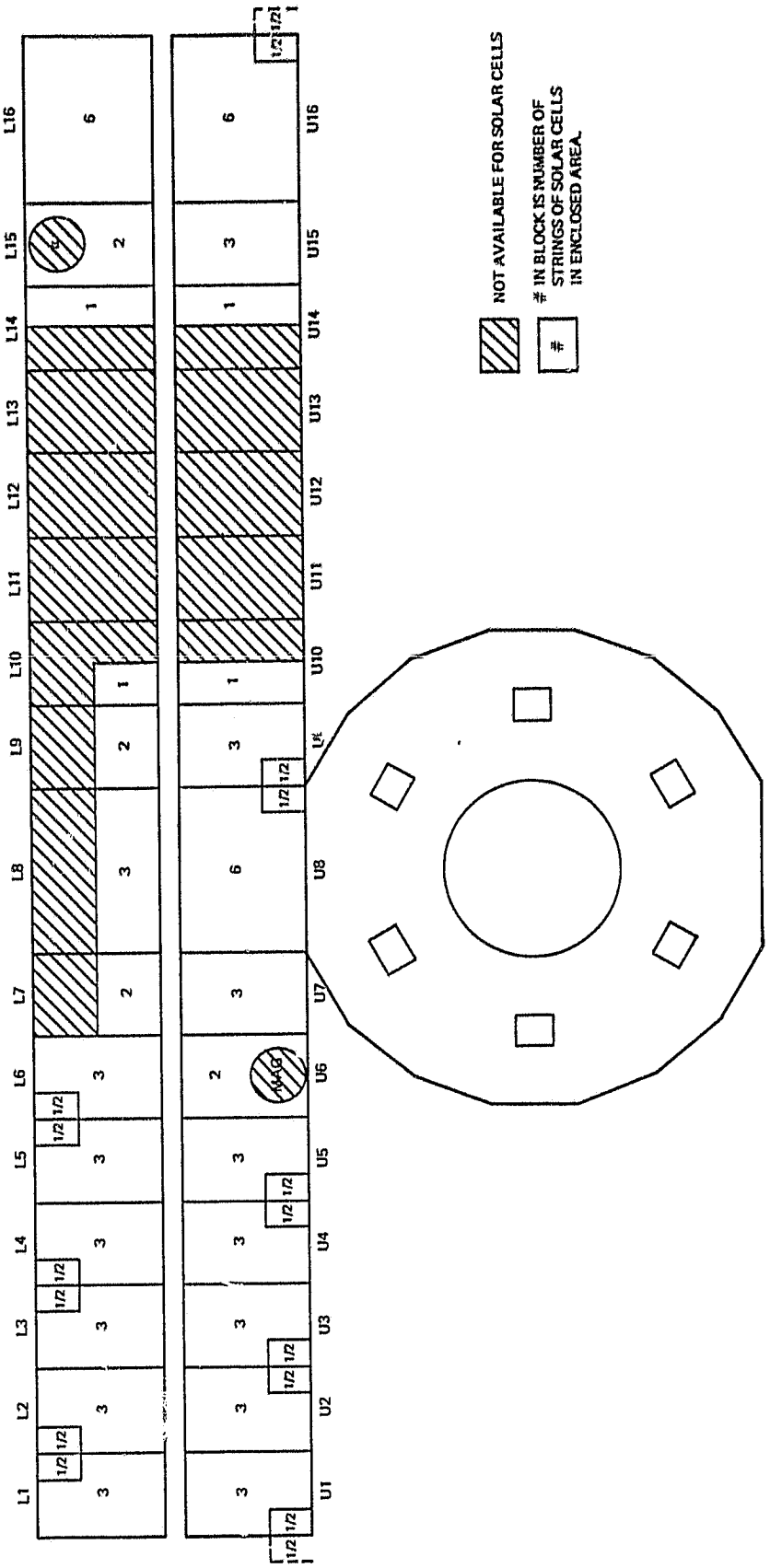

Figure 10-10. Little Bird Developed Array

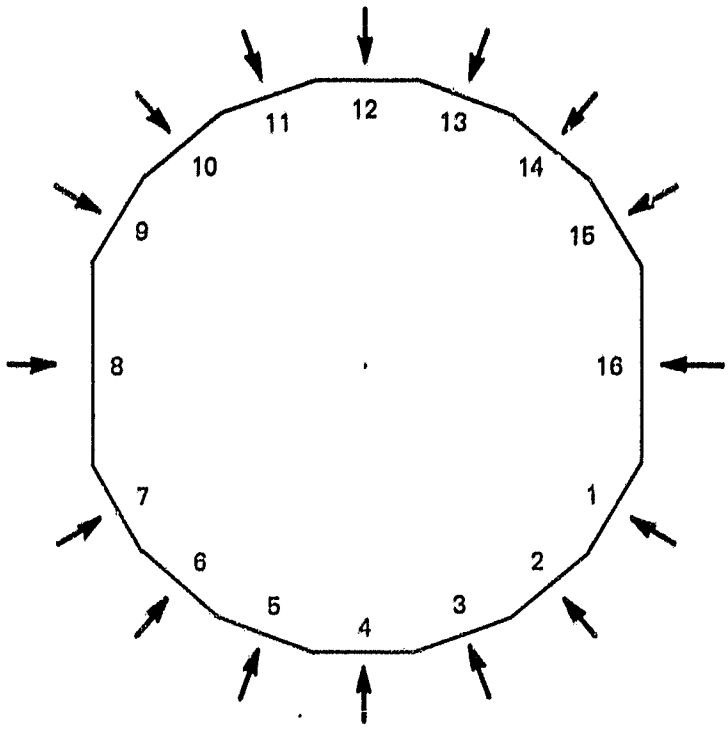

Figure 10-11. Sun Projection Geometry

10.4.1 MGO Power Performance

For each of the three solar array designs, a series of analyses of the power system performance was conducted. Subsystem performance parameters were varied for each of the launch cases: 88I, 90II and 92II. For each case, the following were considered: both a northern and a southern approach, data playback to record ratios of 8:1 and 4:1, and return link data via either X-band or S-band. The loads assumed in constructing the power profile to be used are shown in Table 10-7. The continuous load of the spacecraft, the most clearly defined in terms of accuracy of estimate, is based on the actual values of the corresponding equipment from the DE program, and therefore, only a modest 2 watt margin was applied. Note that the only difference in the proposed equipment is the change to the receiver portion of the transponders selected. Again for convervatism, it has been assumed that both communications receivers are powered continuously during the entire operational mission. An approximate 30 percent margin was allocated to the instrument complement above that defined in the JPL instrument description. Furthermore, the multi-spectral mapper was included at the identified peak value of 12 watts as opposed to the average value of 8 watts. A specific design tape recorder was not selected; however, the allocation of 9 watts in the record mode and 18 watts in the playback mode are judged to be conservative. Similarly, allocation of 9.5 watts to control the pointing of the high gain antenna during the playback operations is also believed to be conservative. Finally, since the detailed operation of the system during the playback mode is the least well defined, an additional power margin of 30.0 watts was allocated to the playback function to allow for contingencies.

TABLE 10-
(SINGL

PANEL	GUN NORM TO 16	GUN NORM TO 1	GUN NORM TO 2	GUN NORM TO 3	GUN NORM TO 4	GUN NO
"½"	P_B cos 15° = 2.136	P_B cos 15 = 2.136	P_B cos 35 = 1.749	P_B cos 55 = 1.225	0	0
U1	$3P_B$ cos 30° = 5.549	$3P_B$ = 6.407	$3P_B$ cos 20 = 6.021	$3P_B$ cos 40 = 4.900	$3P_B$ cos 60 = 3.204	$3P_B$ cos 8
U2	$3P_B$ cos 50 = 4.118	$3P_B$ cos 20 = 6.021	$3P_B$ = 6.407	$3P_B$ cos 20 = 6.021	$3P_B$ cos 20 = 4.908	$3P_B$ cos 6
"½"	P_B cos 50 4.118	P_B cos 30 = 1.850	P_B cos 10 = 2.103	P_B cos 10 = 2.103	P_B cos 30 = 1.450	P_B cos 50
U3	1 (P_B) cos 70 = 2.191	$3P_B$ cos 40 = 4.908	$3P_B$ cos 20 6.02	$3P_B$ = 6.407	$3P_B$ cos 20 = 6.021	$3P_B$ cos 4
U4	0	$3P_B$ cos 60 = 3.204	$3P_B$ cos 40 = 4.908	$3P_B$ cos 20 = 6.021	$3P_B$ = 6.407	$3P_B$ cos 2
"½"	0	P_B cos 70 = .730	P_B cos 50 = 1.373	P_B cos 30 = 1.850	P_B cos 10 = 2.103	P_B cos 10
U5	0	$3P_B$ cos 80 = 1.113	$3P_B$ cos 60 3.204	$3P_B$ cos 40 = 4.908	$3P_B$ cos 20 = 6.021	$3P_B$
U6	0	0	$2P_B$ cos 80 = .742	$2P_B$ cos 60 2.136	$2P_B$ cos 40 = 3.272	$2P_B$ cos 2
U7	0	0	0	$3P_B$ cos 80 = 1.113	$3P_B$ cos 60 = 3.204	$3P_B$ cos 4
U8	0	0	0	0	0	$6P_B$ cos 7
"½"	0	0	0	0	0	0
U9	0	0	0	0	0	0
U10	0	0	0	0	0	0
U14	$1P_B$ cos 50 = 1.373	P_B cos 80° = .371	0	0	0	0
U15	3 (P_B) cos 30 = 5.549	$3P_B$ cos 60 = 3.204	$3P_B$ cos 80° = 1.113	0	0	0
U16	6 x (P_B) = 12.814	$6P_B$ cos 30 = 11.097	$6P_B$ cos 50° = 8.237	$6P_B$ cos 70 = 4.383	0	0
L1	$3P_B$ cos 30 = 5.549	$3P_B$ = 6.407	$3P_B$ cos 20° = 6.021	$3P_B$ cos 40° = 4.908	$3P_B$ cos 60° = 3.204	$3P_B$ cos 8
"½"	P_B cos 40 = 1.636	P_B cos 10 - 2.103	P_B cos 10° = 2.103	P_B cos 30° = 1.850	P_B cos 50 = 1.373	P_B cos 70
L2	$3P_B$ cos 50 = 4.118	$3P_B$ cos 20 = 6.021	$3P_B$ = 6.407	$3P_B$ cos 20 = 6.021	$3P_B$ cos 40 = 4.908	$3P_B$ cos 6
L3	$3P_B$ cos 70 = 2.191	$3P_B$ cos 40 = 4.908	$3P_B$ cos 20° = 6.021	$3P_B$ = 6.407	$3P_B$ cos 20 = 6.021	$3P_B$ cos 4
"½"	0	P_B cos 50 = 1.373	P_B cos 30 = 1.850	P_B cos 10 = 2.103	P_B cos 10 = 2.103	P_B cos 30
L4	0	$3P_B$ cos 60 = 3.204	$3P_B$ cos 40 = 4.908	$3P_B$ cos 20 = 6.021	$3P_B$ = 6.407	$3P_B$ cos 2
L5	0	$3P_B$ cos 80 = 1.113	$3P_B$ cos 60 = 3.204	$3P_B$ cos 40 = 4.908	$3P_B$ cos 20 = 6.021	$3P_B$
"½"	0	0	P_B cos 70 = -.730	P_B cos 50 = 1.373	P_B cos 30 = 1.850	P_B cos 10
L6	0	0	$3P_B$ cos 80 = 1.113	$3P_B$ cos 60 = 3.204	$3P_B$ cos 40 = 4.908	$3P_B$ cos 2
L7	0	0	0	$2P_B$ cos 80 = 0.742	$2P_B$ cos 60 = 2.136	$2P_B$ cos 4
L8	0	0	0	0	0	$3P_B$ cos 7
L9	0	0	0	0	0	0
L10	0	0	0	0	0	0
L14	P_B cos 50 = 1.373	P_B cos 80 = .371	0	0	0	0
L15	$2P_B$ cos 30 = 3.699	$2P_B$ cos 60 = 2.136	$2P_B$ cos 80° = 0.742	0	0	0
L16	$6P_B$ = 12.814	$6P_B$ cos 30°= 11.098	$6P_B$ cos 50° = 8.237	$6P_B$ cos 70 = 4.383	0	0
	= 66.178	79.775	83.214	82,995	75,921	

FOLDOUT FRAME

TABLE 10-4. 30^{o} CONFIGURATION, P_S (SINGLE STRING) = 2.1357W

SUN NORM TO 3	SUN NORM TO 4	SUN NORM TO 5	SUN NORM TO 6
P_B cos 50 = 1.229	0	0	0
$3P_B$ cos 40 = 4.908	$3P_B$ cos 60 = 3.204	$3P_B$ cos 80 = 1.113	0
$3P_B$ cos 20 = 6.021	$3P_B$ cos 20 = 4.908	$3P_B$ cos 60 = 3.204	$3P_B$ cos 80 = 1.113
P_B cos 10 = 2.103	P_B cos 30 = 1.450	P_B cos 50 = 1.373	P_B cos 70 = .730
$3P_B$ = 6.407	$3P_B$ cos 20 = 6.021	$3P_B$ cos 40 = 3.908	$3P_B$ cos 60 = 3.204
$3P_B$ cos 20 = 6.021	$3P_B$ = 6.407	$3P_B$ cos 20 = 6.021	$3P_B$ cos 40 = 4.908
P_B cos 30 = 1.850	P_B cos 10 = 2.103	P_B cos 10 = 2.103	P_B cos 30 = 1.850
$3P_B$ cos 40 = 4.908	$3P_B$ cos 20 = 6.021	$3P_B$ = 6.407	$3P_B$ cos 20 = 6.021
$2P_B$ cos 60 2.136	$2P_B$ cos 40 = 3.272	$2P_B$ cos 20 = 4.014	$2P_B$ = 4.271
$3P_B$ cos 80 = 1.113	$3P_B$ cos 60 = 3.204	$3P_B$ cos 40 = 4.908	$3P_B$ cos 20 = 6.021
0	0	$6P_B$ cos 70 = 4.383	$6P_B$ cos 50 = 8.237
0	0	0	P_B cos 65 = 0.903
0	0	0	$3P_B$ cos 80 = 1.113
0	0	0	0
0	0	0	0
0	0	0	0
$6P_B$ cos 70 = 4.383	0	0	0
$3P_B$ cos 40° = 4.908	$3P_B$ cos 60° = 3.204	$3P_B$ cos 80° = 1.113	0
P_B cos 30° = 1.850	P_B cos 50 = 1.373	P_B cos 70° = 0.730	0
$3P_B$ cos 20 = 6.021	$3P_B$ cos 40 = 4.908	$3P_B$ cos 60° = 3.204	$3P_B$ cos 80° = 1.113
$3P_B$ = 6.407	$3P_B$ cos 20 = 6.021	$3P_B$ cos 40° = 4.908	$3P_B$ cos 60° = 3.204
P_B cos 10 = 2.103	P_B cos 10 = 2.103	P_B cos 30° = 1.850	P_B cos 50 = 1.373
$3P_B$ cos 20 = 6.021	$3P_B$ = 6.407	$3P_B$ cos 20° = 6.021	$3P_B$ cos 40 = 4.908
$3P_B$ cos 40 = 4.908	$3P_B$ cos 20 = 6.021	$3P_B$ = 6.407	$3P_B$ cos 20 = 6.021
P_B cos 50 = 1.373	P_B cos 30 = 1.850	P_B cos 10 = 2.103	P_B cos 10 = 2.103
$3P_B$ cos 60 = 3.204	$3P_B$ cos 40 = 4.908	$3P_B$ cos 20 = 6.021	$3P_B$ = 6.407
$2P_B$ cos 80 = 0.742	$2P_B$ cos 60 = 2.136	$2P_B$ cos 40 = 3.272	$2P_B$ cos 20 = 4.014
0	0	$3P_B$ cos 70 = 2.191	$3P_B$ cos 50 = 4.118
0	0	0	$2P_B$ cos 80 = 0.742
0	0	0	0
0	0	0	0
0	0	0	0
$6P_B$ cos 70 = 4.383	0	0	0
82.995	75.921	76.254	72.464

PANEL	SUN NORM TO 7	SUN NORM TO 8		SUN NORM TO 10	SUN NORM TO 11	SUN NORM T
"½"	0	0	0	0	0	0
U1	0	0	0	0	0	0
U2	0	0	0	0	0	0
"½"	0	0	0	0	0	0
U3	$3P_S$ cos 80 = 1.113	0	0	0	0	0
U4	$3P_S$ cos 60 = 3.204	0	0	0	0	0
"½"	$3P_S$ cos 50 = 1.373	0	0	0	0	0
U5	$3P_S$ cos 40 = 4.908	$3P_S$ cos 70 = 2.191	0	0	0	0
U6	$2P_S$ cos 20 = 4.014	$2P_S$ cos 50 = 2.746	$2P_S$ cos 80 = 0.742	0	0	0
U7	$3P_S$ = 6.407	$3P_S$ cos 30 = 5.549	$3P_S$ cos 60 = 3.204	$3P_S$ cos 80 = 1.113	0	0
U8	$6P_S$ cos 30° = 11.097	$6P_S$ = 12.814	$6P_S$ cos 30 = 11.097	$6P_S$ cos 50 = 8.237	$6P_S$ cos 70 = 4.283	0
"½"	P_S cos 45 = 1.510	P_S cos 15 = 2.136	P_S cos 15 = 2.136	P_S cos 35 = 1.749	P_S cos 55 = 1.225	0
U9	$3P_S$ cos 60 = 3.204	$3P_S$ cos 30 = 5.549	$3P_S$ = 6.407	$3P_S$ cos 20 = 6.021	$3P_S$ cos 40 = 4.908	$3P_S$ cos 60 =
U10	$1P_S$ cos 80 = 0.371	P_S cos 50 = 1.379	P_S cos 20 = 2.007	P_S = 2.136	P_S cos 20 = 2.007	P_S cos 40 = 1
U14	0	0	0	P_S cos 80 = 0.3771	P_S cos 60 = 1.068	P_S cos 60 = 1
U15	0	0	0	0	$3P_S$ cos 80 = 1.113	$3P_S$ cos 80 =
U16	0	0	0	0	0	0
L1	0	0	0	0	0	0
"½"	0	0	0	0		0
L2	0	0	0	0	0	0
L3	$3P_S$ cos 80 = 1.113	0	0	0	0	
"½"	P_S cos 70 = 0.730	0	0	0	0	0
L4	$3P_S$ cos 60 = 3.204	0	0	0	0	0
L5	$3P_S$ cos 40 = 4.908	$3P_S$ cos 70 = 2.191	0	0	0	0
"½"	P_S cos 30 = 1.850	P_S cos 60 = 1.068	0	0	0	0
L6	$3P_S$ cos 20 = 6.021	$3P_S$ cos 50 = 4.118	$3P_S$ cos 80 = 1.113	0	0	0
L7	$2P_S$ = 4.271	$2P_S$ cos 30 = 3.699	$2P_S$ cos 60 = 2.136	$2P_S$ cos 80 = 0.742	0	0
L8	$3P_S$ cos 30 = 5.549	$3P_S$ = 6.407	$3P_S$ cos 30 = 5.549	$3P_S$ cos 50 = 4.118	$3P_S$ cos 70 = 2.191	0
L9	$2P_S$ cos 60 = 2.136	$2P_S$ cos 30 = 3.699	$2P_S$ = 4.271	$2P_S$ cos 20 = 4.014	$2P_S$ cos 60 = 2.136	$2P_S$ cos 60 =
L10	P_S cos 80 = 0.371	P_S cos 50 = 1.373	P_S cos 20 = 2.997	P_S = 2.136	P_S cos 40 = 1.636	P_S cos 40 = 1
L14	0	0	0	P_S cos 80 = 0.371	P_S cos 60 = 1.068	P_S cos 40 = 1
L15	0	0	0	0	$2P_S$ cos 80 = 0.742	$2P_S$ cos 60 =
L16	0	0	0	0	0	0
	67.354	54.919	40.669	31.008	23.984	17.22

FOLDOUT FRAME

TABLE 10-4. 30° CONFIGURATION, P_S (SINGLE STRING) = 2.1357W (Continued)

SUN NORM TO 10	SUN NORM TO 11	SUN NORM TO 12	SUN NORM TO 13	SUN NORM TO 14	SUN NORM TO 15
	0	0	0	P_S cos 65 = 0.903	P_S cos 45 = 1.510
	0	0	0	$3P_S$ cos 80 = 1.113	$3P_S$ cos 60 = 3.204
	0	0	0	0	$3P_S$ cos 80 = 1.113
	0	0	0	0	0
	0	0	0	0	0
	0	0	0	0	0
	0	0	0	0	0
	0	0	0	0	0
	0	0	0	0	0
P_S cos 80 = 1.113	0	0	0	0	0
P_S cos 50 = 8.237	$6P_S$ cos 70 = 4.283	0	0	0	0
cos 35 = 1.749	P_S cos 55 = 1.225	0	0	0	0
P_S cos 20 = 6.021	$3P_S$ cos 40 = 4.908	$3P_S$ cos 60 = 3.204	$3P_S$ cos 80 = 1.113	0	0
= 2.136	P_S cos 20 = 2.007	P_S cos 40 = 1.636	P_S cos 60 = 1.068	P_S cos 80 = 1.636	0
cos 80 = 0.3771	P_S cos 60 = 1.068	P_S cos 60 = 1.636	P_S cos 40 = 2.007	P_S cos = 2.136	P_S cos 20 = 2.007
	$3P_S$ cos 80 = 1.113	$3P_S$ cos 80 = 3.204	$3P_S$ cos 60 = 4.908	$3P_S$ cos 40 = 6.021	$3P_S$ = 6.407
	0	0	$6P_S$ cos 70 = 4.383	$6P_S$ cos 50 = 8.237	$6P_S$ cos 30 = 11.097
	0	0	0	$3P_S$ cos 80 = 1.113	$3P_S$ cos 60 = 3.204
		0	0	0	P_S cos 70 = 0.730
	0	0	0	0	$3P_S$ cos 80° = 1.113
	0				
	0	0	0	0	0
	0	0	0	0	0
	0	0	0	0	0
	0	0	0	0	0
	0	0	0	0	0
P_S cos 80 = 0.742	0	0	0	0	0
P_S cos 50 = 4.118	$3P_S$ cos 70 = 2.191	0	0	0	0
P_S cos 20 = 4.014	$2P_S$ cos 60 = 2.136	$2P_S$ cos 60 = 2.136	$2P_S$ cos 80 = 0.742	0	0
= 2.136	P_S cos 40 = 1.636	P_S cos 40 = 1.636	P_S cos 60 = 1.064	P_S cos 80 = 0.371	0
cos 80 = 0.371	P_S cos 60 = 1.068	P_S cos 40 = 1.636	P_S cos 20 = 2.007	P_S = 2.136	P_S cos 20 = 2.007
	$2P_S$ cos 80 = 0.742	$2P_S$ cos 60 = 2.136	$2P_S$ cos 40 = 3.273	$2P_S$ cos 20 = 4.104	$2P_S$ = 4.271
	0	0	$6P_S$ cos 70 = 4.383	$6P_S$ cos 50 = 8.237	$6P_S$ cos 30 = 11.097
31.008	23.984	17.224	25.015	34.652	47.76

FOLDOUT FRAME

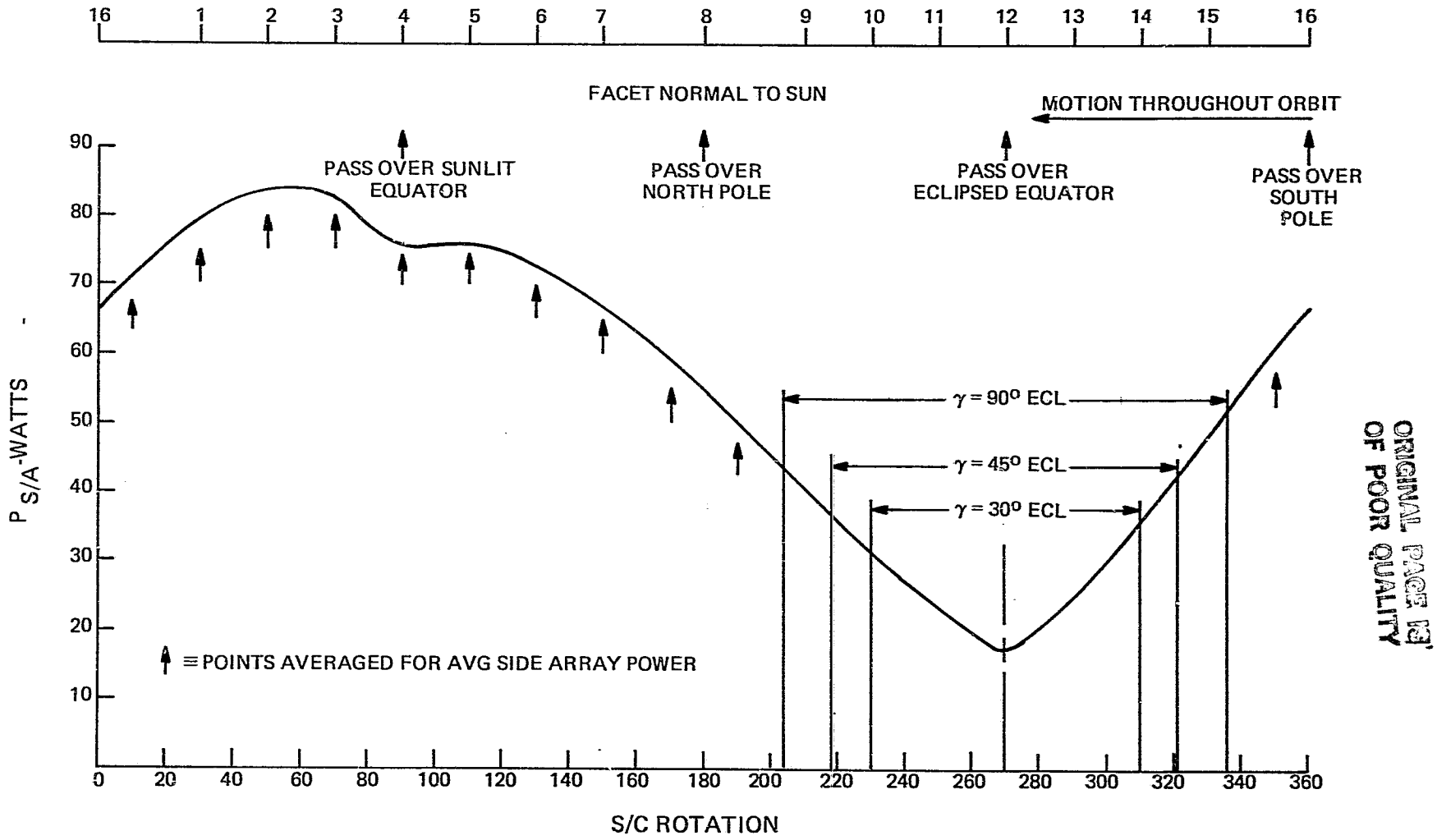

Figure 10-12. 30°γ Array Configuration - Little Bird Side Array Output, Normal Incident Sun, Through 360° S/C Relative to Sun Vector

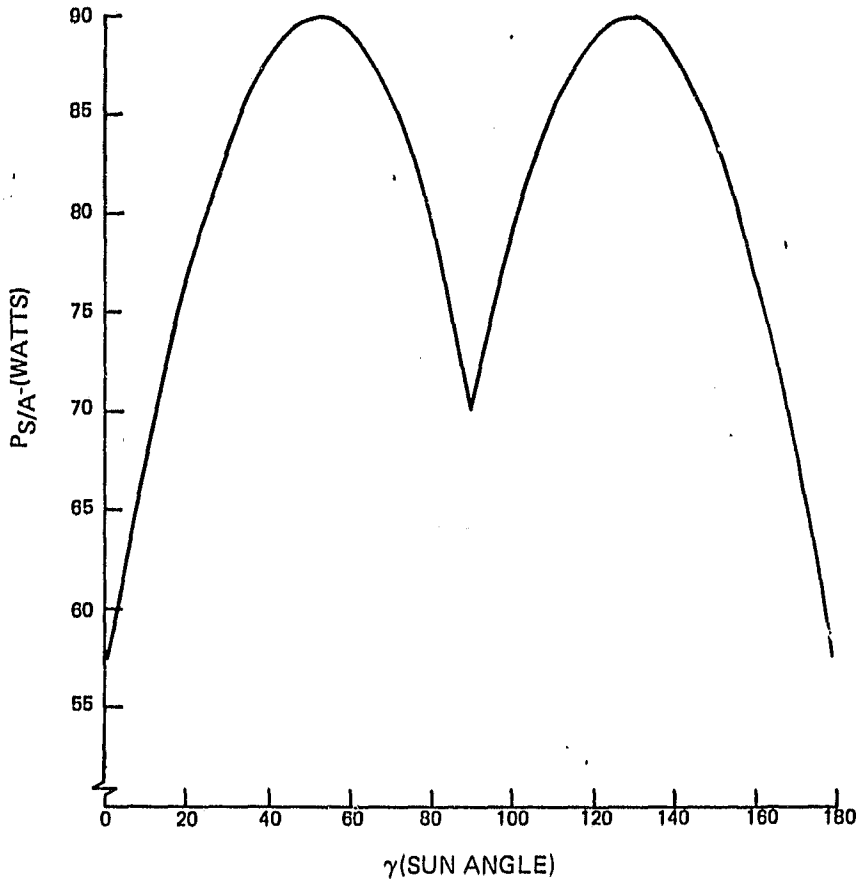

Figure 10-13. Little Bird 30°γ Configuration STINT Curve

TABLE 10-5. LITTLE BIRD SOLAR ARRAY

Effective Sun Angle	Side Temp	End Temp	# Series Cells/Side String	# Series Cell/End String	# Strings/ Side Panel	# Strings End Panel
50°	24°C	40°	79	85	3	28
70°	33°C	14°	75	75	3	32

To illustrate the behavior of the power system, eight sets of the graphical output of the analysis, corresponding to the 88I launch case for the 30° Sun angle solar array (runs 49, 52, 55, 58, 61, 64, 67 and 70), are presented in Figures 10-24 through 10-47. While the analysis provides graphical output for all cases run, only this subset has been included, for purposes of brevity.

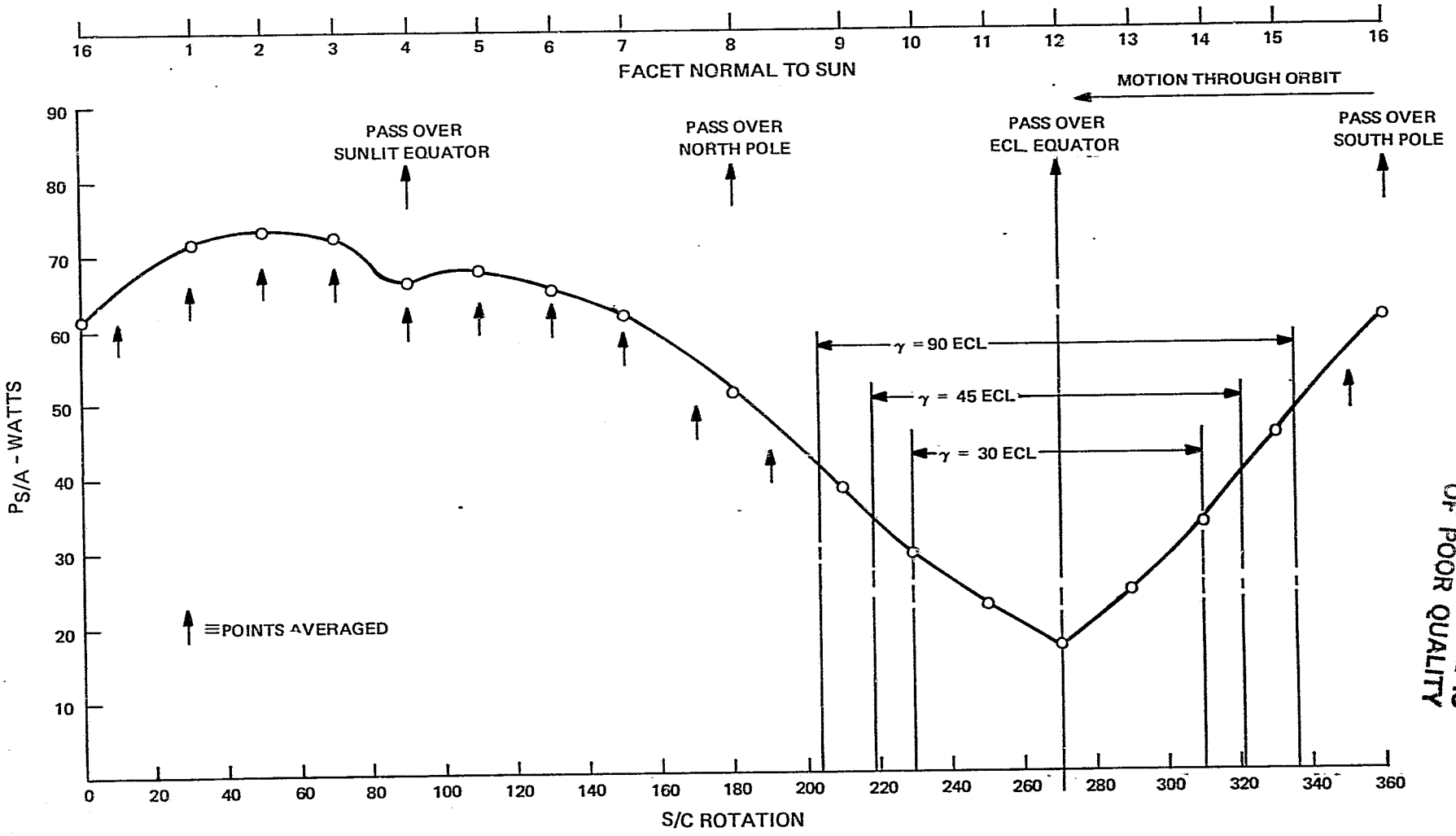

Figure 10-14. 50° and 70°γ Array Configuration - Little Bird Side Array Output, Normal Incident Sun, Through 360° S/C Relative to Sun Vector

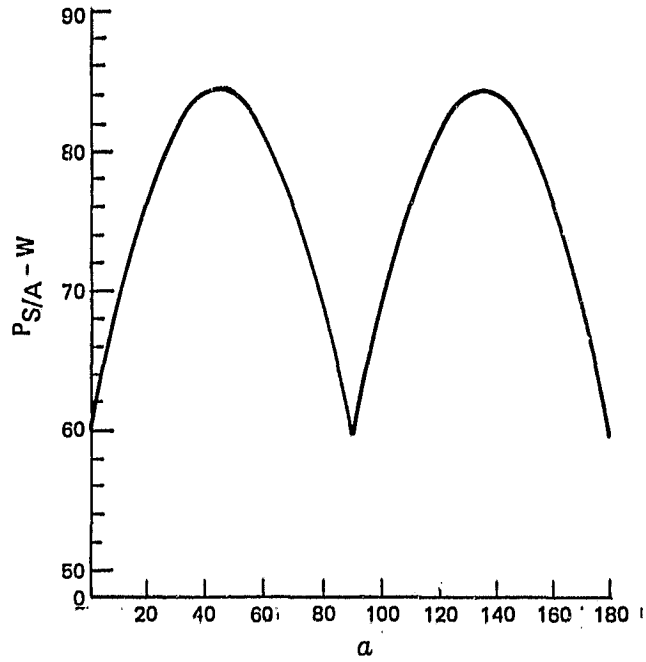

Figure 10-15. Little Bird 50°γ Configuration STINT Curve

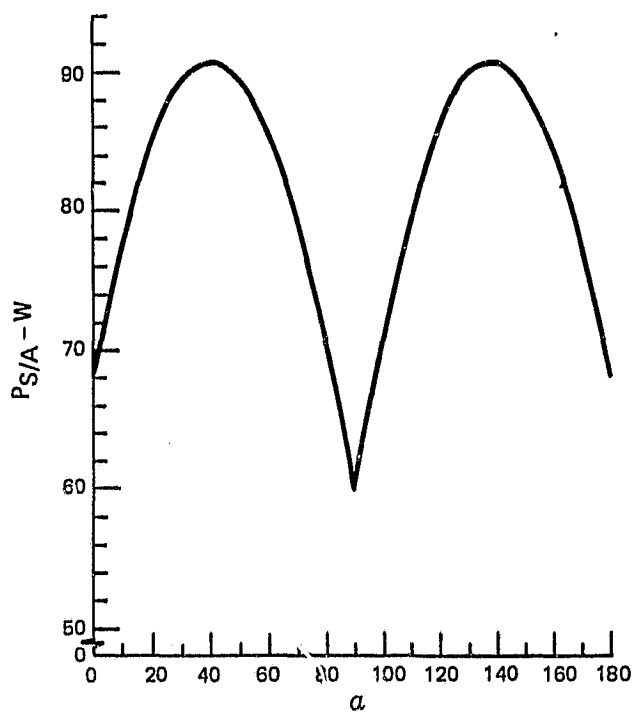

Figure 10-16. Little Bird 70°γ Configuration STINT Curve

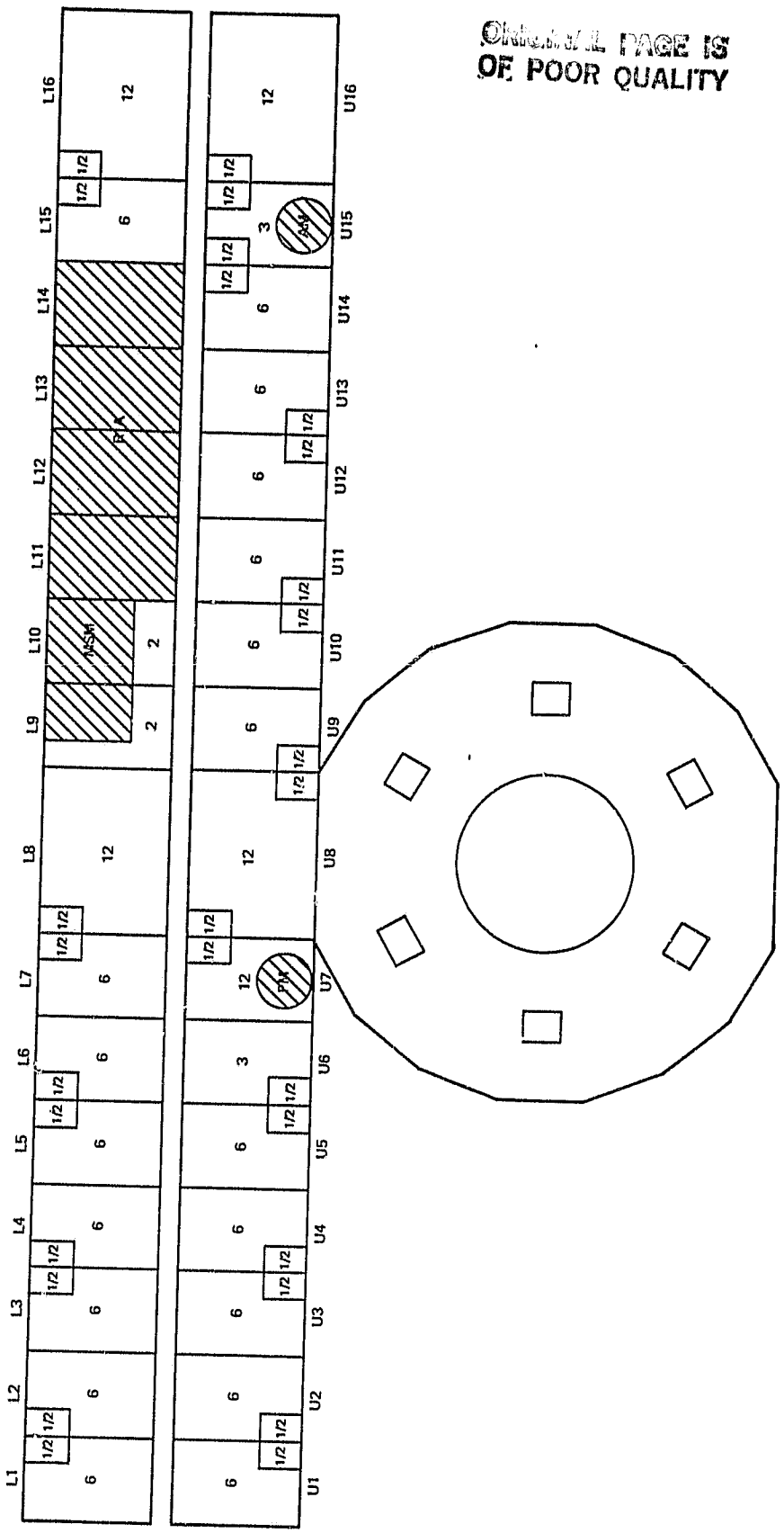

Figure 10-17. Big Bird Developed Array

TABLE 10-6. BIG BIRD SOLAR ARRAY

Effective Sun Angle	Side Array Temp	End Array Temp	Cells/Side Series String	Cells/End Series String	Strings/ Side Panel	Strings/ End Panel
30°	6	50	73	90	6 1/2	50
50°	24	40	79	85	6	53
70°	33	14	82	75	5 1/2	60

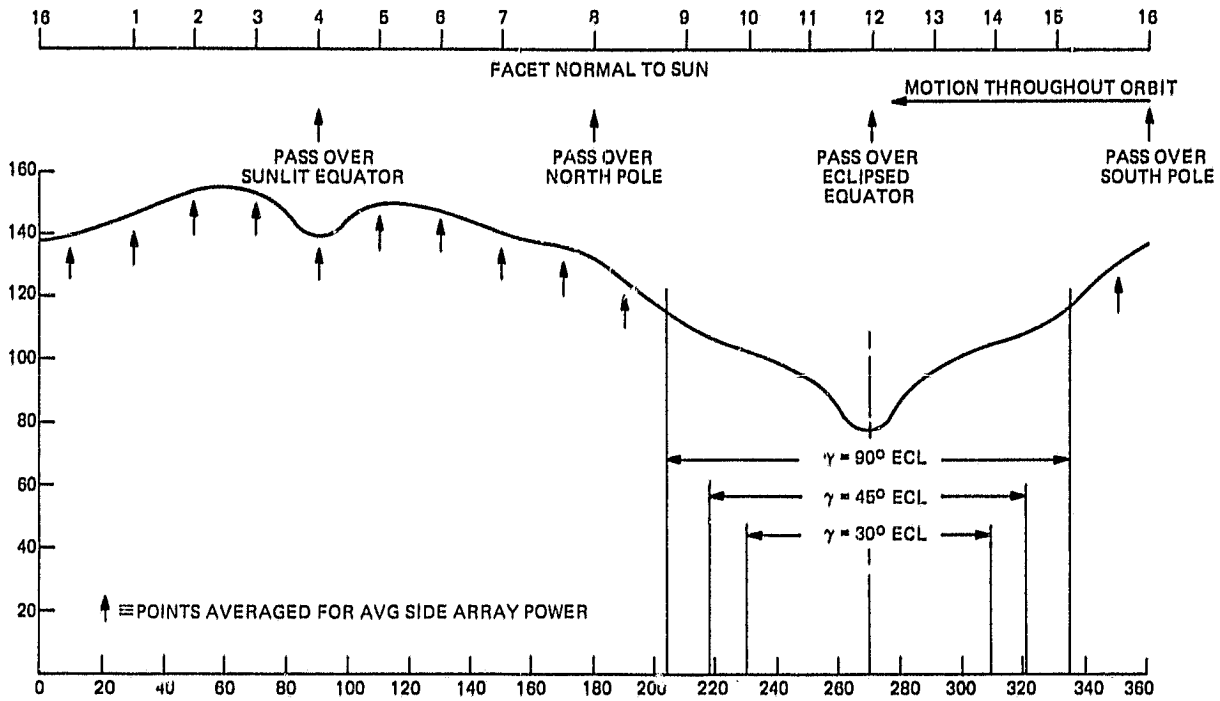

Figure 10-18. γ=30° Configuration - Big Bird Side Array

continuously during the entire operational mission. An approximate 30 percent margin was allocated to the instrument complement above that defined in the JPL instrument description. Furthermore, the multi-spectral mapper was included at the identified peak value of 12 watts as opposed to the average value of 8 watts. A specific design tape recorder was not selected; however, the allocation of 9 watts in the record mode and 18 watts in the playback mode are judged to be conservative. Similarly, allocation of 9.5 watts to control the pointing of the high gain antenna during the playback operations is also believed to be conservative. Finally, since the detailed operation of the system during the playback mode is the least well defined, an additional power margin of 30.0 watts was allocated to the playback function to allow for contingencies.

To illustrate the behavior of the power system, eight sets of the graphical output of the analysis, corresponding to the 88I launch case for the 30° Sun angle solar array (runs 49, 52, 55, 58, 61, 64, 67 and 70), are presented in Figures 10-24 through 10-47. While the analysis provides graphical output for all cases run, only this subset has been included, for purposes of brevity.

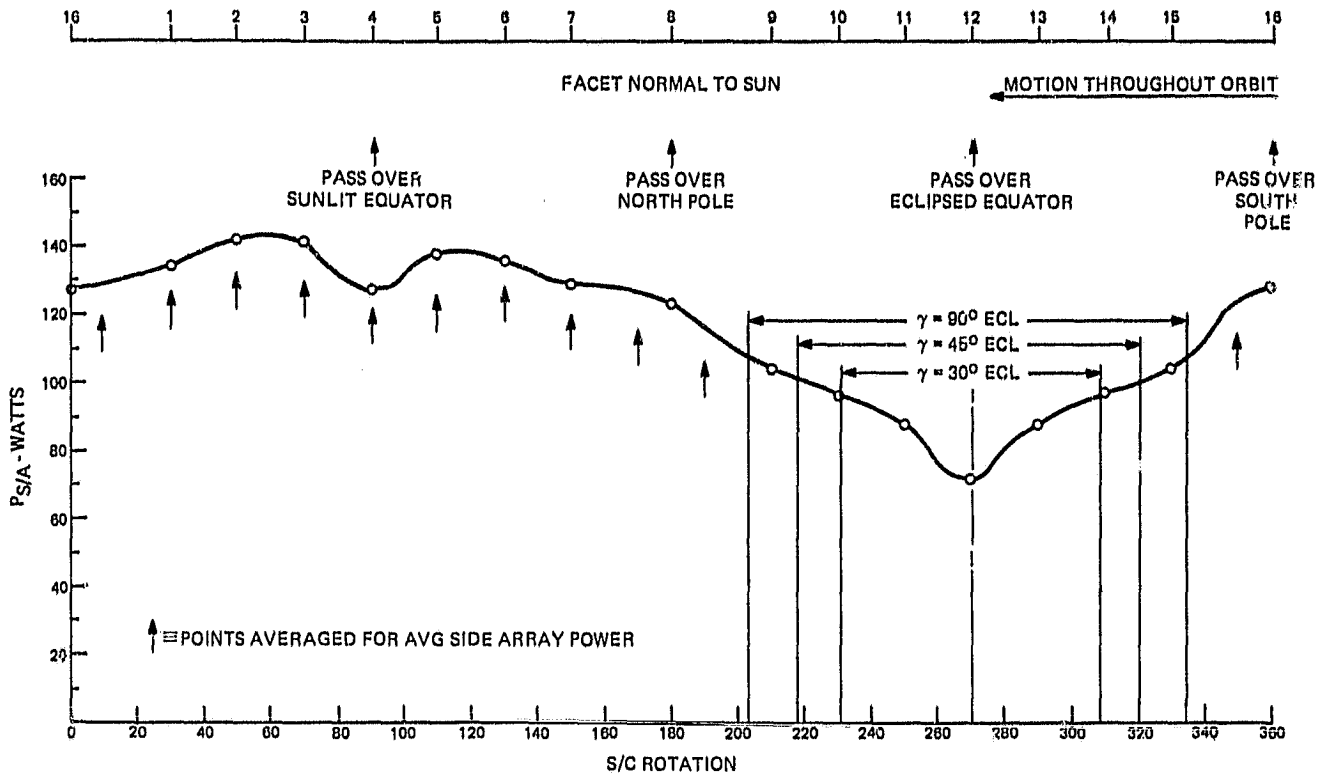

Figure 10-19. γ=50° Configuration - Big Bird Side Array

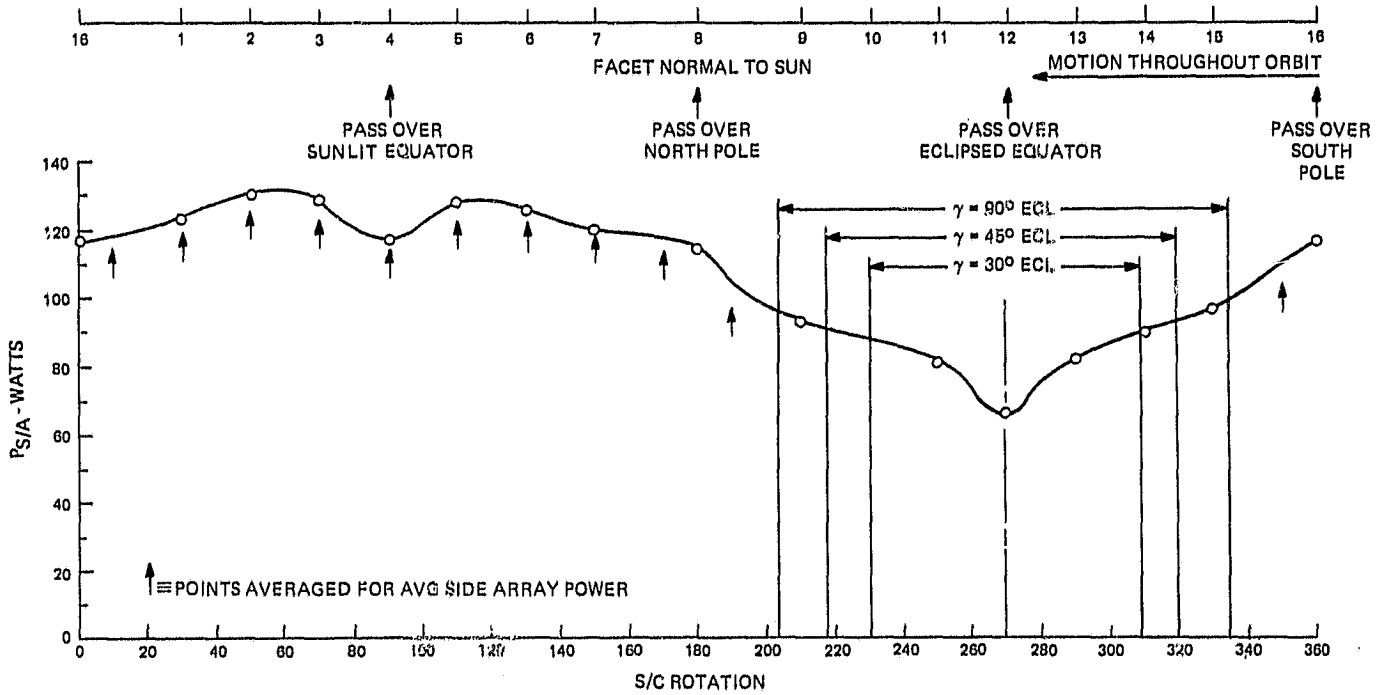

Figure 10-20. γ=70° Configuration - Big Bird Side Array

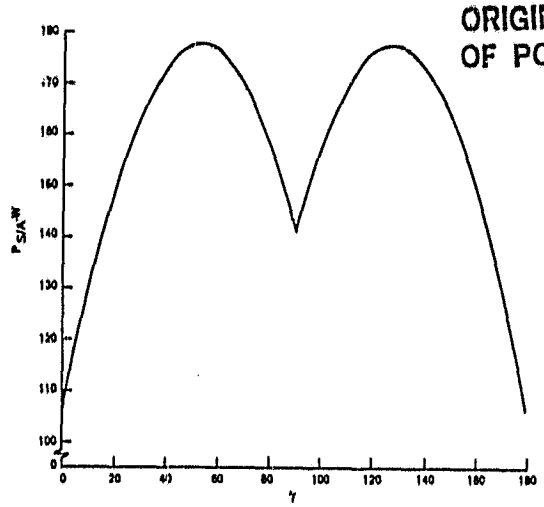

Figure 10-21. Big Bird γ=30° Configuration STINT Data

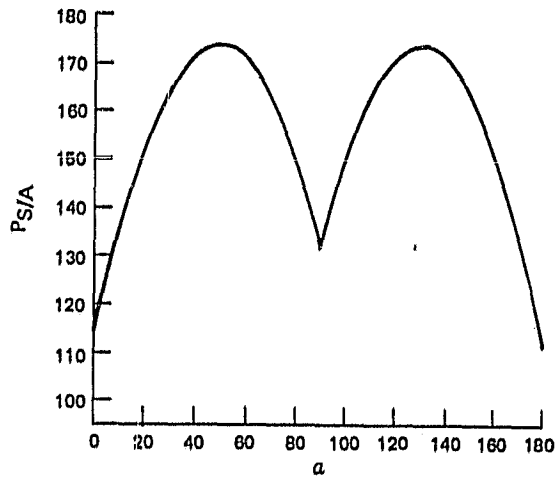

Figure 10-22. Big Bird γ=50° Configuration STINT Data

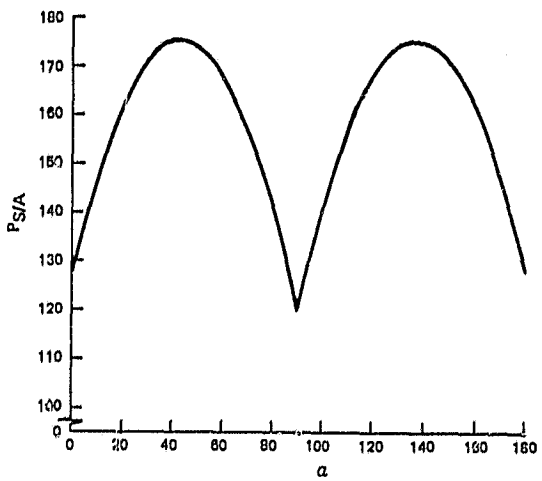

Figure 10-23. Big Bird γ=70° Configuration STINT Data

TABLE 10-7. MGO POWER PROFILE

Subsystem / Bus	Continuous Load			Load Above Continuous					
	Watts			Science Watts			Playback Watts		
	Unreg.	-24.5V	+28V	Unreg.	-24.5V	+28V	Unreg.	-24.5V	+28V
Instruments	0.				57.0				
Communications: X-Band	14.2						116.5		
(S-Band)							(132.8)**		
Attitude Control	3.5		6.5						
Command & Data Handling (C&DH)	1.8		8.0		9.0			18.0	
Power	4.5								
Thermal (50% DC)	2.0								
Margin	2.0								
S/C Total	26		14.5		66.0		116.5	18.0	
							(132.8)		
Unregulated Bus Total Load	45.0			73.0			136.6		
							(152.8)**		

*Assuming efficiency factors: .9 for -24.5V Regulator
.85 for +28V Regulator

**Bracketed numbers are for S-Band Downlink.

TABLE 10-7. MGO POWER PROFILE (Continued)

Subsystem / Bus	Continuous Load			Load Above Continuous					
	Watts			Science Watts			Playback Watts		
	Unreg.	-24.5V	+28V	Unreg.	-24.5V	+28V	Unreg.	-24.5V	+28V
Instruments									
Magnetometer									
Electronics					4.0				
Sensor									
Gamma Ray Spectrometer									
Electronics					10.0				
Sensor									
Multi-Spectral Mapper									
Electronics					12.0				
Sensor									
Radar Altimeter									
Electronics					18.0				
Sensor									
Instrument Margin (30%)					13.0				
Instruments Total					57.0				

TABLE 10-7. MGO POWER PROFILE (Continued)

Subsystem / Bus	Continuous Load			Load Above Continuous					
	Watts			Science Watts			Playback Watts		
	Unreg.	-24.5V	+28V	Unreg.	-24.5V	+28V	Unreg.	-24.5V	+28V
Communications									
Transponder*									
S-Band Receivers X- or S-Band Transmitters (2 powered continuously)	14.2						74.5 (90.8)*		
High Gain Antenna Control							9.5		
Premodulation Processor							2.5		
Communications Margin							30°		
Communications Total	14.2						116.5 (132.8)*		

*Numbers in brackets represents S-band downlink

TABLE 10-7. MGO POWER PROFILE (Continued)

Subsystem / Bus	Continuous Load			Load Above Continuous					
	Watts			Science Watts			Playback Watts		
	Unreg.	-24.5V	+28V	Unreg.	-24.5V	+28V	Unreg.	-24.5V	+28V
C&DH									
Command and Telemetry Processor (CTP)			5.0						
Remote Telemetry Module (RTM)			2.5						
Command Distribution Unit (CDU)			.5						
Tape Recorder					9.0			18.0	
C&DH Total			8.0		9.0			18.0	
Power									
PSE Shunt Loss	3.0								
Bypass Resistor Leakage	.5								
Current Sensor Loss	.5								
+28V Regulator Fixed Loss	.5								
Power Total	4.5								

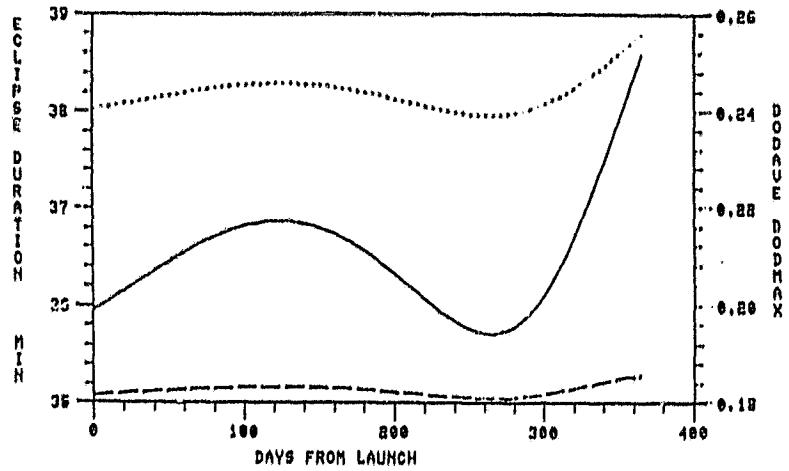

Figure 10-24. Run 049, Array Power and Sun Angle

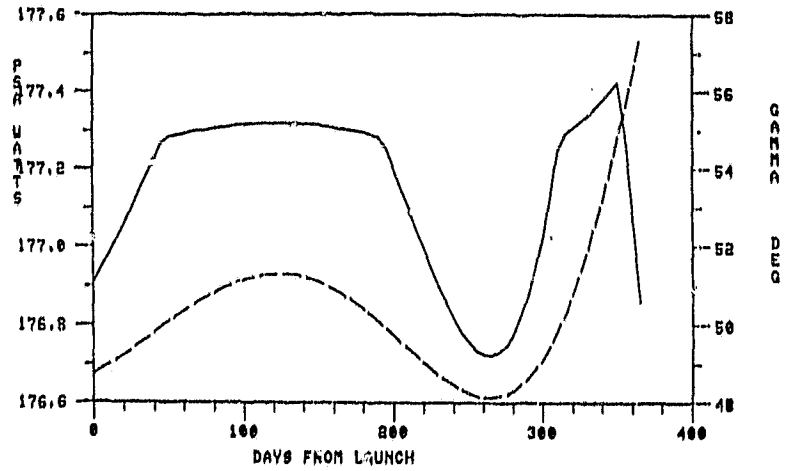

Figure 10-25. Run 049, Eclipse History and DOD Performance

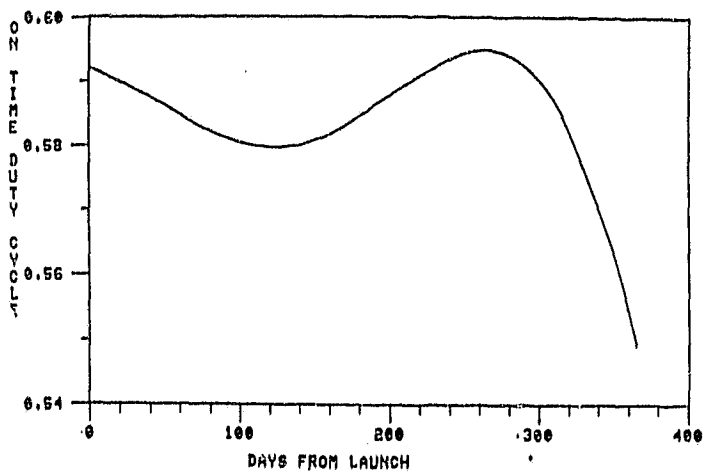

Figure 10-26. Run 049, Duty Cycle Performance

C-3

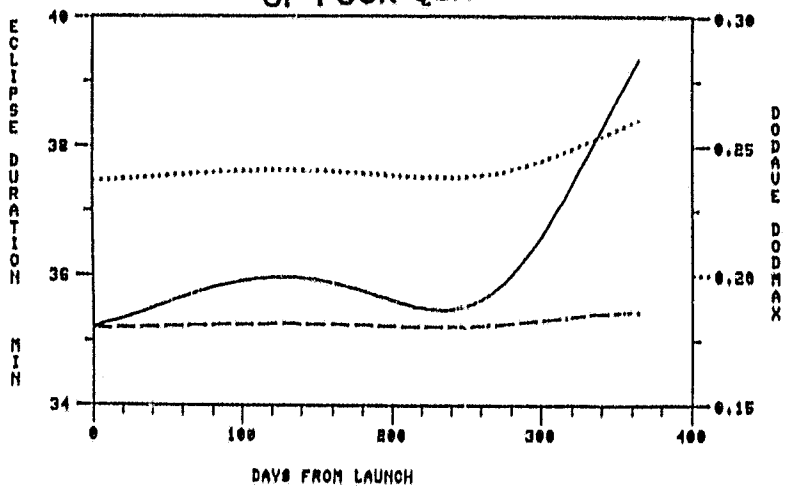

Figure 10-27. Run 052, Array Power and Sun Angl

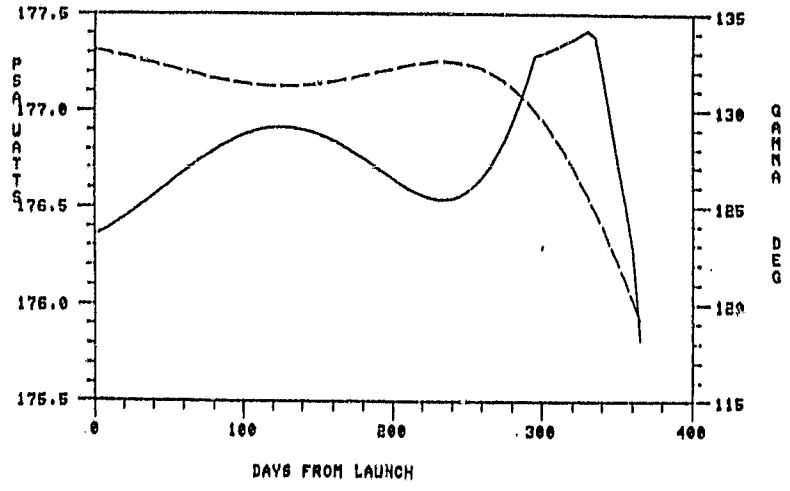

Figure 10-28. Run 052, Eclipse History and DOD Performance

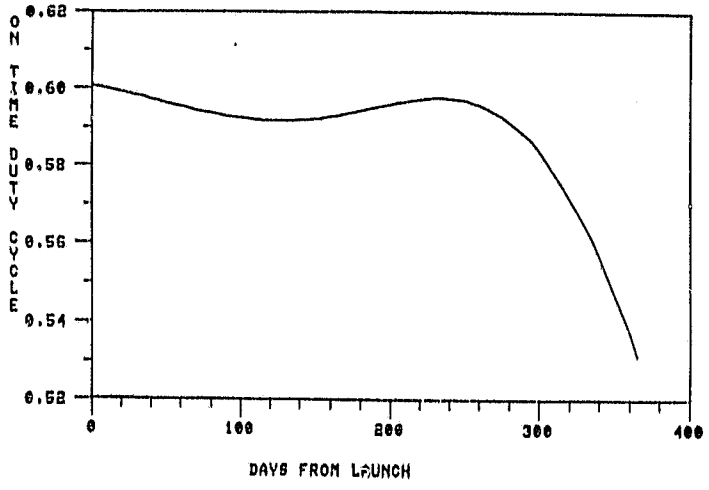

Figure 10-29. Run 052, Duty Cycle Performance

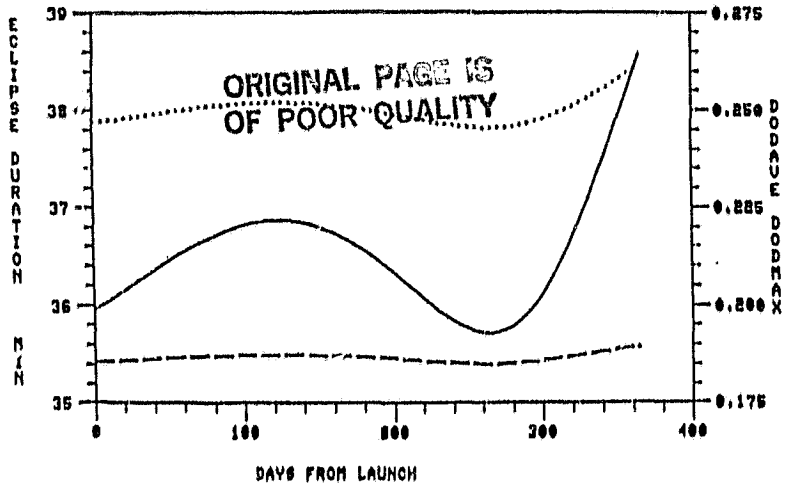

Figure 10-30. Run 055, Array Power and Sun Angle

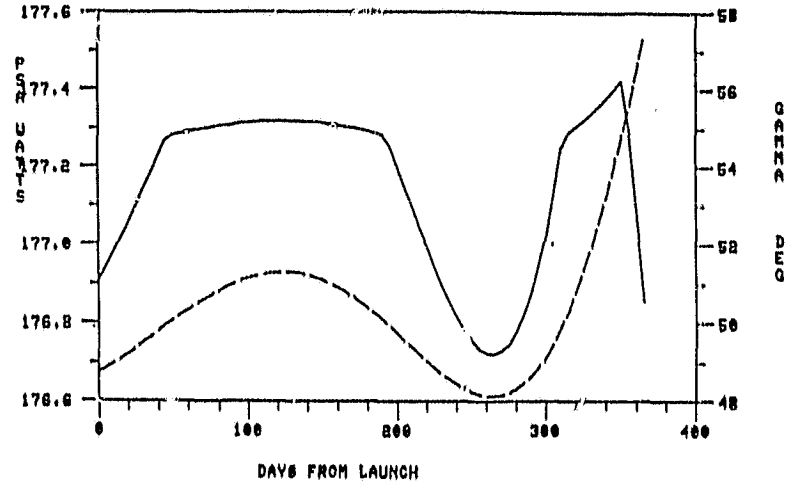

Figure 10-31. Run 055, Eclipse History and DOD Performance

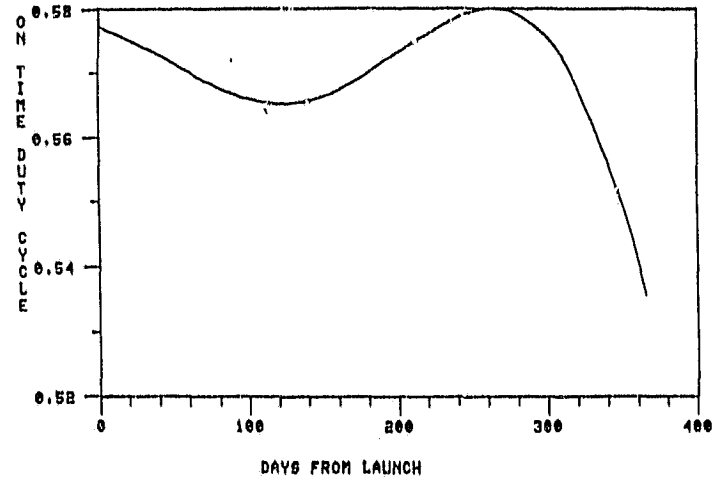

Figure 10-32. Run 055, Duty Cycle Performance

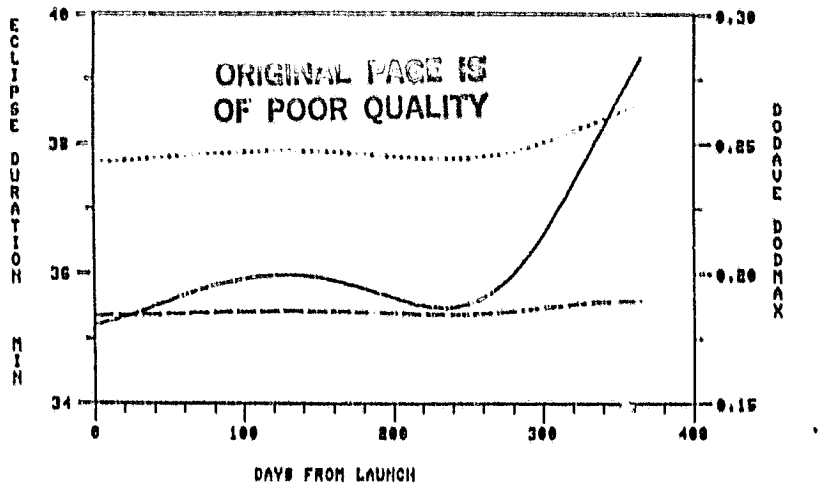

Figure 10-33. Run 058, Array Power and Sun Angle

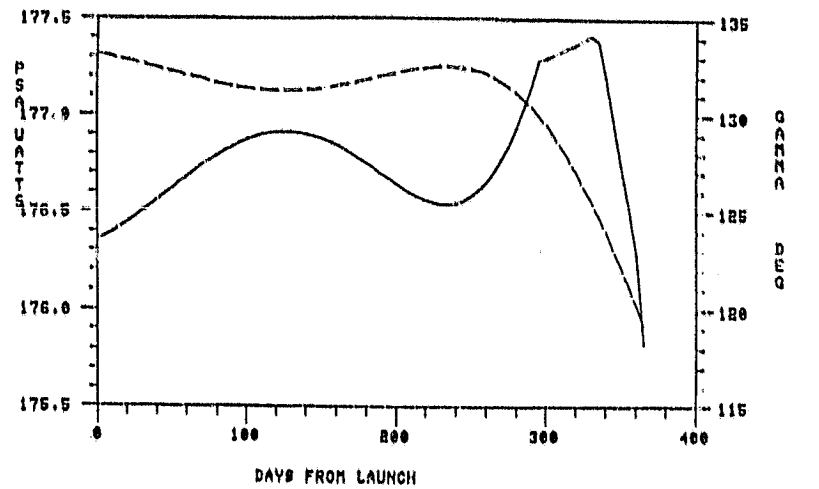

Figure 10-34. Run 058, Eclipse History and DOD Performance

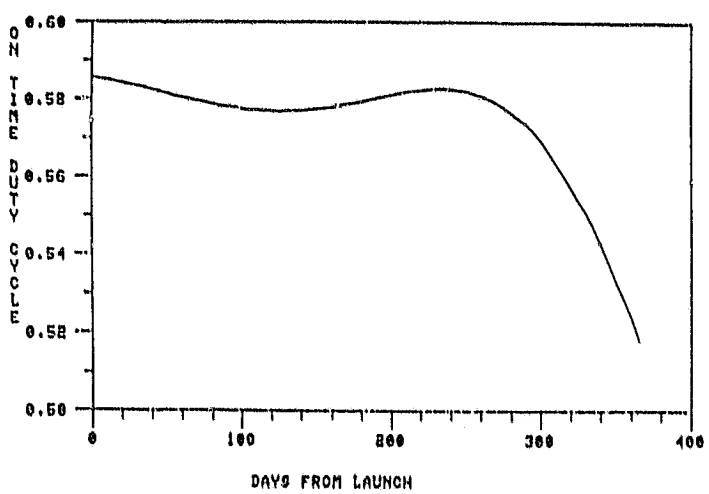

Figure 10-35. Run 058, Duty Cycle Performance

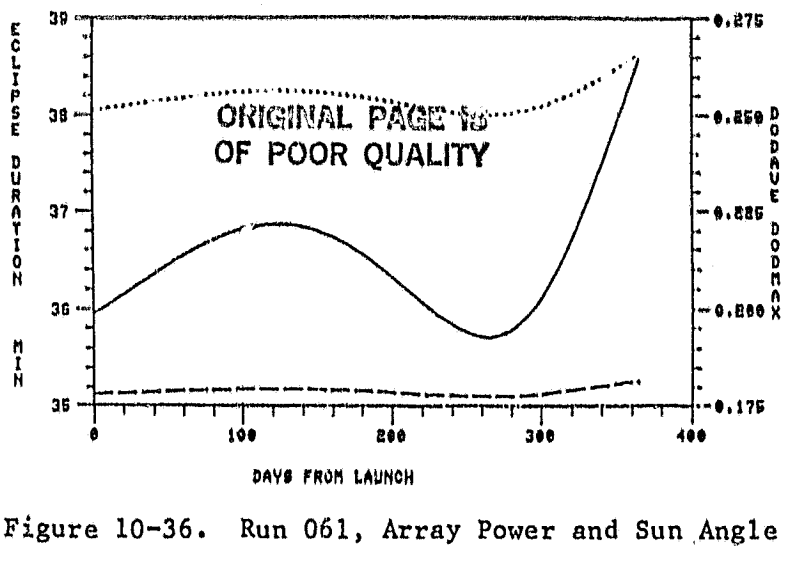

Figure 10-36. Run 061, Array Power and Sun Angle

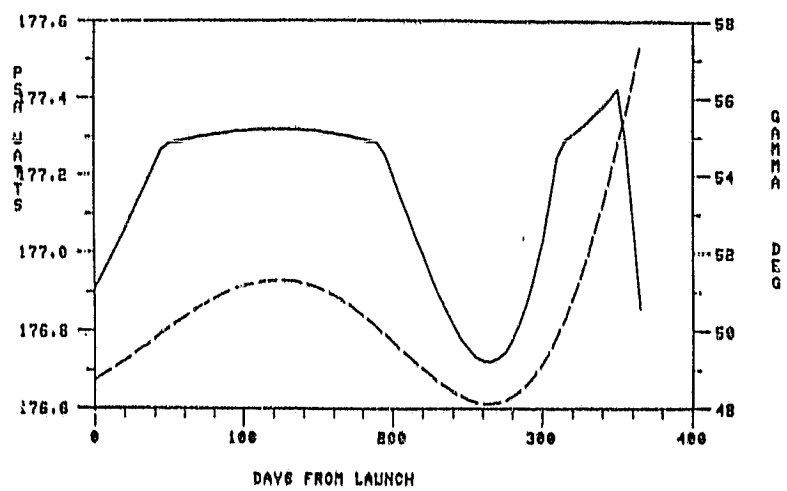

Figure 10-37. Run 061, Eclipse History and DOD Performance

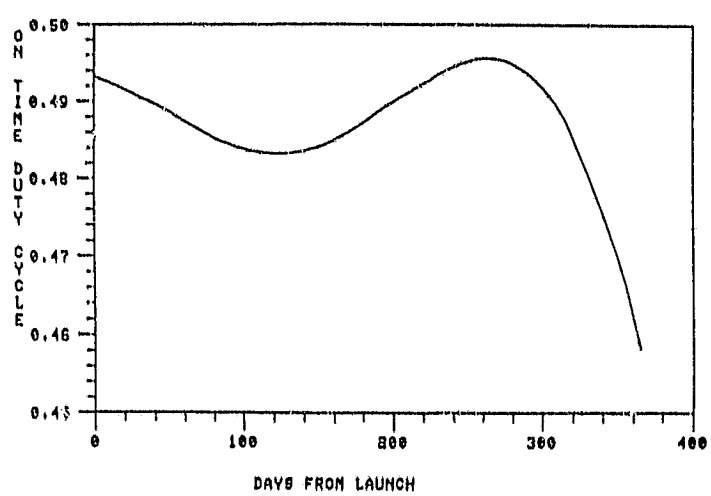

Figure 10-38. Run 061, Duty Cycle Performance

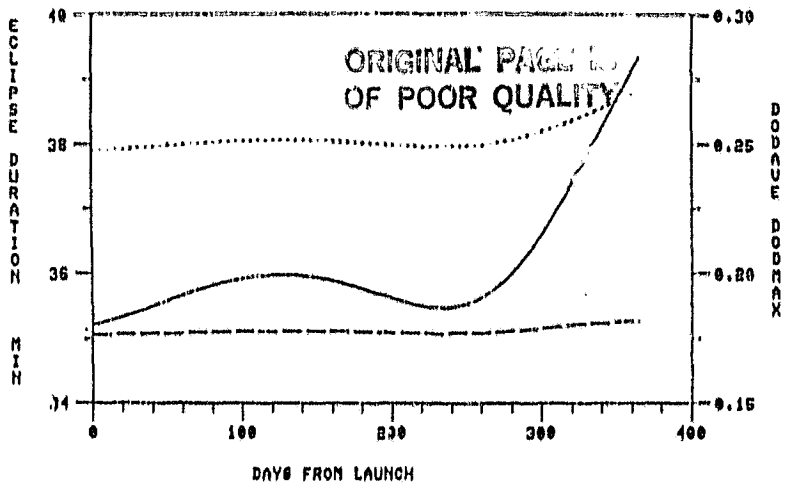

Figure 10-39. Run 064, Array Power and Sun Angle

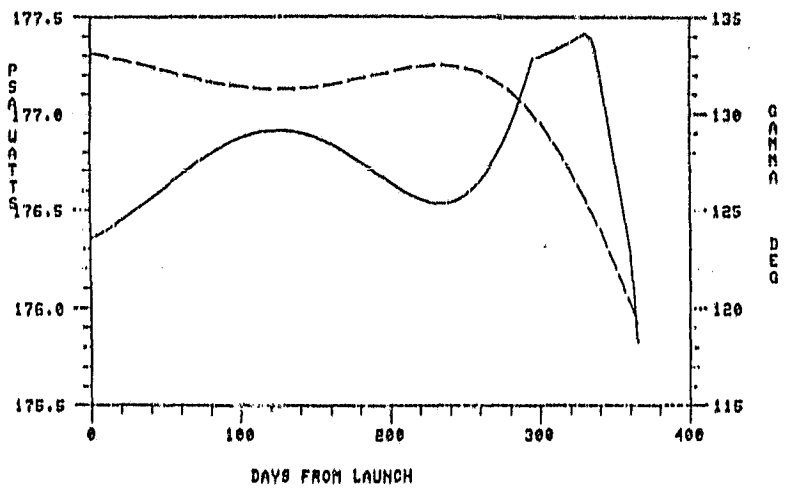

Figure 10-40. Run 064, Eclipse History and DOD Performance

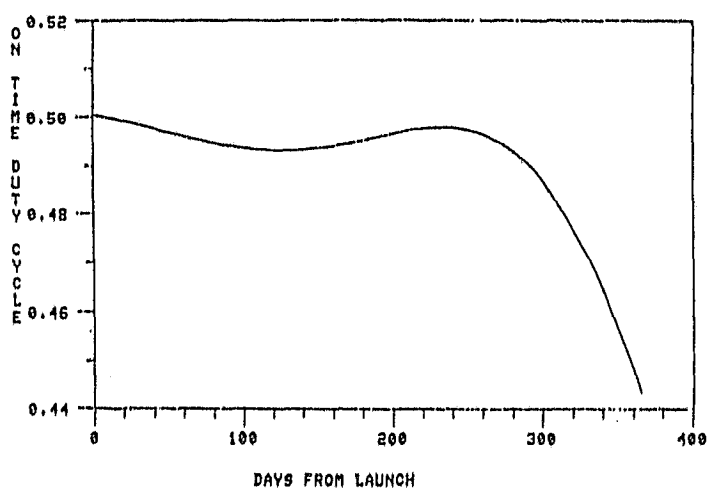

Figure 10-41. Run 064, Duty Cycle Performance

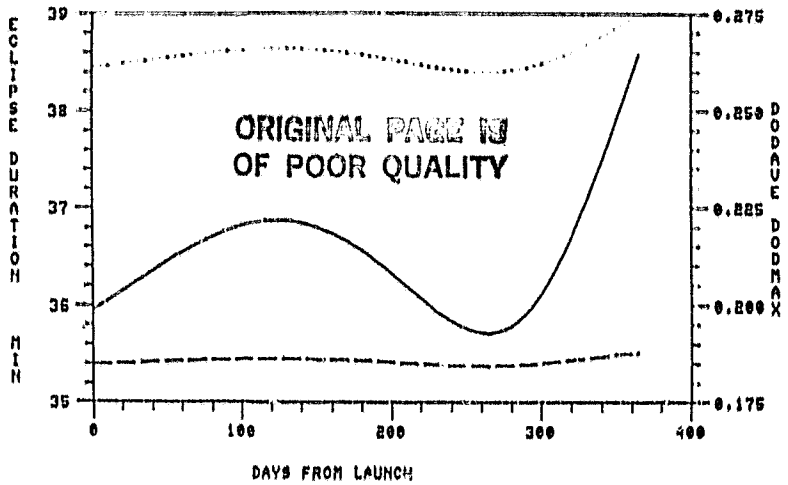

Figure 10-42. Run 067, Array Power and Sun Angle

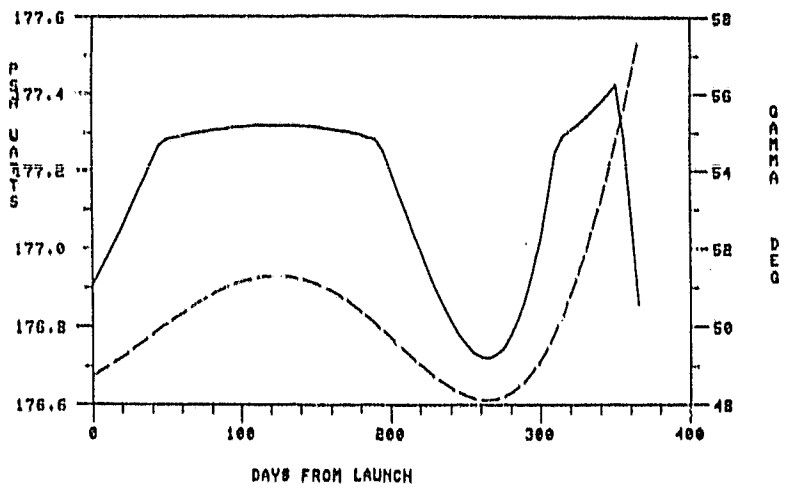

Figure 10-43. Run 067, Eclipse History and DOD Performance

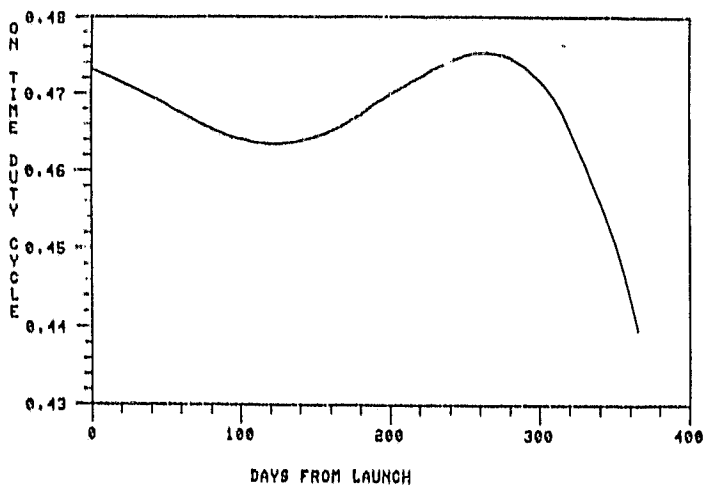

Figure 10-44. Run 067, Duty Cycle Performance

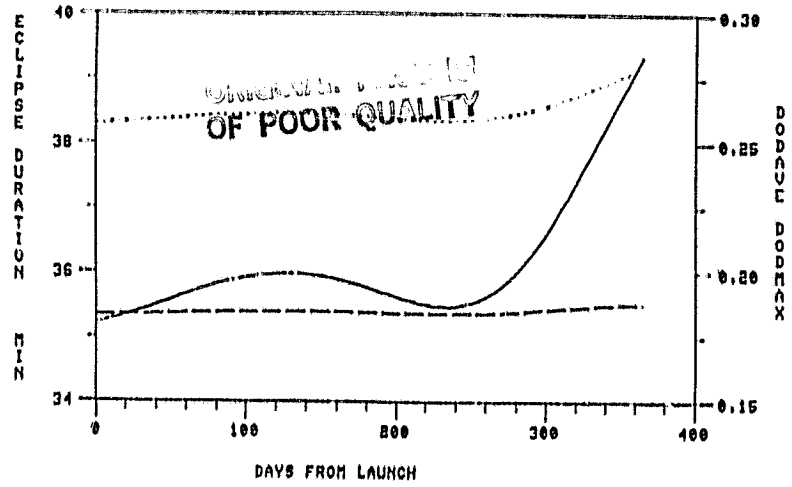

Figure 10-45. Run 070, Array Power and Sun Angle

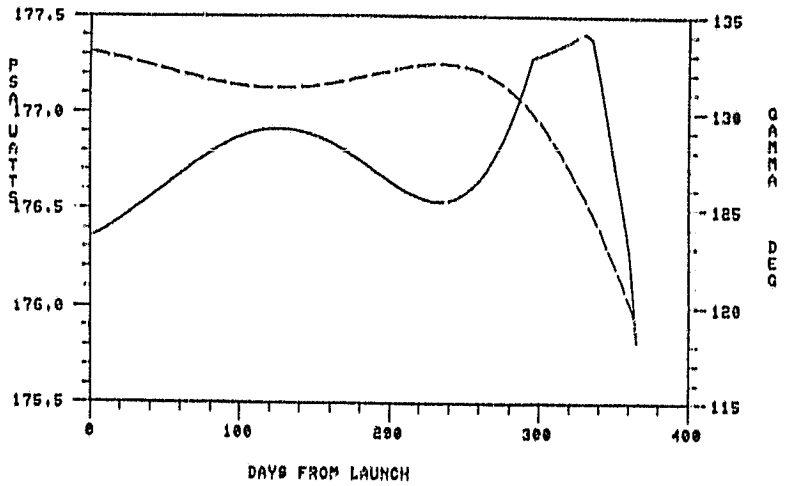

Figure 10-46. Run 070, Eclipse History and DOD Performance

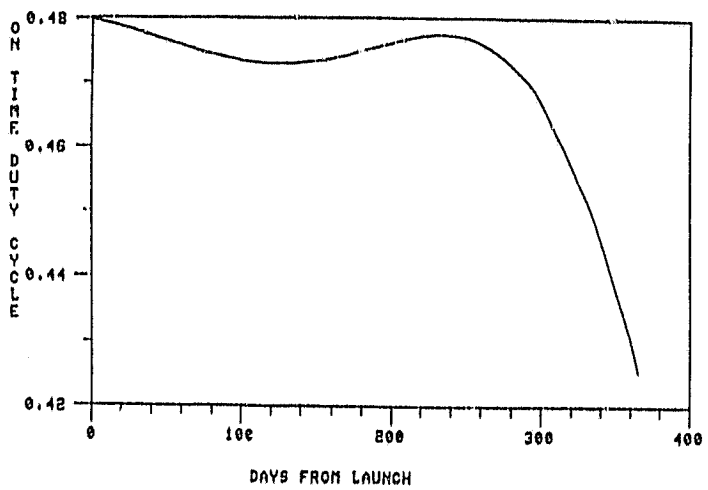

Figure 10-47. Run 070, Duty Cycle Performance

10.5 WORST CASE/NOMINAL CASE COMPARISONS

As stated previously, the analytic model used to predict power performance is extremely conservative to assure that the performance prediction of the available duty cycle is a worst case prediction. To demonstrate this and to establish an expected case to worst case comparison factor, samples of the on-time duty cycle performance actually achieved in the DE-B mission are compared to the worst case predictions. This comparison is shown in Figure 10-48. The continuous curve is the worst case prediction, while the "X" entries are the actual measured performance. It can be seen from this figure that the shape of the prediction curve is rather faithfully followed by the actual performance, but the actual performance was significantly better than the predicted worst case. The ratios of actual to worst case predictions are tabulated in Table 10-8, resulting in an average of the ratios encountered for the 11 samples of 1.61. This factor has been used in this study to predict the expected total science data-gathering time throughout the mission.

Table 10-9 presents a summary of the big bird analyses performed and summarizes the salient power system performance parameters achieved. These are the minimum, maximum, and average-over-mission-life science on-time duty cycle, the maximum depth of discharge encountered, and the total hours of science data gathering time during the one-year operational mission life. (Note that the duty cycle is tabulated as the fraction of the orbit during which science data can be gathered and, by the constraints of the program, cannot be gathered during data playback, thus limiting the on-time duty cycle to .899 for 8:1 playbacks and .800 for 4:1 playbacks.)

The results of these runs are presented in Figure 10-49, with the critical performance parameter being the "worst case" science data on time throughout the mission. As the analysis is very conservative (see Section 10.5), a second ordinate has been added to the figure, utilizing the Dynamics Explorer actual in-flight performance to develop a correlation factor from worst case to expected case. As can be seen using this ordinate, data gathering throughout all of the 88I launch cases for 8:1 playbacks can be achieved, and both 88I and 90II cases can be achieved for 4:1 playback conditions. Finally, without removing the power margin factors contained in all of the analyses conducted, it can be seen from this figure that significant missions can be performed for all conditions considered. Furthermore, it must be noted that the power design (solar array) was not optimized in terms of mission performance but merely used the available area resulting from scaling up the structure to accommodate the required hydrazine tanks.

For completeness, and to establish a scaling factor for the size change between the little bird MGO and a big bird MGO, a set of computer analyses was performed for the little bird 50° Sun angle solar array over the same set of parametric conditions as that for the big bird. These runs are tabulated in Table 10-10. As can be seen, for each case considered, the little bird design provided insufficient science collection to perform any meaningful mission and in some cases was unable to achieve energy balance for zero duty cycle (also implying zero operating time in the playback mode). One set of the graphics from these runs, corresponding to run 73, is shown in Figures 10-50 through 10-52. For comparative purposes, these performance plots should be compared to run 49 of the big bird plots presented earlier.

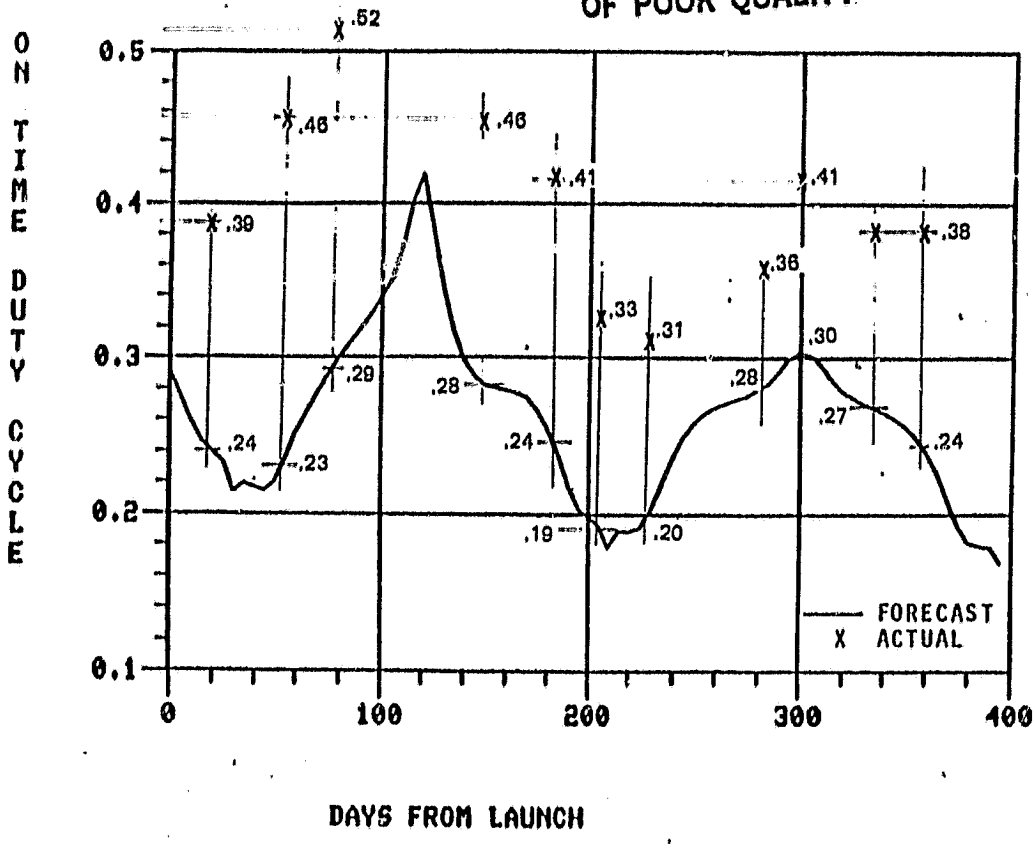

Figure 10-48. DE-B Duty Cycle Performance

TABLE 10-8. ACTUAL TO WORST CASE DUTY CYCLE COMPARISON

Days From Launch	Predicted Duty Cycle	Actual Duty Cycle	Ratio
20	.24	.39	1.625
50	.23	.46	2.0
75	.29	.52	1.793
150	.28	.46	1.643
180	.24	.41	1.708
205	.19	.33	1.737
230	.20	.31	1.55
280	.28	.36	1.286
300	.30	.41	1.367
330	.27	.38	1.407
360	.24	.38	1.583
Average Value of Ratio = 1.61			

TABLE 10-9. MGO BIG BIRD CASES CONSIDERED (γ=50° OPT. S/A)

Run	Launch Case	Injection Start	Comm Link	PB Ratio	Duty Cycle Min	Duty Cycle* Max	Duty Cycle Average	DOD Max	Total SCI Data Hours
25	88I	South	X-Band	8:1	.52	.57	.561	.256	4918.2
26	90II	South	↓	↓	.33	.58	.508	.224	4446.6
27	92II	South	↓	↓	.32	.58	.446	.275	3903.0
28	88I	North	↓	↓	.50	.58	.567	.261	4962.7
29	90II	North	↓	↓	.32	.58	.503	.274	4407.8
30	92II	North	↓	↓	.32	.59	.445	.274	3900.5
31	88I	South	S-Band	↓	.51	.56	.547	.262	4795.6
32	90II	South	↓	↓	.32	.56	.495	.278	4336.3
33	92II	South	↓	↓	.32	.57	.442	.278	3868.6
34	88I	North	↓	↓	.49	.57	.552	.266	4838.9
35	90II	North	↓	↓	.31	.57	.491	.278	4298.4
36	92II	North	↓	↓	.31	.58	.434	.278	3804.1
37	88I	South	X-Band	4:1	.43	.48	.468	.267	4097.0
38	90II	South	↓	↓	.28	.48	.423	.281	3704.1
39	92II	South	↓	↓	.27	.49	.377	.281	3303.1
40	88I	North	↓	↓	.42	.48	.472	.271	4133.1
41	90II	North	↓	↓	.27	.48	.419	.281	3671.1
42	92II	North	↓	↓	.27	.49	.371	.281	3247.8
43	88I	South	S-Band	↓	.42	.46	.449	.276	3929.7
44	90II	South	↓	↓	.27	.46	.406	.287	3553.4
45	92II	South	↓	↓	.26	.47	.362	.287	3169.3
46	88I	North	↓	↓	.40	.46	.453	.280	3964.2
47	90II	North	↓	↓	.26	.46	.402	.287	3521.8
48	92II	North	↓	↓	.26	.47	.356	.287	3116.4

TABLE 10-9. MGO BIG BIRD CASES CONSIDERED (γ=30° OPT. S/A) (Continued)

Run	Launch Case	Injection Start	Comm Link	PB Ratio	Duty Cycle Min	Duty Cycle* Max	Duty Cycle Average	DOD Max	Total SCI Data Hours
49	88I	South	X-Band	8:1	.55	.59	.584	.256	5118.2
50	90II				.38	.60	.538	.275	4709.6
51	92II				.38	.61	.489	.276	4286.0
52	88I	North			.53	.60	.588	.260	5153.5
53	90II				.37	.60	.533	.276	4672.9
54	92II				.37	.61	.483	.276	4227.0
55	88I	South	S-Band		.54	.58	.57	.262	4990.6
56	90II				.37	.58	.524	.279	4592.6
57	92II				.37	.59	.477	.279	4179.9
58	88I	North			.52	.59	.524	.266	5024.8
59	90II				.36	.59	.520	.280	4556.8
60	92II				.36	.59	.471	.280	4122.5
61	88I	South	X-Band	4:1	.46	.50	.487	.266	4266.1
62	90II				.32	.50	.448	.283	3926.0
63	92II				.31	.50	.408	.283	3572.2
64	88I	North			.44	.50	.490	.270	4294.4
65	90II				.31	.50	.445	.283	3894.7
66	92II				.31	.51	.402	.283	3522.9
67	80I	South	S-Band		.44	.48	.467	.275	4091.6
68	90II				.31	.48	.430	.289	3766.1
69	92II				.30	.48	.391	.289	3427.3
70	88I	North			.43	.48	.470	.279	4118.7
71	90II				.30	.48	.426	.289	3736.1
72	92II				.30	.49	.386	.289	3380.1

TABLE 10-9. MGO BIG BIRD CASES CONSIDERED (γ=50° OPT. S/A)

Run	Launch Case	Injection Start	Comm Link	PB Ratio	Duty Cycle Min	Duty Cycle* Max	Duty Cycle Average	DOD Max	Total SCI Data Bits
97	88I	South	X-Band	8:1	.51	.58	.567	.257	4964.0
98	90II	↓	↓	↓	.28	.59	.499	.273	4371.2
99	92II	↓	↓	↓	2.8	.60	.432	.273	3780.1
100	88I	North	↓	↓	.48	.59	.574	.261	5025.1
101	90II	↓	↓	↓	.27	.59	.494	.273	4327.9
102	92II	↓	↓	↓	.27	.61	.422	.273	3700.6
103	88I	South	S-Band	↓	.50	.57	.553	.262	4840.2
104	90II	↓	↓	↓	.28	.57	.487	.276	4262.7
105	92II	↓	↓	↓	.27	.59	.421	.276	3686.6
106	88I	North	↓	↓	.47	.58	.559	.266	4899.7
107	90II	↓	↓	↓	.26	.58	.482	.276	4220.4
108	92II	↓	↓	↓	.27	.59	.412	.276	3609.1
109	88I	South	X-Band	4:1	.43	.49	.472	.267	4135.7
110	90II	↓	↓	↓	.24	.49	.416	.279	3640.8
111	92II	↓	↓	↓	.23	.50	.359	.279	3146.7
112	81I	North	↓	↓	.40	.49	.478	.272	4195.9
113	90II	↓	↓	↓	.22	.49	.411	2.79	3604.1
114	92II	↓	↓	↓	.23	.51	.352	.279	3080.2
115	88I	South	S-Band	↓	.41	.47	.453	.276	3966.7
116	90II	↓	↓	↓	.23	.47	.399	.285	3492.7
117	92II	↓	↓	↓	.22	.48	.345	.285	3019.2
118	80I	North	↓	↓	.39	.47	.458	.280	4014.7
119	90II	↓	↓	↓	.22	.47	.395	.285	3457.5
120	92II	↓	↓	↓	.22	.49	.337	.285	2955.5

10.6 LGO POWER PERFORMANCE

For the LGO, a series of 32 power analyses were performed similar to the MGO studies. The power profiles utilized are shown in Table 10-11. In the case of LGO, the communications subsystem configuration was listed to S-band, but in two configurations, one using the high gain antenna (and associated antenna control) and a second using the high power amplifier and only the low gain antenna.

In sizing the solar array, rather than addressing the problem as rigorously as was done for MGO, two solar arrays were considered. The first, ignoring the physical requirements of the hydrazine storage, assumed that the spacecraft was the size of the Dynamics Explorer and used the STINT table of the DE-B spacecraft. Since this spacecraft was designed for the temperatures encountered in an Earth orbit, and since both DE-B and LGO are 1 rpo orbiters, it was assumed that this would make a viable candidate. Second, a big bird configuration was assumed consistent with the spacecraft shown in Section 4 for LGO. The array for this spacecraft was based on the MGO big bird design for an effective Sun angle of 50°. To obtain the equivalent power output, the STINT tables for the MGO design were scaled up by a factor of 1/0.4, the ratio of solar constants for the LGO to MGO missions. This results in an optimistic power prediction as the solar flux will dictate a hotter solar array in the LGO case. Analysis shows, however, that this design results in a significant "overkill," indicating that such a scaled array would be capable of supporting a significantly larger power drain than that analyzed. The cases considered are shown in Tables 10-12 and 10-13 for the LGO little bird and LGO big bird, respectively. For completeness, two sets of graphics output, corresponding to runs 1 and 17, have been included in Figures 10-53 through 10-58.

A variable addressed in the LGO analyses was the right ascension of the ascending node (RAAN). Since this was not specified, the analyses were run for the full range of RAAN in 45° increments from 0° through 315°. As can be seen from the tables, the DE-B spacecraft array design will support a relatively modest mission in the LGO orbit, whereas, as noted above, the LGO "big bird" design has a significant margin. Since the LGO design would require a physical size such as that of the big bird, under the assumptions of this study, the question of available power for the mission becomes non-critical. Furthermore, as was noted in the introduction of the power system studies, the claim that the MGO case is by far the dominant one in terms of driving the design is substantiated.

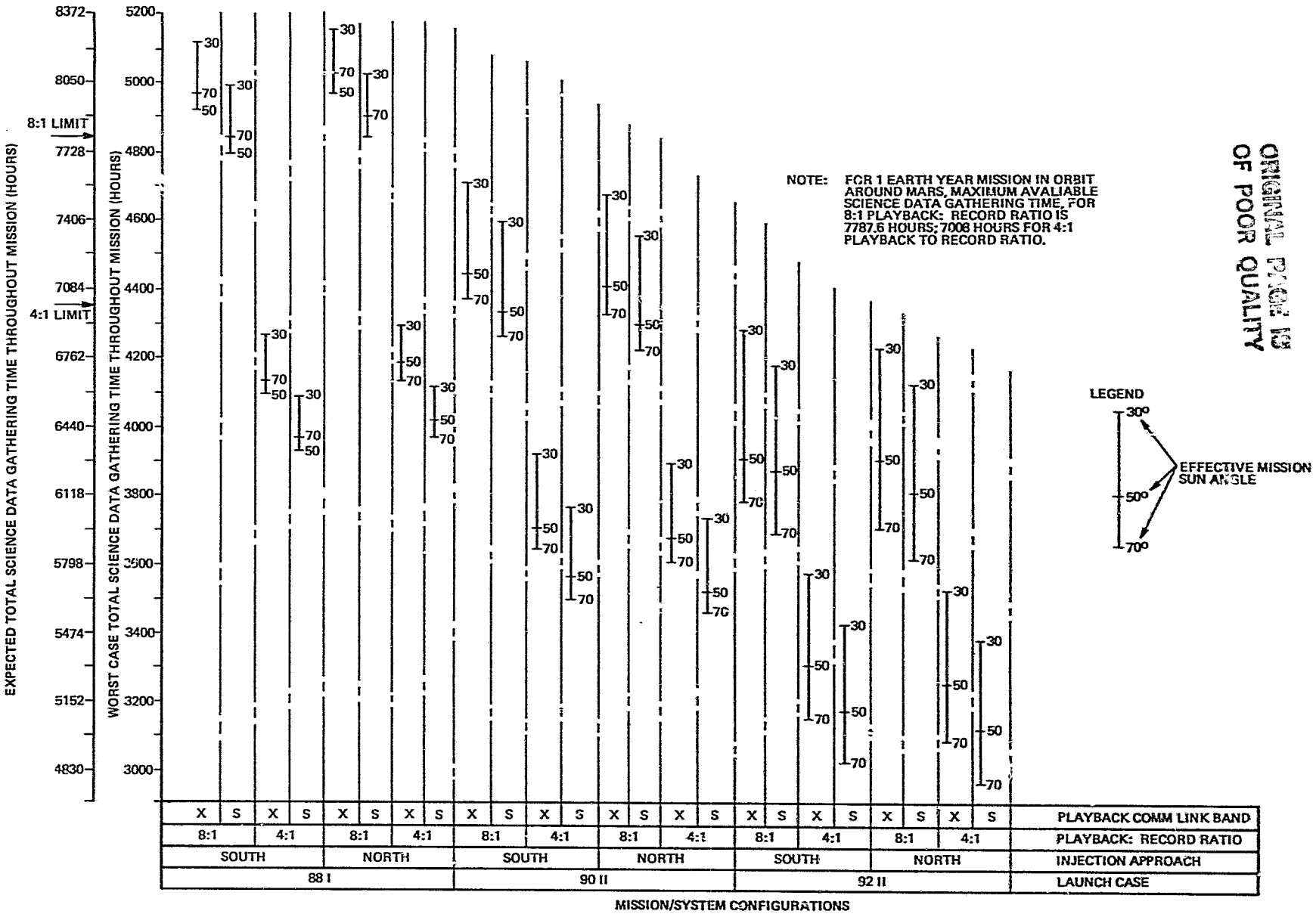

ORIGINAL PAGE IS
OF POOR QUALITY

Figure 10-49. MGO Power Performance as a Function of Launch Case, Injection Approach, System Configuration and Effective Sun Angle

TABLE 10-10. MGO LITTLE BIRD CASES CONSIDERED LITTLE BIRD γ50°

Run	Launch Case	Injection Start	Comm Link	PB Ratio	Duty Cycle Min	Duty Cycle* Max	Duty Cycle Average	DOD Max	Total SCI Data Hours
73	88I	South	X-Band	8:1	.02	.04	.036	.102	317.5
74	90II				-.06	.04	.012	.102	107.5
75	92II				-.07	.05	-.012	.103	-102.5
76	80I	North			.01	.05	.039	.103	338.6
77	90II				-.07	.05	.010	.103	91.6
78	92II				-0.7	.05	-.015	.104	-131.1
79	88I	South	S-Band		.02	.04	.036	.102	311.3
80	90II				-.06	.04	.012	.102	105.4
81	92II				-0.7	.05	-.011	.103	-100.6
82	88I	North			.01	.04	.038	.103	332.0
83	90II				-.07	.04	.010	.103	89.8
84	92II				-.07	.05	-.015	.104	-128.6
85	88I	South	X-Band	4:1	.01	.04	.031	.102	271.0
86	90II				-.05	.04	.010	.102	91.7
87	92II				-.06	.04	-.010	.103	-87.5
88	88I	North			.01	.04	.033	.102	289.0
89	90II				-.06	.04	.009	.102	78.2
90	92II				-.06	.04	-.013	.103	-111.9
91	88I	South	S-Band		.01	.03	.030	.102	262.1
92	90II				-.05	.04	.010	.102	88.7
93	92II				-.06	.04	-.010	.103	-84.7
94	88I	North			.01	.04	.032	.102	279.5
95	90II				-.06	.04	.009	.102	75.5
96	92II				-.06	.04	-.012	.103	-108.3

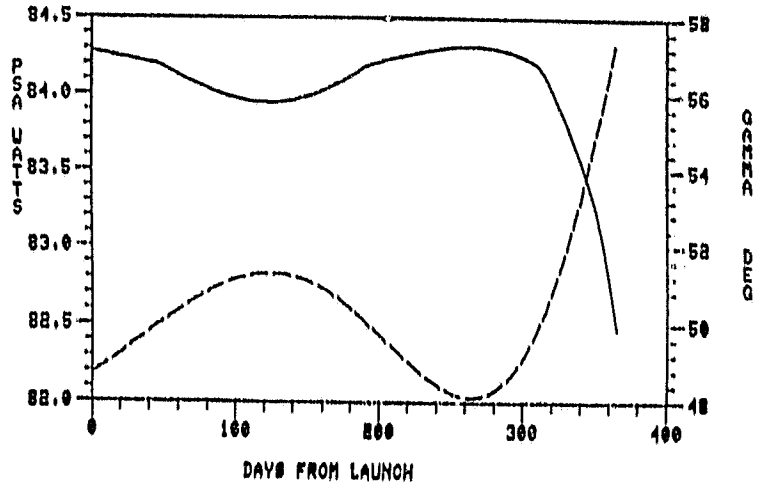

Figure 10-50. Run 073, Array Power and Sun Angle

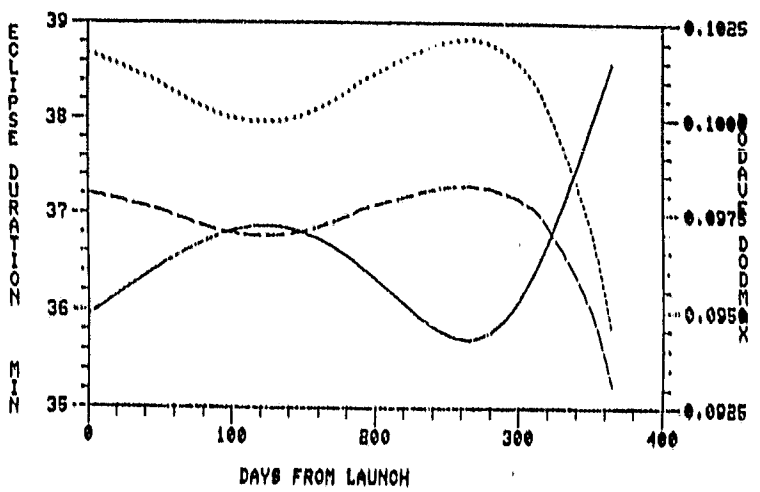

Figure 10-51. Run 073, Eclipse History and DOD Performance

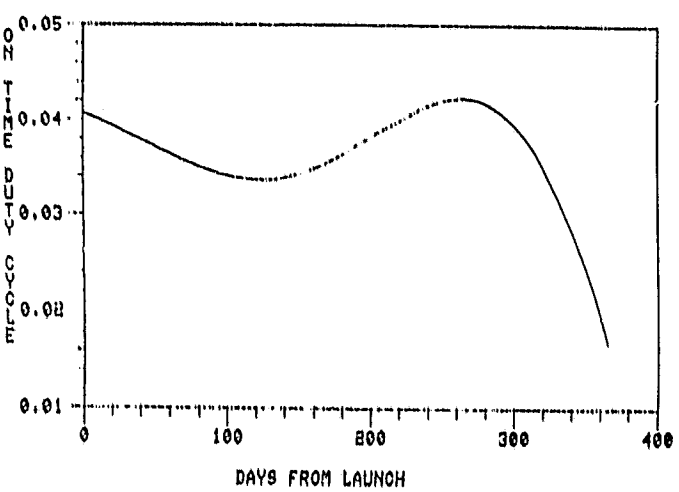

Figure 10-52. Run 073, Duty Cycle Performance

TABLE 10-11. LGO POWER PROFILE

Subsystem / Bus	Continuous Load			Load Above Continuous					
	Watts			Science Watts			Playback Watts		
	Unreg.	-24.5V	+28V	Unreg.	-24.5V	+28V	Unreg.	-24.5V	+28V
Instruments	0				57.0				
Communications:							44.7 (120.7)**		
S-Band (S-Band without high gain antenna)	14.2							18.0	
Attitude Control	3.5		6.5						
C&DH	1.8		8.0		9.0				
Power	4.5								
Thermal Margin (50% dc)	2.0								
S/C Total	26.0		14.5		66.0		44.7 (120.7)	18.0	
Unregulated Bus Total Load	45.0			73.0			64.7 (140.7)**		

*Assuming efficiency factors: .9 for -24.5V Regulator
.85 for +28V Regulator

**Bracketed numbers are for S-Band Downlink without high gain antenna.

TABLE 10-11. LGO POWER PROFILE (Continued)

Subsystem / Bus	Continuous Load Watts			Load Above Continuous					
				Science Watts			Playback Watts		
	Unreg.	-24.5V	+28V	Unreg.	-24.5V	+28V	Unreg.	-24.5V	+28V
Instruments	0				57.0				
Magnetometer									
Electronics					4.0				
Sensor									
X-Ray Spectrometer									
Electronics					10.0				
Sensor									
Multi-Spectral Mapper									
Electronics					12.0				
Sensor									
Radar Altimeter									
Electronics					18.0				
Sensor									
X-Ray Spectrometer									
Electronics					10.0				
Sensor									
Electron Reflector									
Electronics					5.0				
Sensor									
Margin					12.0				
Instrument Total					71.0				

TABLE 10-11. LGO POWER PROFILE (Continued)

Subsystem / Bus	Continuous Load			Load Above Continuous					
	Watts			Science Watts			Playback Watts		
	Unreg.	-24.5V	+28V	Unreg.	-24.5V	+28V	Unreg.	-24.5V	+28V
Communications									
Transponder*									
S-Band Receivers (2 powered continuously)	14.2								
S-Band Transmitters							20.2 (79.9*)		
High Gain Antenna Control (if antenna is used)							9.5		
Premodulation Processor							2.5		
Communications Margin							12.5 (38.5*)		
Communications Total and 20 watts rf power	14.2						44.7 (120.7)*		

*Numbers in brackets represent S-Band downlink without high gain antenna and include power amp and 20 watts rf power.

TABLE 10-11. LGO POWER PROFILE (Continued)

Subsystem Component / Bus	Continuous Load			Load Above Continuous					
	Watts			Science Watts			Playback Watts		
	Unreg.	-24.5V	+28V	Unreg.	-24.5V	+28V	Unreg.	-24.5V	+28V
ADACS									
Sun Sensor Electronics		1.5							
Pitch Control Electronics (PCE)	1.0	5.0							
Momentum Wheel Assembly (MWA)	2.5								
ADACS Total	3.5	6.5							
C&DH									
Command and Telemetry Processor (CTP)		5.0							
Remote Telemetry Module (RTM)		2.5							
Command Distribution Unit (CDU)	1.8	.5							
Tape Recorder					9.0			18.0	
C&DH Total	1.8	8.0			9.0			18.0	
POWER									
PSE Shut Loss	3.0								
Bypass Resistor Leakage	.5								
Current Sensor Loss	.5								
+28V Regulator Fixed Loss	.5								
Power Total	4.5								

TABLE 10-12. LGO DE-B STINT

Run	S-band	LG Antenna	PB 8:1	RAAN	Duty Cycle Min.	Duty Cycle Max	Duty Cycle Avg.	DOD Max.	Total Worst Case Data Hours
1		Yes		0	.03	.12	.076	.162	669.1
2				45	.03	.19	.089	.162	779.6
3				90	.02	.29	.117	.162	1021.5
4				135	.03	.29	.116	.162	1013.3
5				180	.03	.30	.103	.162	899.3
6				225	.02	.30	.115	.162	1010.3
7				270	.03	.30	.117	.162	1026.3
8				315	.03	.19	.089	.162	783.2
9		No		0	.02	.11	.070	.162	609.3
10				45	.02	.18	.081	.162	711.8
11				90	.02	.27	.107	.162	936.1
12				135	.02	.27	.106	.162	928.0
13				180	.02	.28	.094	.162	822.2
14				225	.02	.27	.106	.162	925.0
15				270	.02	.27	.107	.162	939.9
16				315	.02	.18	.082	.162	715.6

TABLE 10-13. LGO MOD MGO 50° STINT

Run	S-Band	LG Antenna	PB 8:1	RAAN	Duty Cycle Min.	Duty Cycle Max.	Duty Cycle Ave.	DOD Max.	Total Worst Case Data Hours
17		Yes		0	.889	.889	.889	.354	7786.6
18				45					
19				90					
20				135					
21				180					
22				225					
23				270					
24				315					
25		No		0					
26				45					
27				90					
28				135					
29				180					
30				225					
31				270					
32				315					

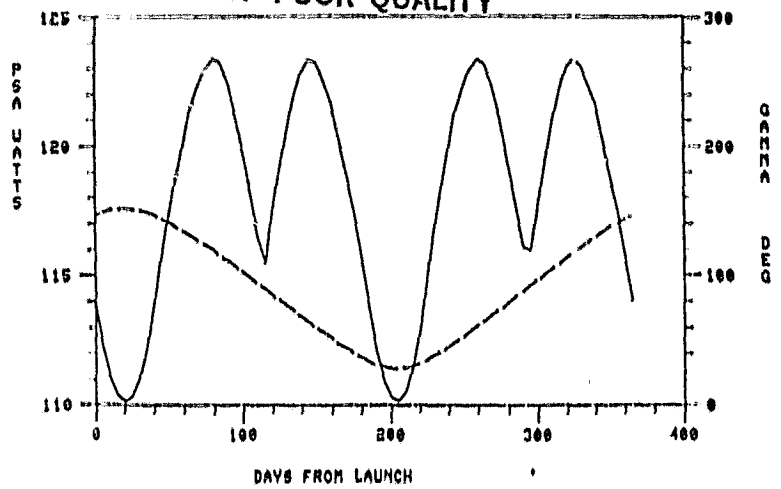

Figure 10-53. Run 001, Array Power and Sun Angle

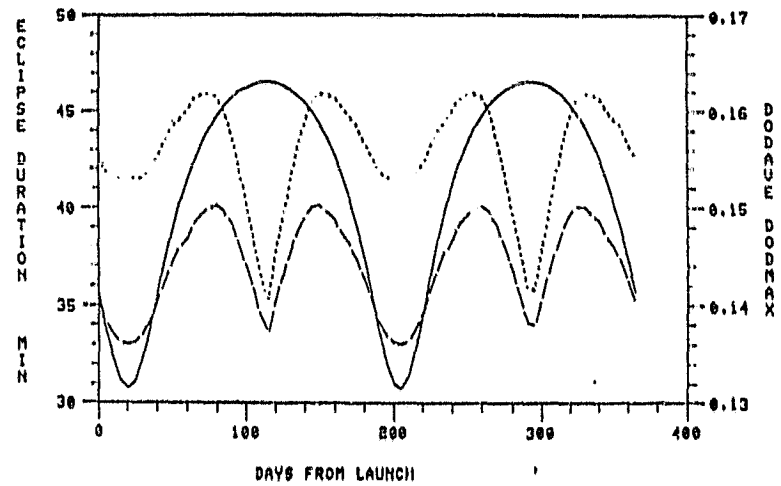

Figure 10-54. Run 001, Eclipse History and DOD Performance

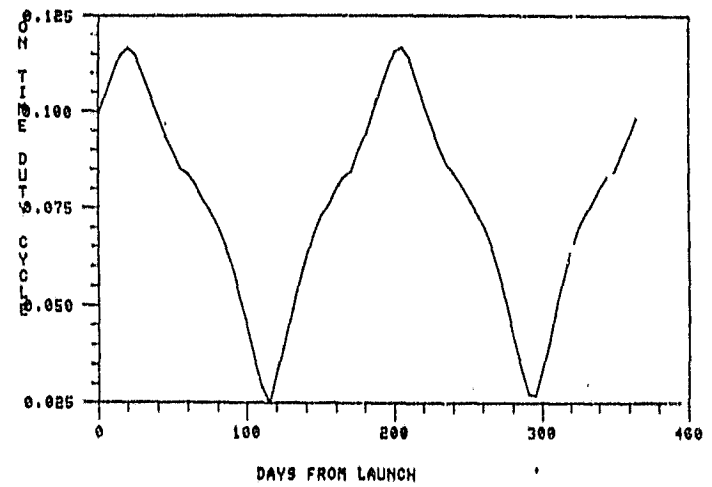

Figure 10-55. Run 001, Duty Cycle Performance

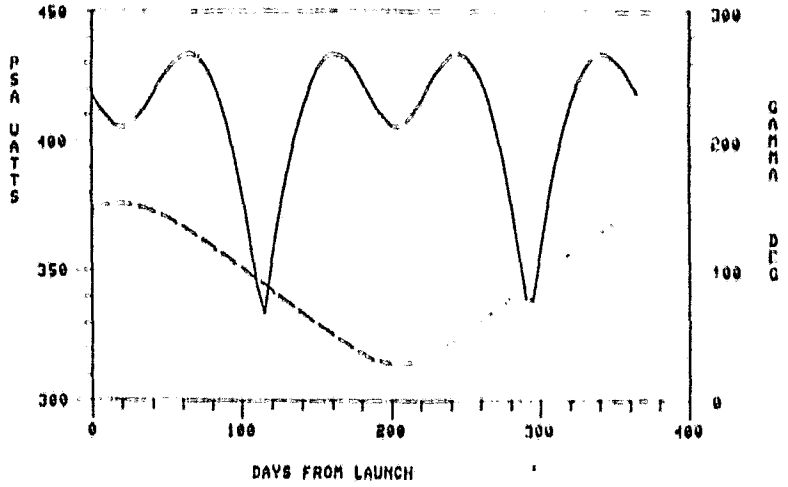

Figure 10-56. Run 017, Array Power and Sun Angle

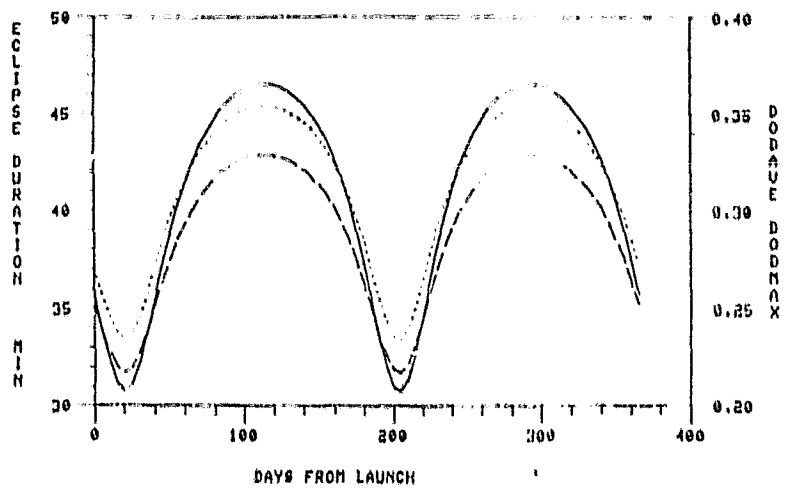

Figure 10-57. Run 017, Eclipse History and DOD Performance

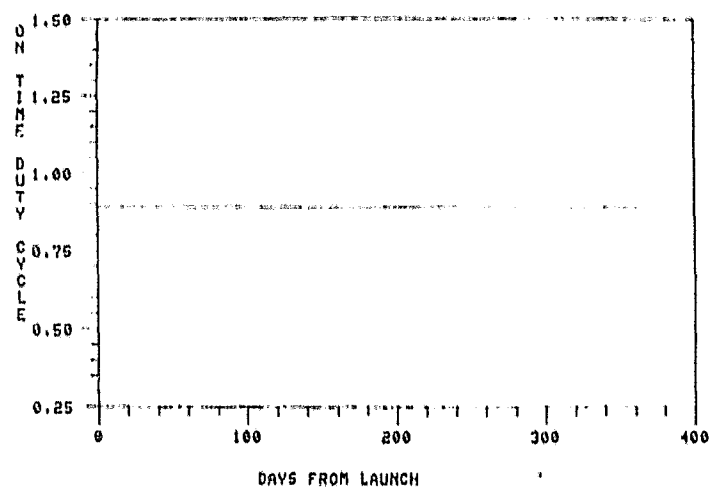

Figure 10-58. Run 017, Duty Cycle Performance

APPENDIX A
MGO MASS PROPERTIES AND INERTIA CHARACTERISTICS LISTING

MGO – STOWED 30C WEIGHT INPUT DATA – AUGUST 18, 1982

ID	NAME	DATE	ZONE	EST/ACT WEIGHT	QTY	TARGET WEIGHT	DRWG. NO	SOURCE
1000000	MGO (STOWED)	0	0	0.0	1	0.0		
1010000	UPPER STRUCT/EQUIP	0	0	0.0	1	0.0		
1010100	UPPER EQUIP	0	0	229.340	1	0.0		
1010200	UPPER HAT	0	0	37.710	1	0.0		
1010300	UPPER BASEPLATE	0	0	0.0	1	0.0		
1010301	BASEPLATE STRUCT	0	0	53.340	1	0.0		
1010302	BALANCE AND MARGIN	0	0	111.300	1	0.0		
1020000	LOWER STRUCT/EQUIP	0	0	0.0	1	0.0		
1020100	LOWER EQUIP	0	0	254.110	1	0.0		
1020200	LOWER HAT	0	0	37.710	1	0.0		
1020300	LOWER BASEPLATE	0	0	0.0	1	0.0		
1020301	BASEPLATE STRUCT	0	0	52.780	1	0.0		
1020302	MARGIN AND BALANCE	0	0	111.300	1	0.0		
1030000	CENTER COL/SHR PNLS	0	0	73.190	1	0.0		
1040000	ALTIMETER ASS'Y	0	0	0.0	1	0.0		
1040100	ALTIMETER ANT	0	0	4.410	1	0.0		
1040200	ALTIMETER ELECT	0	0	17.640	1	0.0		
1050000	M/S MAPPER	0	0	37.480	1	0.0		
1060000	CS ASS'Y	0	0	0.0	1	0.0		
1060100	CS 1	0	0	6.500	1	0.0		
1060200	CS 2	0	0	6.500	1	0.0		
1070000	MWA ASS'Y	0	0	0.0	1	0.0		
1070100	MWA	0	0	39.640	1	0.0		
1070200	MWA SUPPORT	0	0	6.540	1	0.0		
1080000	HI GAIN ANT ASS'Y	0	0	0.0	1	0.0		
1080100	HI GAIN ANTENNA	0	0	15.000	1	0.0		
1080200	ANT BOOM/INDEX	0	0	11.000	1	0.0		
1090000	GRS ASS'Y	0	0	0.0	1	0.0		
1090100	GRS	0	0	26.500	1	0.0		
1090200	GRS DPPL PTG	0	0	4.410	1	0.0		
1090300	GRS ASTROMAST	0	0	0.0	1	0.0		
1090301	ASTROMAST CAN	0	0	18.000	1	0.0		
1090302	ASTROMAST BOOM	0	0	6.100	1	0.0		
1100000	MAG ASS'Y	0	0	0.0	1	0.0		
1100100	MAGNETOMETER	0	0	6.610	1	0.0		
1100250	MAG ASTROMAST	0	0	0.0	1	0.0		
1100251	ASTROMAST CAN	0	0	18.000	1	0.0		
1100252	ASTROMAST BOOM	0	0	6.100	1	0.0		
1110000	LOW/MED GAIN ANT	0	0	10.000	1	0.0		
1120000	PROPELLANT TANKS	0	0	17.250	5	0.0		
1130000	PROPULSION	0	0	0.0	1	0.0		
1130100	ENGINES	0	0	35.270	1	0.0		
1130200	PLUMBING/VALVES	0	0	15.430	1	0.0		
1130300	TANK & ENG HEATERS	0	0	11.920	1	0.0		
1140000	PROPELLANT	0	0	157.000	6	0.0		
1150000	AKM EXPEND & MOTOR	0	0	1326.000	1	0.0		
1160000	SEP ADAPTER	0	0	132.000	1	0.0		

APPENDIX A
MGO MASS PROPERTIES AND
INERTIA CHARACTERISTICS LISTING

MGO – STOWED 30C WEIGHT REPORT – AUGUST 18, 1982

ID	NAME	TARGET WEIGHT	CURRENT ESTIMATED ACT WT WEIGHT	QTY	DRWNG NO	SOURCE	ZONE
1000000	MGO (STOWED)	0.0	3857.920	1			0
1100000	.UPPER STRUCT/EQUIP	0.0	431.030	1			0
1101100	..UPPER EQUIP	0.0	229.040	1			0
1101200	..UPPER MAT	0.0	37.710	1			0
1101300	..UPPER BASEPLATE	0.0	164.340	1			0
1101301	BASEPLATE STRUCT	0.0	53.240	1			0
1101302	BALANCE AND MARGIN	0.0	111.300	1			0
1200000	.LOWER STRUCT/EQUIP	0.0	425.900	1			0
1201100	..LOWER EQUIP	0.0	294.110	1			0
1201200	..LOWER MAT	0.0	37.710	1			0
1201300	..LOWER BASEPLATE	0.0	164.080	1			0
1201301	BASEPLATE STRUCT	0.0	52.780	1			0
1201302	MARGIN AND BALANCE	0	111.300	1			0
1300000	.CENTER COL/SHR PNLS	0.0	73.190	1			0
1400000	.ALTIMETER ASS'Y	0.0	22.050	1			0
1401100	..ALTIMETER ANT	0.0	4.410	1			0
1401200	..ALTIMETER ELECT	0.0	17.640	1			0
1500000	.MMS MAPPER	0.0	37.480	1			0
1600000	.CS ASS'Y	0.0	13.000	1			0
1601100	..CS 1	0.0	6.500	1			0
1601200	..CS 2	0.0	6.500	1			0
1700000	.MWA ASS'Y	0.0	48.280	1			0
1701100	..MWA	0.0	39.640	1			0
1701200	..MWA SUPPORT	0.0	8.640	1			0
1800000	.HI GAIN ANT ASS'Y	0.0	26.000	1			0
1801100	..HI GAIN ANTENNA	0.0	15.000	1			0
1801200	..ANT BOOM/INDEX	0.0	11.000	1			0
1900000	.GRS ASS'Y	0.0	55.710	1			0
1901100	..GRS	0.0	26.500	1			0
1901200	..GRS DEPL FTG	0.0	4.410	1			0
1901300	..GRS ASTROMAST	0.0	24.100	1			0
1901301	ASTROMAST CAN	0.0	18.000	1			0
1901302	ASTROMAST BOOM	0.0	6.100	1			0
1100000	.MAG ASS'Y	0.0	30.710	1			0
1101100	..MAGNETOMETER	0.0	6.610	1			0
1101200	..MAG ASTROMAST	0.0	24.100	1			0

1103231	ASTROMAST CAN	0.0	18.000	1	3
1103262	ASTROMAST BOOM	0.0	6.100	1	3
1110000	.LOW/MED GAIN ANT	0.0	10.000	1	3
1120000	.PROPELLANT TANKS	0.0	133.500	6	0
1130000	.PROPULSION	0.0	51.720	1	3
1131100	..ENGINES	0.0	35.270	1	3
1132300	..PLUMBING/VALVES	0.0	15.430	1	3
1133000	..TANK & ENG HEATERS	0.0	11.020	1	0
1140000	.PROPELLANT	0.0	1002.000	6	3
1150000	.ASM EXPEND & MOTOR	0.0	1326.000	1	3
1160000	.SEP ADAPTER	0.0	132.000	1	3

MGO - STOWED 30C WEIGHT AND INERTIA SUMMARY INPUT MOMENT OF INERTIA AND CG INFORMATION AUGUST 18, 1982

ID.NO	NAME	T°	ROT	X Y Z LOCAL BOX COORDINATE AXES LX/IXX	LY/IYY	LZ/IZZ	RAD.O/IXY	RAD.I/IXZ	IYZ	X Y Z S/C COORDINATES XBAR	YBAR	ZBAR	WEIGHT
1010100	UPPER EQUIP	9	0	0.0	0.0	19.00	36.00	10.00	0.0	0.0	0.0	54.900	229.54
1010200	UPPER HAT	12	0	0.0	0.0	19.00	36.00	0.0	0.0	0.0	0.0	51.500	37.71
1010300	UPPER BASEPLATE	9	0	0.0	0.0	1.00	36.00	10.00	0.0	0.0	0.0	44.700	154.34
1020100	LOWER EQUIP	9	0	0.0	0.0	19.00	36.00	10.00	0.0	0.0	0.0	12.600	284.11
1020200	LOWER HAT	12	0	0.0	0.0	19.00	36.00	0.0	0.0	0.0	0.0	15.000	37.71
1020300	LOWER BASEPLATE	9	0	0.0	0.0	1.00	36.00	10.00	0.0	0.0	0.0	21.910	154.33
1030000	CENTER COL/SHR PNLS	12	0	0.0	0.0	61.40	9.00	0.0	0.0	0.0	0.0	32.500	73.19
1040100	ALTIMETER ANT	15	0	0.0	0.0	0.0	20.00	0.0	0.0	-7.300	41.000	3.900	4.41
1040200	ALTIMETER ELECT	1	0	32.00	16.00	9.00	0.0	0.0	0.0	-0.500	22.800	17.000	17.54
1050000	M/S WAPPER	1	0	15.40	32.70	14.60	0.0	0.0	0.0	24.500	12.000	14.000	37.48
1060100	CS 1	1	0	9.00	9.00	9.00	0.0	0.0	0.0	9.000	-15.600	9.000	5.50
1060200	CS 2	1	0	9.00	9.00	9.00	0.0	0.0	0.0	-16.900	6.200	9.000	5.50
1070100	MWA	13	0	0.0	0.0	0.0	0.0	0.0	0.0	0.0	0.0	58.300	39.54
1070200	MWA SUPPORT	4	0	0.0	0.0	5.00	4.00	0.0	0.0	0.0	0.0	53.300	8.54
1080100	HI GAIN ANTENNA	15	1	0.0	0.0	0.0	30.00	0.0	0.0	-33.100	-33.500	12.200	15.30
1080200	ANT 300°/INDEX	2	1	42.00	0.0	0.0	2.00	0.0	0.0	-28.000	-33.300	52.500	11.00
1090100	GRS	1	0	11.40	19.70	12.60	0.0	0.0	0.0	-41.300	2.000	43.500	25.50
1090200	GRS DEPL FTG	1	0	6.00	28.00	5.00	0.0	0.0	0.0	-36.000	15.500	51.500	4.41
1100301	ASTROMAST CAN	10	1	7.00	0.0	0.0	5.25	0.0	0.0	-27.600	15.100	50.000	18.00
1100302	ASTROMAST BOOM	2	1	7.00	0.0	0.0	5.25	0.0	0.0	-27.500	15.100	50.000	5.10
1100100	MAGNETOMETER	1	1	2.00	2.00	3.20	0.0	0.0	0.0	32.200	-18.600	50.000	5.51
1100201	ASTROMAST CAN	10	1	7.00	0.0	0.0	5.25	0.0	0.0	27.800	-15.100	50.000	18.00
1100202	ASTROMAST BOOM	2	1	7.00	0.0	0.0	5.25	0.0	0.0	27.700	-15.100	50.000	5.10
1110000	LOW/MED GAIN ANT	9	0	0.0	0.0	4.00	36.00	35.00	0.0	0.0	0.0	33.300	10.00
1120000	PROPELLANT TANKS	5	0	0.0	0.0	0.0	11.05	0.0	0.0	0.0	-23.000	33.300	17.25
1120000	PROPELLANT TANKS	5	0	0.0	0.0	0.0	11.05	0.0	0.0	19.900	-11.500	33.300	17.25
1120000	PROPELLANT TANKS	5	0	0.0	0.0	0.0	11.05	0.0	0.0	19.900	11.500	33.300	17.25
1120000	PROPELLANT TANKS	5	0	0.0	0.0	0.0	11.05	0.0	0.0	0.0	23.000	33.300	17.25
1120000	PROPELLANT TANKS	5	0	0.0	0.0	0.0	11.05	0.0	0.0	-19.900	11.500	33.300	17.25
1120000	PROPELLANT TANKS	5	0	0.0	0.0	0.0	11.05	0.0	0.0	-19.900	-11.500	33.300	17.25
1130000	PROPULSION	4	0	0.0	0.0	3.00	36.00	0.0	0.0	0.0	0.0	33.300	61.72
1140000	PROPELLANT	5	0	0.0	0.0	0.0	10.55	0.0	0.0	0.0	24.000	33.300	167.00
1140000	PROPELLANT	5	0	0.0	0.0	0.0	10.55	0.0	0.0	0.0	-24.000	33.300	167.00
1140000	PROPELLANT	5	0	0.0	0.0	0.0	10.55	0.0	0.0	20.400	12.400	33.300	167.00
1140000	PROPELLANT	5	0	0.0	0.0	0.0	10.55	0.0	0.0	20.400	-12.400	33.300	167.00
1140000	PROPELLANT	5	0	0.0	0.0	0.0	10.55	0.0	0.0	-20.400	12.400	33.300	167.00
1140000	PROPELLANT	5	0	0.0	0.0	0.0	10.55	0.0	0.0	-20.400	-12.400	33.300	167.00
1150000	AKM EXPEND & MOTOR	13	0	138786.00	138786.00	143849.00	0.0	0.0	0.0	0.0	0.0	-25.350	1325.00
1160000	SEP ADAPTER	12	0	0.0	0.0	30.00	13.75	0.0	0.0	0.0	0.0	-15.900	132.00

MGO – STOWED 30C OVERALL WEIGHT AND INERTIA SUMMARY S/C MOMENTS OF INERTIA – AUGUST 18, 1982

THE WEIGHT AND INERTIA SUM TOTALS ARE:

SUM OF WEIGHTS	=	0.38573287E+04
SUM OF WEIGHTS * X DISTANCE	=	-0.10189727E+04
SUM OF WEIGHTS * Y DISTANCE	=	0.11270264E+02
SUM OF WEIGHTS * Z DISTANCE	=	0.42630582E+05
SUM OF WEIGHTS * X * Y DISTANCE	=	0.75906580E+04
SUM OF WEIGHTS * X * Z DISTANCE	=	-0.55248525E+05
SUM OF WEIGHTS * Y * Z DISTANCE	=	-0.13503687E+05
SUM OF WEIGHTS * X2	=	0.45051719E+06
SUM OF WEIGHTS * Y2	=	0.39783051E+06
SUM OF WEIGHTS * Z2	=	0.39620030E+07
SUM OF IXX (LB-IN2)	=	0.70260337E+06
SUM OF IYY (LB-IN2)	=	0.70140269E+06
SUM OF IZZ (LB-IN2)	=	0.98194867E+06
SUM OF IXY (LB-IN2)	=	-0.22866577E+04
SUM OF IXZ (LB-IN2)	=	0.0
SUM OF IYZ (LB-IN2)	=	0.0

THE C.G. COMPONENTS ARE -- X= -0.264124E+00 Y= 0.292132E-02 Z= 0.110501E+02

MGO - STOWED 30C OVERALL INERTIA SUMMARY S/C MOMENTS OF INERTIA - AUGUST 18, 1982

S/C MOMENT OF INERTIA SUM TOTALS ARE:

* THE FOLLOWING VALUES HAVE UNITS OF LB-IN2

IXX = 0.4591363?E+07
IYY = 0.4542574?E+07
IZZ = 0.1333026?E+07
IXY = 0.5329?5?4E+04
IXZ =-0.4?39?6?5?E+05
IYZ =-0.1353422?E+05
IMAX = 0.4543121?E+07
IMIN = 0.4?2?61?5E+07

* THE FOLLOWING VALUES HAVE UNITS OF IN-LBS-SEC2

IXX = 0.11?434?8E+05
IYY = 0.1232615?E+05
IZZ = 0.47?15?7?E+04
IXY = 0.1374723?E+02
IXZ =-0.1139437?E+03
IYZ =-0.3531814?E+02
IMAX = 0.1232755?E+05
IMIN = 0.1139207?E+05

INERTIA RATIO

I SPIN / I TRANSVERSE MAX = 0.394

APPENDIX B
ACTIVE NUTATION DAMPING DURING MGO CRUISE PHASE

APPENDIX B
ACTIVE NUTATION DAMPING DURING MGO CRUISE PHASE

The need for active nutation damping arises whenever a simple minor-axis spinner must maintain stability over a period of time longer than the destabilizing time constant. This is definitely the case with the MGO cruise phase, because the mass distribution in that configuration represents a long spinning vehicle with a significant liquid mass fraction due to the need for maneuvers about Mars. This vehicle is "prolate", i.e., a minor-axis spinner. Thus, the inherent instability of a prolate spinner plus the need for stability in cruise situations lead to the requirement for active nutation control (ANC). The fundamental driving aspect of such a control function is the energy dissipation rate within the liquid propellant tanks.

The function of an active nutation damper is to control the magnitude of nutation angle with specified response characteristics. In a prolate spinner, the rate of nutation angle increase is directly related to the dissipation rate. In fact, this rate can generally be characterized via an exponential decay (illustrated in Figure B-1) of rotational kinetic energy from a maximum to a minimum. The dissipation time constant, τ, is a key parameter in the design of the ANC, as it is an indication of propellant and thrust requirements for the attitude control system.

A more realistic dissipation profile would account for the physical nature of propellant slosh at low and high coning angles. Such considerations would lead to a bell-shaped curve, as illustrated with the exponential form of Figure B-1. It is clear that the exponential assumption leads to conservative estimates of propellant requirements for nutation control.

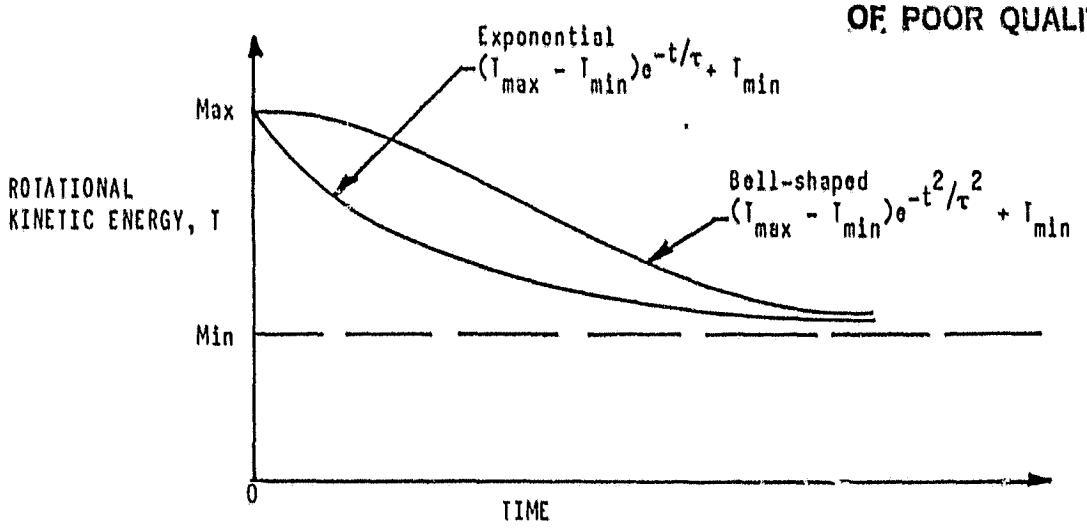

Figure B-1. General Model of Energy Dissipation

Figure B-2 illustrates an exponential coning angle profile consistent with the one for kinetic energy. However, the associated time constant, τ_θ, is different than τ. Expressions for τ and τ_θ are developed along with a conservative estimate of propellant usage for nutation control. Again, an account of the physical nature of slosh would yield a bell-shaped curve for θ, as illustrated in Figure B-2.

Assuming the exponential model, the dissipation rate is simply the time derivative of

$$(T_{max} - T_{min})e^{-t/\tau} + T_{min}$$

or

$$\dot{T} = (T_{max} - T_{min})(-\frac{1}{\tau})e^{-t/\tau}$$

Since the nutation angle, θ, must be kept small, only the initial value of $\dot{T}$ need be considered. This is also the maximum value of $\dot{T}$. Thus, at $t = 0$,

$$\dot{T}_{(t = 0)} = -(\frac{T_{max} - T_{min}}{\tau})$$

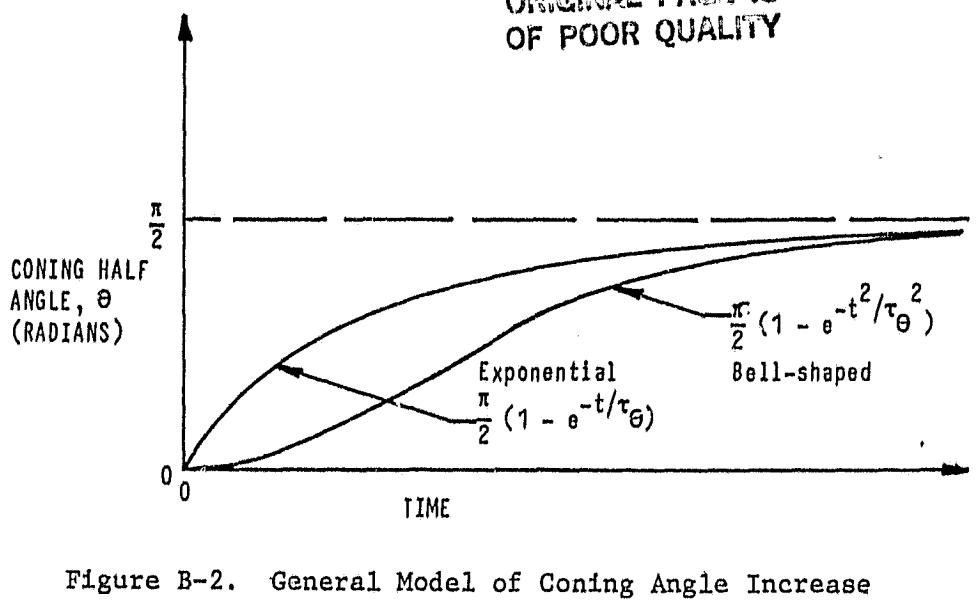

Figure B-2. General Model of Coning Angle Increase

Since angular momentum, h, is conserved and

$$T_{min} = \tfrac{1}{2} I_{max}\omega_f^2 = \frac{h^2}{2 I_{max}}$$

and

$$T_{max} = \tfrac{1}{2} I_{min}\omega_o^2 = \frac{h^2}{2 I_{min}}$$

where ω_f is the final flat-spin rate and ω_o is the initial spin rate then

$$\dot{T}_{(t = 0)} = \tfrac{1}{2} \frac{h^2}{\tau}\left(\frac{1}{I_{min}} - \frac{1}{I_{max}}\right) .$$

Kinetic relations (Reference 1) lead to

$$\dot{T} = \frac{h^2}{I_{min}} \left(\frac{I_{min}}{I_{max}} - 1\right) \theta\dot{\theta}$$

Equating these two forms for dissipation gives a relation between τ and θ for small values of θ,

$$\theta\dot{\theta} = \frac{1}{2\tau}$$

which integrates to

$$\theta^2 = \frac{\Delta t}{\tau}$$

Thus, the time to reach a value of θ from $\theta = 0$ is

$$\Delta t = \theta^2 \tau$$

To correct θ to zero, a torque impulse equal to $h\theta$ must be applied. Thus, the total impulse required to maintain $\theta \approx 0$ over a period of time can be estimated as follows. Assuming a precession thruster, F, at a moment arm, d, the thrust impulse is Ft_f, where t_f is the thrust time. The torque impulse is $Ft_f d$. However, the moment arm d is not constant in the typical case, leading to an impulse form, I_t, of

$$2\int_0^{\Delta\Phi/2} FR\cos\Phi \frac{d\Phi}{\omega} = -\frac{2FR}{\omega}\sin\left(\frac{\Delta\Phi}{2}\right) \text{ per revolution,}$$

where $d = R\cos\Phi$

Φ = precession thruster azimuthal position

ω = MGO spin rate

R = radial position of thruster from spin axis

$\Delta\Phi$ = precession thrust arc, i.e., thrust time per cycle is $\frac{\Delta\Phi}{\omega}$

Since $h = I_{spin}\omega$, the value of I_t needed is

$$I_t = I_{spin}\omega\theta$$

To roughly estimate the propellant required for ANC, assume a corrective precession thrust per revolution, leading to a time, Δt, of $2\pi/\omega$ and a value of θ equal to $\sqrt{2\pi/\omega\tau}$. The needed torque impulse per cycle is $I_{spin}\omega\sqrt{\frac{2\pi}{\omega\tau}}$. Equating this to the form for precession impulse and solving for thrust impulse $F(\frac{\Delta\Phi}{\omega})$, gives

$$I_f = F\left(\frac{\Delta\Phi}{\omega}\right) = \frac{I_{spin}\omega(\Delta\Phi/2)}{R\sin\frac{\Delta\Phi}{2}} \sqrt{2\pi/\omega\tau}$$

which is the thrust impulse per cycle of spin. Thus, the corrective impulse per day is

$$I_f \frac{\omega}{2\pi} (86,400) \quad lb_f\text{-sec/day}$$

when ω is in rad/sec and I_f is in lb_f-sec.

Now propellant mass required is related to impulse by

$$M_p = \frac{\text{Impulse}}{I_{sp} g}$$

or the mass/day is

$$\frac{dM_p}{d\ day} = \frac{I_f}{I_{sp} g} \frac{\omega}{2\pi} (86,400)$$

or

$$\frac{dM_p}{d\ day} = \frac{I_{spin} \omega^2 (86,400)(\Delta\Phi/2)}{RI_{sp} \sqrt{2\pi\omega\tau}\ \sin(\frac{\Delta\Phi}{2})} .$$

Thus, propellant usage is proportional to $1/\sqrt{\tau}$, which indicates a desire for large time constants. Determination of τ for MGO represents a major technical effort. The number of important parameters is large and interactions are highly nonlinear.

The MGO vehicle has not been designed sufficiently to formulate specific dissipation models. However, the propellant usage can be estimated. Given two or four spherical tanks placed equidistant from the spin axis and knowing the propellant properties, it remains only to set the problem in the required combination of spin rates and tank fill-fractions. A spin rate of 5 rpm is to be expected. The fill fraction during cruise is "near-full" or 75% taken as an average. Nearly-full tanks can be modeled as inviscid liquid except at the boundary layer. Nutation causes each tank to experience two types of cyclic motion: translations and rotations. Such motion occurs at the nutation frequency.

Although the spacecraft is nominally in low-g, spinning creates a body-force field in the propellants similar to a spatially non-uniform gravitational acceleration. The magnitude of the $\Omega^2 r$ field with respect to surface tension forces determines whether the liquid responds in a low-g or high-g way, in accordance with the numerical value of the non-dimensional Bond number: $N_B = \rho g R_o^2/\sigma = \rho d\Omega^2 R_o^2/\sigma$. The data for MGO-type show the minimum N_B occurs for N_2H_4 when the spin rate is 1 RPM. This minimum exceeds $N_B = 80$. Since N_B less than 10 is generally taken to separate low-g from high-g (Reference 2), it is clear that the propellant dynamics are controlled by "gravity" forces, not surface tension. Thus, technology developed for high-g sloshing can be applied here and is represented dynamically by: (1) a pendulum chosen to duplicate the forces on the tank walls caused by the part of the liquid that participates in the sloshing, and (2) an immobile, or rigid, mass which represents the rest of the liquid mass (Reference 3).

This model leads to the dissipation caused by sloshing,

$$\varepsilon = K_s \theta^2 \Omega^{1.64}$$

where ε is in in-lb per nutation cycle, θ is again the nutation half cone angle in radians, and Ω is the spin rate in rad/sec. K_s varies from 69 at 25% fill to 27 at 75% fill. Slosh resonances are not predicted to occur in the nutation frequency range of interest here. However, available test data on spherical tanks are contradictory on the possibility of resonances. The value of K_s for 75% fill-fraction is estimated as $27(\text{in-lb/rad})(\text{rad/sec})^{1.64}$.

The cyclic rotations set up a viscous boundary layer at the tank walls because some of the liquid is dragged along by wall motion. However, the bulk of liquid in the tank does not participate in this motion. Assuming boundary layer motion is decoupled from sloshing, the boundary

layer dynamics can be determined analytically. This leads to the boundary layer dissipation,

$$\varepsilon = K_{BL}\theta^2\Omega^{1.5}$$

where K_{BL} varies from about 11 at 25% fill to about 18 at 75% fill. Thus, use 18 (in-lb/rad)(rad/sec)$^{1.5}$.

Nutation frequency, λ, can be derived from a perturbed form of Euler's moment equations (Reference 1). For principal axes, x, y, z, these equations have the form,

$$I_x\dot{\omega}_x + \omega_y\omega_z(I_z - I_y) = 0$$

$$I_y\dot{\omega}_y + \omega_x\omega_z(I_x - I_z) = 0$$

$$I_z\dot{\omega}_z + \omega_z\omega_y(I_y - I_x) = 0$$

for torque-free space. In the nominal case

$$\omega_x = \Omega$$

$$\omega_y = \omega_z = 0$$

where x is the axis of spin. In the perturbed case

$$\omega_x = \Omega + \omega_x$$

$$\omega_y = \omega_y$$

$$\omega_z = \omega_z$$

These equations become, to first order in small values ω_x, ω_y, ω_z

$$I_x\dot{\omega}_x = 0$$

$$I_y\dot{\omega}_y + \Omega\omega_z(I_x - I_z) = 0$$

$$I_z\dot{\omega}_z + \Omega\omega_y(I_y - I_x) = 0$$

which leads to ω_x = constant, and

$$\dot{\omega}_y + \Omega \left(\frac{I_x - I_z}{I_y} \right) \omega_z = 0$$

$$\dot{\omega}_z - \Omega \left(\frac{I_x - I_y}{I_z} \right) \omega_y = 0.$$

Differentiating the first and substituting the second gives

$$\ddot{\omega}_y + \lambda^2 \omega_y = 0$$

where

$$\lambda = \Omega \sqrt{\left(\frac{I_z - I_x}{I_y} \right) \left(\frac{I_y - I_x}{I_z} \right)}$$

the nutation frequency.

The mass properties assumed for MGO at 75% fill fraction are

$$I_x = 5640 \text{ in-lb-s}^2$$

$$I_y = 9590 \text{ in-lb-s}^2$$

$$I_z = 9590 \text{ in-lb-s}^2.$$

This data is used to generate values of λ for three spin rates:

Spin rate, Ω	λ(rad/sec)
1 RPM	0.0431
5 RPM	0.2157
30 RPM	1.2940

Worst case dissipation rates are estimated conservatively by using four times the slosh dissipation plus four times the boundary layer dissipation. These results are tabulated in Table B-1 for nutation angles of 1° and 3°.

$$\dot{T} = -\frac{\epsilon\lambda}{2\pi} \text{ (in-lb/sec)}$$

and kinetic relations gave

$$\dot{T} = \frac{h^2}{I_{min}} \left(\frac{I_{min}}{I_{max}} - 1\right) \theta\dot{\theta}$$

where

$$\theta\dot{\theta} = \frac{1}{2\tau}$$

for small θ values, then the time constant expression becomes

$$\tau = -\frac{h^2}{I_{min}} \left(\frac{I_{min}}{I_{max}} - 1\right) \frac{\pi}{\epsilon\lambda}$$

Values of τ for the worst case situation are listed in Table B-2. This information is then used to calculate the propellant requirement to maintain a given value of nutation angle, i.e., 1° or 3°, using values of

$$\Delta\Phi = 60°$$

$$I_{sp} = 220 \text{ sec}$$

$$R = 3.0 \text{ ft.}$$

with

$$\frac{dM_p}{d\ day} = \frac{I_{spin}\omega^2(86,400)\Delta\Phi/2}{RI_{sp}\sqrt{2\pi\omega\tau}\ \sin(\Delta\Phi/2)}$$

Table B-3 presents the results for the cases studied. Unfortunately, these values are unacceptably high. Refinement in estimates and adjustments in design will significantaly reduce these values.

TABLE B-1. WORST CASE DISSIPATION RATES (in-lb/nutation cycle)

Spin Rate	1 rpm		2 rpm		30 rpm	
Nutation Angle	1°	3°	1°	3°	1°	3°
Slosh	0.000813	0.00732	0.0114	0.102	0.215	1.935
Boundary Layer	0.000743	0.00669	0.00831	0.0748	0.122	1.099
Sum	0.001556	0.01401	0.01971	0.1768	0.337	3.034

TABLE B-2. DISSIPATION TIME CONSTANTS (sec)

Nutation Angle	Spin Rate, Ω		
	1 rpm	5 rpm	30 rpm
1°	1.1934×10^6	4.7062×10^5	1.652×10^5
3°	1.325×10^5	5.2465×10^4	1.8347×10^4

TABLE B-3. PROPELLANT CONSUMPTION FOR NUTATION CONTROL (lbs/day)

Nutation Angle	Spin Rate, Ω		
	1 rpm	5 rpm	30 rpm
1°	0.7973	14.195	352.1
3°	2.393	42.515	1056.6